RESEARCH REPORT

INVESTIGATION OF THE PROPERTIES OF FIBER METAL ACOUSTICAL MATERIALS

By J. J. Cimerol, A. R. Erickson and J. I. Fisher

HUYCK METALS COMPANY
Division of Huyck Corporation
45 WOODMONT ROAD, MILFORD, CONN. 06460
TEL. (203) 878-5981

NASA CR-66643

INVESTIGATION OF THE PROPERTIES OF FIBER METAL ACOUSTICAL MATERIALS

By J. J. Cimerol, A. R. Erickson
and J. I. Fisher

Prepared under Contract No. NAS 1-6990 by
HUYCK METALS COMPANY
MILFORD, CONNECTICUT

for

Langley Research Center

NATIONAL AERONAUTICS AND SPACE ADMINISTRATION

September 1968

ABSTRACT

Porous fiber metal materials are potentially useful in absorbing noise generated by turbofan jet engines by installing the materials in the engine nacelles. The program simulated a number of environmental conditions to which the materials may be exposed in service. Detailed mechanical and physical property information was obtained, and the effects of air erosion, water saturation and freezing, fuel combustion, high temperatures, and salt spray corrosion were measured. Also, tests were performed to assess the relative ease with which the materials could be cleaned of dust and soot contamination. In general, at least type 347 stainless steel fiber metal materials were considered to have passed all of the tests imposed.

TABLE OF CONTENTS

	Page
SUMMARY	1
INTRODUCTION	4
RESULTS AND DISCUSSION	
Task A--Thermal Expansivity	7
Task B--Air Erosion	14
Task C--Freeze-Thaw Cycling	21
Task D--Water Saturation	24
Task E--Fuel Saturation and Combustion Tests	32
Task F--Air Oxidation	37
Task G--Salt Corrosion	58
Task H--Cleanability	68
Task I--Mechanical Properties	80
SUMMARY OF CONCLUSIONS	115
APPENDIX	
Appendix A--Thermal Expansivity	120
Appendix B--Air Erosion	122
Appendix C--Freeze-Thaw Cycling	125
Appendix D--Water Saturation	127
Appendix E--Fuel Saturation and Combustion Tests	130
Appendix F--Air Oxidation	132
Appendix G--Salt Corrosion	135
Appendix H--Cleanability	137
Appendix I--Mechanical Properties	151

TABLE OF CONTENTS (continued)

Page

Appendix J--Flow Resistance Testing - Tasks B Through G 160

Appendix K--Mechanical Properties Testing - Tasks C, E, F, and G 162

Appendix L--Apparent Density and Dimensional Inspection 164

REFERENCES 165

LIST OF FIGURES

Figure		Page
A-1	Percentage Elongation of 347SS Fiber Metal as Compared to Solid Wrought 347SS	12
A-2	Percentage Elongation of Aluminum Fiber Metal as Compared to Solid Wrought Aluminum	13
B-1	Effect of Air Erosion on FM125C. 347SS-C38 Fiber	18
B-2	Effect of Air Erosion on FM138. 347SS-C18 Fiber	19
B-3	Effect of Air Erosion on FM161. 347SS-E18 Fiber	20
D-1	Effect of Water Saturation on Differential Pressure and Flow Resistance. FM152B-Aluminum-E58 Fiber	27
D-2	Effect of Water Saturation on Differential Pressure and Flow Resistance. FMS180-17-4PHSS-C18 and C38 Fibers	28
D-3	Effect of Water Saturation on Differential Pressure and Flow Resistance. FM125C-347SS-C38 Fiber	29
D-4	Effect of Water Saturation on Differential Pressure and Flow Resistance. FM150-347SS-C28 Fiber	30
D-5	Effect of Water Saturation on Differential Pressure and Flow Resistance. FM161-347SS-E18 Fiber	31
E-1	Relationship Between Average Combustion Period and Pore Volume	36
F-1	Effect of Air Oxidation on Ultimate Tensile Strength. FM151B-Aluminum-E58 Fiber	44
F-2	Effect of Air Oxidation on Ultimate Tensile Strength. FMS180-17-4PHSS-C18 and C38 Fiber . .	45
F-3	Effect of Air Oxidation on Ultimate Tensile Strength. FM125C-347SS-C38 Fiber	46
F-4	Effect of Air Oxidation on Ultimate Tensile Strength. FM137-347SS-C28 Fiber	47

LIST OF FIGURES (continued)

Figure		Page
F-5	Effect of Air Oxidation on Ultimate Tensile Strength. FM138-347SS-C18 Fiber	48
F-6	Effect of Air Oxidation on Ultimate Tensile Strength. FM139-347SS-E18 Fiber	49
F-7	Effect of Air Oxidation on Air Flow Resistance. FM151B-Aluminum-E58 Fiber	50
F-8	Effect of Air Oxidation on Air Flow Resistance. FMS180-17-4PHSS-C18 and C38 Fiber	50
F-9	Effect of Air Oxidation on Air Flow Resistance. FM125C-347SS-C38 Fiber	51
F-10	Effect of Air Oxidation on Air Flow Resistance. FM137-347SS-C28 Fiber	51
F-11	Effect of Air Oxidation on Air Flow Resistance. FM138-347SS-C18 Fiber	52
F-12	Effect of Air Oxidation on Air Flow Resistance. FM139-347SS-E18 Fiber	52
F-13	Effect of Air Oxidation on Weight. FM151B-Aluminum-E58 Fiber	53
F-14	Effect of Air Oxidation on Weight. FMS180-17-4PHSS-C18 and C38 Fiber	53
F-15	Effect of Air Oxidation on Weight. FM125C-347SS-C38 Fiber	54
F-16	Effect of Air Oxidation on Weight. FM137-347SS-C28 Fiber	54
F-17	Effect of Air Oxidation on Weight. FM138-347SS-C18 Fiber	55
F-18	Effect of Air Oxidation on Weight. FM139-347SS-E18 Fiber	55
F-19	Oxidation Rate Constants for 347SS and 17-4PHSS .	56
F-20	Calculated and Observed Weight Gain From Oxidation. FMS180-17-4PHSS-C18 and C38 Fiber . .	57

LIST OF FIGURES (continued)

Figure		Page
F-21	Calculated and Observed Weight Gain From Oxidation. FM137-347SS-C28 Fiber	57
G-1	Effect of Salt Corrosion Exposure on Ultimate Tensile Strength. FM151B-Aluminum-E58 Fiber . .	65
G-2	Effect of Salt Corrosion Exposure on Ultimate Tensile Strength. FMS180-17-4PHSS-C18 and C38 Fiber	65
G-3	Effect of Salt Corrosion Exposure on Ultimate Tensile Strength. FM125C-347SS-C38 Fiber	66
G-4	Effect of Salt Corrosion Exposure on Ultimate Tensile Strength. FM137-347SS-C28 Fiber	66
G-5	Effect of Salt Corrosion Exposure on Ultimate Tensile Strength. FM138-347SS-C18 Fiber	67
G-6	Effect of Salt Corrosion Exposure on Ultimate Tensile Strength. FM139-347SS-E18 Fiber	67
H-1	Unsupported Fiber Metal and Bonded Sample Configurations	75
H-2	Effect of Cleaning on FM171. Part I Testing-Unsupported Fiber Metal	76
H-3	Effect of Cleaning on FM171. Part I Testing-Unsupported Fiber Metal	77
H-4	Effect of Cleaning on FM171. Part II Testing-Fiber Metal Bonded to 1 in. (2.54 cm) Honeycomb	78
H-5	Effect of Cleaning on FM125C and FM171. Part III Testing-Double Layer Fiber Metal Bonded to Two Layers of Honeycomb	79
I-1	Typical Stress-Strain Plot for 347SS Fiber Metal. 25.8 Percent Dense C18 Fiber	91
I-2	Effect of Prestrain on Young's Modulus of 347SS Fiber Metal. 25.8 Percent Dense C18 Fiber . . .	92
I-3	Effect of Prestrain on the Yield Strength of 347SS Fiber Metal. 25.8 Percent Dense C18 Fiber	93

LIST OF FIGURES (continued)

Figure		Page
I-4	Cantilever Beam Deflection Testing for Young's Modulus Determination. 347SS Fiber Metal	94
I-5	Apparent Young's Modulus vs Apparent Density. 347SS Fiber Metal Type C38 Fiber	95
I-6	Photomicrograph at 56x of FM128A Fiber Metal Acoustical Material. 347SS Type C18 Fiber With 18 Mesh x 0.009 in. (0.023 cm) Diameter Wire Screen Reinforcement on Both Sides	96
I-7	Apparent Young's Modulus vs Apparent Density. 347SS Fiber Metal Type C18 Fiber	97
I-8	Apparent Young's Modulus vs Apparent Density. Aluminum Fiber Metal Type E58 Fiber	98
I-9	Apparent Shear Modulus vs Apparent Density. 347SS Fiber Metal Type C38 Fiber	99
I-10	Apparent Shear Modulus vs Apparent Density. 347SS Fiber Metal Type C18 Fiber	100
I-11	Apparent Shear Modulus vs Apparent Density. Aluminum Fiber Metal Type E58 Fiber	101
I-12	Influence of Apparent Density on Ultimate Tensile Strength. 347SS Fiber Metal, C38 Fiber	102
I-13	Influence of Apparent Density on Yield Strength. 347SS Fiber Metal, C38 Fiber	103
I-14	Increase in Ultimate Strength of Thin 347SS Fiber Metal by Wire Screen Reinforcement	104
I-15	Increase in Ultimate Tensile Strength Caused by 18 Mesh x 0.009 in. (0.023 cm) Diameter Wire Screen Reinforcement. Type 347SS Fiber Metal . .	105
I-16	Influence of Apparent Density on Ultimate Tensile Strength. 347SS Fiber Metal C18 Fiber .	106
I-17	Influence of Apparent Density on Yield Strength. 347SS Fiber Metal, C18 Fiber	107
I-18	Influence of Apparent Density on Ultimate Tensile Strength. Aluminum Fiber Metal, E58 Fiber . . .	108

LIST OF FIGURES (continued)

Figure		Page
I-19	Influence of Apparent Density on Yield Strength. Aluminum Fiber Metal, E58 Fiber	108
I-20	Apparent Values of Ultimate Tensile Strength, Young's and Shear Modulus for Fiber Metal	109
I-21	Influence of Apparent Density on Elongation of Fiber Metal. 7.0 in. (17.8 cm) Test Gauge Length	110
I-22	Effect of Thickness on the Ductility of Screen Reinforced Type 347SS Fiber Metal Materials . . .	111
I-23	Torsional Damping Capacity of 347SS Type C38 Fiber Metal	112
I-24	Torsional Damping Capacity of 347SS Type C18 Fiber Metal	113
I-25	Torsional Damping Capacity of Aluminum Type E58 Fiber Metal	114

FIGURES IN APPENDICES

AB-1	Air Erosion Test Apparatus	124
AD-1	Water Saturation Test Apparatus	129
AE-1	Burning Combustion Specimen	131
AH-1	Low Velocity Flow Resistance Apparatus. 5 to 20 cm per sec (0.16 to 0.65 ft per sec)	146
AH-2	High Velocity Flow Resistance Apparatus. 27 to 500 cm per sec (0.89 to 16.4 ft per sec)	147
AH-3	Contamination Apparatus	148
AH-4	Detail of Contamination Test Fixture	149
AH-5	Cleaning Method 4A used in Part II and III Testing. Impervious Backing Plate in Place . . .	150
AI-1	Young's Modulus Test Apparatus. Cantilever Beam Method	156

LIST OF FIGURES (continued)

Figure		Page
AI-2	Young's Modulus Test Apparatus. Simply Supported Beam Method	157
AI-3	Damping Capacity and Shear Modulus Test Apparatus	158
AI-4	Mechanical Properties Test Specimen	159
AJ-1	Flow Resistance Test Apparatus	161

LIST OF TABLES

Table		Page
I	Fiber Metal Acoustical Materials Evaluated in NAS 1-6990 Study Program	6
A-I	Samples Tested in Thermal Expansivity Study . . .	9
A-II	Changes in Length for 347 Stainless Steel Samples	10
A-III	Changes in Length for Aluminum Samples	11
B-I	Influence of Air Erosion on Fiber Metal Weight . .	16
B-II	Influence of Air Erosion on Thickness and Flow Resistance	17
C-I	Effect of Freeze-Thaw Cycling on Fiber Metal Thickness and Flow Resistance	22
C-II	Effect of Freeze-Thaw Cycling on Ultimate Tensile Strength and Percentage Elongation	23
D-I	Break Through Differential Pressures and Air Velocities Required to Totally Dry Out Water Saturated Fiber Metal Acoustical Materials	26
E-I	Influence of Six Cycles of Fuel Combustion on Flow Resistance and Weight Gain	34
E-II	Affect of Six Cycles of Fuel Combustion on Ultimate Tensile Strength and Percentage Elongation	35
E-III	Observed Combustion Periods of Fiber Metal Materials	36
F-I	Effect of Air Oxidation on Percentage Elongation .	42
F-II	Appearance of Stainless Steel Fiber Metal Materials Resulting from Air Oxidation	43
G-I	Effect of Salt Corrosion Exposure on Weight . . .	61
G-II	Effect of Salt Corrosion Exposure on Flow Resistance	62
G-III	Appearance of Samples After Salt Corrosion Exposure	63

LIST OF TABLES (continued)

Table		Page
G-IV	Effect of Salt Corrosion Exposure on Percentage Elongation	64
H-I	Results of Cleaning Experiments. Part I of Program-Unsupported Fiber Metal	73
H-II	Results of Cleaning Experiments. Parts II and III of Program-Fiber Metal-Honeycomb Configurations	74
I-I	Mechanical Properties of Fiber Metal	89
I-II	Effect of Fabrication Techniques on the Mechanical Properties of Fiber Metal	90

INVESTIGATION OF THE PROPERTIES OF FIBER METAL ACOUSTICAL MATERIALS

by J. J. Cimerol
A. R. Erickson
J. I. Fisher

Huyck Metals Company

SUMMARY

Twenty-eight alternative fiber metal acoustical materials were evaluated in environmental tests under conditions simulating those expected to be encountered in the silencing of turbofan jet engines. Three different metal alloys at four fiber diameters were employed at apparent densities ranging from 40 to 70%. An austenitic (type 347) and a precipitation hardening (17-4PH) stainless steel were tested, as well as a hybrid aluminum alloy. The test materials were produced to four basic air flow resistances: 10, 25, 50, and 80 cgs rayls.

The effect of the environmental testing conditions was measured on visual appearance, air flow resistance, weight change, tensile strength, and elongation to failure in tension.

Thermal Expansivity

Fiber metal has essentially the same thermal expansivity as the solid metal counterparts at temperatures ranging from -275°F (-170°C) to 1000°F (538°C).

Air Erosion

There was no measurable effect of any kind due to air jets impinging on fiber metal for time periods up to 100 hours.

Freeze Thaw Cycling

Fiber metal materials were not affected by repetitive water filling, freezing and thawing between the temperatures of -109°F (-78°C) and 220°F (104°C).

Water Saturation

Saturation of fiber metal materials with water causes a marked increase in their air flow resistance. This water is physically expelled from the pores and the dry air flow resistance is restored when air is forced through the materials at high direct current air flow velocities. These measured velocities are similar to those particle velocities found in sound waves of the intensities experienced in turbofan jet engines.

Fuel Combustion

Repetitive burning of jet fuel from fuel saturated specimens had no effect on the properties of fiber metal materials. The short duration of combustion is related to the small pore volume of the fiber metal materials.

Air Oxidation

The rate of air oxidation was measured with several materials at various temperatures for up to 50 hours exposure. The maximum operating temperature recommended for type 347 stainless steel fiber metal is 1000°F (538°C).

Salt Spray Corrosion

There is a progressive increase in air flow resistance resulting from the corrosion deposits in aluminum and 17-4PH fiber metal exposed to salt spray. These deposits could be removed with appropriate cleaning procedures. The type 347 stainless steel materials were demonstrated to have satisfactory resistance to up to 96 hours of salt spray corrosion

Cleanability

Simulated engine contaminants (silica dust, carbon black and turbine oil) can be cleaned from clogged panels mounted on honeycomb supports. Solvent action was required to remove oils while positive liquid flushing is required to remove oil-free solid contaminants. Cleaning with liquids is aided by the mechanical action of vacuum cleaning, air blasting, and ultrasonic energy.

Mechanical Properties

Young's modulus, shear modulus, yield strength, tensile strength, elongation to failure in tension, and torsional damping capacity were measured on the materials of interest in this program but over a wider range of apparent densities than is normally encountered with acoustical materials. The results are presented as graphical correlations and are explained in terms of the physical composition of fiber metal. Apparent density and screen reinforcement have the largest effects upon these properties.

INTRODUCTION

Requirements have been increasing recently for materials which both are highly effective sound absorbers and are sufficiently durable to withstand a number of adverse environmental conditions. With the developing need to reduce the noise generated by turbofan jet engines, even more interest has been focused on porous metal absorptive materials. Fiber metal materials have been applied for noise control in a number of situations involving elevated temperatures, high flow rates, and high sound pressure levels. For example, these materials have been successfully employed to treat the inlet and exhaust of small gas turbines, high performance fans, and aircraft air conditioning systems.

Fiber metallurgy is a relatively new technology, with its roots in powder metallurgy. The metallurgical procedure common to both is the sintering process, a high temperature treatment in a protective atmosphere which produces metallurgical bonds between metal particles analogous to welds. Whereas metal powders are most frequently compacted to very high apparent densities (percent of the apparent volume occupied by metal), it is the objective in fiber metallurgy to produce relatively low density (high porosity) parts. This is easily done with metal fibers, and densities as low as 10 percent are not uncommon. By controlling both density and fiber size, close control of pore size and fluid permeability is achieved.

Controlled permeability to air, combined with the capability to produce large, thin and light weight sheets, has therefore made fiber metal materials highly interesting in the field of aircraft noise control. The acoustician requires materials with a controlled acoustic flow resistance, which is simply permeability to air expressed in units useful in acoustical computations, cgs rayls. Thus, acoustic flow resistance of a permeable material is:

$$R_f = \frac{\Delta P}{\mu}$$

Where

R_f is acoustic flow resistance in cgs rayls, dyne sec/cm^3

ΔP is pressure differential, dynes/cm^2

μ is flow velocity, cm/sec

The work reported here has been aimed primarily at supplying design and performance information not previously available on fiber metal materials. It is also intended that this report provide insight both into the design tradeoffs which can be made, and the effectiveness of fiber metal when subjected to the adverse environments which might be encountered in aircraft turbofan jet engine applications.

Many of the tests to which the materials were subjected derived from suggestions provided by members of the airframe and jet engine industry, prior to undertaking the work.

A careful selection of candidate materials was made, in order to represent as wide a range of acoustical and mechanical properties as would likely be of interest. As shown in Table I, both conventional (type 347) and precipitation hardening (17-4 PH) stainless steels were chosen. Also, an aluminum alloy fiber metal was subjected to some of the testing.

The work to be reported included a detailed survey of mechanical properties, conducted under a joint program between Huyck Metals Company and Illinois Institute of Technology Research Institute. The properties determined were yield and ultimate tensile strengths, ductility, tension and shear moduli and torsional damping. The effects of elevated temperature air oxidation, high velocity air impingement and salt fog corrosion exposure were determined. The possible adverse effects were measured of water saturating then freezing in the pores of the porous metals, as were the effects of fuel saturating the pores and then burning there. Determinations were made of thermal expansivity at elevated and sub-zero temperatures. Finally, a careful study was performed by the Douglas Aircraft Division, McConnell Douglas Corporation, of the problems likely to be encountered in maintaining porous fiber metal materials installations. This study centered around cleaning the materials of deliberately added contaminants.

TABLE I

FIBER METAL ACOUSTICAL MATERIALS EVALUATED IN NAS 1-6990 STUDY PROGRAM

Fiber metal spec no.	Nominal flow resistance, rayls	Material	Fiber type	No. of reinf screen layers	Nominal total apparent density, %	Nominal thickness		Nominal total area density	
						in.	cm	lb/ft^2	kg/m^2
Number Screen Reinforcement									
FM151B	10	Aluminum	E58	0	47.8	0.060	0.152	0.405	1.98
FM152B	50	Aluminum	E58	0	64.7	0.060	0.152	0.548	2.68
FMS180	10	17-4PHSS	(1)	0	56.3	0.015	0.038	0.342	1.67
FMS181	25	17-4PHSS	(1)	0	75.5	0.010	0.025	0.323	1.58
FMS182	50	17-4PHSS	C18	0	53.0	0.017	0.043	0.377	1.84
FMS183	80	17-4PHSS	C18	0	63.0	0.014	0.036	0.373	1.82
18 mesh x 0.009 in. (0.023 cm) Diameter Wire Screen Reinforcement									
FM125C	10	347SS	C38	2	51.5	0.040	0.102	0.854	4.18
FM137	10	347SS	C28	2	49.1	0.030	0.076	0.610	2.98
FM138	10	347SS	C18	2	49.9	0.020	0.051	0.415	2.03
FM139	10	347SS	E18	2	49.9	0.020	0.051	0.415	2.03
FM129B	25	347SS	C38	2	56.0	0.040	0.102	0.931	4.56
FM150	25	347SS	C28	2	59.2	0.030	0.076	0.740	3.62
FM140	25	347SS	C18	2	60.1	0.020	0.051	0.500	2.45
FM141	25	347SS	E18	2	60.1	0.020	0.051	0.500	2.45
FM171	40	347SS	C38	2	67.8	0.040	0.102	1.125	5.51
FM172	40	347SS	C18	2	67.3	0.020	0.051	0.557	2.72
FM123A	50	347SS	C38	1	61.0	0.040	0.102	1.016	4.97
FM126B	50	347SS	C28	2	60.4	0.030	0.076	0.755	3.69
FM128A	50	347SS	C18	2	68.8	0.020	0.051	0.572	2.80
FM145	50	347SS	E18	2	68.8	0.020	0.051	0.572	2.80
FM158	80	347SS	C38	1	69.5	0.040	0.102	1.153	5.65
FM159	80	347SS	C28	1	64.7	0.030	0.076	0.810	3.96
FM160	80	347SS	C18	1	63.8	0.020	0.051	0.530	2.59
FM161	80	347SS	E18	1	63.8	0.020	0.051	0.530	2.59
30 mesh x 0.0065 in. (0.0165 cm) Diameter Wire Screen Reinforcement									
FM146	10	347SS	C38	2	50.0	0.040	0.102	0.830	4.06
FM147	25	347SS	C38	2	61.2	0.040	0.102	1.020	4.99
FM149	50	347SS	C38	2	68.6	0.040	0.102	1.140	5.58
FM167	80	347SS	C38	1	68.8	0.040	0.102	1.140	5.58

Fiber Code

Type	E58	C38	C28	C18	E18
Diam (in.)	0.006	0.004	0.003	0.002	0.002
Diam (cm)	0.0152	0.0102	0.0076	0.0051	0.0051

[1]Fiber type 13% C18, 87% C38

RESULTS AND DISCUSSION

TASK A--THERMAL EXPANSIVITY

Introduction.- There has been a need, for design purposes, to know the thermal expansivity of fiber metal rather than to assume that the thermal expansivity of fiber metal is equal to that of the solid metal from which it is fabricated. In addition, fiber metal is normally anisotropic, the metal fibers tend to orient themselves with their major dimension in the plane of the sheet. It is, therefore, possible that fiber metal has different thermal expansivity characteristics in and normal to the plane of formation.

The purpose of this work was to answer these questions over the broadest range of material type and density from which fiber metal for engine silencing would be produced. On this basis, aluminum and 347 SS fiber metal were evaluated, over a density range of 35 to 66 percent. The samples tested are shown in Table A-I.

Experimental apparatus and procedure.- A vitreous silica dilatometer, fitted with an extensometer, was used to determine the thermal expansion characteristics of 2 in. long rods of fiber metal. The 347 stainless steel specimens were evaluated over a temperature range of -275°F (-170.5°C) to 1000°F (537.7°C), while the aluminum fiber metal was evaluated over a range of -275°F (-170.5°C) to 400°F (204.1°C). Details of apparatus and procedure are given in Appendix A.

Discussion of results.- The specimens tested in the program are shown in Table A-I. The basic data from the program are shown in Tables A-II and A-III. There was no change in gauge length for any of the specimens resulting from the temperature excursions. These data were initially evaluated for differences in expansivity as the orientation of the gauge lengths changed from parallel to normal to the plane of formation. This analysis indicated that no trends in the data existed and, therefore, fiber metal is isotropic with respect to thermal expansivity.

Next, the percentage elongation values for specimens 1 and 2, 3 and 4, 5 and 6, 7 and 8 were averaged in order to determine if apparent density influenced thermal expansivity. These data are plotted in Figures A-1 and A-2 along with the values for the solid wrought materials, Reference 1. The figures indicate that apparent density does not significantly influence the thermal expansivity of fiber metal. Above ambient temperatures, the thermal expansion of 347 SS and aluminum fiber metal is about 95 percent that of the solid wrought material. Below ambient temperatures, there is no significant difference in thermal elongation between fiber metal and the solid wrought material.

Conclusions.- The following conclusions can be drawn from this work:

1. Fiber metal is isotropic in thermal expansivity with respect to compaction direction. That is, thermal expansion is the same parallel or perpendicular to the plane of the sheet.

2. Thermal expansion characteristics are independent of apparent density of the fiber metal.

3. Above ambient temperature, both 347 SS and aluminum fiber metal have about 95 percent of the thermal expansivity of the solid wrought material. Below ambient temperature, both fiber metals have essentially the same thermal expansivities as the solid wrought material.

TABLE A-I

SAMPLES TESTED IN THERMAL EXPANSIVITY STUDY

Sample number	Material type	Fiber type	Apparent density, percent	Sample length		Gauge length orientation relative to formation plane
				in.	cm	
1	347 SS	C-38	39.4	1.947	4.945	parallel
2	347 SS	C-38	40.0	1.947	4.945	normal
3	347 SS	C-38	62.5	2.000	5.080	parallel
4	347 SS	C-38	66.9	2.003	5.088	normal
5	aluminum	E-58	37.5	1.987	5.047	parallel
6	aluminum	E-58	35.6	2.046	4.963	normal
7	aluminum	E-58	58.3	2.000	5.080	parallel
8	aluminum	E-58	60.5	2.001	5.083	normal

TABLE A-II

CHANGES IN LENGTH FOR
347 STAINLESS STEEL SAMPLES

Temperature,		Cumulative length change, in. per in. (cm per cm)			
		Test sample number			
°F	°C	1	2	3	4
75	23.9	0	0	0	0
100	37.8	0.00026	0.00018	0.00020	0.00018
200	93.3	0.00118	0.00101	0.00100	0.00105
300	148.9	0.00206	0.00185	0.00188	0.00190
400	204.1	0.00300	0.00280	0.00283	0.00280
500	260.0	0.00396	0.00375	0.00380	0.00382
600	315.6	0.00494	0.00475	0.00478	0.00479
700	371.1	0.00601	0.00578	0.00575	0.00579
800	426.6	0.00707	0.00688	0.00678	0.00682
900	482.2	0.00812	0.00791	0.00780	0.00787
1000	537.7	0.00919	0.00904	0.00880	0.00884
75	23.9	0	0	0	0
50	10.0	-0.00018	-0.00018	-0.00015	-0.00010
0	- 17.8	-0.00069	-0.00072	-0.00088	-0.00065
- 50	- 45.6	-0.00113	-0.00121	-0.00130	-0.00105
-100	- 73.3	-0.00159	-0.00165	-0.00175	-0.00145
-150	-101.1	-0.00203	-0.00209	-0.00220	-0.00183
-200	-128.9	-0.00239	-0.00247	-0.00260	-0.00219
-250	-156.7	-0.00265	-0.00270	-0.00280	-0.00240
-275	-170.6	-0.00278	-0.00283	-0.00290	-0.00255

TABLE A-III

CHANGES IN LENGTH FOR
ALUMINUM SAMPLES

Temperature,		Cumulative length change, in. per in. (cm per cm)			
		Test sample number			
°F	°C	5	6	7	8
75	23.9	0	0	0	0
100	37.8	0.00033	0.00027	0.00033	0.00020
150	65.6	0.00099	0.00091	0.00095	0.00083
200	93.3	0.00159	0.00152	0.00158	0.00143
250	121.1	0.00227	0.00215	0.00225	0.00210
300	148.9	0.00290	0.00286	0.00293	0.00285
350	176.7	0.00352	0.00350	0.00363	0.00345
400	204.1	0.00418	0.00420	0.00430	0.00405
75	23.9	0	0	0	0
50	10.0	-0.00025	-0.00027	-0.00014	-0.00020
0	- 17.8	-0.00103	-0.00098	-0.00120	-0.00123
- 50	- 45.6	-0.00161	-0.00152	-0.00163	-0.00165
-100	- 73.3	-0.00219	-0.00213	-0.00210	-0.00208
-150	-101.1	-0.00277	-0.00269	-0.00255	-0.00258
-200	-128.9	-0.00322	-0.00313	-0.00300	-0.00295
-250	-156.7	-0.00352	-0.00347	-0.00335	-0.00340
-275	-170.6	-0.00367	-0.00362	-0.00350	-0.00355

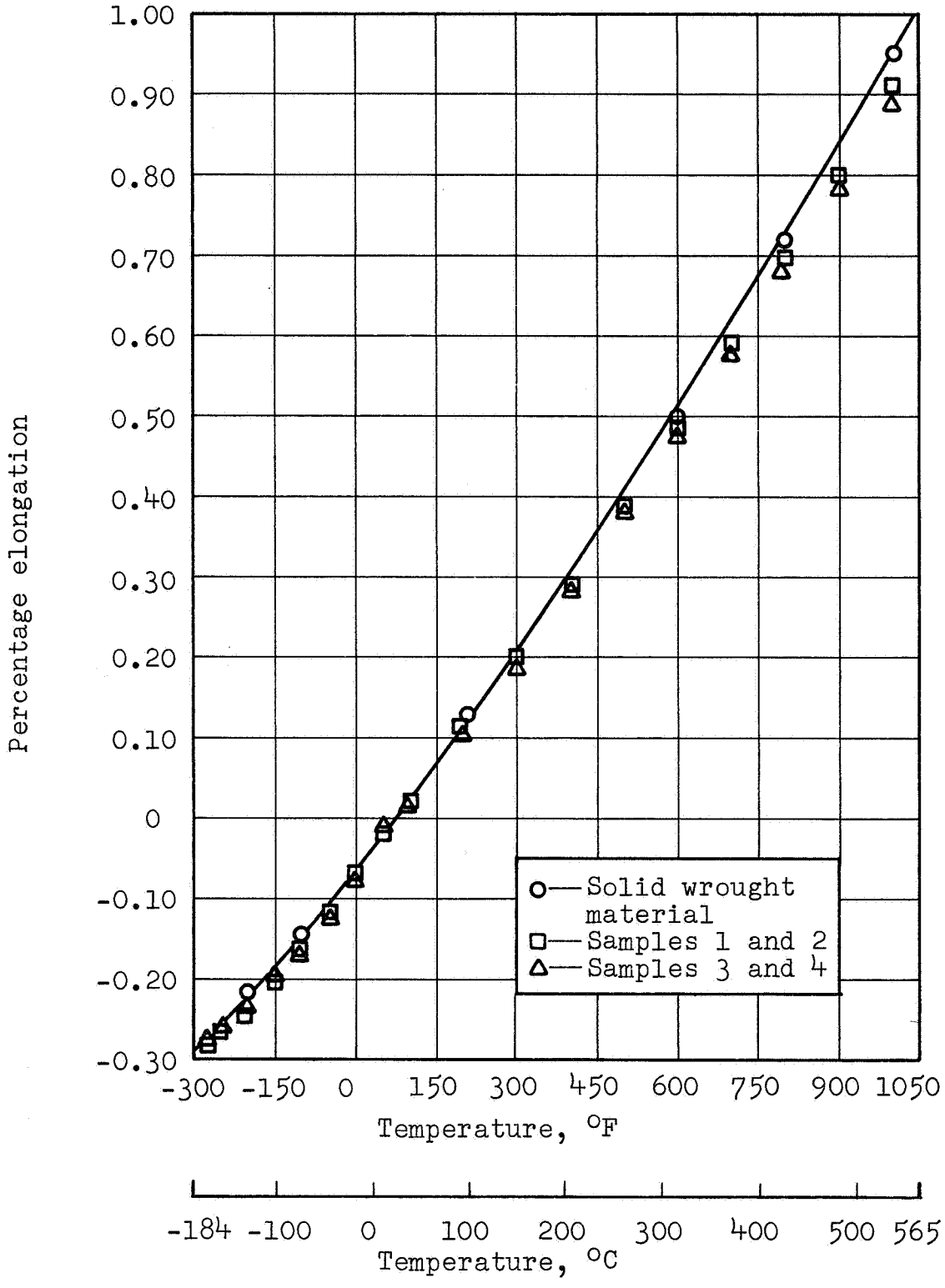

FIGURE A-1

PERCENTAGE ELONGATION OF 347 SS FIBER METAL
AS COMPARED TO SOLID WROUGHT 347 SS

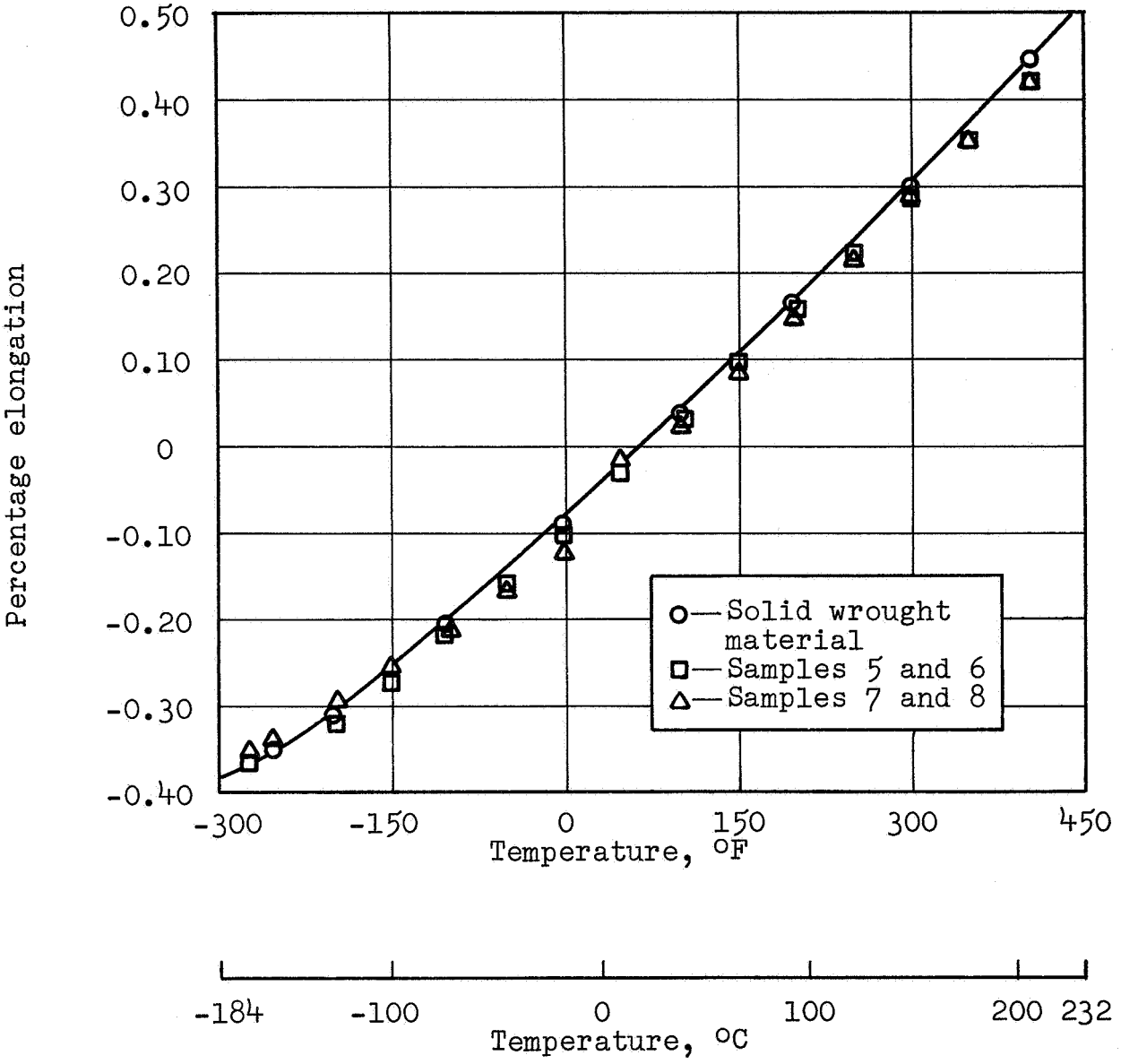

FIGURE A-2

PERCENTAGE ELONGATION OF ALUMINUM FIBER METAL AS COMPARED TO SOLID WROUGHT ALUMINUM

TASK B--AIR EROSION

Introduction.- The porous metal component of an engine sound absorptive treatment will be subjected to high velocity air streams, of at least grazing incidence. It was the intention of this test series to determine the erosion effects, of both a mechanical and an acoustical nature, that might be produced by such a stream acting on fiber metal materials. A particular objective was the determination of whether high velocity air streams would work on individual fibers sufficiently to break their metallurgical bonds, leading to progressive deterioration of the material. The severity of the test was maximized by increasing the angle of air impingement to 45 degrees.

All of the materials shown in Table I were evaluated in this program.

Experimental apparatus and procedure.- The environmental exposure in this test series consisted of directing a sonic velocity air blast, from 0.055 in. (0.139 cm) diameter flow orifices, onto the surface of the fiber metal materials. The angle of incidence was 45 degrees. The erosion effects were determined by observing the visual, acoustical, and mechanical changes on the specimens. Details of experimental apparatus and procedure are given in Appendix B.

Discussion of results.- The basic data gathered in this program are shown in Tables B-I and B-II.

Table B-I shows that all specimens lost some weight in the test. The predominant value for weight lost is 2 milligrams, with a few values at 3 and 4 milligrams and one value at 13 milligrams. Considering that the weight per lineal inch of 0.004 in. (0.010 cm) (C38) diameter stainless steel wire is 0.0016 grams, these results would indicate that fibers amounting to 1.25 in. (3.18 cm) were lost from these materials for a 2 milligram loss. Correspondingly, 2 milligrams lost from 0.003 in. (0.0076 cm) (C28) and 0.002 in. (0.0051 cm) (C18) diameter wire materials would amount to a respective 2.16 in. (5.48 cm) and 4.88 in. (12.4 cm) of wire loss. Photomicrographs at 21X, of all the target areas, before and after testing, refute the wire loss theory. In no instance was there any evidence of erosion or removal or loosening of fibers. In the interest of brevity, three typical pairs of photographs are shown in Figures B-1 through B-3. Thickness changes, shown in Table B-II, also tend to disprove wire loss. Decreases of 0.0001 to 0.0003 in. (0.00025 to 0.00076 cm) predominate, which represent only a small fraction of the minimum fiber diameter employed.

A more probable explanation for the weight losses is the ultrasonic cleaning given the specimens, both before and after testing. It would be very unlikely that the same degree of cleaning could be achieved each time, and if the cleaning after exposure was slightly more vigorous than before testing, then uniformly lower specimen weights would result.

Flow resistance changes, resulting from the test, are shown in Table B-II. Values of -5 to +5 percent predominate, with one value at -16 percent. Variations of this order are not considered significant.

Conclusions.- It is concluded that the impingement of a sonic blast of clean air for 100 hours caused no erosion or dislodging of fibers from any of the fiber metal specimens evaluated.

TABLE B-I

INFLUENCE OF AIR EROSION
ON FIBER METAL WEIGHT

Fiber metal spec no	Material type	Fiber type	Weight of specimens, gms	
			Initial	Loss after exposure
FM151B	aluminum	E58	3.712	0.004
FM152B	aluminum	E58	3.966	0.002
FMS180	17-4PHSS	C18,C38	2.567	0.004
FMS181	17-4PHSS	C18,C38	2.265	0.002
FMS182	17-4PHSS	C18	2.861	0.003
FMS183	17-4PHSS	C18	2.707	0.002
FM125C	347 SS	C38	5.258	0.002
FM137	347 SS	C28	4.632	0.002
FM138	347 SS	C18	2.912	0.002
FM139	347 SS	E18	3.078	0.002
FM129B	347 SS	C38	6.638	0.002
FM150	347 SS	C28	5.174	0.002
FM140	347 SS	C18	3.524	0.002
FM141	347 SS	E18	3.618	0.002
FM123A	347 SS	C38	7.280	0.003
FM126B	347 SS	C28	5.440	0.004
FM128A	347 SS	C18	3.992	0.003
FM145	347 SS	E18	4.266	0.002
FM158	347 SS	C38	9.105	0.013
FM159	347 SS	C28	6.258	0.002
FM160	347 SS	C18	3.860	0.001
FM161	347 SS	E18	4.019	0.004
FM146	347 SS	C38	5.908	0.003
FM147	347 SS	C38	7.420	0.002
FM149	347 SS	C38	8.753	0.003
FM162	347 SS	C38	8.195	0.003

TABLE B-II

INFLUENCE OF AIR EROSION ON THICKNESS AND FLOW RESISTANCE

Fiber metal spec no	Air flow resistance			Target area thickness			
	before erosion, rayls	after erosion, rayls	change, percent	initial		change	
				in.	cm	in.	cm
FM151B	14.0	13.2	- 5.7	0.0531	0.1349	-0.0002	-0.0005
FM152B	47.0	41.2	-12.3	0.0651	0.1652	0.0001	0.0002
FMS180	7.4	7.1	- 4.1	0.0167	0.0424	-0.0004	-0.0010
FMS181	22.8	19.4	-14.9	0.0111	0.0282	-0.0001	-0.0002
FMS182	66.9	55.9	-16.5	0.0161	0.0409	-0.0001	-0.0002
FMS183	75.7	69.1	- 9.0	0.0153	0.0389	-0.0001	-0.0002
FM125C	6.9	6.6	- 4.4	0.0409	0.1040	-0.0003	-0.0007
FM137	7.1	7.4	4.2	0.0391	0.0992	-0.0003	-0.0007
FM138	5.0	4.6	- 8.0	0.0272	0.0691	0.0001	0.0002
FM139	6.6	6.2	- 6.1	0.0274	0.0696	-0.0016	-0.0040
FM129B	24.5	24.3	- 0.8	0.0419	0.1064	0.0002	0.0005
FM150	14.7	15.4	4.8	0.0370	0.0939	0	0
FM140	23.5	23.1	- 1.7	0.0244	0.0620	-0.0007	-0.0017
FM141	17.6	17.6	0	0.0276	0.0701	-0.0014	-0.0035
FM123A	42.2	37.9	-10.2	0.0416	0.1055	0	0
FM126B	31.6	29.1	- 7.9	0.0338	0.0859	-0.0002	-0.0005
FM128A	20.6	20.6	0	0.0277	0.0704	-0.0003	-0.0007
FM145	34.6	36.0	4.1	0.0289	0.0734	-0.0008	-0.0020
FM158	55.1	52.9	- 4.0	0.0502	0.1274	-0.0005	-0.0012
FM159	55.1	52.9	- 4.0	0.0345	0.0876	-0.0003	-0.0007
FM160	91.1	91.1	0	0.0210	0.0534	-0.0001	-0.0002
FM161	86.0	83.1	- 3.4	0.0246	0.0625	-0.0003	-0.0007
FM146	8.1	7.4	- 8.6	0.0496	0.1258	-0.0002	-0.0005
FM147	23.5	24.6	4.7	0.0498	0.1265	-0.0002	-0.0005
FM149	46.6	45.6	- 2.2	0.0491	0.1247	-0.0002	-0.0005
FM162	45.6	46.6	2.2	0.0497	0.1262	-0.0002	-0.0005

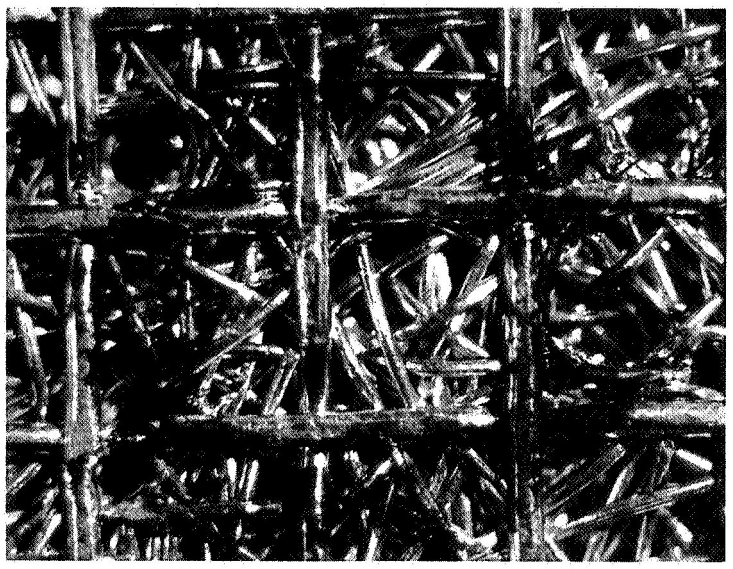

(a) Before erosion
Magnification factor - 21

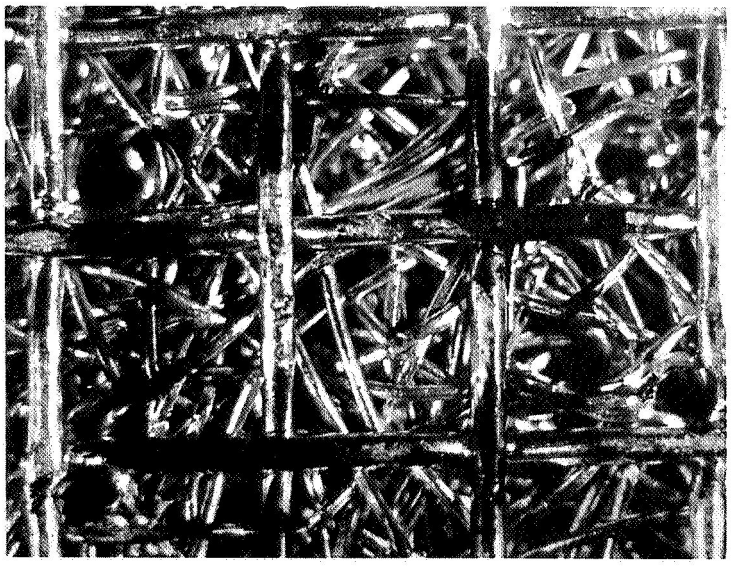

(b) After erosion
Magnification factor - 21

FIGURE B-1

EFFECT OF AIR EROSION
ON FM125C 347SS - C38 FIBER

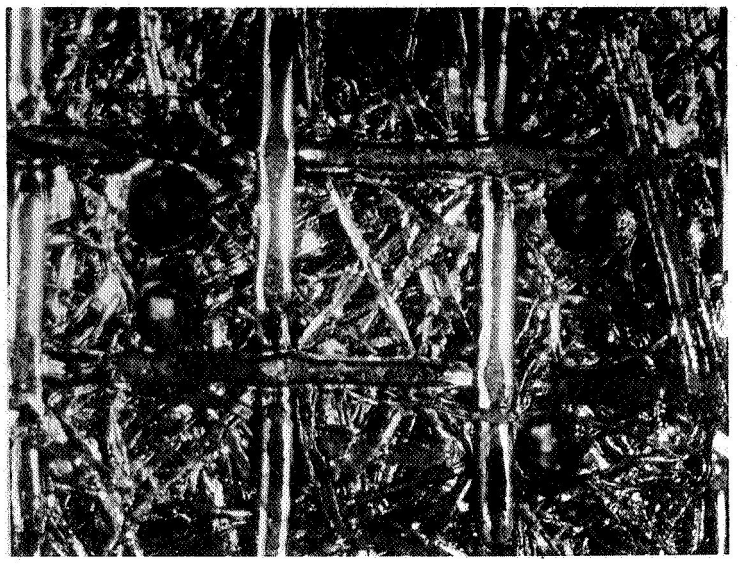

(a) Before erosion
Magnification factor - 21

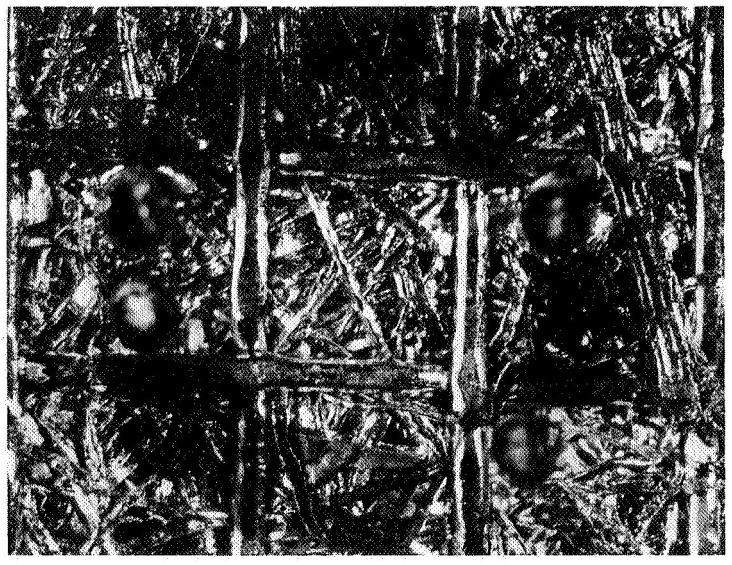

(b) After erosion
Magnification factor - 21

FIGURE B-2

EFFECT OF AIR EROSION
ON FM138 347SS - C18 FIBER

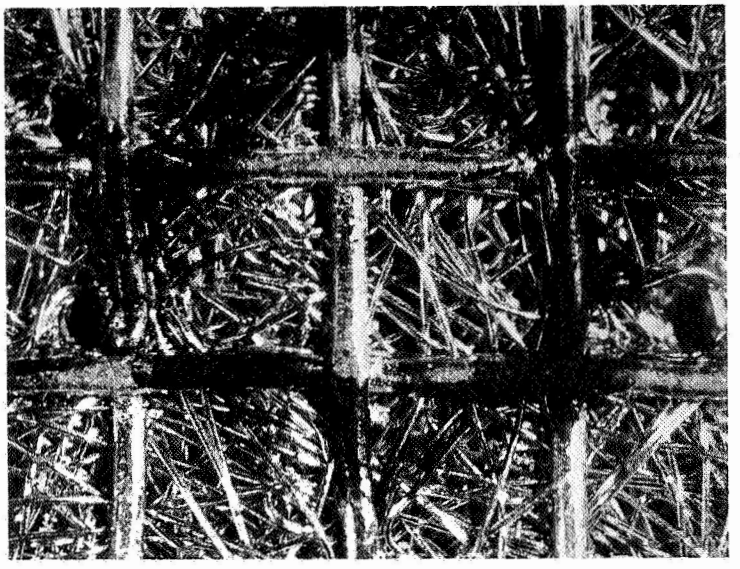

(a) Before erosion
Magnification factor - 21

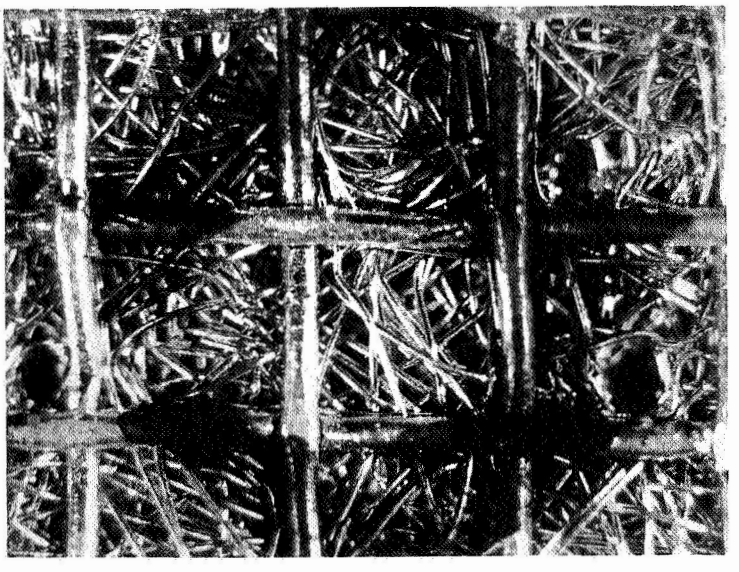

(b) After erosion
Magnification factor - 21

FIGURE B-3

EFFECT OF AIR EROSION
ON FM161 347SS - E18 FIBER

TASK C--FREEZE-THAW CYCLING

Introduction.- A porous metal liner will be exposed at least partially to weather effects. It is certain that some of the material will undergo cycles of water saturation followed by freezing. The objective of this series of tests was to determine whether repeated cycles of freezing and thawing would have any degrading effects on the mechanical and/or acoustical properties of the materials.

The candidate materials were chosen from Table I. The basis for selection was to sample the full range of material type, apparent density, and fiber diameter. On this basis FM151B, FM152B, FMS180, FMS183, FM125C, FM138, FM128A, and FM158 were subjected to testing.

Experimental apparatus and procedure.- Specimens of each material were subjected to ten cycles of water saturation, freezing, sub-cooling to -109°F (-78°C), and thawing, with measurements of flow resistance and dimensions being performed before and after each freeze-thaw cycle. After exposure, tensile strengths and percent elongations were measured in comparison with unexposed control specimens. Details of the experimental apparatus and procedure are given in Appendix C.

Discussion of results.- The effects of 10 freeze-thaw cycles are shown for all specimens in Tables C-I and C-II. The cycling did not affect the dimensions of the test specimens as shown in the before and after thickness values of Table C-I. Table C-I also shows that the freeze-thaw cycling did not significantly affect the flow resistance of the test specimens.

The effects of the cycling on the mechanical properties of the materials are shown in Table C-II. In each instance, the group averages represent the average values of two specimens. By inspection, it is apparent that the alternate freezing and thawing did not affect either the ultimate tensile strength or the percentage elongation at failure for any of the materials.

Conclusions.- Freeze-thaw cycling has no effect on fiber metal dimensions, flow resistance, ultimate tensile strength, or elongation to failure.

TABLE C-I

EFFECT OF FREEZE-THAW CYCLING ON FIBER METAL THICKNESS AND FLOW RESISTANCE

Fiber metal spec no	Fiber metal thickness				Flow resistance, rayls	
	before cycling,		after cycling,		before cycling	after cycling
	in.	cm	in.	cm		
FM151B	0.054	0.137	0.054	0.137	10.2	9.0
FM152B	0.064	0.162	0.064	0.162	46.6	45.0
FMS180	0.016	0.041	0.016	0.041	8.0	7.9
FMS183	0.015	0.038	0.015	0.038	66.8	72.8
FM125C	0.041	0.104	0.041	0.104	8.7	7.7
FM138	0.027	0.069	0.027	0.069	7.2	6.5
FM128A	0.027	0.069	0.027	0.069	45.3	43.5
FM158	0.050	0.127	0.050	0.127	61.2	56.0

TABLE C-II

EFFECT OF FREEZE-THAW CYCLING
ON ULTIMATE TENSILE STRENGTH
AND PERCENTAGE ELONGATION

Fiber metal spec no	Specimen type	Group av apparent density, percent	Group av ultimate tensile strength		Group av elongation, percent
			psi	MN/m^2	
FM151B	control	55.3	3 260	22.5	3.0
FM151B	test	55.3	3 010	20.8	2.9
FM152B	control	58.2	4 195	28.9	2.7
FM152B	test	57.3	4 290	29.6	2.9
FMS180	control	54.8	31 700	218.0	4.4
FMS180	test	53.0	32 250	222.0	4.2
FMS183	control	62.3	46 350	319.0	3.1
FMS183	test	60.3	45 750	316.0	3.8
FM125C	control	44.6	12 875	88.7	13.1
FM125C	test	43.9	12 340	85.1	12.9
FM138	control	35.6	9 725	67.1	14.6
FM138	test	35.9	9 940	68.5	16.5
FM128A	control	53.5	16 725	115.0	12.6
FM128A	test	53.0	16 150	111.0	16.5
FM158	control	53.5	12 030	82.7	15.2
FM158	test	55.2	12 650	87.2	16.9

TASK D--WATER SATURATION

Introduction.- A porous acoustical material exposed to weather is certain to become partially or totally saturated with water. Since retained water will alter the flow resistance of the material, the question must be answered as to the relative ease with which water can be forced from the material. It was the object of this test series to determine the air velocity that would result in complete dryout and total restoration of the flow resistance properties of fiber metal, along with the initial point at which water would begin to be forced from the material by exceeding the pressure drop required to overcome the surface tension of the water in the largest pores. The most severe test was imposed, wherein the saturated fiber metal rested in a horizontal position.

Since pore size, thickness, and wetting angle can play a role in the degree of retention of water, all of the fiber metal materials shown in Table I were tested.

Experimental apparatus and procedure.- Each material was fixtured in a holder and flow resistance-air velocity relationships were established for the dry samples over a velocity range of 0.008 to 11.1 ft per sec (0.244 -339 cm per sec).

The materials were then saturated with water and the testing repeated, noting, in addition, the initial differential pressures at which the water began to be forced from the materials. Detailed descriptions of the apparatus and procedure are presented in Appendix D.

Discussion of results.- Typical plots interrelating air velocity, flow resistance, and differential pressure, for both dry and wet fiber metal, are shown in Figures D-1 through D-5. These figures encompass the extremes of rayl number, fiber diameter, and metal type. They all indicate that the higher the velocity, the more nearly a water wet fiber metal approaches the performance of the dry material.

The air velocities and pressure drops required to achieve dryout of the water saturated fiber metal materials are shown in Table D-I, along with the initial break through pressures. Inspection of the data indicates that all but three of the dryout velocities fell into the range of 11.5 to 16.5 ft per sec (351 to 503 cm per sec). Results outside of this range were 18, 28, and 55 ft per sec (549, 854, and 1675 cm per sec). The test was severe in that the saturated fiber metal rested horizontally.

The particle velocity of a plane acoustic wave can be calculated from the following formula, Reference 2.

$$SPL_{eg} = 20 \log u + 106.4 \text{ dB re } 0.0002 \mu \text{ bar}$$

where

SPL_{eg} the equivalent sound pressure level in dB re 0.0002 micro bar

u the particle velocity in cm/sec

Sound pressure levels of 160-165 dB are ordinarily created in jet engines. These noise levels create wave front velocities of 16 to 30 ft per sec (488 -915 cm per sec), which are greater than all but one of the experimental results. It is therefore apparent that fiber metal acoustical materials which become water saturated, under the severest of circumstances, will dry out very rapidly with engine operation and regain their normal, dry, flow resistance characteristics.

The break through differential pressures ranged from 0.65 to 2.12 in. (1.65 to 5.35 cm) of water. Ten rayl fiber metal, at sound pressure levels of 160-165 dB, should produce differential pressures of about 4 in. (10.15 cm) of water, so no problem should be encountered in obtaining the initial pressure drop required to force water out of the largest pores.

Conclusions.- The following conclusions can be drawn from this test series:

1. The wave front velocities, created at the sound pressure levels of ordinary jet engine operation, are more than sufficient to rapidly dry out water saturated fiber metal.

2. The differential pressures, created at the sound pressure levels of ordinary jet engine operation, are more than sufficient to begin to force water from water saturated fiber metal materials.

TABLE D-I

BREAK THROUGH DIFFERENTIAL PRESSURES AND AIR VELOCITIES REQUIRED TO TOTALLY DRY OUT WATER SATURATED FIBER METAL ACOUSTICAL MATERIALS

Fiber metal spec no	Material type	Fiber type	Break through differential pressure,		Conditions for total displacement of water from pores			
					Air velocity,		Differential pressure,	
			in. H_2O	cm H_2O	ft/sec	cm/sec	in. H_2O	cm H_2O
FM151B	aluminum	E58	0.70	1.78	14.0	427	4.8	12.2
FM152B	aluminum	E58	0.64	1.62	11.5	350	32.0	81.3
FMS180	17-4PHSS	C18,C38	1.58	4.01	15.0	457	5.0	12.7
FMS181	17-4PHSS	C18,C38	1.35	3.43	15.5	472	16.0	40.6
FMS182	17-4PHSS	C18	2.12	5.38	15.5	472	30.0	76.2
FMS183	17-4PHSS	C18	1.83	4.65	12.0	366	20.0	50.8
FM125C	347 SS	C38	1.10	2.79	11.5	350	3.5	8.9
FM137	347 SS	C28	0.83	2.11	12.0	366	3.0	7.6
FM138	347 SS	C18	0.85	2.16	15.5	472	3.0	7.6
FM139	347 SS	E18	0.85	2.16	28.0	853	6.5	16.5
FM129B	347 SS	C38	0.87	2.21	11.5	350	15.0	38.1
FM150	347 SS	C28	0.94	2.39	11.5	350	6.5	16.5
FM140	347 SS	C18	1.55	3.94	16.5	503	10.0	25.4
FM141	347 SS	E18	1.02	2.59	14.5	442	11.0	27.9
FM123A	347 SS	C38	0.78	1.98	15.5	472	30.0	76.2
FM126B	347 SS	C28	0.95	2.41	15.5	472	17.0	43.2
FM128A	347 SS	C18	1.13	2.87	16.0	487	17.0	43.2
FM145	347 SS	E18	1.58	4.01	15.0	457	22.0	55.9
FM158	347 SS	C38	1.95	4.95	12.0	366	22.0	55.9
FM159	347 SS	C28	1.10	2.79	16.5	503	30.0	76.2
FM160	347 SS	C18	1.35	3.43	12.0	366	33.0	83.8
FM161	347 SS	E18	1.65	4.19	12.0	366	25.0	63.5
FM146	347 SS	C38	0.65	1.65	18.0	548	4.5	11.4
FM147	347 SS	C38	0.75	1.91	55.0	1675	20.0	50.8
FM149	347 SS	C38	1.08	2.74	13.0	396	20.0	50.8
FM162	347 SS	C38	1.36	3.45	12.0	366	27.0	68.6

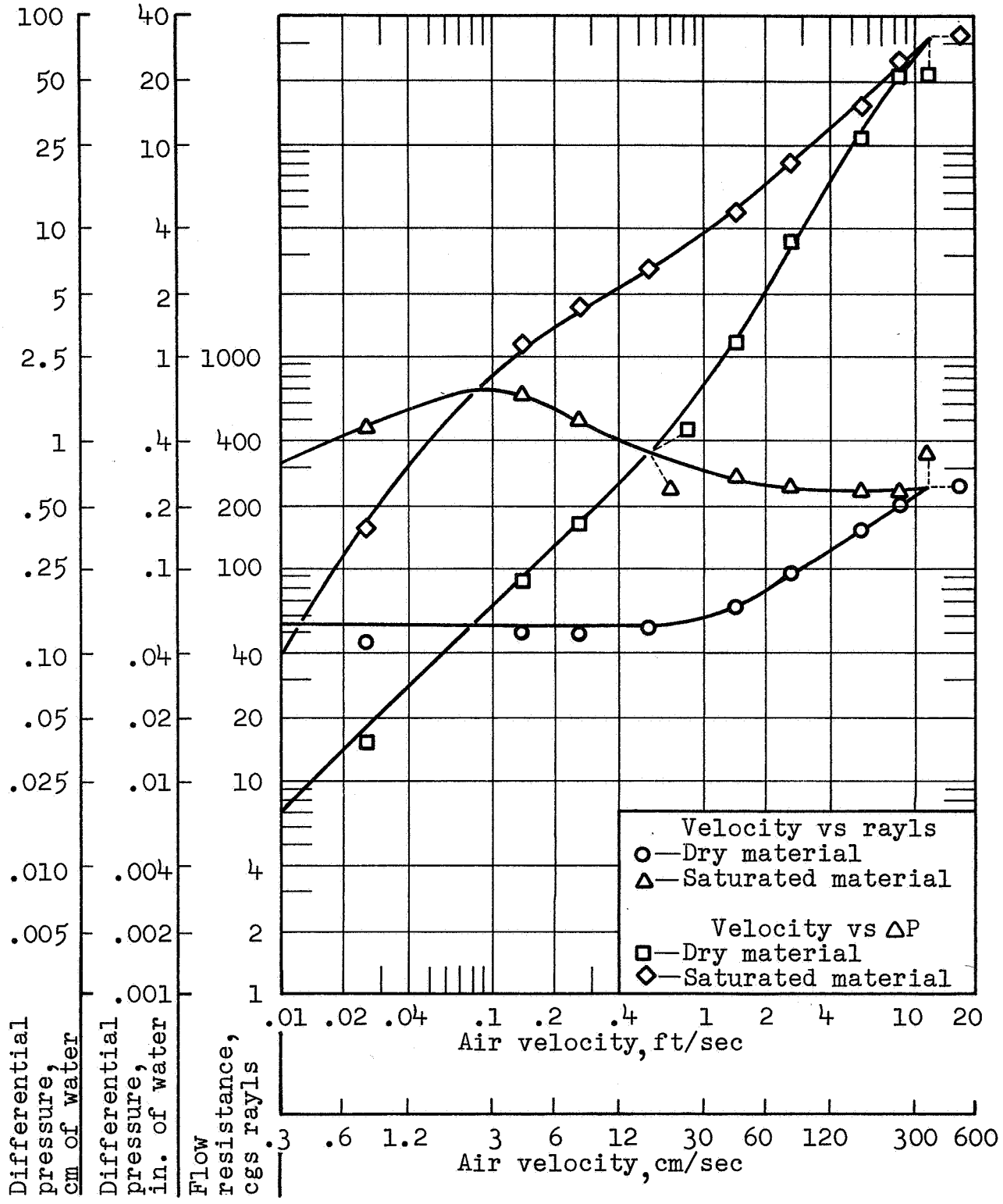

FIGURE D-1

EFFECT OF WATER SATURATION ON DIFFERENTIAL PRESSURE AND FLOW RESISTANCE, FM152B - ALUMINUM - E58 FIBER

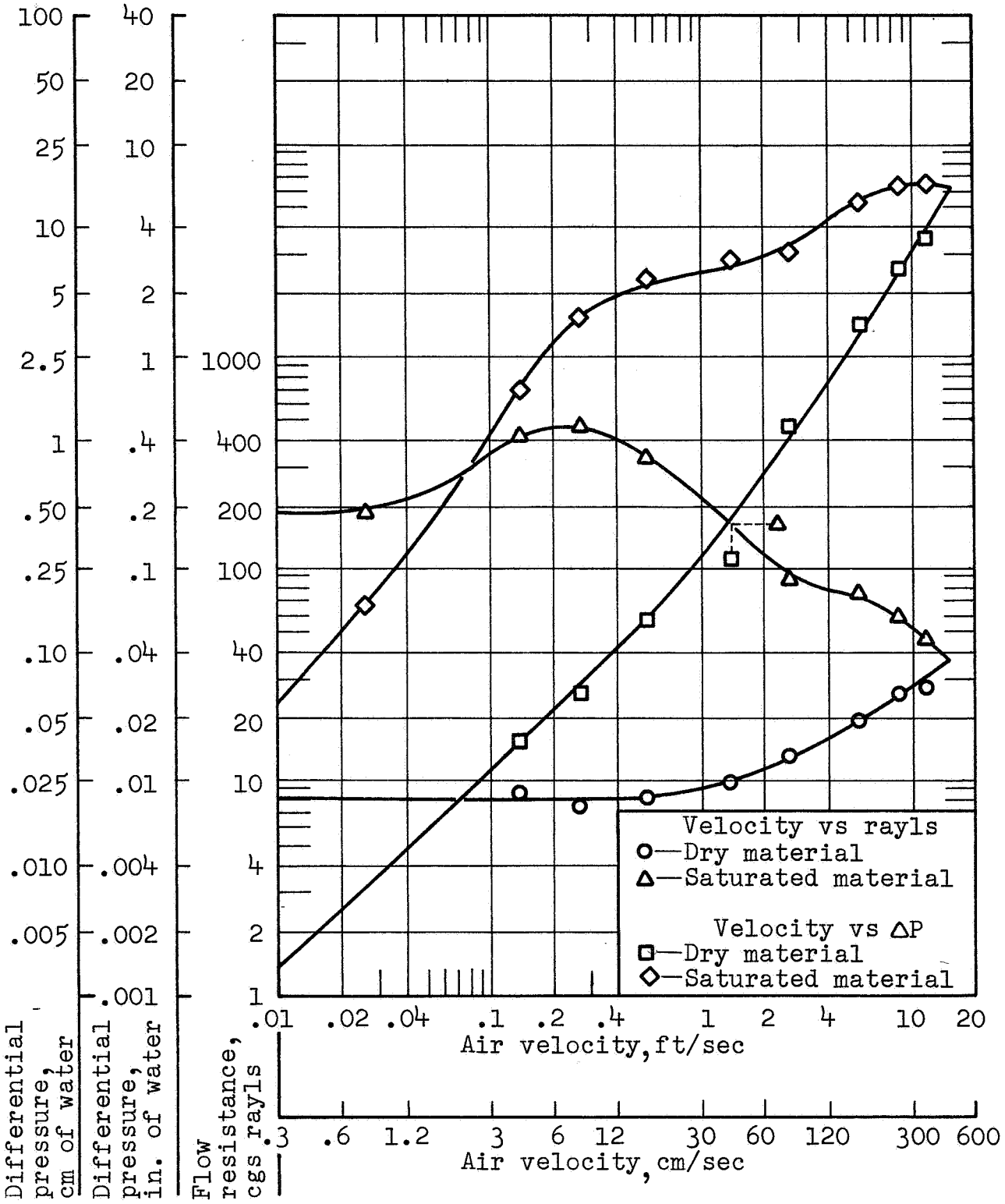

FIGURE D-2

EFFECT OF WATER SATURATION ON DIFFERENTIAL PRESSURE AND FLOW RESISTANCE, FMS180 - 17-4PHSS - C18 AND C38 FIBERS

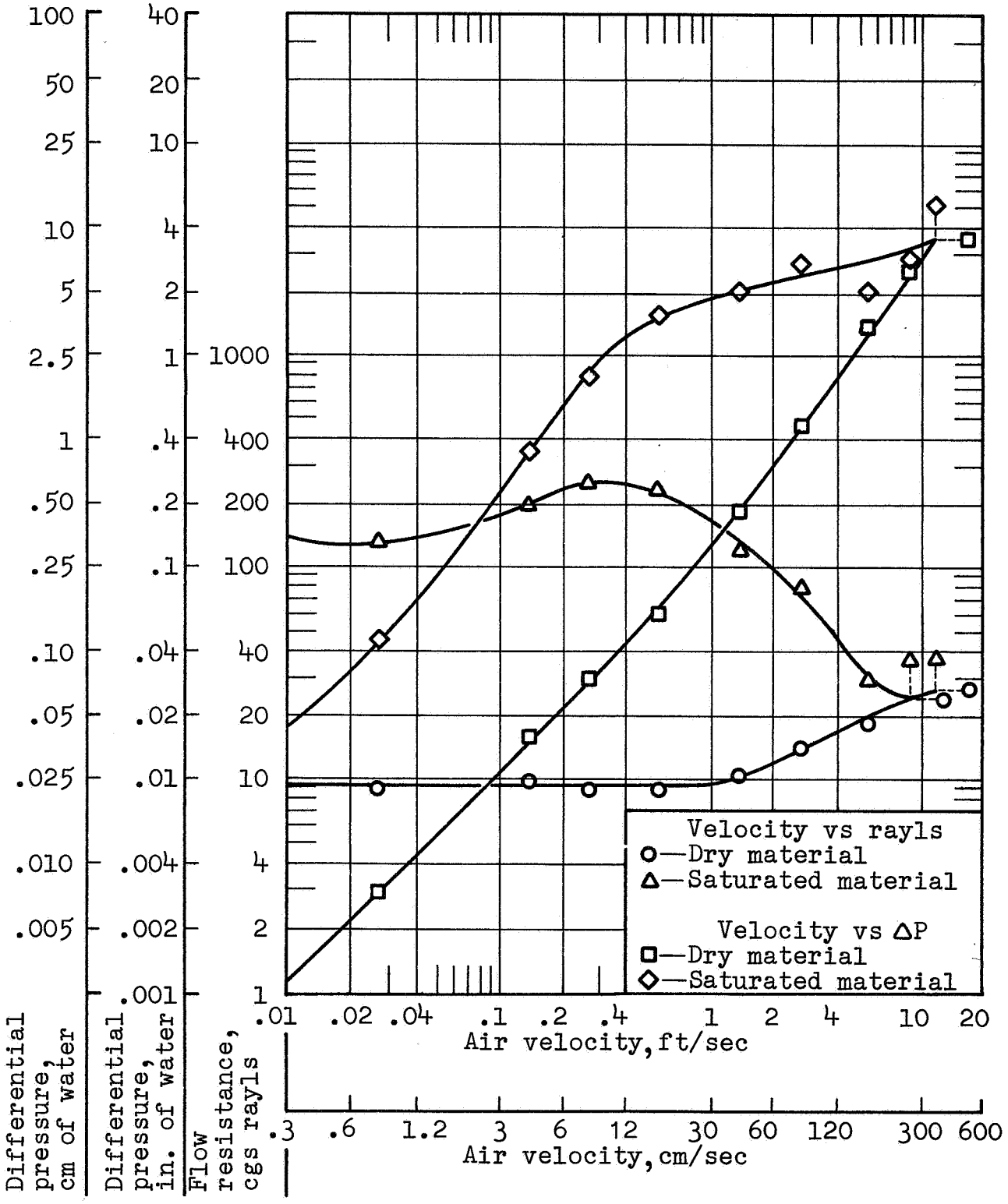

FIGURE D-3

EFFECT OF WATER SATURATION ON DIFFERENTIAL PRESSURE AND FLOW RESISTANCE, FM125C - 347 SS - C38 FIBER

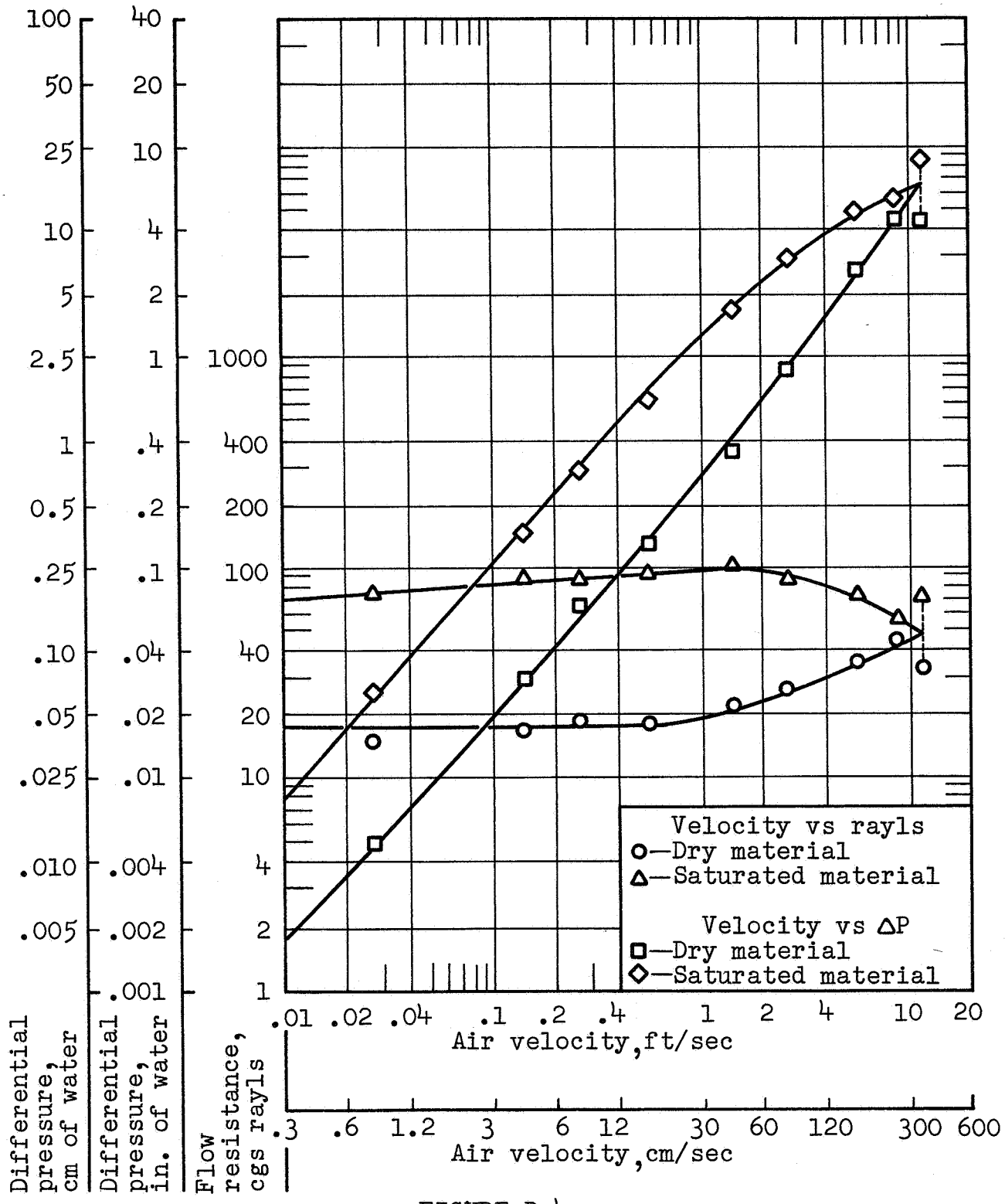

FIGURE D-4

EFFECT OF WATER SATURATION ON DIFFERENTIAL PRESSURE AND FLOW RESISTANCE, FM150 - 347 SS - C28 FIBER

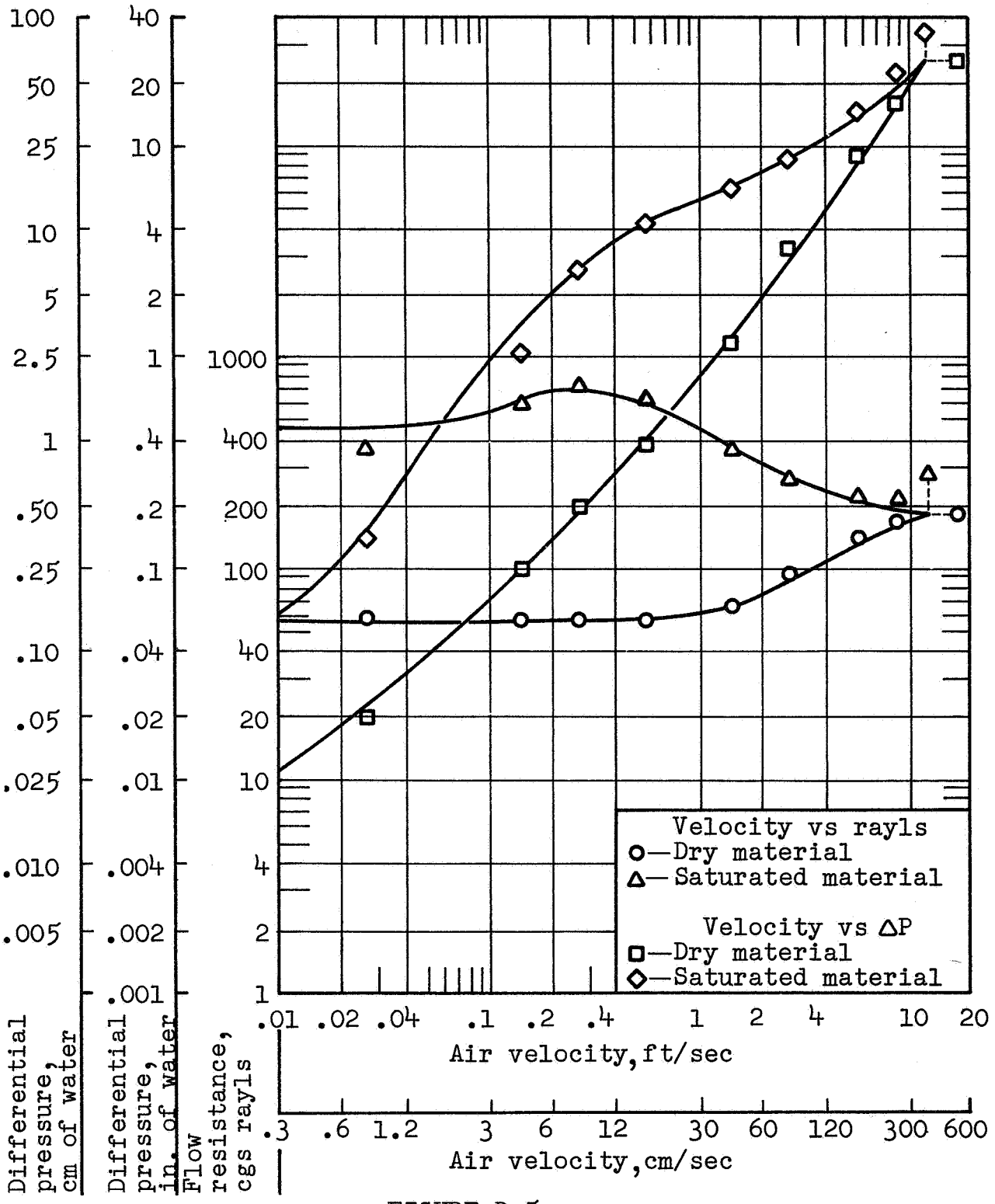

FIGURE D-5

EFFECT OF WATER SATURATION ON DIFFERENTIAL PRESSURE AND FLOW RESISTANCE, FM161 - 347 SS - E18 FIBER

TASK E--FUEL SATURATION AND COMBUSTION TESTS

Introduction.- Porous metals may be employed in the jet pipes of engines. Therefore, the materials may occasionally be the victim of a wet start when they become saturated with fuel and are then ignited. This test series was designed to appraise the effect of such exposure on mechanical and acoustical properties.

The candidate materials were selected from Table I. Selections were made to sample the full range of metal type, fiber type and apparent density. On this basis FM151B, FM152B, FMS180, FMS183, FM125C, FM138, FM128A and FM158 were selected for testing.

Experimental Apparatus And Procedure.- All of the test specimens were subjected to a total of six combustion cycles wherein the specimens were saturated with JP-4 fuel and combusted on a permeable grating. The weights, dimensions, and flow resistances of all specimens were measured before testing and again after each combustion cycle. At the conclusion of the environmental exposures, the tensile strengths and elongation to failure were measured for all test and control specimens. Details of the experimental apparatus and procedure are presented in Appendix E.

Discussion Of Results.- The results of the testing, as they influenced the flow resistance and weight of the test specimens, are shown in Table E-I. Inspection of this table shows that, except for a 17 percent increase for one specimen, flow resistance changes remained within plus or minus 8 percent of original values. These changes are considered to be of minor significance. The weight increases of the test specimens resulting from oxides, fuel or combustion residuals were insignificant.

The influence of the testing on mechanical properties is shown in Table E-II. The results show that the ultimate tensile strengths of the materials were totally unaffected by repeated fuel combustion. The elongation characteristics of the aluminum and 17-4 PH stainless steel materials appear unaltered. The 347 stainless steel specimens appear to have had slightly lower percentage elongations than the reference specimens. However, these changes are considered insignificant when compared to the normal variations in percentage elongation that result from testing duplicate samples.

Observations were made concerning the average periods of combustion for the respective materials. These are shown in Table E-III. Resulting correlation attempts involving mean pore size, thickness and combustion times yielded the correlation shown in Figure E-1. It is concluded that the quantity of fuel that a material can hold at saturation (total pore volume) and not mean pore size determines the period of combustion.

FM151B, FM125C and FM158 had an even, light soot coating after six cycles of fuel combustion. FM152B, FM138, FM128A, FMS180 and FMS183 had a spotted, light coating of soot.

Conclusions.- The following conclusions can be drawn concerning the effects of repeated fuel combustion.

1. Combustion of jet fuel wicked into fiber metal has no significant effect upon weight, dimensions, flow resistance, ultimate tensile strength or elongation to failure.

2. The time required for complete combustion of the fuel saturating the materials was short (between 27 and 64 seconds) and was dependent upon the pore volume but not upon pore size.

TABLE E-I

INFLUENCE OF SIX CYCLES OF FUEL COMBUSTION
ON FLOW RESISTANCE AND WEIGHT GAIN

Fiber metal spec no	Flow resistance			Weight		
	before, rayls	after, rayls	change, percent	before, gms	after, gms	change, percent
FM151B	5.4	5.9	8.1	21.644	21.632	-0.055
FM152B	52.0	47.9	-7.9	24.689	24.658	-0.125
FMS180	9.3	10.1	8.6	18.303	18.306	0.016
FMS183	67.5	66.8	-1.0	20.275	20.277	0.010
FM125C	9.7	10.4	7.4	44.569	44.572	0.007
FM138	7.1	7.4	4.2	24.554	24.555	0.004
FM128A	43.4	44.5	2.7	34.475	34.476	0.003
FM158	79.1	92.6	17.1	70.984	70.984	0

TABLE E-II

AFFECT OF SIX CYCLES OF FUEL COMBUSTION
ON ULTIMATE TENSILE STRENGTH AND
PERCENTAGE ELONGATION

Fiber metal spec no	Material type	Specimen class	Group av apparent density, percent	Group av UTS		Group av elongation, percent
				psi	MN/m^2	
FM151B	aluminum	reference	45.9	1 945	13.4	4.0
FM151B	aluminum	test	49.2	2 950	20.3	4.2
FM152B	aluminum	reference	64.8	5 220	36.0	7.0
FM152B	aluminum	test	58.8	4 900	33.8	6.1
FMS180	17-4PHSS	reference	53.2	29 700	205.0	5.1
FMS180	17-4PHSS	test	53.0	32 170	222.0	5.6
FMS183	17-4PHSS	reference	59.9	45 500	314.0	4.9
FMS183	17-4PHSS	test	60.9	47 025	324.0	4.1
FM125C	347 SS	reference	47.4	14 750	102.0	17.0
FM125C	347 SS	test	47.8	14 200	98.0	14.8
FM138	347 SS	reference	38.7	11 230	77.5	17.3
FM138	347 SS	test	39.1	11 340	78.3	16.4
FM128A	347 SS	reference	52.9	17 830	123.0	15.9
FM128A	347 SS	test	53.6	17 315	119.0	13.3
FM158	347 SS	reference	62.3	12 060	83.2	13.8
FM158	347 SS	test	59.6	11 850	81.7	13.3

TABLE E-III

OBSERVED COMBUSTION PERIODS
OF FIBER METAL MATERIALS

Fiber metal spec no	Fiber type	Apparent density, percent	Mean pore size, microns	Thickness		Average combustion time, sec
				in.	cm	
FM151B	E58	52.5	140	0.054	0.137	43
FM152B	E58	59.9	105	0.064	0.162	43
FMS180	C38,C18	55.0	83	0.015	0.038	29
FMS183	C18	63.2	60	0.014	0.035	27
FM125C	C38	48.3	170	0.040	0.101	38
FM138	C18	39.5	185	0.027	0.069	33
FM128A	C18	55.2	85	0.027	0.069	33
FM158	C38	54.1	102	0.050	0.127	64

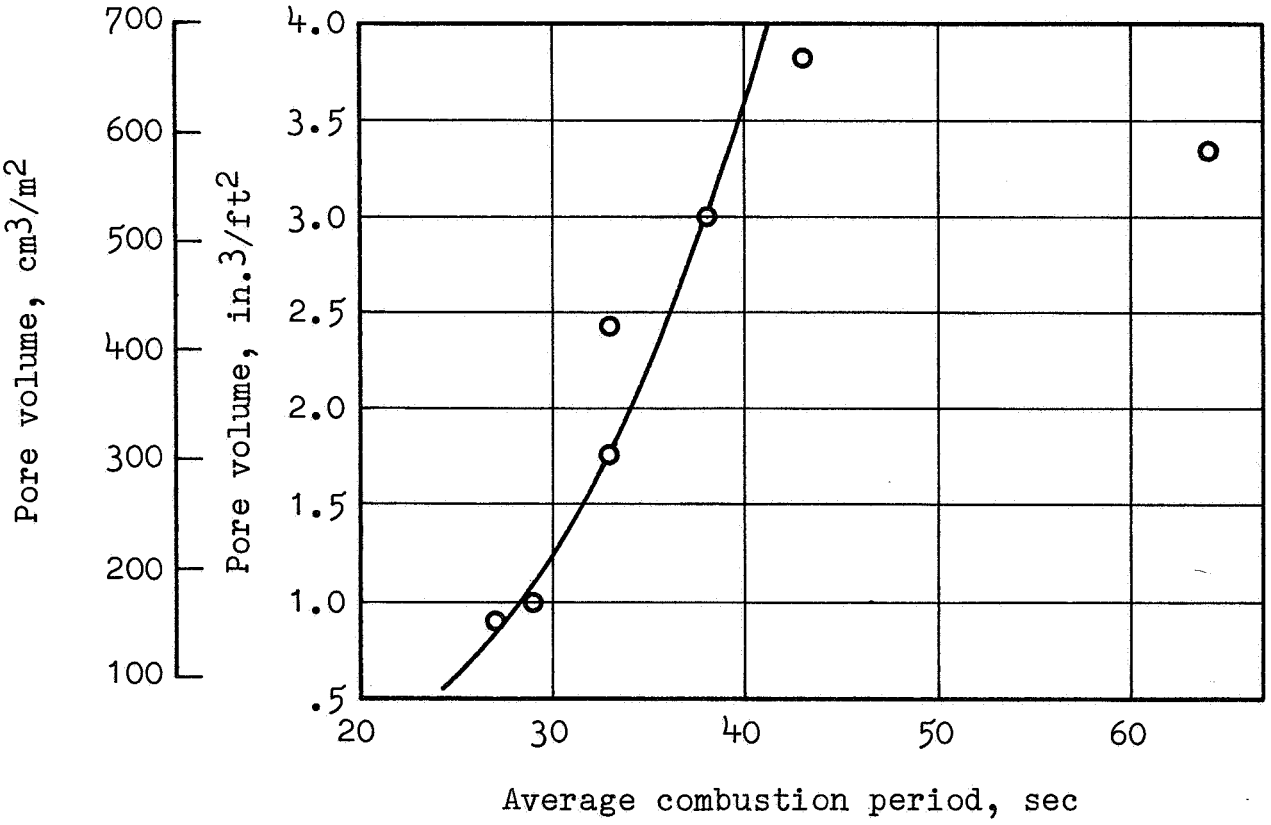

FIGURE E-1

RELATIONSHIP BETWEEN AVERAGE
COMBUSTION PERIOD AND PORE VOLUME

TASK F--AIR OXIDATION

Introduction.- The objective of this task was to obtain a measure of the elevated temperature oxidation resistance of the fiber metal materials, as a function of alloy type and fiber diameter. FM151B, FMS180, FM125C, FM137, FM138, and FM139 were selected from Table I for testing.

Apparatus and procedure.- Oxidation damage was assessed through weight, flow resistance, and mechanical property changes.

The stainless steel materials were exposed to temperatures of 800 to 1100°F (427-593°C) for periods up to 50 hours.

The aluminum materials were exposed to temperatures of 500 to 700°F (260 to 372°C), again for up to 50 hours. Exposure was in static air in an electrical laboratory furnace. A detailed description of apparatus and procedure is given in Appendix F.

Discussion of results.- The effects of air oxidation on ultimate tensile strength (UTS) are shown in Figures F-1 through F-6. The points as plotted represent the average of two tensile results for the indicated time at the indicated temperature. In a manner analogous to solid materials, minor variations within fiber metal materials can cause a varying UTS at a given apparent density. It was therefore necessary to compare the tensile strength results with the normal variations encountered in testing replicated samples of unoxidized fiber metal. Previous testing of fiber metal indicated that standard deviations of 13 percent existed in the measured ultimate tensile strengths for the 347SS, and aluminum materials. A 6 percent standard deviation could be expected for the 17-4 PH SS. Therefore, the one standard deviation lines in each of these figures represent limits within which 2 out of every 3 specimens should lie. The results indicate that for 347SS so significant loss in tensile strength was observed. For aluminum, no significant changes were noted up to 600°F (316°C) but a loss in strength of about 20 percent was noted at 700°F (372°C). The data indicate that the effect is temperature rather than time dependent and is probably the result of over-aging of the alloy. For 17-4 PH SS, no significant effect was observed up to 900°F (482°C). At 1000°F, (538°C) indications began to appear that some strength loss was developing. At 1100°F, (593°C) a strength loss of about 22 percent is evident. This loss appears to be more temperature than time dependent. These results agree with what might be expected for the solid metal. If solid 17-4 PH SS is initially age hardened at 900°F, (482°C) a loss in UTS of at least 20 percent can be expected when exposed to 1100°F, (593°C) without any decrease in its elongation characteristics as is confirmed below.

A summary of results for the total percentage elongations at failure are shown in Table F-I.

For 347 SS, 15-18 percent elongation values were generally observed. For 17-4 PH SS and aluminum, 3.5-5 percent were found. No significant change in this property was observed at any of the environments evaluated.

The effects of air oxidation on flow resistance are shown in Figures F-7 through F-12. In general, no dependency on temperature or time was observed. For 347 SS specimens, the air flow resistance change varied from a 10 percent decrease to a 30 percent increase, with a 10-20 percent increase the most common. The 17-4 PH SS samples normally experienced a -5 to 5 percent change. The aluminum samples normally experienced a 0-10 percent decrease in flow resistance. In summary, the changes in air flow resistance, within the limits evaluated, were random in character and minor in magnitude.

The effect of oxidation on sample weight is shown in Figures F-13 through F-18. The largest weight gain experienced was 0.32 percent. The results for 347 SS were as anticipated. The weight gain from oxide pickup was both temperature and time dependent, with temperature the more dominent variable. The weight increased most noticeably at 1100°F (593°C). As anticipated, the finer the fiber (C18 and E18 vs C38) the greater was the percentage weight increase. This is due to the greater specific surface area (cm^2/cm^3) for the finer fibers. The weight gain for the 17-4 PH SS also followed a time-temperature dependency. On the other hand, the aluminum specimens always lost weight.

The appearance of the stainless steel samples after oxidation is described in Table F-II. The aluminum materials remained silvery in appearance but with a reduced luster. The 347 SS materials ranged from golden to rust brown at low temperatures and short times to a dark to blackish brown at 1100°F (593°C) and 50 hours. The 17-4 PH SS specimens started at a medium shade of brown and qucikly reached a blackish brown.

Of all the physical properties evaluated, the resultant change in weight seems to be the most sensitive means of measuring the extent of oxidation. The weight gain for the stainless steels increases with increasing temperature, time, and fiber surface area. Inspection of Figures F-14 through F-18 shows that 1000°F (538°C) and approximately 900°F (482°C) are the maximum temperatures for the 347 SS and 17-4 PH SS respectively, at which the weight increases tend to level out with time. Higher temperatures give additional weight increases with time and will probably result in eventual deterioration of the fiber metal in service. In order to illustrate this point and to permit extrapolation of the data to much longer periods of time, the data represented by Figures F-14 through F-18 were evaluated to determine a suitable reaction rate equation and reaction rate constants. Details of this work are described in Appendix F. The resulting reaction rate constants are shown as a function of temperature in Figure F-19. Below 900°F (482°C) the constants are comparable for the

347 SS and 17-4 PH SS. Above 900°F (482°C) the 17-4 PH SS exhibits an increasingly greater reaction rate than the 347 SS. The following equation represents the weight gain of fiber metal resulting from air oxidation.

$$W^3 = 3Kt$$

where

W Is the cumulative weight gain of oxides per unit area of fiber surface, gm per cm^2

K Is the reaction rate constant, gm per cm^2 per hr

t Is the time in hours

If W is multiplied by the specific surface of the fiber metal material, expressed in cm^2 per gm, and then by 100, the percentage increase in weight of the fiber metal is obtained. Calculated and experimentally observed values for typical materials (FMS180 and FM137) are shown in Figures F-20 and F-21.

In addition, some weight gains for 5000 hours of air oxidation for FMS180 (17-4 PH SS) and FM137 (347 SS) were calculated and are shown below, along with experimentally observed values at 1100°F (593°C) and 50 hours. A temperature of 1000°F (538°C) was assumed for the 347 SS and 900°F (482°C) for the 17-4 PH SS.

	FMS180 17-4 PHSS	FM137 347SS
Calculated wt gain, % at 5000 hrs	0.30	0.54
Temperature, °F (°C)	900 (482)	1000 (538)
Observed wt gain, % at 50 hrs	0.20	0.32
Temperature, °F (°C)	1100 (593)	1100 (593)

As has been discussed previously, the observed oxidation weight gains produced no significant effect on flow resistance and provided that the temperature was maintained below 1000°F (538°C) for the 17-4 PH SS, no loss in tensile strength was observed. It is not anticipated that the relatively modest increases in these oxidation weight gains, caused by these long term exposures, will significantly alter these conclusions. It is therefore concluded that 5000 hours of operation at 1000°F (538°C) and 900°F (482°C) for 347 SS and 17-4 PH SS fiber metal respectively will not produce harmful results.

Conclusions.- The following conclusions can be drawn concerning the effects of air oxidation:

As with solid aluminum, aluminum fiber metal is extremely resistant to air oxidation. The only harmful effect produced by air oxidation, was a 20 percent reduction of ultimate tensile strength (UTS) after exposure to 700°F (372°C). This was probably the result of over-aging of the particular aluminum alloy used. Otherwise, air oxidation did not cause any significant changes in appearance, flow resistance, or total elongation at failure. Assuming that the 300-400°F (149-205°C) limitation on fatigue strength of aluminum does not impose a serious design problem, aluminum fiber metal can be used at temperatures up to 600°F, (316°C) in air, without harmful effect.

The remaining conclusions deal with the air oxidation of the 17-4 PH and 347 stainless steel alloys. They resulted from exposure times of up to 50 hours at temperatures to 1100°F (593°C).

1. Of all the parameters observed, weight change was the most sensitive variable for evaluating air oxidation. There were small weight increases for all specimens tested resulting from oxide formation. The largest weight increase observed was 0.32 wt percent. The percent weight gain increased with increasing surface area, time, and temperature and was generally somewhat greater for 17-4 PH SS than for 347 SS.

2. Quantitative relationships were developed which express oxidation weight increases as a function of surface area, time, and temperature for each alloy. These relationships were used for estimating weight gains for long term (5000 hours) air oxidation and indicate that no harmful effects should be produced at 1000°F (538°C) for 347 SS and 900°F (482°C) for 17-4 PH SS.

3. Random changes, both increases and decreases, in flow resistance were observed. These changes could not be related to the weight gain of oxides on the fiber metal. Since even the largest percentage weight gains had no significant effect on flow resistance, it is concluded that flow resistance was not significantly affected by the relatively mild oxidation conditions employed in this study.

4. 347 SS fiber metal has satisfactory resistance to air oxidation at temperatures up to 1000°F (538°C), and is not recommended for use above this temperature. Although no significant loss in ultimate tensile strength was observed after 50 hours exposure at 1100°F (593°C), estimates of long term oxidation weight gains indicate the possibility of enough oxidation to cause some significant loss of strength.

5. 17-4 PH SS fiber metal has satisfactory air oxidation resistance up to 900°F (482°C). It is not recommended for operation at temperatures above this because of losses in strength resulting from over-aging of the alloy and estimated excessive long term oxidation.

6. There was no significant loss in ductility evidenced by total elongation to failure of tensile specimens.

7. There was a general tendency for increasing discoloration with increasing time and temperature. More discoloration was observed with the 17-4 PH·SS.

TABLE F-I

EFFECT OF AIR OXIDATION ON
PERCENTAGE ELONGATION

Fiber metal spec no	Material type	Fiber type	Observed elongation range	
			before oxidation, percent	after oxidation, percent
FM151B	aluminum	E58	4.0- 4.4	3.4- 5.1
FMS180	17-4PHSS	C18,C38	4.0- 4.3	3.5- 5.2
FM125C	347 SS	C38	13.0-14.8	12.7-16.0
FM137	347 SS	C28	13.0-17.2	12.7-18.7
FM138	347 SS	C18	16.7-17.4	13.2-19.5
FM139	347 SS	E18	19.3-21.5	16.9-20.5

TABLE F-II

APPEARANCE OF STAINLESS STEEL FIBER METAL MATERIALS RESULTING FROM AIR OXIDATION

Fiber metal spec no	SS alloy	Fiber type	Oxidation period, hours	Oxidation[a] temperature, °F (°C)			
				800 (427)	900 (482)	1000 (533)	1100 (593)
FM125C	347	C38	2	1	4	4	4
FM125C	347	C38	4	1	4	4	4
FM125C	347	C38	10	3	4	4	4
FM125C	347	C38	20	3	4	4	4
FM125C	347	C38	50	3	4	4	5
FM137	347	C28	2	1	4	4	4
FM137	347	C28	4	1	4	4	4
FM137	347	C28	10	1	4	4	5
FM137	347	C28	20	3	4	4	5
FM137	347	C28	50	3	4	4	5
FM138	347	C18	2	1	3	3	3
FM138	347	C18	4	1	3	3	3
FM138	347	C18	10	1	3	3	5
FM138	347	C18	20	3	3	3	5
FM138	347	C18	50	3	3	3	5
FM139	347	E18	2	2	3	3	4
FM139	347	E18	4	2	3	3	4
FM139	347	E18	10	2	3	4	4
FM139	347	E18	20	2	3	4	4
FM139	347	E18	50	3	3	4	5
FMS180	17-4 PH	C38,C18	2	3	3	5	5
FMS180	17-4 PH	C38,C18	4	3	3	5	5
FMS180	17-4 PH	C38,C18	10	3	3	5	5
FMS180	17-4 PH	C38,C18	20	3	3	5	5
FMS180	17-4 PH	C38,C18	50	3	5	5	5

[a]Appearance code as follows:

1 - Rust brown
2 - Golden brown
3 - Medium brown
4 - Dark brown
5 - Blackish brown

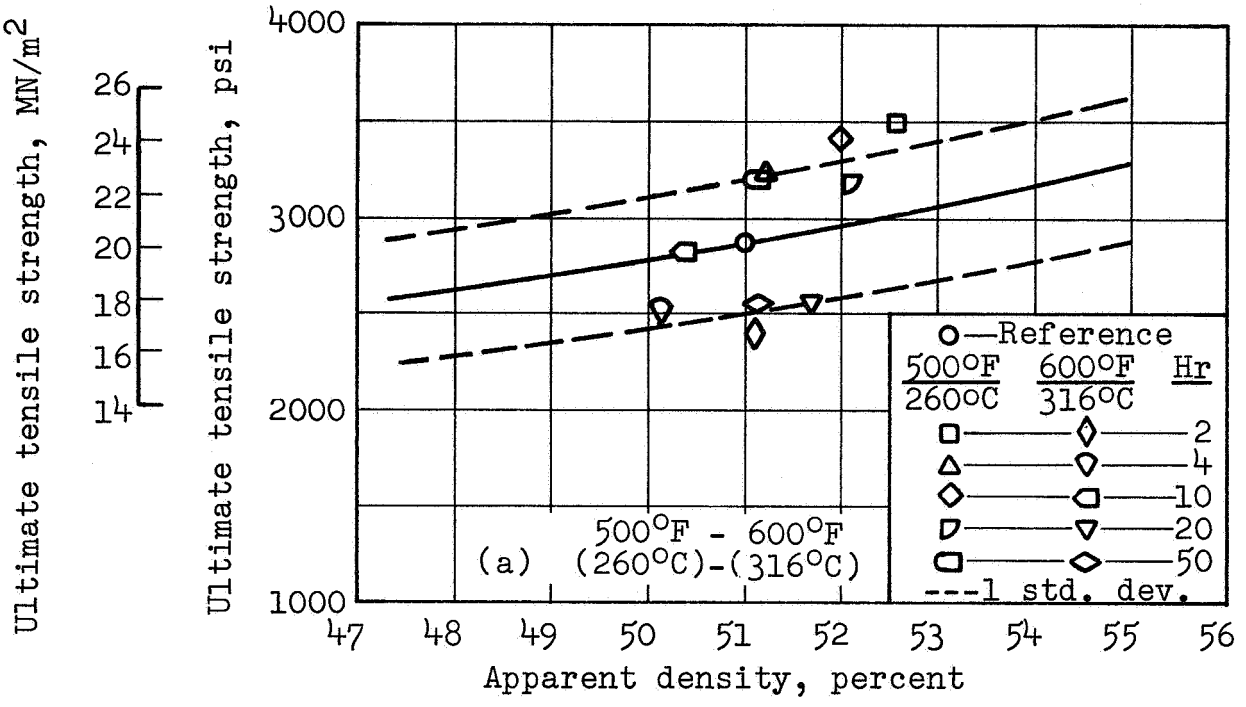

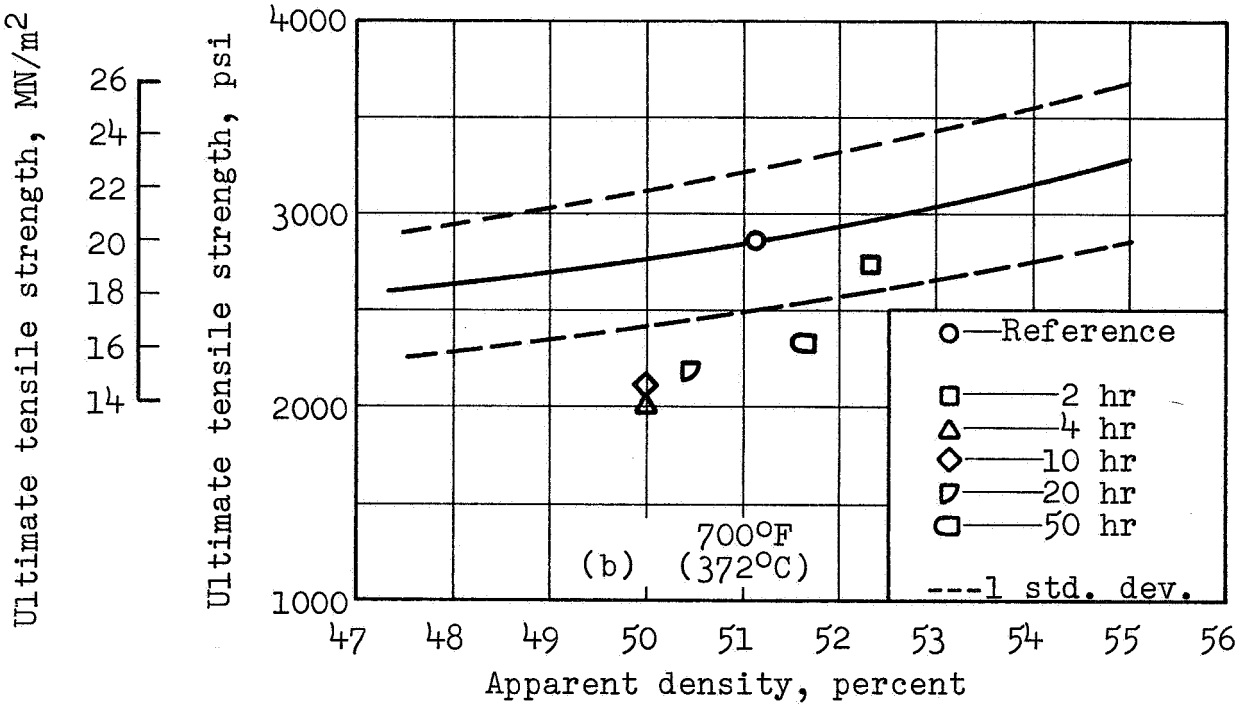

FIGURE F-1

EFFECT OF AIR OXIDATION ON ULTIMATE TENSILE STRENGTH, FM151B - ALUMINUM - E58 FIBER

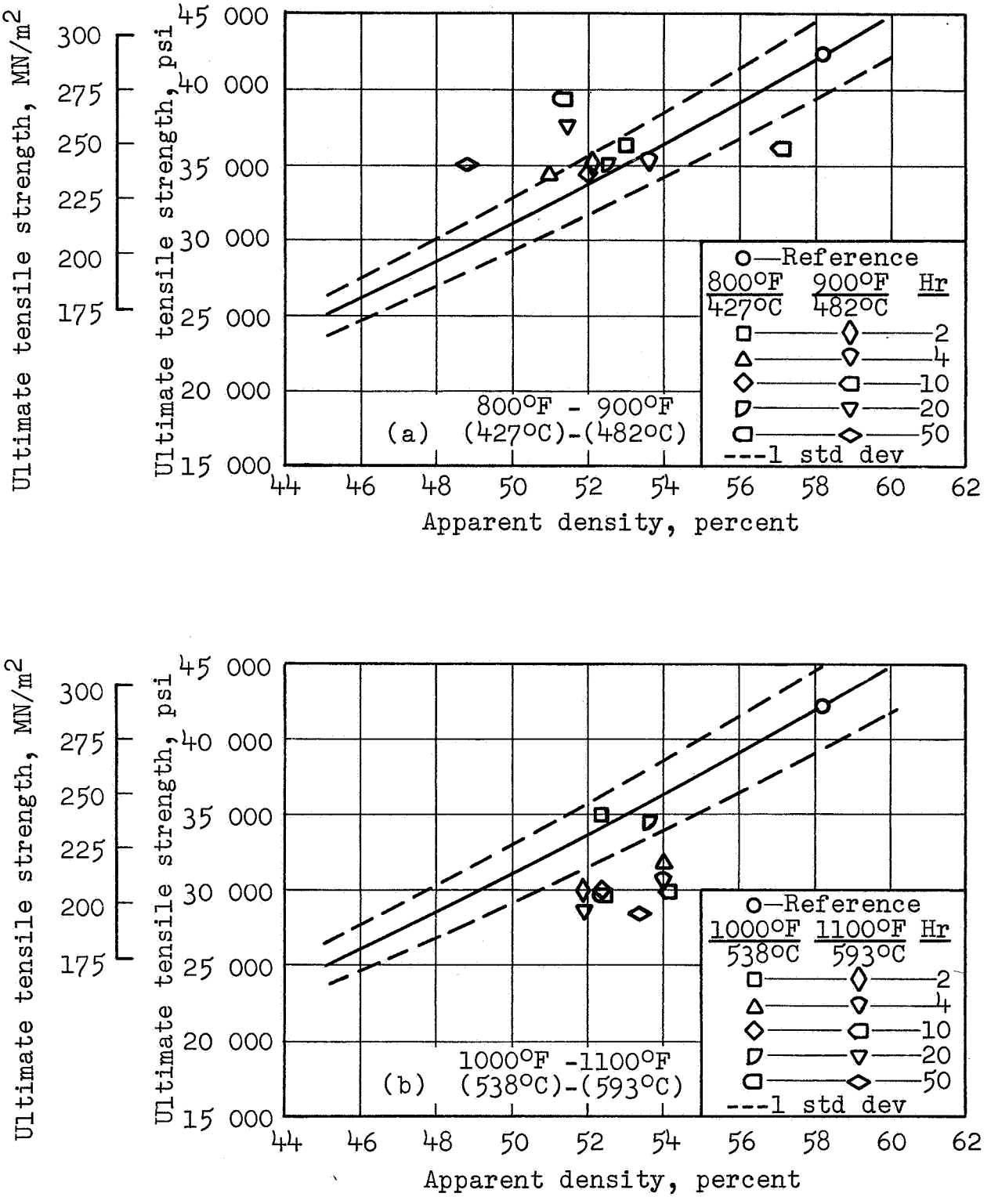

FIGURE F-2

EFFECT OF AIR OXIDATION ON ULTIMATE TENSILE STRENGTH, FMS180 - 17-4PHSS - C38-C18 FIBER

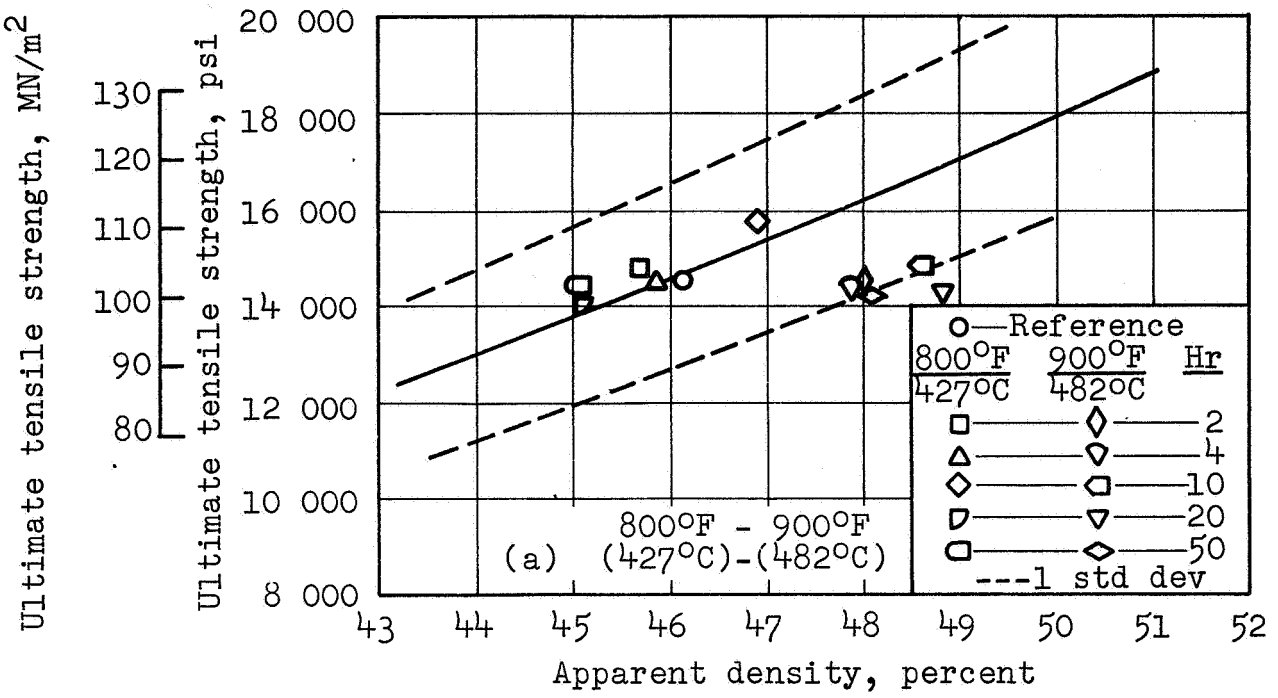

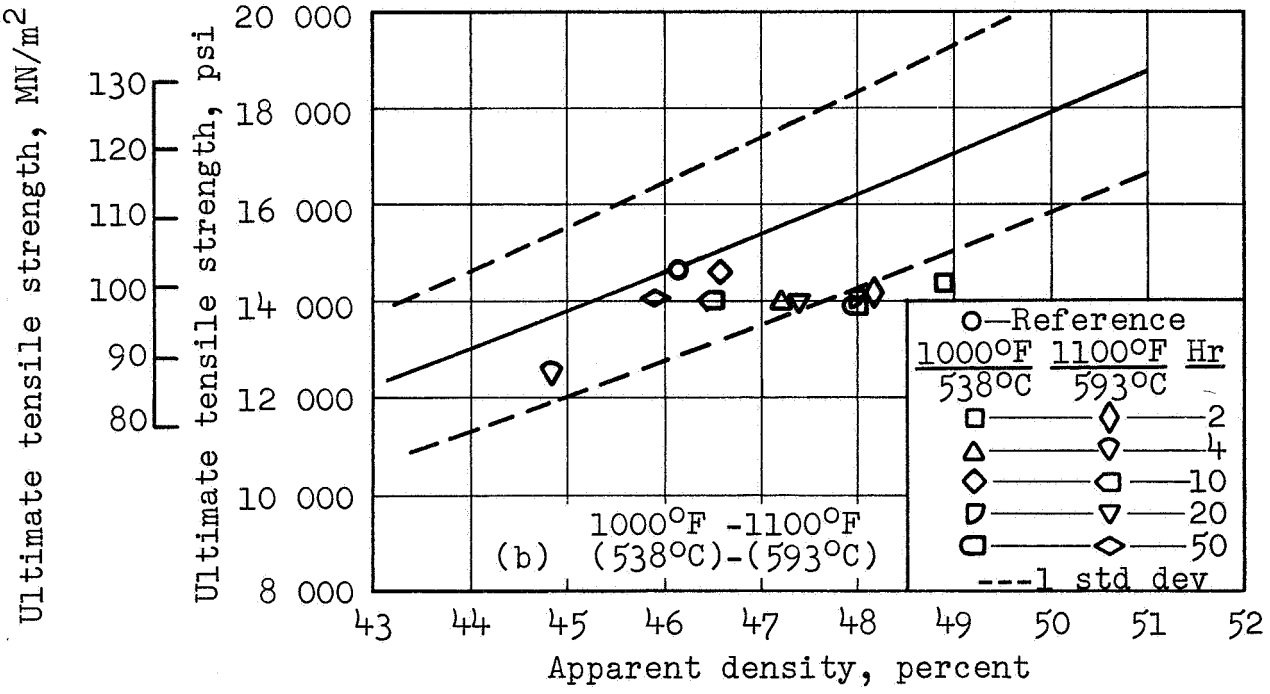

FIGURE F-3

EFFECT OF AIR OXIDATION ON ULTIMATE TENSILE STRENGTH, FM125C - 347SS - C38 FIBER

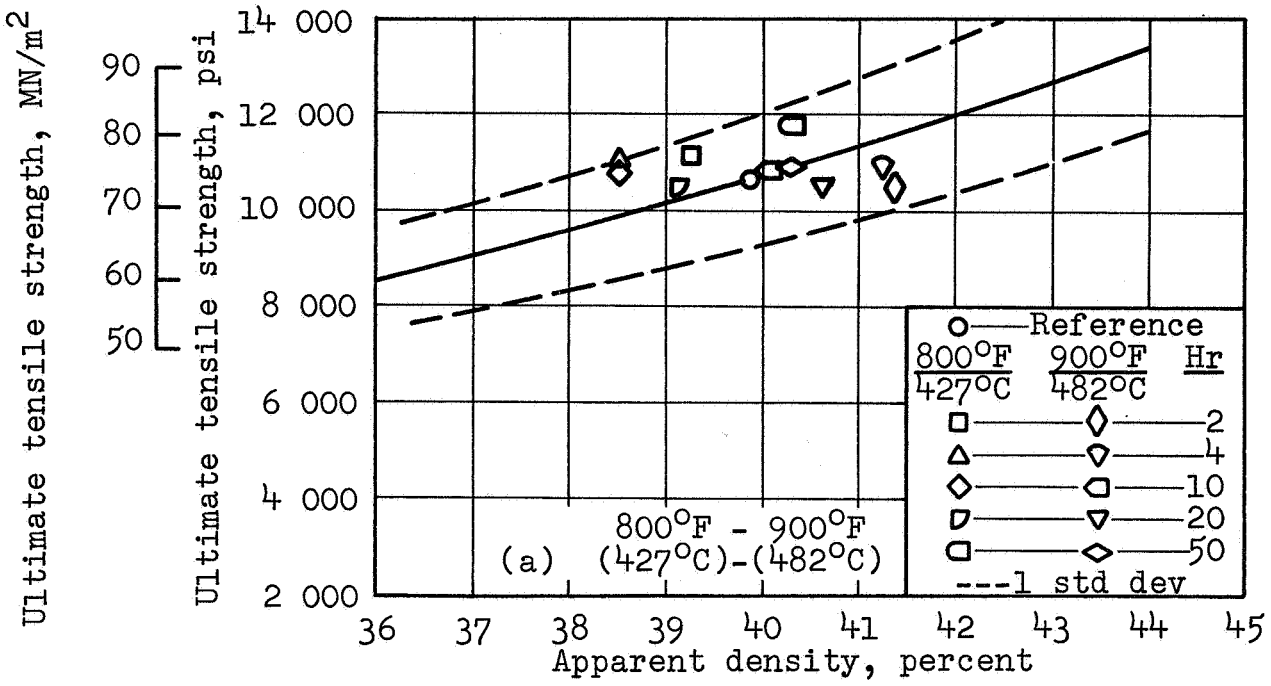

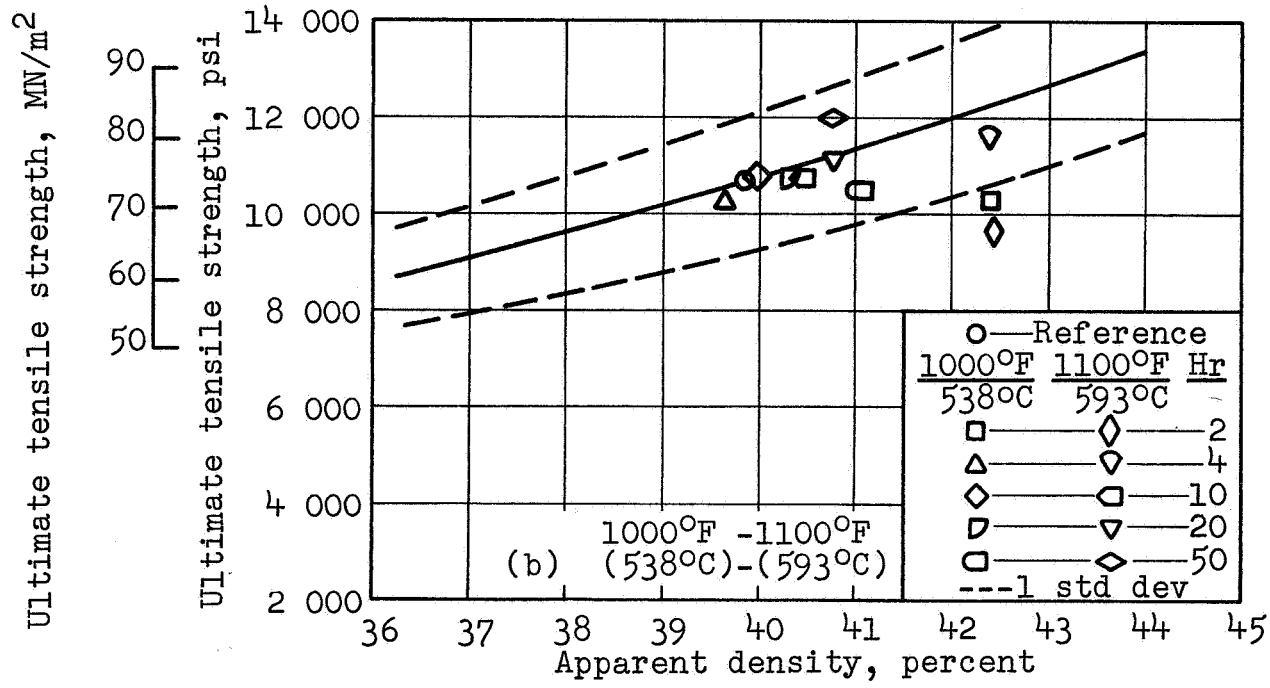

FIGURE F-4

EFFECT OF AIR OXIDATION ON ULTIMATE TENSILE STRENGTH, FM137 - 347SS - C28 FIBER

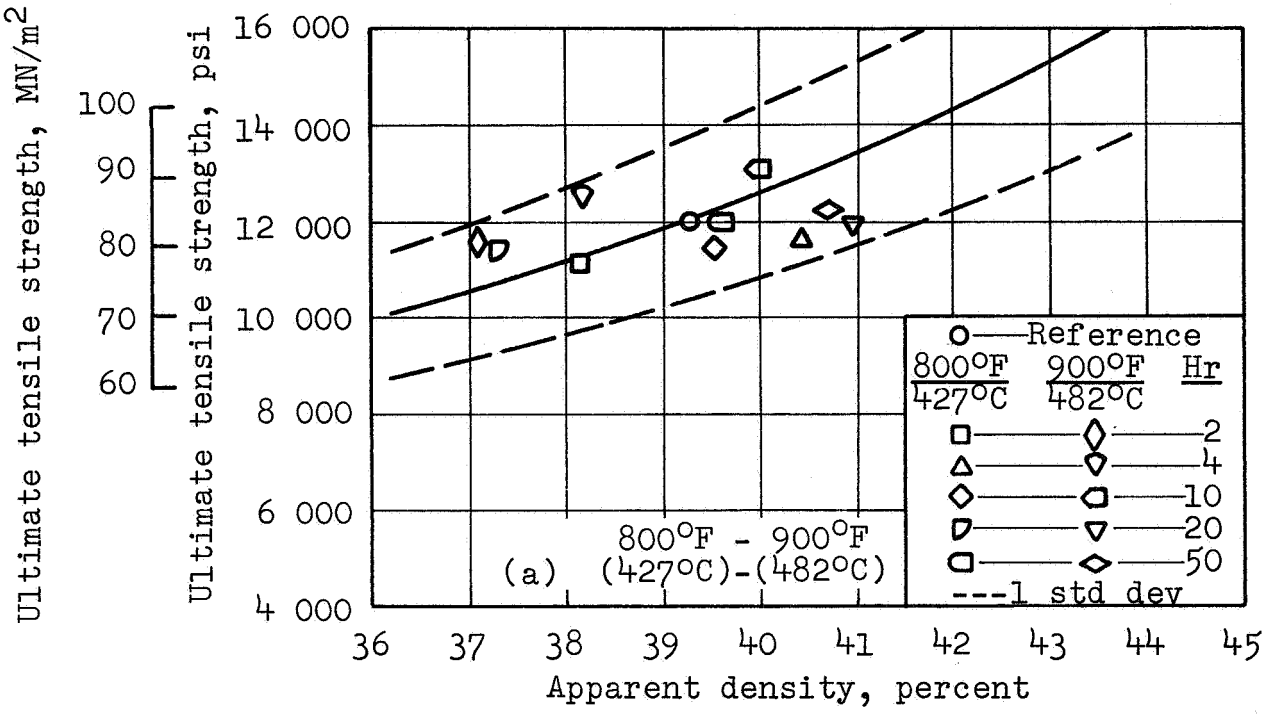

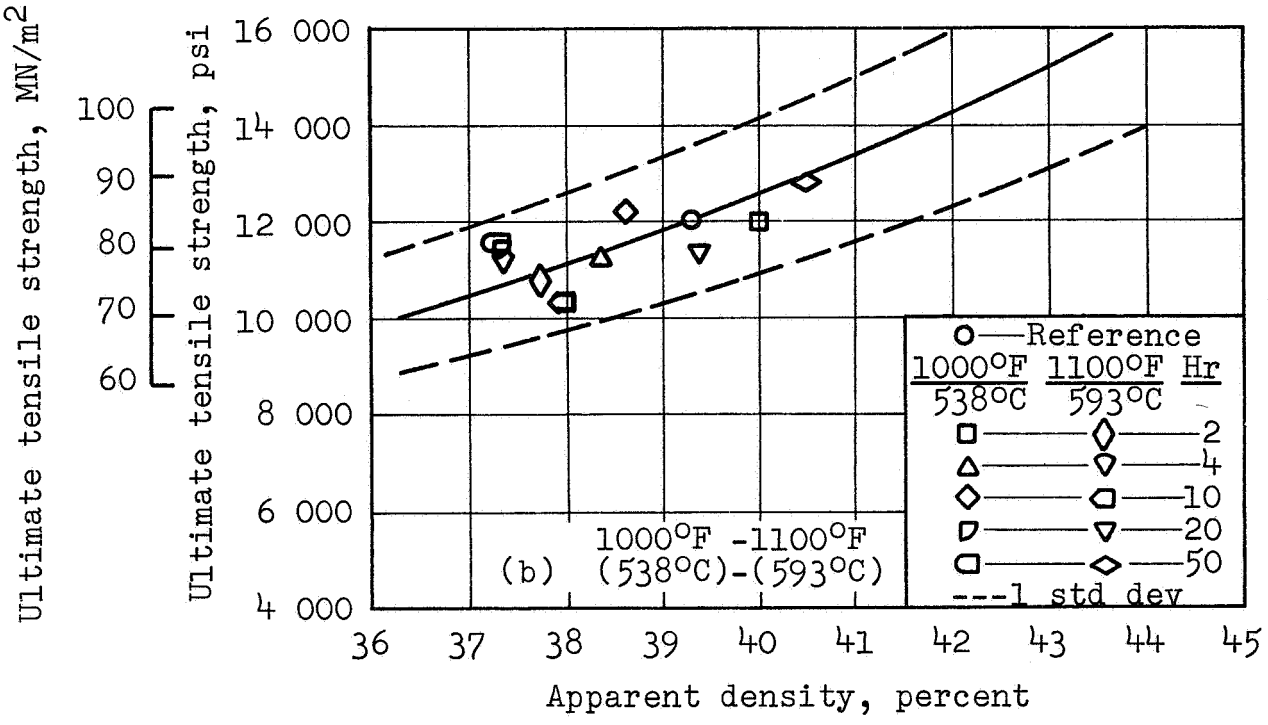

FIGURE F-5

EFFECT OF AIR OXIDATION ON ULTIMATE TENSILE STRENGTH, FM138 - 347SS - C18 FIBER

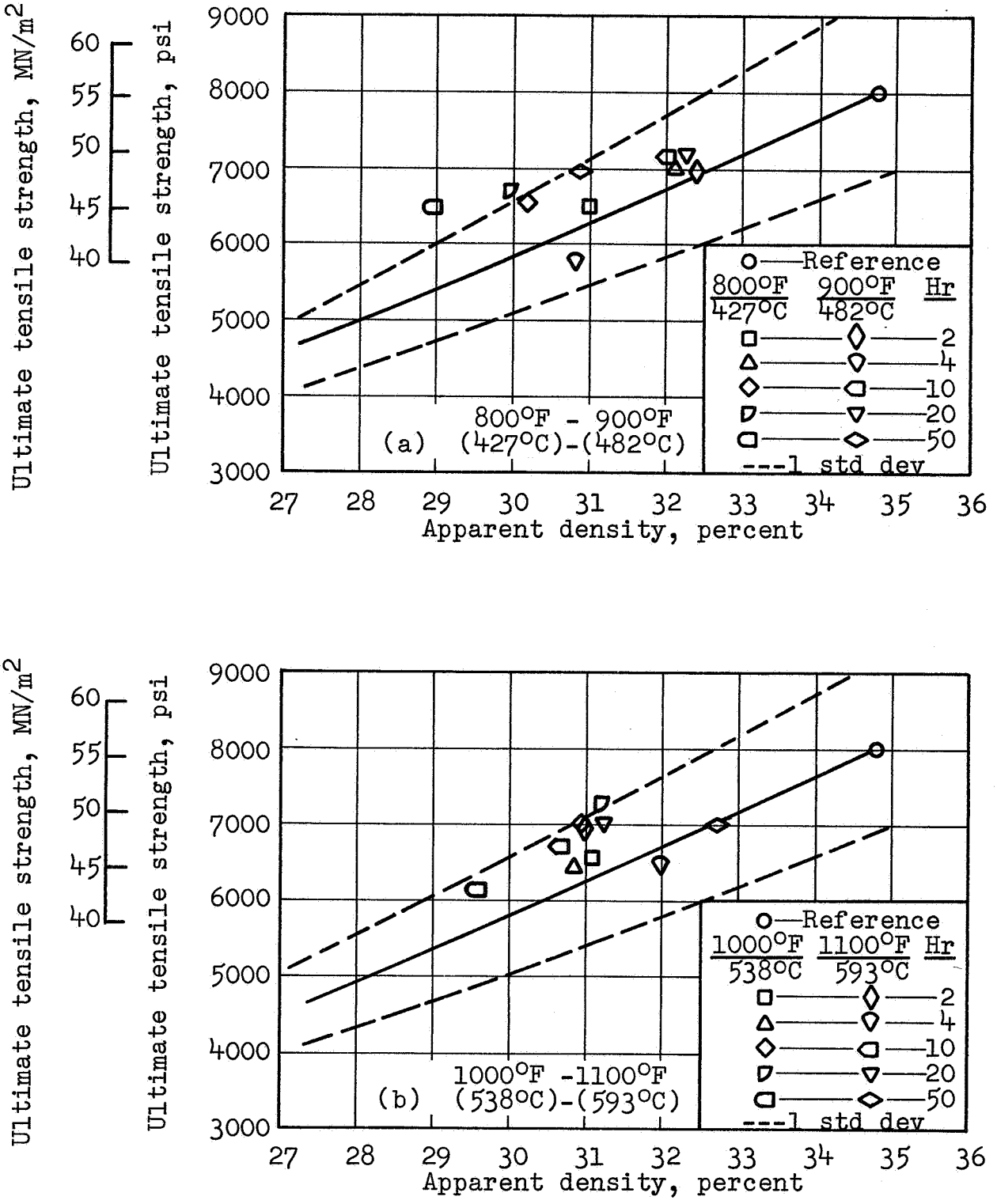

FIGURE F-6

EFFECT OF AIR OXIDATION ON ULTIMATE TENSILE STRENGTH, FM139 - 347SS - E18 FIBER

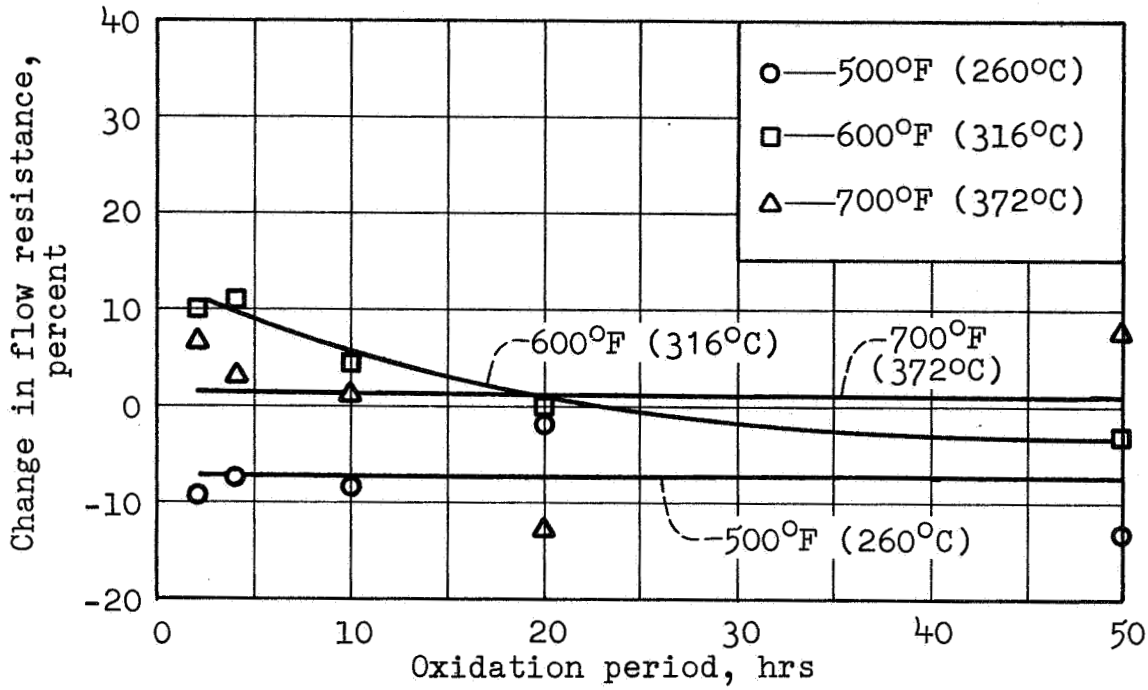

FIGURE F-7.- EFFECT OF AIR OXIDATION ON AIR FLOW RESISTANCE, FM151B - ALUMINUM - E58 FIBER

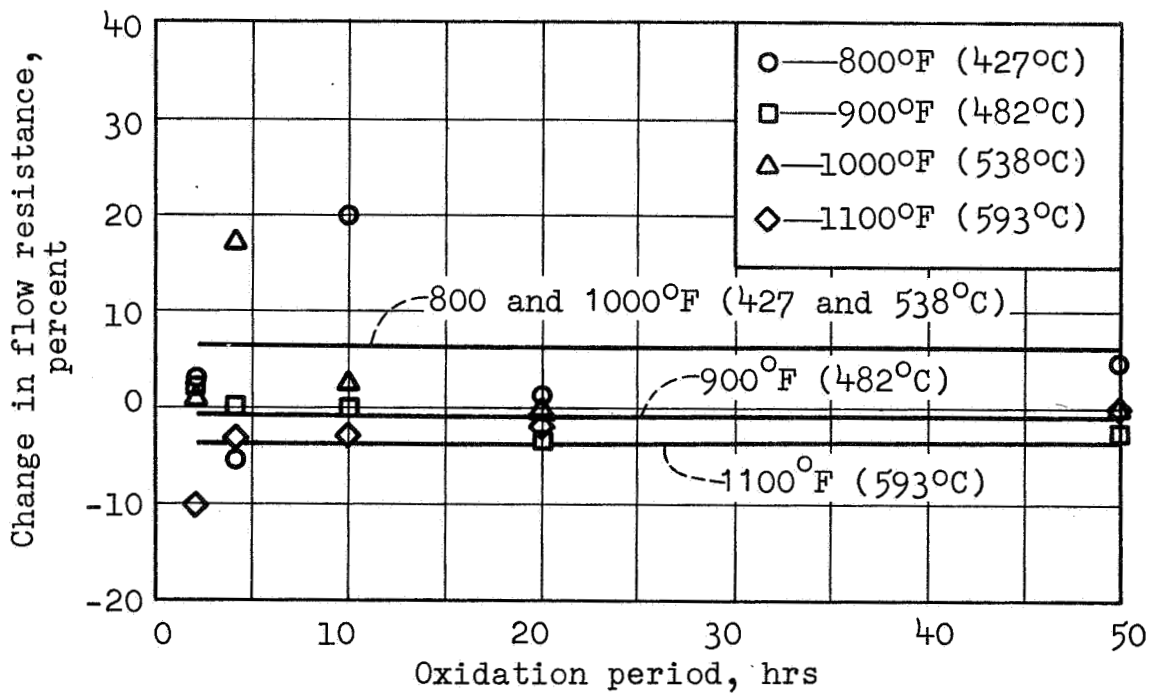

FIGURE F-8.- EFFECT OF AIR OXIDATION ON AIR FLOW RESISTANCE, FMS180 - 17-4PHSS - C18 - C38

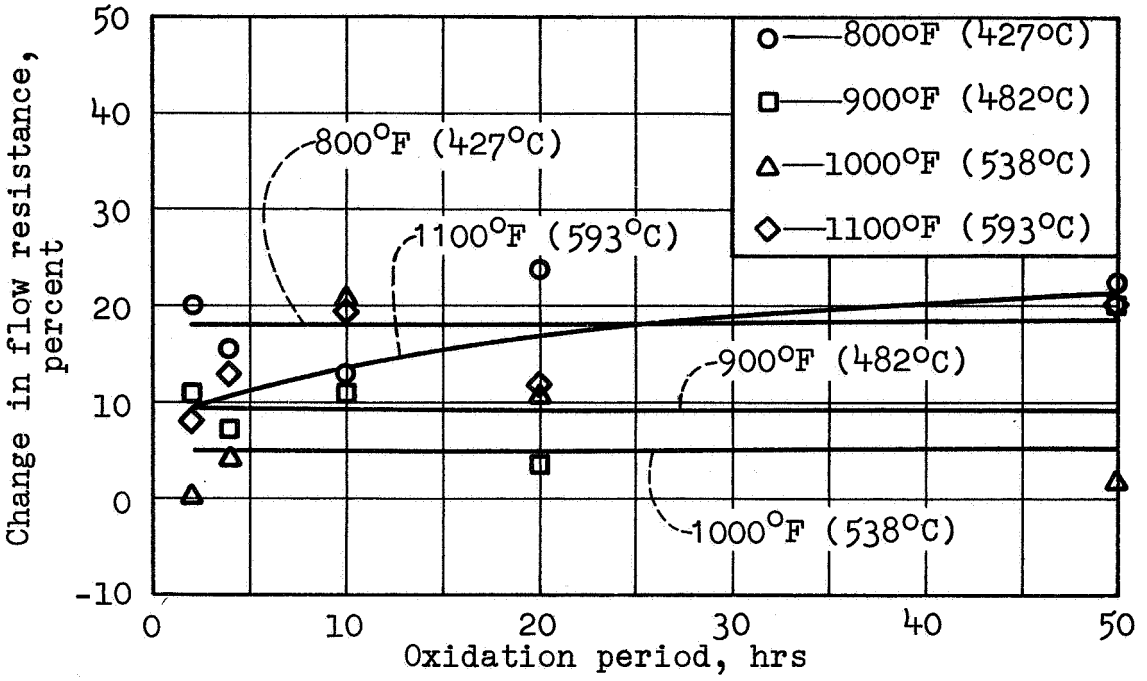

FIGURE F-9.- EFFECT OF AIR OXIDATION ON AIR FLOW RESISTANCE, FM125C - 347SS - C38 FIBER

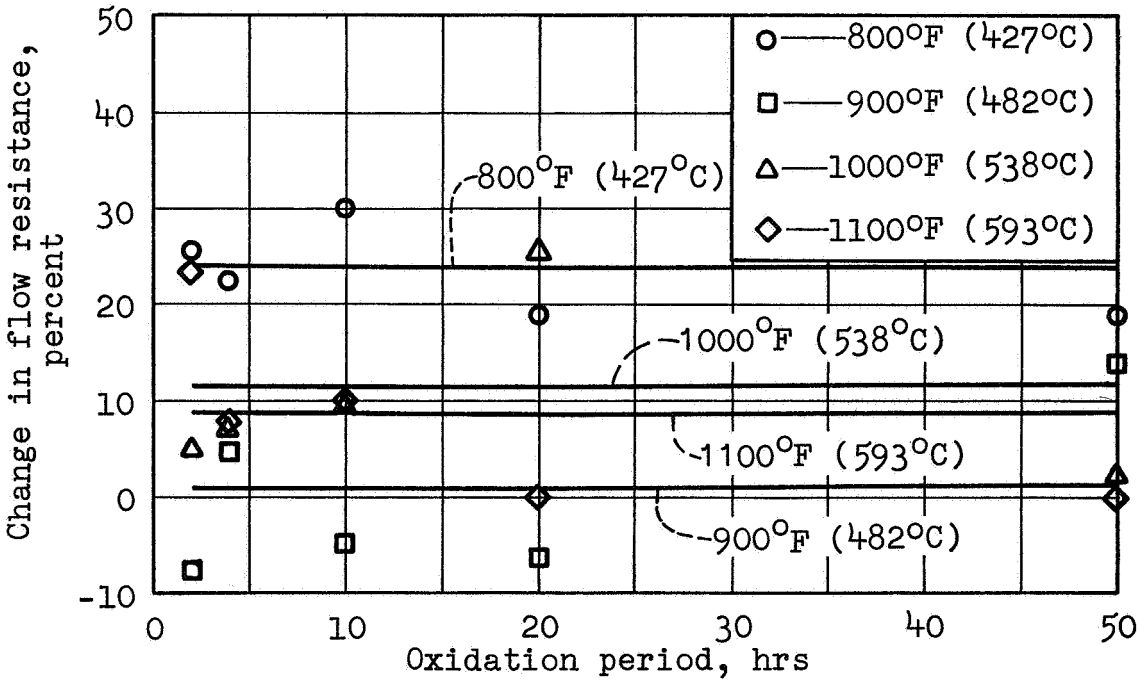

FIGURE F-10.- EFFECT OF AIR OXIDATION ON AIR FLOW RESISTANCE, FM137 - 347SS - C28 FIBER

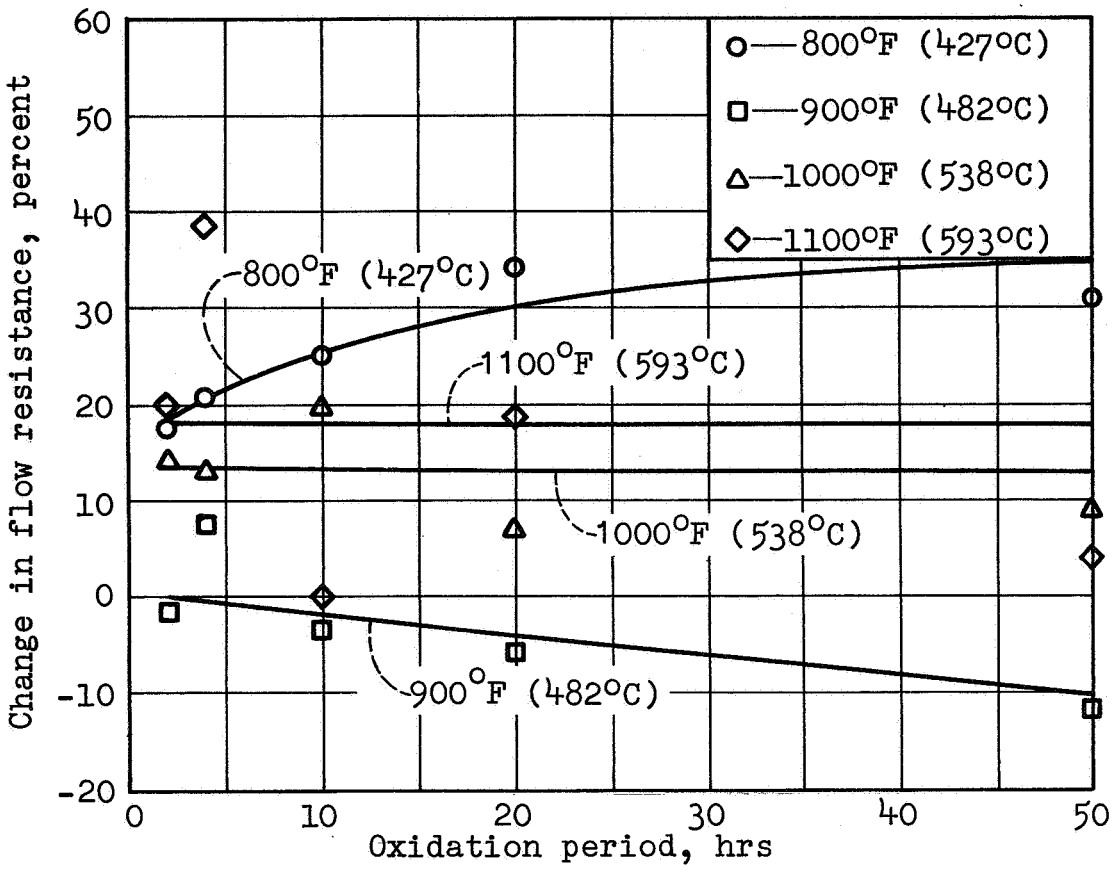

FIGURE F-11.- EFFECT OF AIR OXIDATION ON AIR FLOW RESISTANCE, FM138 - 347SS - C18 FIBER

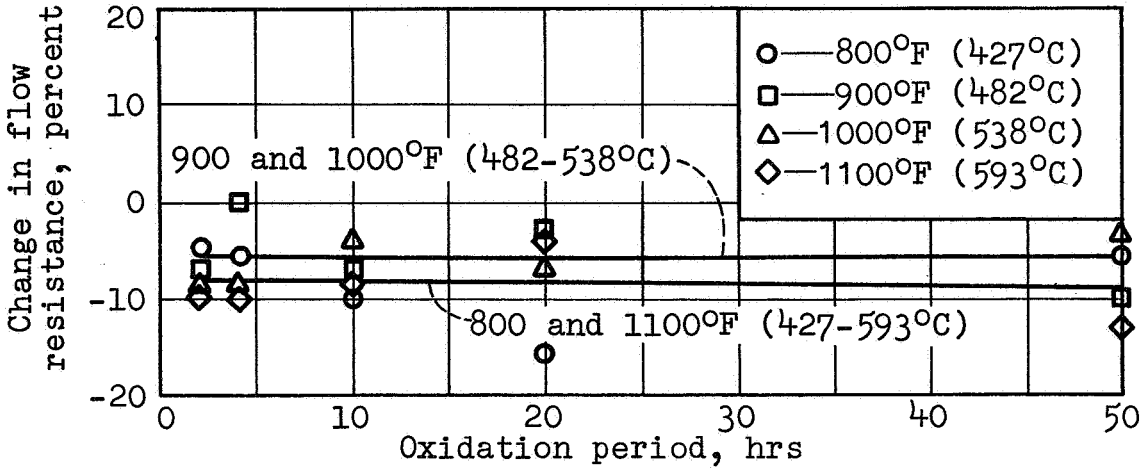

FIGURE F-12.- EFFECT OF AIR OXIDATION ON AIR FLOW RESISTANCE, FM139 - 347SS - E18 FIBER

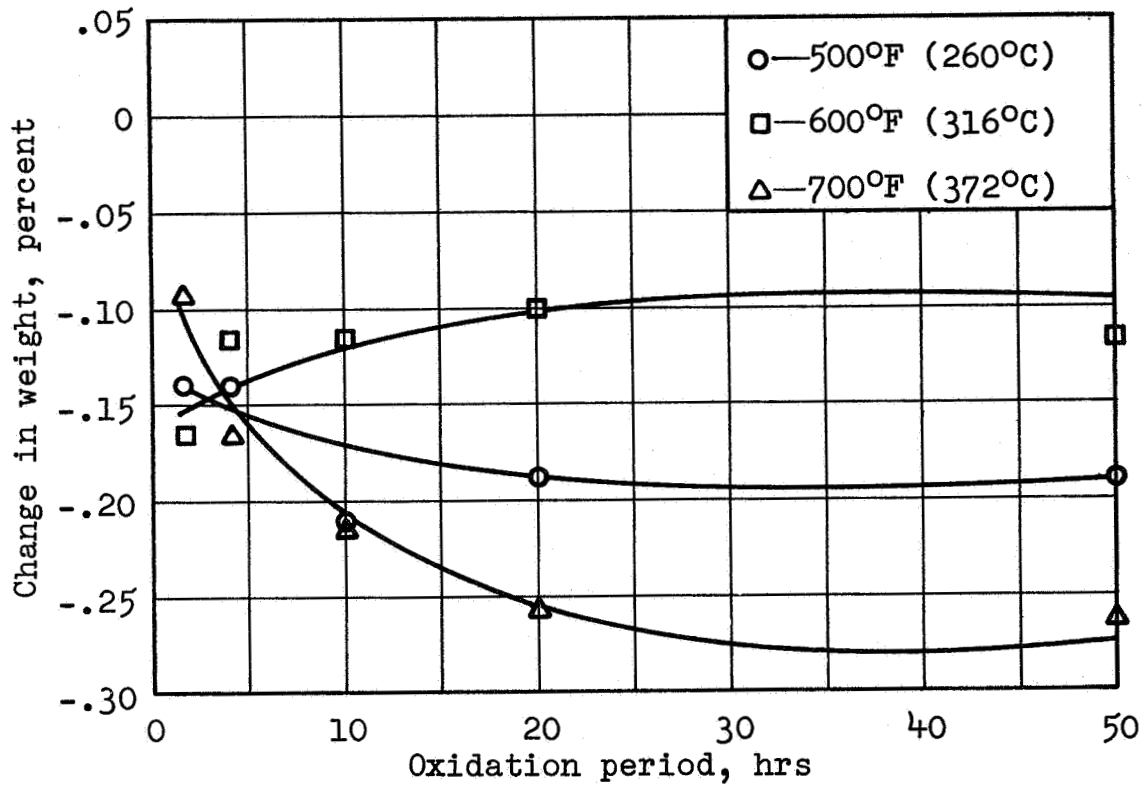

FIGURE F-13.- EFFECT OF AIR OXIDATION ON WEIGHT, FM151B - ALUMINUM - E58 FIBER

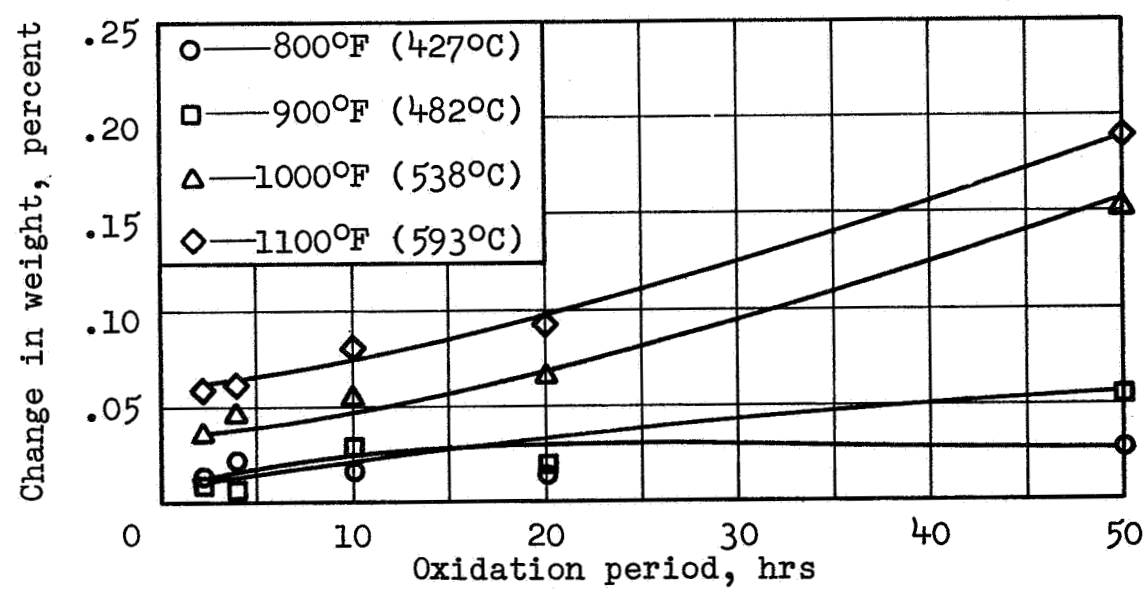

FIGURE F-14.- EFFECT OF AIR OXIDATION ON WEIGHT, FMS180 - 17-4PHSS - C18 - C38 FIBER

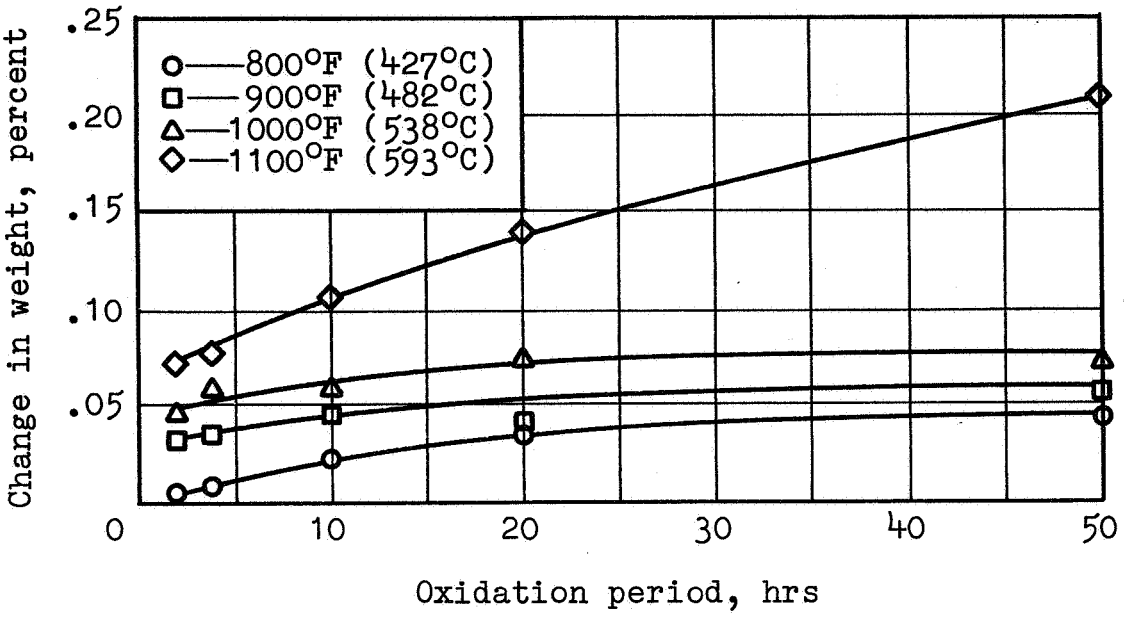

FIGURE F-15.- EFFECT OF AIR OXIDATION ON WEIGHT, FM125C - 347SS - C38 FIBER

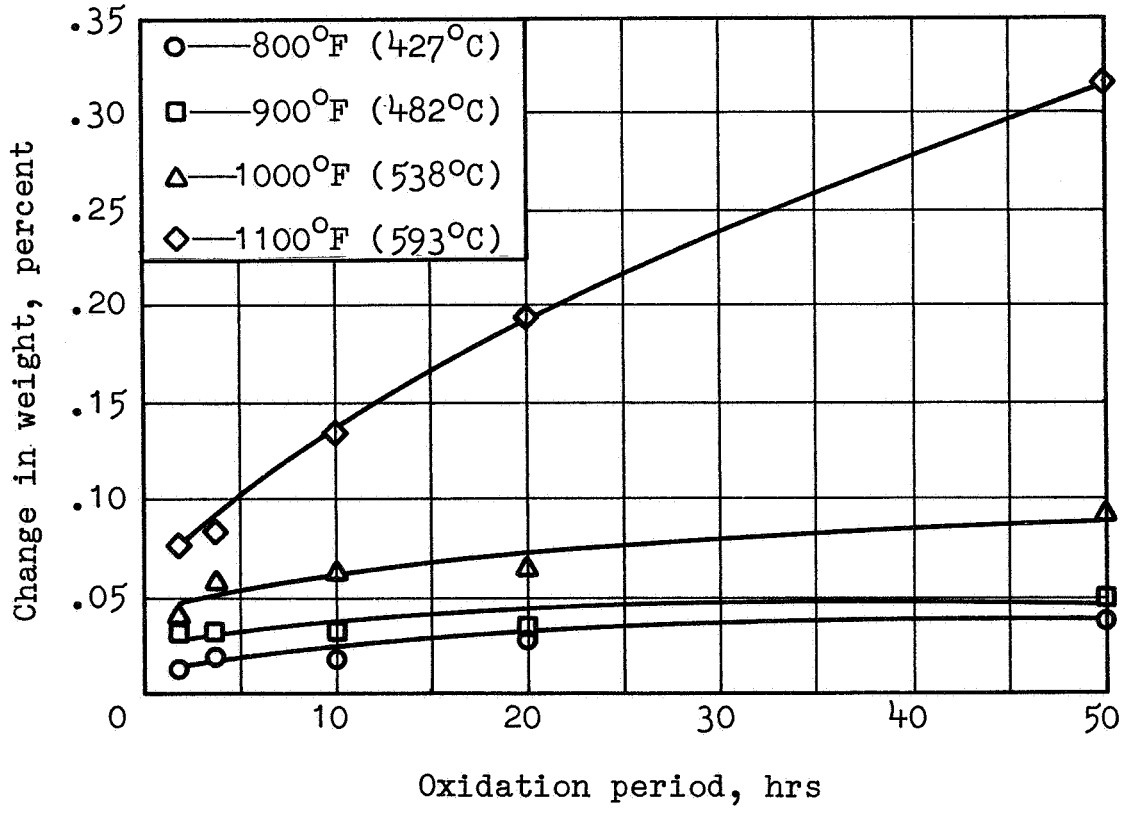

FIGURE F-16.- EFFECT OF AIR OXIDATION ON WEIGHT, FM137 - 347SS - C28 FIBER

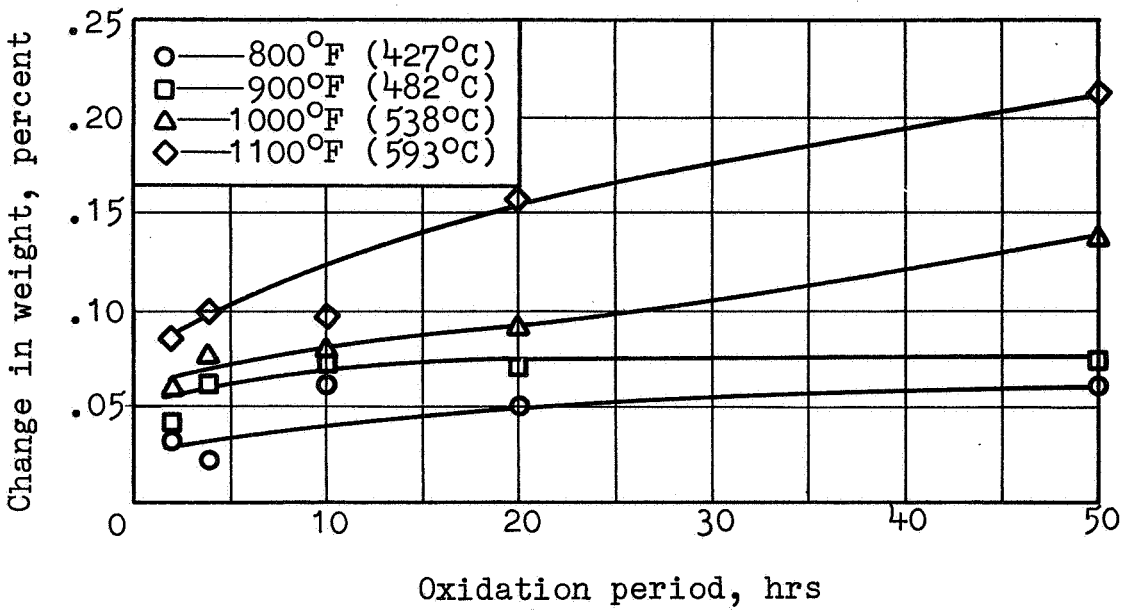

FIGURE F-17.- EFFECT OF AIR OXIDATION ON WEIGHT, FM138 - 347SS - C18 FIBER

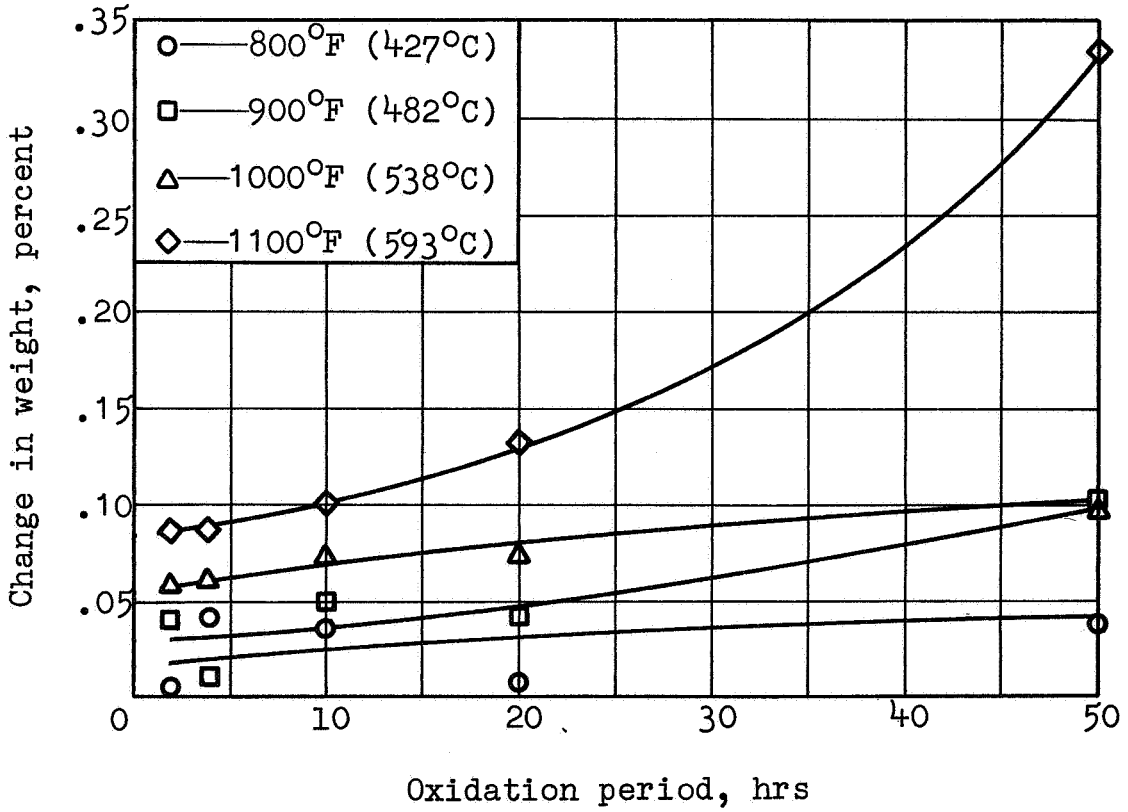

FIGURE F-18.- EFFECT OF AIR OXIDATION ON WEIGHT, FM139 - 347SS - E18 FIBER

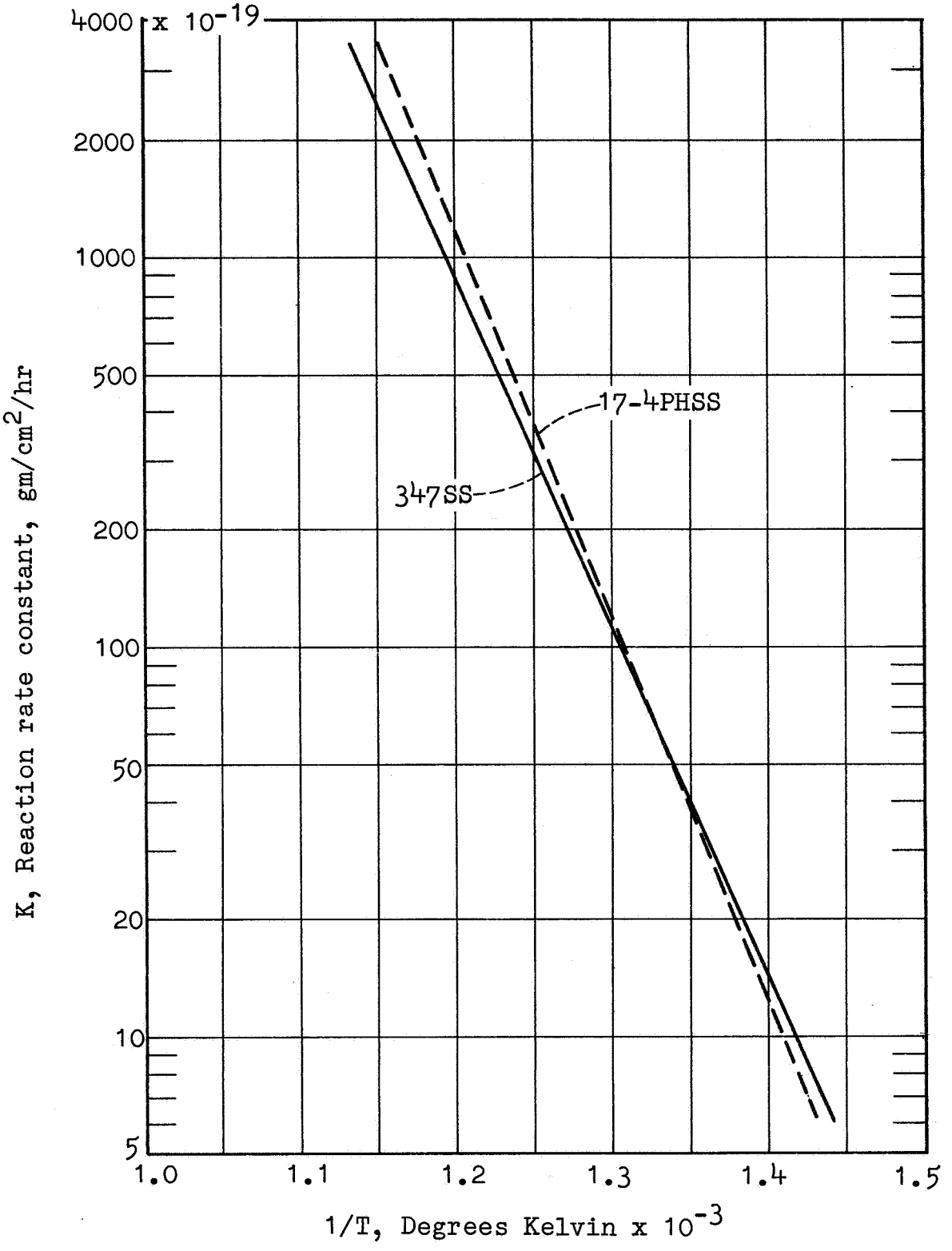

FIGURE F-19

OXIDATION RATE CONSTANTS FOR 347SS AND 17-4PHSS

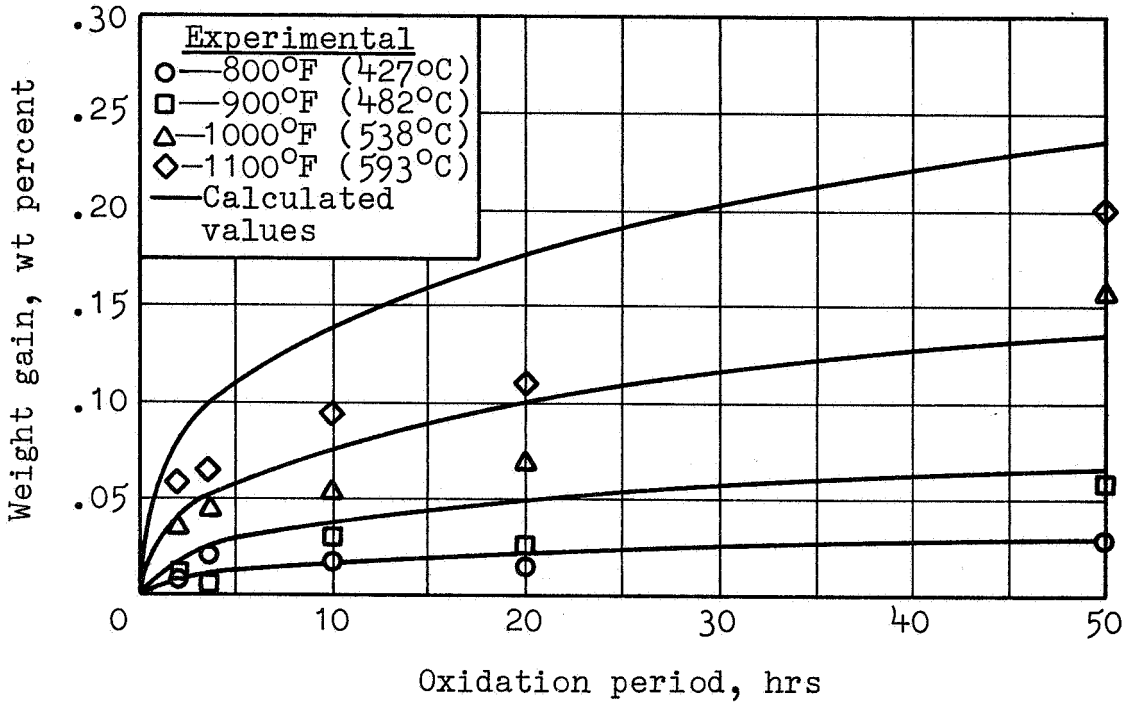

FIGURE F-20.- CALCULATED AND OBSERVED WEIGHT GAIN FROM OXIDATION, FMS180 - 17-4PHSS - C18 AND C38 FIBER

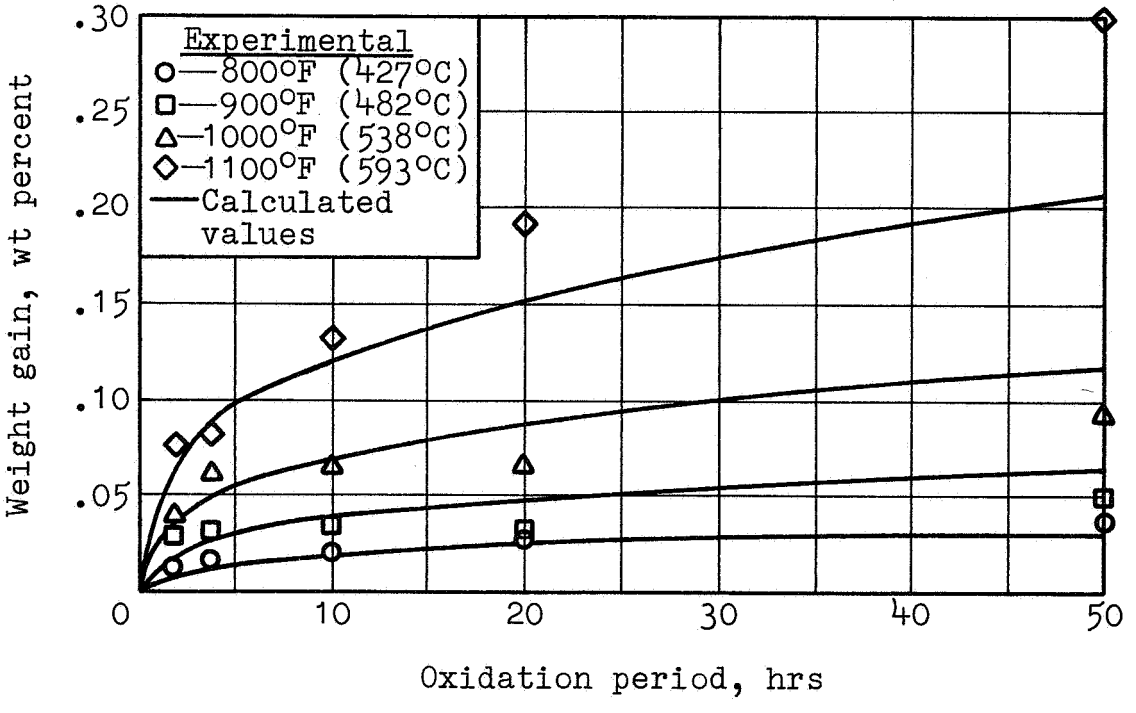

FIGURE F-21.- CALCULATED AND OBSERVED WEIGHT GAIN FROM OXIDATION, FM137 - 347SS - C28 FIBER

TASK G--SALT CORROSION

Introduction.- The porous metal component of an engine silencer is virtually certain to be subjected to humid, salty, atmospheres when the aircraft is flying low over salt water. In addition, it is possible that some entrained salt water may be left in contact with the porous metallic element for extended periods of time, should the aircraft remain parked at seacoast airports. The objective of this test series was to determine the effects of such exposures on the mechanical and flow resistance properties of a number of fiber metal materials.

The candidate materials were chosen from Table I. It was intended to cover the full range of materials and fiber types. The most adverse effects should be noted on the lower density fiber metal materials possessing the smallest areas of inter-fiber metallurgical bonds. On this basis FM151B, FMS180, FM125C, FM137, FM138, and FM139 were selected for testing.

Experimental apparatus and procedure.- The environmental exposures were conducted by York Research Corporation in Stamford, Connecticut, utilizing a standard salt spray chamber as the principal piece of test apparatus. A total of four specimens of each material type were tested. Three of the specimens were tested in Program A, which subjected the specimens to a salt spray for periods of 24, 48 and 96 hours. The fourth specimen was tested in Program B, which subjected the specimens to a two week contacting with synthetic sea water.

All specimens were tested for changes in flow resistance and mechanical properties that resulted from the two exposures. Details of apparatus and procedure are given in Appendix G.

Discussion of results.- The changes in weight and flow resistance caused by up to 96 hours of salt spray exposure, Program A, and two weeks of contacting with synthetic sea water, Program B, are shown in Tables G-I and G-II. The weight increases were highest for the Program B samples. The largest weight change observed was 1.6 percent. For Program A, the weights of the aluminum and 17-4 PH SS samples increased with time. The weight increase for the 347 SS samples indicated no significant time dependency.

Table G-II indicates that the 347 SS samples experienced no significant change in flow resistance as a result of either method of corrosion exposure. The flow resistance of the aluminum samples was not significantly affected for up to 48 hours; however, a slight increase in flow resistance was observed after 96 hours of salt spray. The two-week exposure to salt water produced a significant increase in flow resistance. The increasing flow resistance for the aluminum samples was accompanied by a commensurate weight gain. White corrosion products were observed in the aluminum specimens. The 17-4 PH

SS samples showed minor to moderate increases in flow resistance. These increases exhibited no dependency to time or type of exposure. They are attributed directly to rust and scale, which even in the 0.1 to 0.15 weight percent range was sufficient to partially clog the pores of these very thin (0.010-0.015 in.) (.025-.037 cm) materials. Ultrasonic cleaning for 1-2 minutes removed the corrosion products and totally restored the original flow resistance of these samples.

The more noticeable corrosion of the 17-4 PH SS samples, as compared to the other materials, is shown in Table G-III which summarizes the appearance of the samples after exposure. This result was anticipated since 17-4 PH SS does not have the same degree of resistance to chloride attack as does 347 SS. In general, 96 hours of salt spray affected sample appearance more than two weeks exposure to salt water.

The effect of the exposures on ultimate tensile strengths (UTS) are shown in Figures G-1 through G-6. Each point represents the average of two tensile specimens. The dashed lines in each figure represent one standard deviation from the mean value. These values for standard deviation were developed from previous strength testing of fiber metal. The results indicate that the 347 SS and aluminum samples did not suffer any loss in UTS in either the salt spray or salt water testing. The 17-4 PH SS samples did not lose strength in the salt water exposure or after 48 hours in the salt spray. However, after 96 hours, a loss of about 14 percent is evident.

The effects of the testing on percentage elongation at failure are shown in Table G-IV. No effect was noted in any of the materials, excepting aluminum. The aluminum samples experienced a 33 percent reduction in elongation, for both exposures and this loss appears to increase with time in the salt spray testing.

Conclusions.- The following conclusions summarize the effects of salt corrosion on fiber metal materials:

1. Aluminum fiber metal is currently considered to be unsatisfactory for a salt spray environment. White corrosion products resulting from salt spray exposure cause increases in weight and flow resistance and losses in ductility, although no loss in ultimate tensile strength was observed. It may be possible to develop ultrasonic cleaning techniques to remove these deposits or to develop surface coatings to prevent corrosion, however, this is not recommended since stronger, more corrosion resistant, low weight materials are available in austenitic stainless steels.

2. Fiber metal produced from 17-4 PH stainless steel is marginal to unsatisfactory in a salt spray environment. Corrosion products produced from the exposure caused some small weight increases, along with significant increases in flow resistance

and a small loss in tensile strength, although no loss in ductility was observed. This result was not surprising since this high strength martensitic alloy is not as resistant to corrosion as the austenitic stainless steels. A short period of ultrasonic cleaning can remove the loose corrosion products and restore the original flow resistance of the fiber metal.

3. Fiber metal, produced from 347 SS, is satisfactory in a salt spray environment. No significant changes were observed in flow resistance, weight, tensile strength or elongation. A few minor rust spots were produced on most of the specimens. Over long periods of time, this could increase the flow resistance, however, routine cleaning procedures used for removing other contaminants should remove trace rust contamination resulting from salt spray corrosion.

TABLE G-I

EFFECT OF SALT CORROSION
EXPOSURE ON WEIGHT

Fiber metal spec no	Material type	Fiber type	Sample number	Sample weight		
				before, gms	change, gms	change, percent
FM151B	aluminum	E58	A-24	20.533	0.012	0.06
FM151B	aluminum	E58	A-48	22.770	0.084	0.37
FM151B	aluminum	E58	A-96	23.977	0.207	0.86
FM151B	aluminum	E58	B	23.927	0.388	1.62
FMS180	17-4PHSS	C18,C38	A-24	19.319	0.019	0.10
FMS180	17-4PHSS	C18,C38	A-48	19.772	0.023	0.12
FMS180	17-4PHSS	C18,C38	A-96	19.612	0.025	0.13
FMS180	17-4PHSS	C18,C38	B	19.332	0.029	0.15
FM125C	347 SS	C38	A-24	36.210	0.020	0.06
FM125C	347 SS	C38	A-48	37.011	0.035	0.10
FM125C	347 SS	C38	A-96	36.932	0.027	0.07
FM125C	347 SS	C38	B	36.875	0.148	0.40
FM137	347 SS	C28	A-24	43.525	0.022	0.05
FM137	347 SS	C28	A-48	43.806	0.056	0.13
FM137	347 SS	C28	A-96	43.072	0.060	0.14
FM137	347 SS	C28	B	44.079	0.062	0.14
FM138	347 SS	C18	A-24	22.768	0.012	0.05
FM138	347 SS	C18	A-48	23.189	0.028	0.12
FM138	347 SS	C18	A-96	22.779	0.010	0.04
FM138	347 SS	C18	B	22.769	0.029	0.13
FM139	347 SS	E18	A-24	24.789	0.003	0.01
FM139	347 SS	E18	A-48	24.327	0.008	0.04
FM139	347 SS	E18	A-96	24.474	0.006	0.03
FM139	347 SS	E18	B	24.644	0.018	0.07

TABLE G-II

EFFECT OF SALT CORROSION EXPOSURE
ON FLOW RESISTANCE

Fiber metal spec no	Material type	Fiber type	Sample number	Flow resistance		
				before, rayls	after, rayls	change, percent
FM151B	aluminum	E58	A-24	5.9	5.5	- 6.8
FM151B	aluminum	E58	A-48	7.7	7.0	- 9.1
FM151B	aluminum	E58	A-96	8.8	10.3	17.0
FM151B	aluminum	E58	B	8.4	14.0	66.0
FMS180	17-4PHSS	C18,C38	A-24	8.8	13.0	47.5
FMS180	17-4PHSS	C18,C38	A-48	9.6	10.4	8.3
FMS180	17-4PHSS	C18,C38	A-96	8.8	10.8	22.7
FMS180	17-4PHSS	C18,C38	B	14.1	18.7	31.6
FM125C	347 SS	C38	A-24	8.4	8.8	4.8
FM125C	347 SS	C38	A-48	8.4	8.8	4.6
FM125C	347 SS	C38	A-96	9.5	9.9	4.4
FM125C	347 SS	C38	B	8.8	9.0	1.9
FM137	347 SS	C28	A-24	9.1	8.8	- 3.3
FM137	347 SS	C28	A-48	10.3	10.7	3.9
FM137	347 SS	C28	A-96	8.8	8.8	0
FM137	347 SS	C28	B	9.9	10.2	2.5
FM138	347 SS	C18	A-24	7.7	7.4	- 4.5
FM138	347 SS	C18	A-48	8.1	8.5	4.3
FM138	347 SS	C18	A-96	6.6	7.2	9.1
FM138	347 SS	C18	B	7.3	7.4	0.7
FM139	347 SS	E18	A-24	8.8	7.7	-12.5
FM139	347 SS	E18	A-48	9.6	9.6	0
FM139	347 SS	E18	A-96	8.5	7.4	-13.0
FM139	347 SS	E18	B	8.1	7.5	- 7.4

TABLE G-III

APPEARANCE OF SAMPLES AFTER
SALT CORROSION EXPOSURE

Fiber metal spec no	Material type	Sample number	Appearance
FM151B	aluminum	A-24	Through white streak discoloration
FM151B	aluminum	A-48	Through white streak discoloration
FM151B	aluminum	A-96	Through white streak discoloration
FM151B	aluminum	B	Through white streak discoloration
FMS180	17-4PHSS	A-24	Through rust staining, 50% of area
FMS180	17-4PHSS	A-48	Through rust staining, 90% of area
FMS180	17-4PHSS	A-96	Through rust staining, 80% of area
FMS180	17-4PHSS	B	Through rust staining, 50% of area
FM125C	347 SS	A-24	Three through rust stains
FM125C	347 SS	A-48	Six through rust stains
FM125C	347 SS	A-96	Many faint through rust stains
FM125C	347 SS	B	Two faint through rust stains
FM137	347 SS	A-24	Five rust streaks, one side
FM137	347 SS	A-48	Through rust staining, one corner
FM137	347 SS	A-96	Through rust staining, one corner
FM137	347 SS	B	Faint rust staining, one edge
FM138	347 SS	A-24	No change
FM138	347 SS	A-48	Two faint rust streaks, one side
FM138	347 SS	A-96	Two faint through rust streaks
FM138	347 SS	B	One very faint streak, one side
FM139	347 SS	A-24	Three small rust spots, one side
FM139	347 SS	A-48	Rust spots and staining on one end
FM139	347 SS	A-96	Three through rust stains
FM139	347 SS	B	Through rust staining, one corner

TABLE G-IV

EFFECT OF SALT CORROSION EXPOSURE
ON PERCENTAGE ELONGATION

Fiber metal spec no	Material type	Sample number	Group averages for elongation		
			before, percent	after, percent	change, percent
FM151B	aluminum	reference	4.2		
FM151B	aluminum	A-24		3.6	-14.3
FM151B	aluminum	A-48		3.4	-19.0
FM151B	aluminum	A-96		2.9	-31.0
FM151B	aluminum	B		2.8	-33.0
FMS180	17-4PHSS	reference	4.2		
FMS180	17-4PHSS	A-24		5.4	28.6
FMS180	17-4PHSS	A-48		5.8	38.0
FMS180	17-4PHSS	A-96		4.4	4.8
FMS180	17-4PHSS	B		4.9	16.6
FM125C	347 SS	reference	14.0		
FM125C	347 SS	A-24		17.4	24.3
FM125C	347 SS	A-48		16.6	18.6
FM125C	347 SS	A-96		15.7	12.1
FM125C	347 SS	B		17.9	27.9
FM137	347 SS	reference	15.1		
FM137	347 SS	A-24		15.6	3.3
FM137	347 SS	A-48		14.2	- 6.0
FM137	347 SS	A-96		14.0	- 7.3
FM137	347 SS	B		15.1	0
FM138	347 SS	reference	17.0		
FM138	347 SS	A-24		16.6	- 2.4
FM138	347 SS	A-48		15.1	-11.2
FM138	347 SS	A-96		14.0	-17.5
FM138	347 SS	B		14.9	-12.4
FM139	347 SS	reference	19.9		
FM139	347 SS	A-24		17.2	-13.6
FM139	347 SS	A-48		19.3	- 3.0
FM139	347 SS	A-96		17.1	-14.0
FM139	347 SS	B		17.2	-13.5

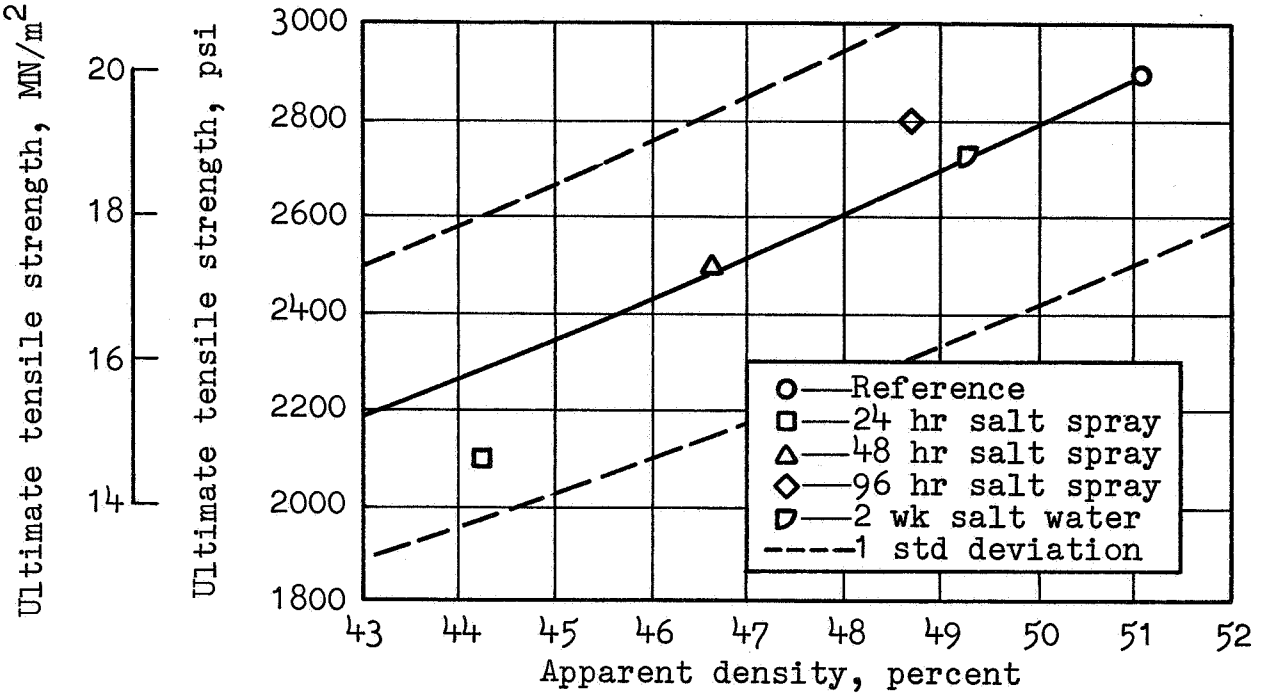

FIGURE G-1.- EFFECT OF SALT CORROSION EXPOSURE ON ULTIMATE TENSILE STRENGTH,FM151B-Aluminum-E58 FIBER

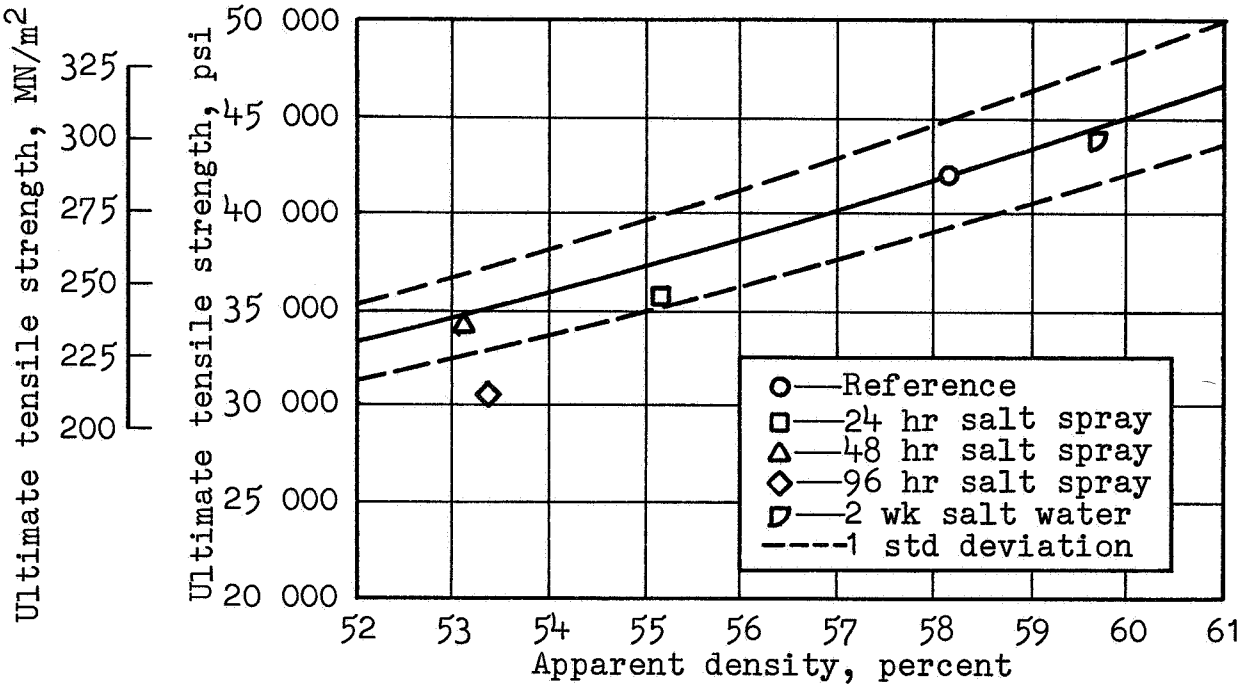

FIGURE G-2.- EFFECT OF SALT CORROSION EXPOSURE ON ULTIMATE TENSILE STRENGTH,FMS180-17-4PHSS-C18, C38 FIBER

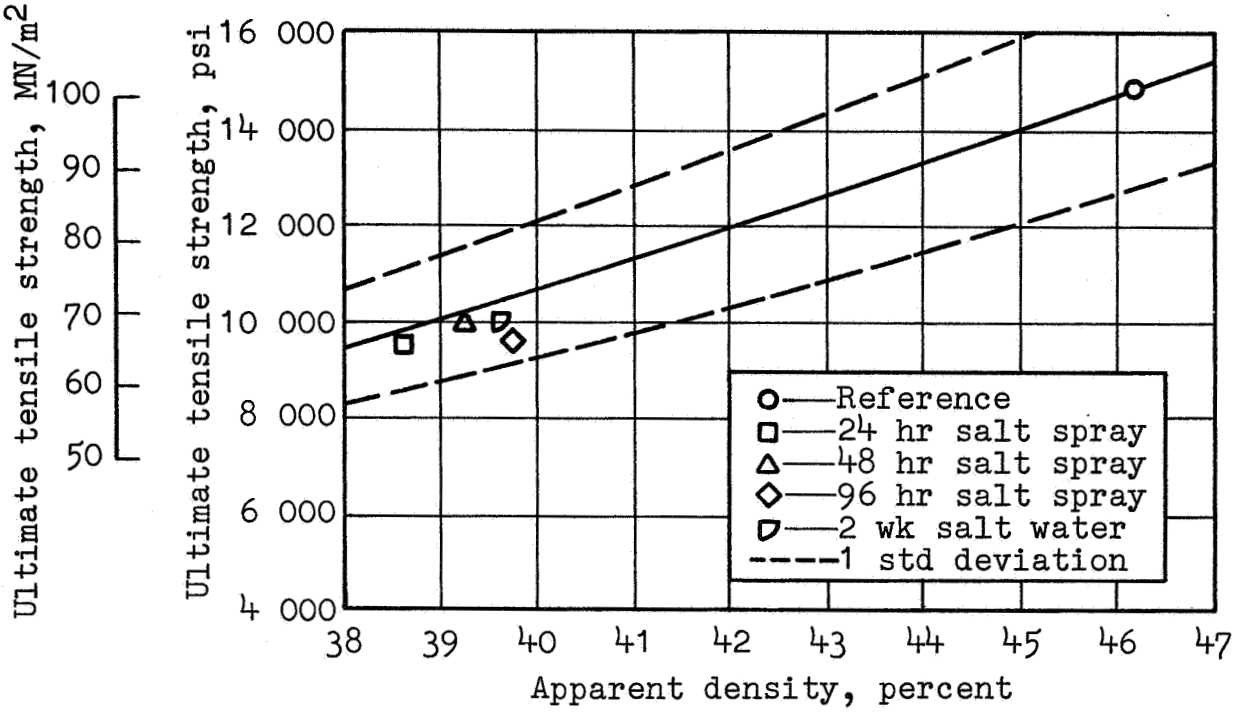

FIGURE G-3.- EFFECT OF SALT CORROSION EXPOSURE ON ULTIMATE TENSILE STRENGTH,FM125C-347SS-C38 FIBER

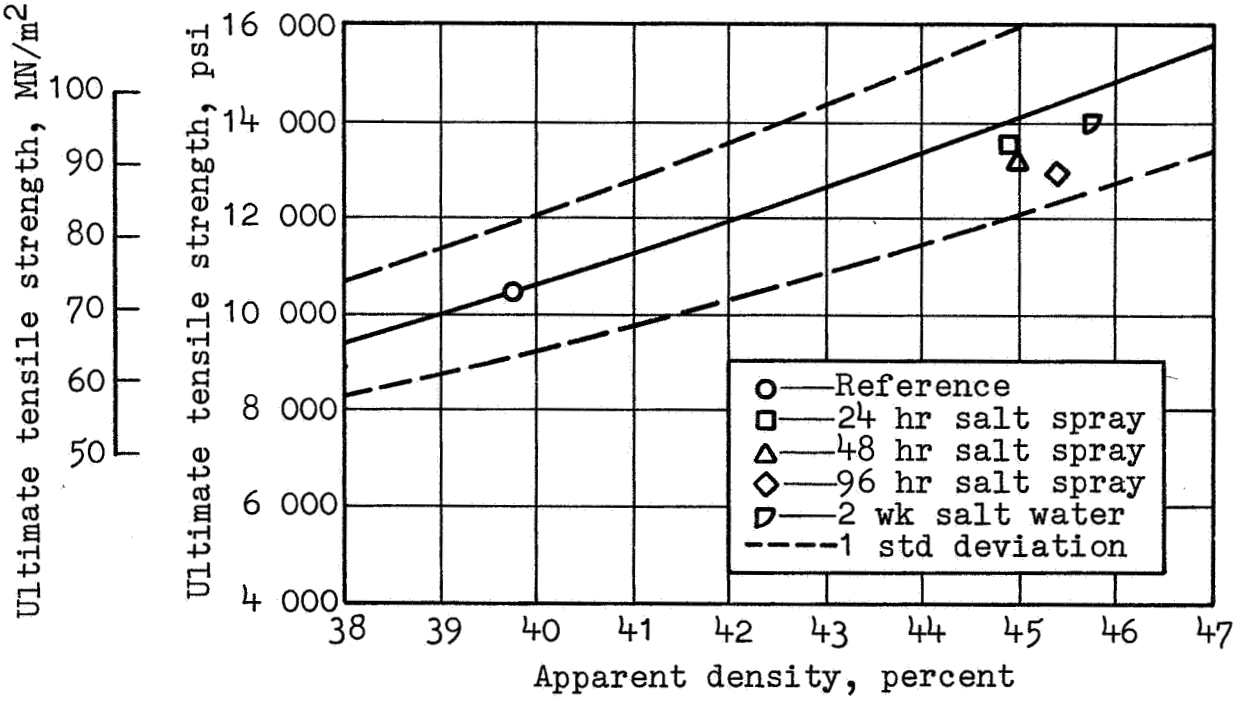

FIGURE G-4.- EFFECT OF SALT CORROSION EXPOSURE ON ULTIMATE TENSILE STRENGTH,FM137-347SS-C28 FIBER

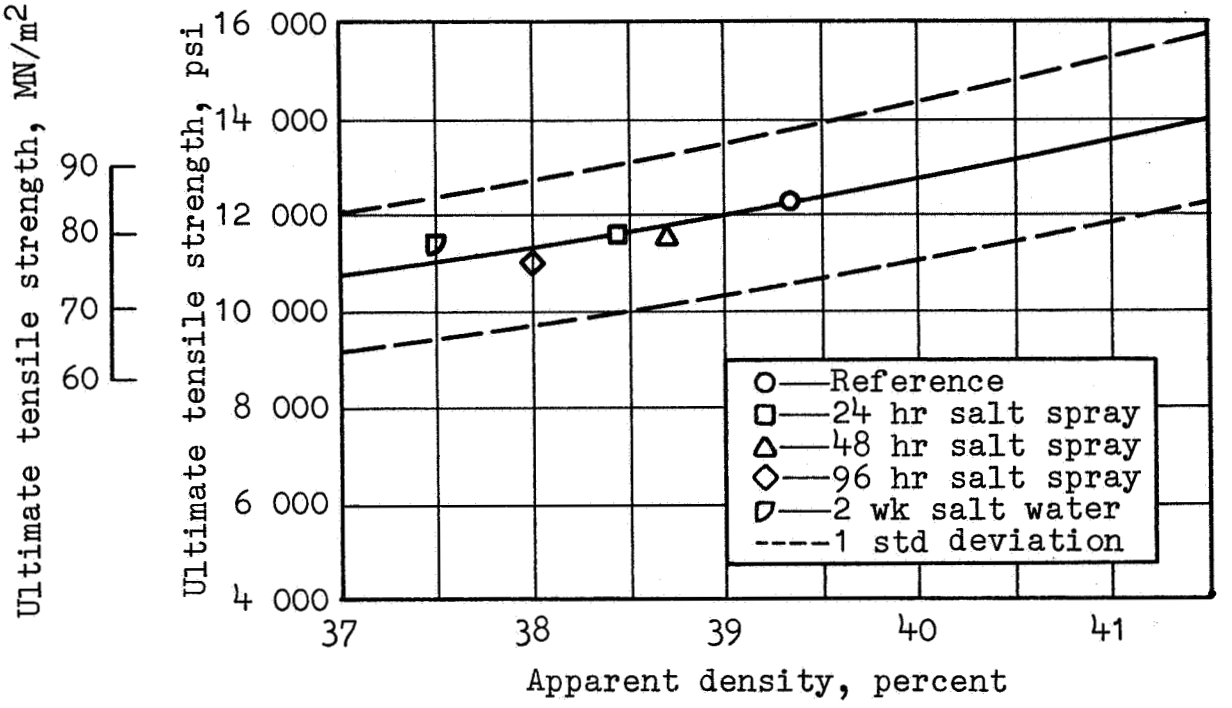

FIGURE G-5.- EFFECT OF SALT CORROSION EXPOSURE ON ULTIMATE TENSILE STRENGTH,FM138-347SS-C18 FIBER

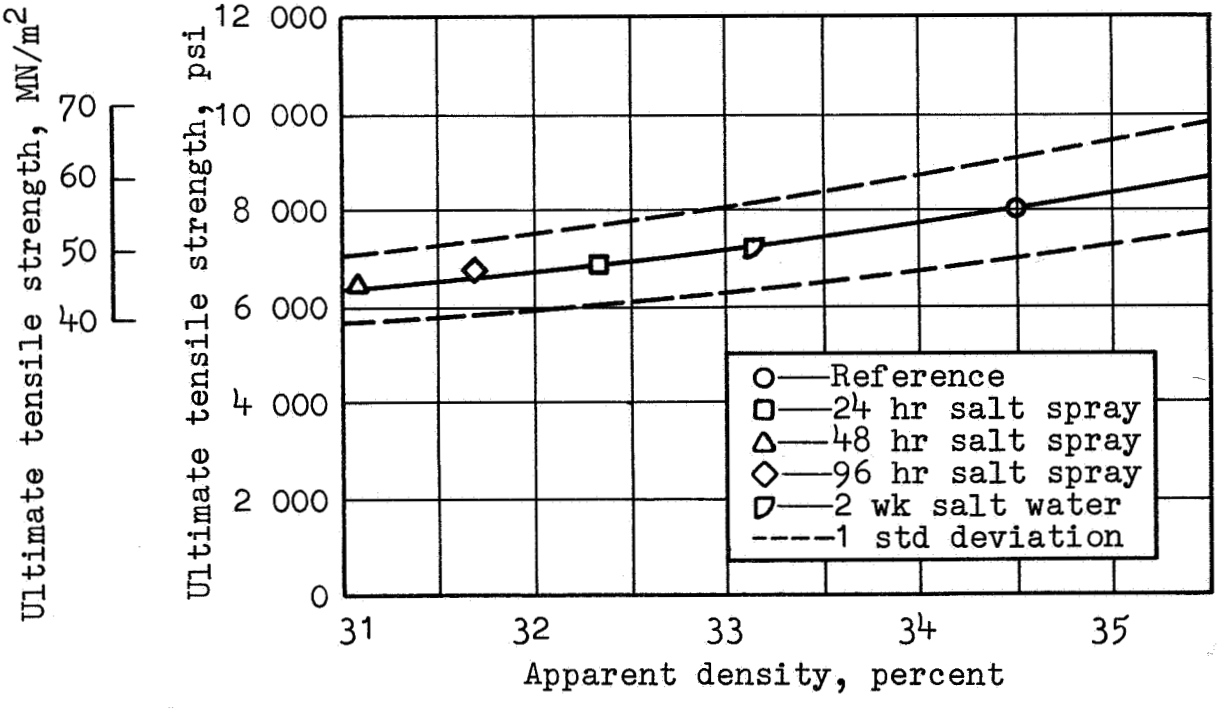

FIGURE G-6.- EFFECT OF SALT CORROSION EXPOSURE ON ULTIMATE TENSILE STRENGTH,FM139-347SS-E18 FIBER

TASK H - CLEANABILITY

Introduction

Fiber metal acoustical materials, because they have sufficiently fine pores which enable them to act as moderately effective air filters, are expected to suffer some degree of contamination in service. This contamination will alter the materials' acoustical flow resistance and thus reduce their sound absorbing effectiveness. Although no knowledge of the degree of rate of contamination is available under typical service conditions, it was the objective of this component of the program to attempt to simulate contaminating processes and then to evaluate the effectiveness of several practical cleaning procedures.

All of the experimental work on contamination and cleanability was performed by the Douglas Aircraft Division of the McDonnell Douglas Corporation, Long Beach, California (Reference 3).

Materials, Contaminants, Experimental Apparatus, and Procedure

Materials.- The fiber metal materials selected for evaluation were FM125C, FM171, and FM172 as described in Table I. These materials represented extremes in pore size and an extreme and a typical flow resistance from the candidate materials. In some tests, two layers of fiber metal were employed, separated by a layer of honeycomb material, in order to simulate an absorber configuration currently employed by some investigators. Also, fiber metal specimens were tested with and without honeycomb backing.

Contaminants.- Two types of contaminants were chosen for the tests. These were: Contaminant A, dust laden dry air and Contaminant B, dust laden dry air blown through specimens that had been immersed in turbine oil. In each case, the dust consisted of fine grain sand (140 mesh silica flour) combined with 10 percent by volume of lampblack. The choice of contaminating agents was based on estimates as to the contaminants that might be expected to be encountered in airline service. Fine grain sand will assuredly be encountered on runways; lampblack represents the unburned hydrocarbons emitted in the engine exhausts; turbine oil represents the oily coatings that might accumulate on the duct surfaces.

Apparatus and procedure.- In conducting the tests, the clean fiber metal specimens first were carefully measured in

flow resistance at several air flow velocities. The specimens were then mounted in the contaminating apparatus, which provided for continuous air flow through the specimens while contaminants were introduced into the air stream. A pressure drop of 6.9 in. (17.5 cm) of water was maintained across each specimen during contamination. This differential pressure was chosen as being representative of the greatest pressure gradient that might occur along a short section of fiber metal lining as installed in an inlet or fan exhaust duct in a JT3D turbo fan engine. The pressure drop was kept approximately constant across the test specimen to simulate the force acting to drive contaminating particles into a porous lining and the decision to terminate the test when the air flow rate had decreased to approximately half its initial value was selected arbitrarily to provide a convenient and reasonable test procedure.

Several cleaning procedures were evaluated, briefly described as follows:

Method 1: Brush with brass wire brush, followed by brushing and vacuuming.

Method 2: Air blast (both sides).

Method 3: Solvent (trichlorethane) wipe, followed by brushing and vacuuming.

Method 4: Immerse in solvent, followed by brushing and vacuuming.

Method 5: Immerse in solvent, followed by air blast.

Method 6: Solvent wipe, followed by air blast.

Method 7: Immerse in ultrasonically agitated solvent.

Evaluation of the cleaning procedure's effectiveness was determined by air flow resistance testing and visual examination. Each specimen was contaminated and cleaned for two or three cycles.

A detailed description of the apparatus and procedure is given in Appendix H.

Discussion of Results

Program description.- The program was divided into three parts, each of which evaluated a different specimen configuration. Part I evaluated unsupported or fiber metal only specimens. Part II studied fiber metal epoxy bonded to 1 inch (2.54 cm) thick, 0.75 inch (1.91 cm) celled fiber glass honeycomb, and

Part III evaluated a fiber metal-honeycomb-fiber metal-honeycomb configuration. The honeycomb in Part III was 0.5 inch (1.27 cm) thick and of the same type as used in Part II. All three sample configurations are shown in Figure H-1.

The results of the program are shown in Tables H-I and H-II. Typical plots of flow resistance vs air flow velocity for all phases of the program are shown in Figures H-2 through H-5.

Part I tests.- The flow resistance of the specimens exposed to contaminant B was always more than twice that of the uncontaminated specimens as shown in Figure H-2. The fact that this increase was always greater than the nominal factor of two that would be anticipated from the contamination procedure employed is attributable to the variable increase in the flow resistance of the oil soaked specimens (before being contaminated by the dust laden dry air) over the flow resistance of the uncontaminated specimens. Also, for samples contaminated by contaminant B, the slope of the flow resistance-air flow velocity curves generally decreased rather than increased with increasing air flow, reference Figure H-2 with contaminant B vs Figure H-3 with contaminant A. This factor is at least partly due to the self cleaning action (oil removal) induced by the high air flow velocities. Similar behavior was observed with water saturated specimens described under Task D of this report.

Inspection of Table H-1 shows that a definite trend developed in Part I concerning the degree of restoration of flow resistance for all the materials tested. For the dry mixture of dust and lampblack (contaminant A) blasting with a jet of air (method 2) was always superior to brushing and vacuuming of the contaminated air side surface (method 1) and always completely restored the original flow resistance. For the fiber metal that had been prewetted with turbine oil (contaminant B) successful restoration of the original flow resistance had to include a complete soaking action by the 1-1-1 trichlorethane solvent in order to loosen the contaminant. Otherwise, blasting with an air jet or vacuuming and brushing were not completely effective. Ultrasonic cleaning in the solvent also completely restored the flow resistance properties of the fiber metal. The successful cleaning methods completely restored the original flow resistance values to fiber metal for three successive cycles.

The problem of residual contamination is one that must be considered when selecting a cleaning method. The unsatisfactory results with cleaning methods 1, 3 and 6 indicate that the contaminant must be removed not only from the surface but also from the pores of fiber metal for effective and complete cleaning. This observation can be understood better if the fiber metal materials are considered to be air filters. It is well established that filters will remove considerably finer particles from a gas

stream than from a liquid stream. As a corollary, filters can be more readily cleaned with a liquid, particularly if the cleaning procedure allows for a velocity of liquid to flush through the pores. Thus cleaning methods 4 and 5, which allowed for some solvent thru flushing of the fiber metal pores and method 7 which provided an ultrasonically induced high velocity pumping action were successful.

Parts II and III testing.- The results of Parts II and III testing are shown in Table H-II. Only the successful cleaning methods from Part I were evaluated in these series, and these cleaning procedures again all proved 100 percent effective in restoring the original flow resistance of the specimens. Figures H-4 and H-5 show that the test specimens exposed to contaminant B again contaminated by a factor of greater than 2 for the reason discussed in Part I testing.

An impervious aluminum plate backing was installed to complete the honeycomb sandwich prior to the last cleaning cycles for methods 4, 5, and 7. The results indicate that the flow resistance after cleaning is independent of whether or not the specimens were cleaned with the backing plate in place.

In addition, a prime objective of Part III testing was to determine whether the outer layer of fiber metal (that first is exposed to the contaminating air flow) would act as a filter for the inner layer. It is most likely that the outer layer did collect all or almost all of the contaminant applied to the specimens for the following reasons:

1. In the presence of the impervious aluminum backing plate, cleaning method 4 was amended to 4A. The solvent was poured directly onto the contaminated surface concurrent with the vacuum removal of a slurry of dust, oil and solvent. The procedure was continued until the contaminated surface appeared clean. When the sandwich was flow resistance tested, the uncontaminated flow resistance was restored.

2. With the aluminum backing plate in place, cleaning method 5 was amended to 5A. The solvent was poured onto the outer layer of the specimen. Then the fiber metal-honeycomb sandwich was inverted and the solvent and contaminant poured out. It is most likely that the scouring of the outer surface by the air jet which followed could only have served to evaporate residual solvent and push any remaining contaminant deeper into the outer layer or into the inner layer of fiber metal. Since the as cleaned sandwich flow resistance tested at precontamination values and since there were no traces of contaminant on the backing plate it is concluded that all of the contaminant was back flushed out of the outer layer by the solvent.

Conclusions

The following conclusions can be drawn from this test series:

1. For the contaminants and contaminating techniques employed, the results show that fiber metal alone or bonded single or double layer fiber metal-honeycomb sandwiches can be cleaned so as to restore the flow resistance to that measured before contamination.

2. The second layer of a double layer fiber metal and honeycomb configuration did not appear to become contaminated. The first or upstream layer appeared to act as an effective filter for the second layer in the contaminating procedure employed.

3. When fiber metal linings are in place in an engine, it is recommended that a procedure be developed that combines forceful spraying of a suitable solvent onto the surface and into the pores of the lining with simultaneous removal of the slurry of solvent and contaminant by a high suction vacuum cleaner.

4. When the fiber metal linings are removed from the engine, it is recommended that a procedure be developed in which the duct is immersed in a tank of a suitable solvent and exposed to ultrasonic energy.

5. It is recommended that further work be conducted in the following areas:

    a. Conduct tests to more accurately determine if the contaminants and contamination techniques employed in this test series are representative of what will occur in service.

    b. Conduct standing wave tube tests to determine acoustical absorption coefficients and acoustical impedance components of contaminated and cleaned specimens.

TABLE H-I

RESULTS OF CLEANING EXPERIMENTS
PART I OF PROGRAM UNSUPPORTED FIBER METAL

Fiber metal spec no	Contaminant employed	Cleaning method employed	Degree of restoration of flow resistance
FM125C	A	1	Partial
FM125C	A	2	Complete
FM125C	B	3	Partial
FM125C	B	4	Complete
FM125C	B	5	Complete
FM125C	B	6	Partial
FM125C	B	7	Complete
FM171	A	1	Partial
FM171	A	2	Complete
FM171	B	3	Partial
FM171	B	4	Complete
FM171	B	5	Complete
FM171	B	6	Partial
FM171	B	7	Complete
FM172	A	1	Partial
FM172	A	2	Complete
FM172	B	3	Partial
FM172	B	4	Complete
FM172	B	5	Complete
FM172	B	6	Partial
FM172	B	7	Complete

TABLE H-II

RESULTS OF CLEANING EXPERIMENTS
PARTS II AND III OF PROGRAM
FIBER METAL - HONEYCOMB CONFIGURATIONS

Fiber metal spec no.	Contaminant employed	Cleaning method employed	Degree of restoration of flow resistance
Part II - Single Layer Bonded Fiber Metal - Honeycomb			
FM171	A	2	Complete
FM171	B	4-4A	Complete
FM171	B	5-5A	Complete
FM171	B	7	Complete
Part III - Two Layer Bonded Fiber Metal - Honeycomb			
FM125C FM171	A	2	Complete
FM125C FM171	B	4-4A	Complete
FM125C FM171	B	5-5A	Complete
FM125C FM171	B	7	Complete
FM171 FM125C	A	2	Complete
FM17L FM125C	B	4-4A	Complete
FM171 FM125C	B	5-5A	Complete
FM171 FM125C	B	7	Complete

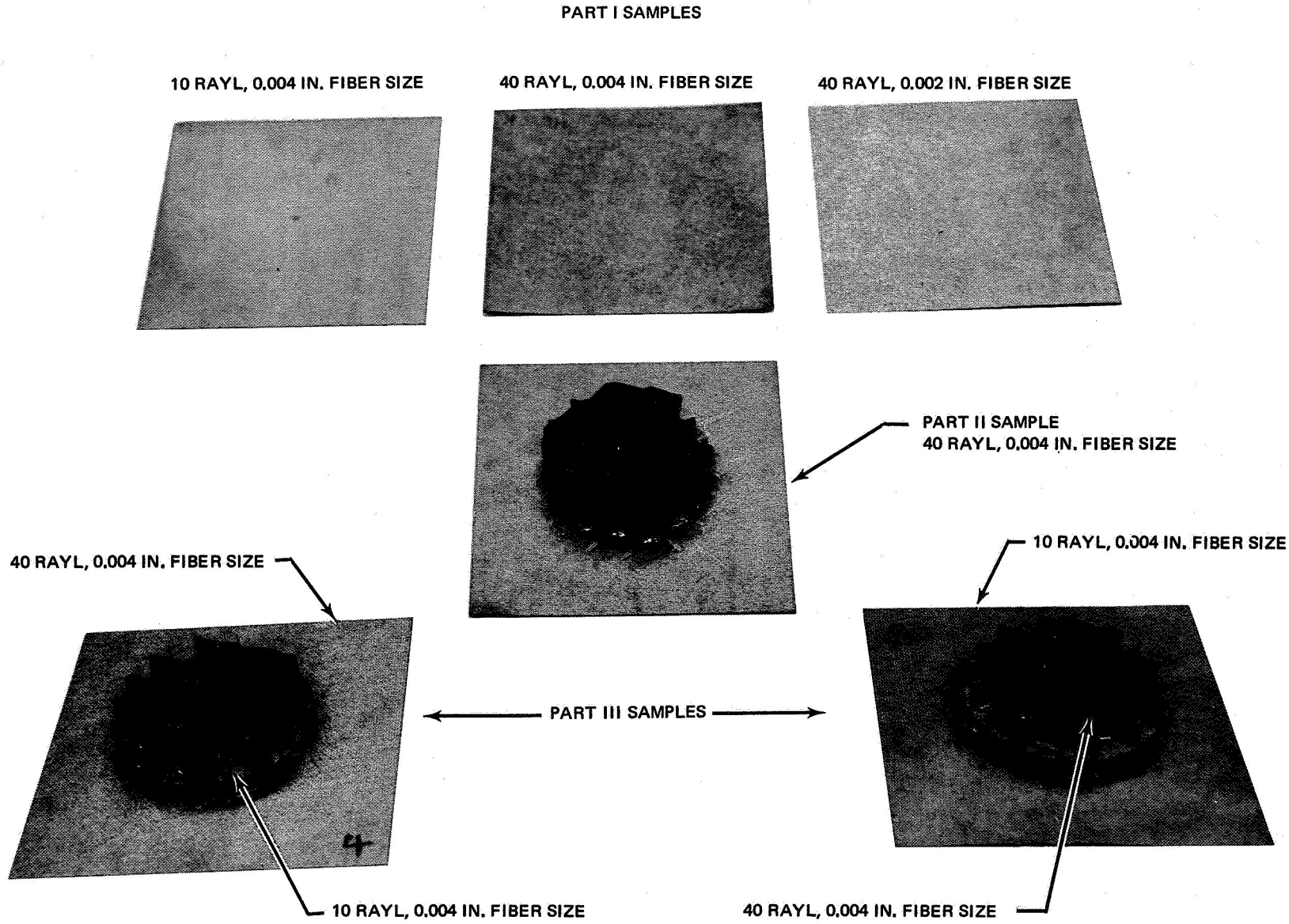

FIGURE H-1

UNSUPPORTED FIBER METAL AND BONDED SAMPLE CONFIGURATIONS

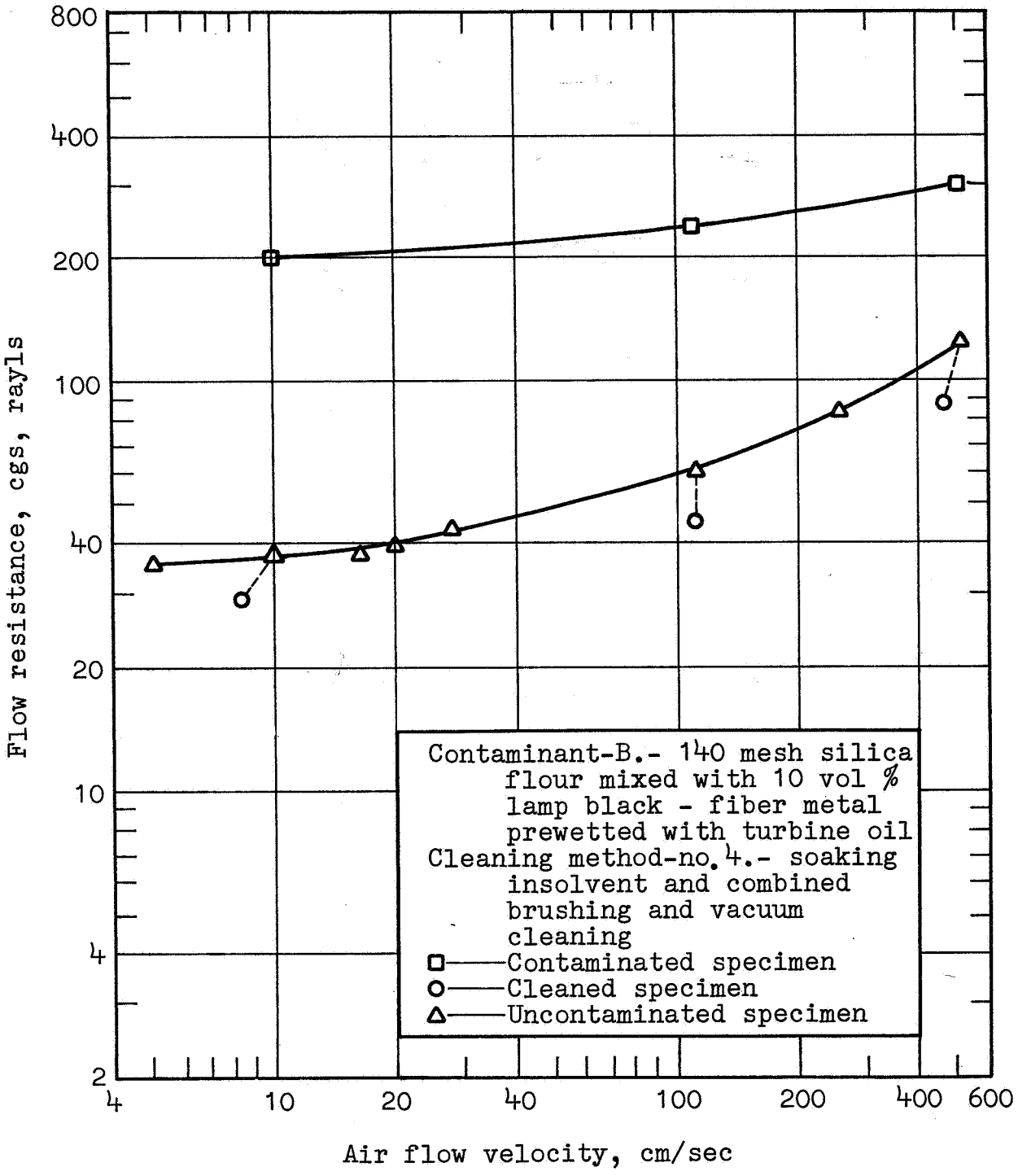

FIGURE H-2

EFFECT OF CLEANING ON FM171
PART I TESTING UNSUPPORTED FIBER METAL

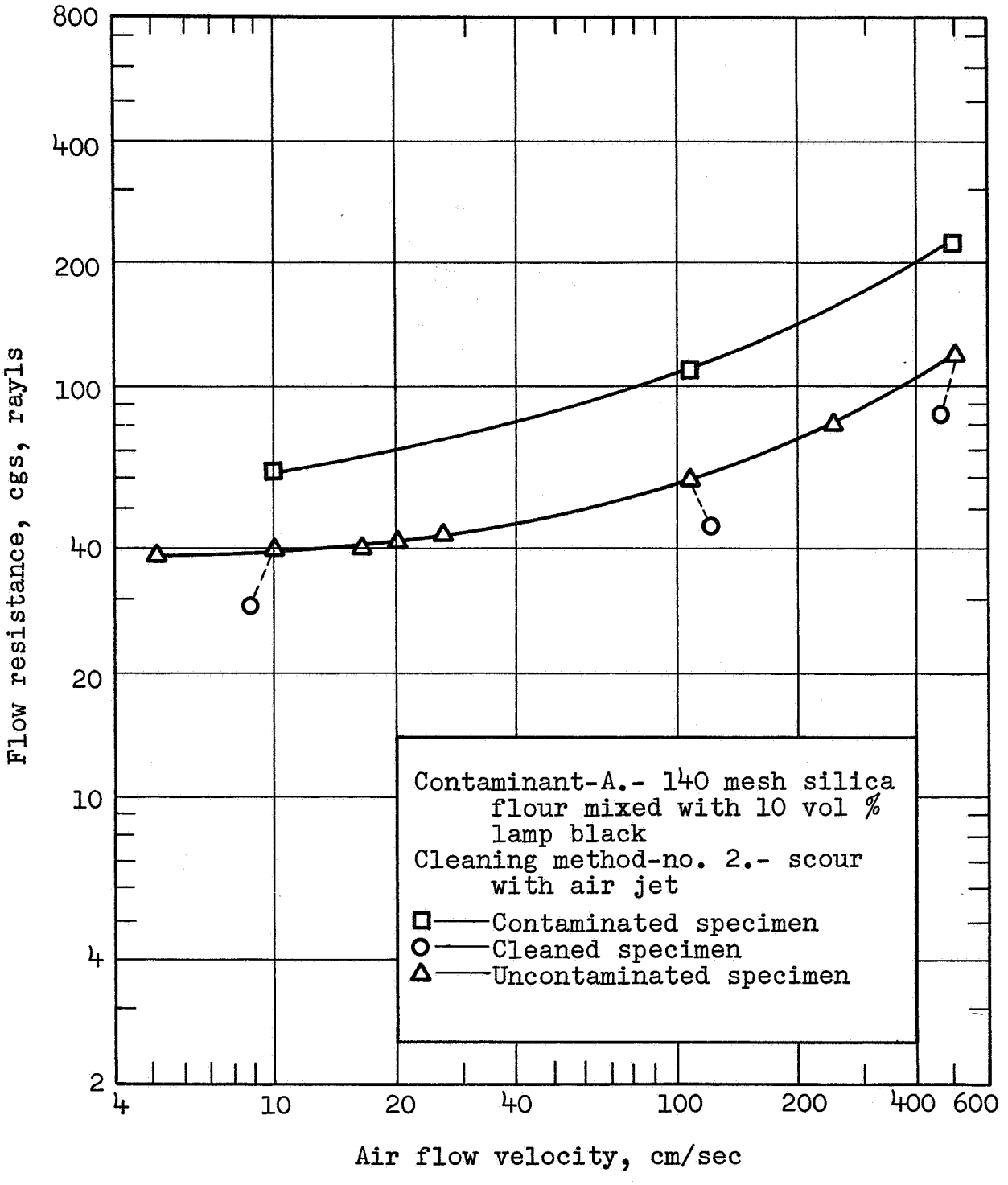

FIGURE H-3

EFFECT OF CLEANING ON FM171
PART I TESTING UNSUPPORTED FIBER METAL

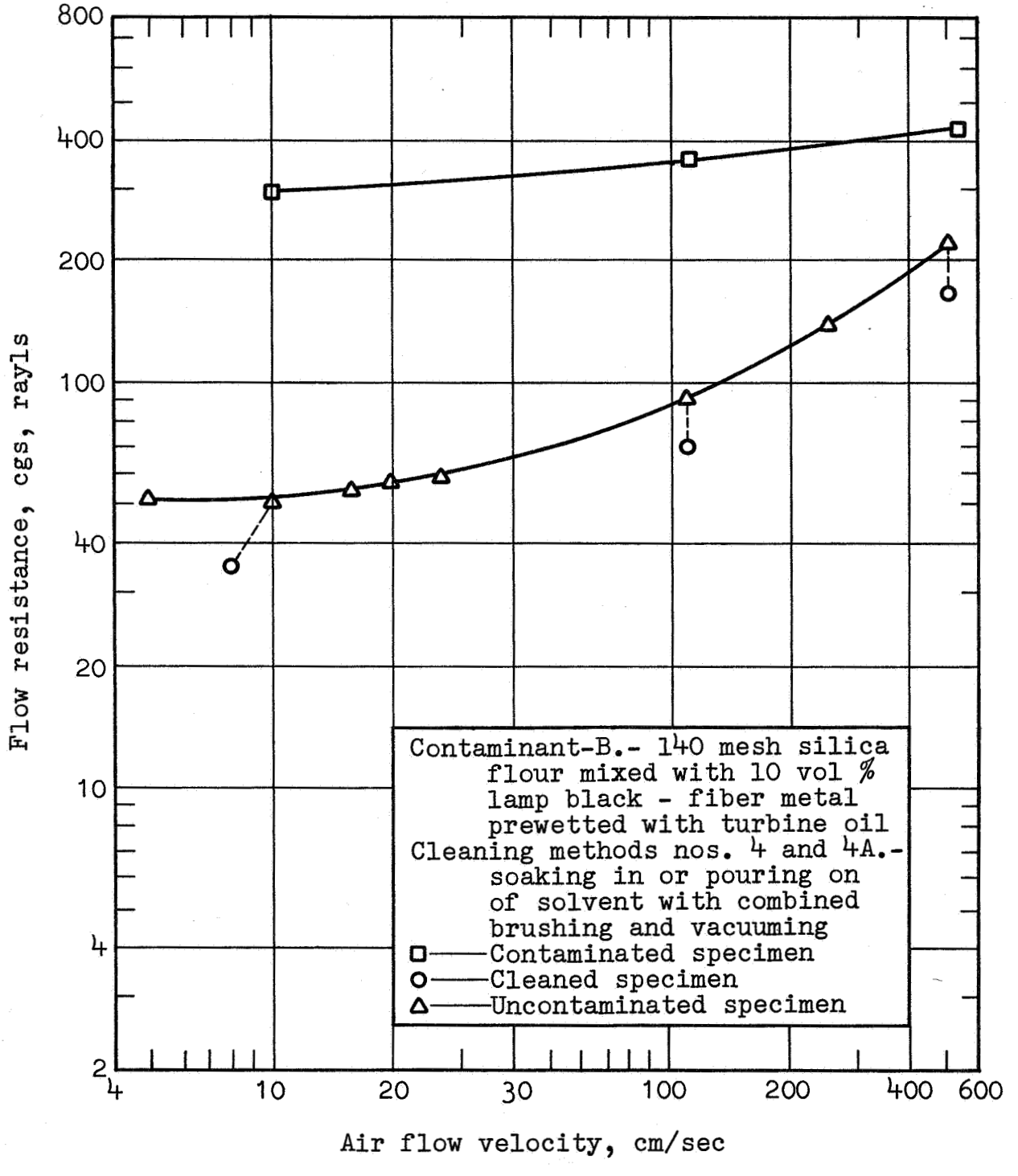

FIGURE H-4

EFFECT OF CLEANING ON FM171 PART II TESTING
FIBER METAL BONDED TO 1 in. (2.54 cm) HONEYCOMB

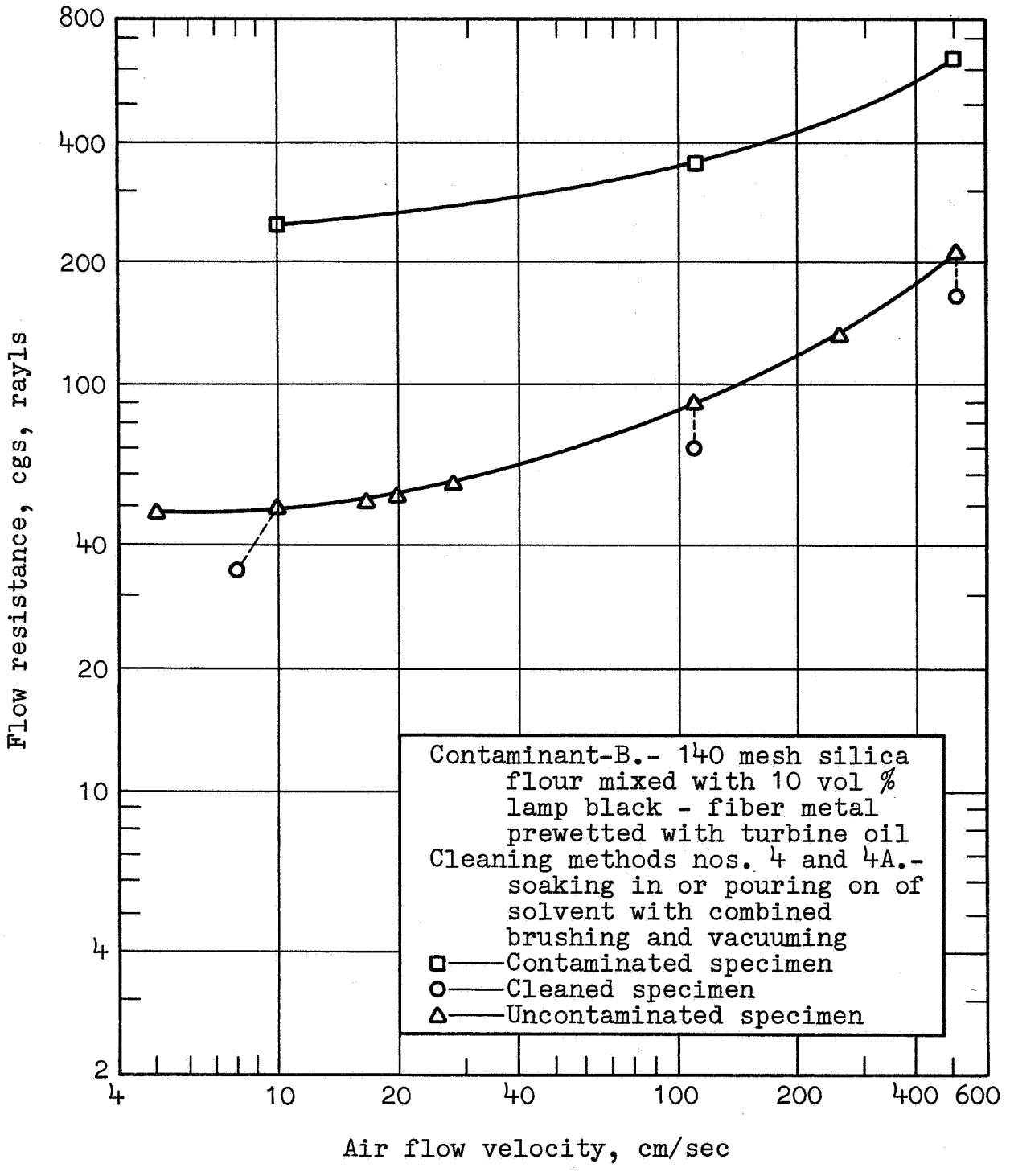

FIGURE H-5

EFFECT OF CLEANING ON FM125C AND FM171 PART III TESTING
DOUBLE LAYER FIBER METAL BONDED TO TWO LAYERS HONEYCOMB

TASK I--MECHANICAL PROPERTIES

Introduction

The information reported in this section is the result of an independent program conducted jointly by Huyck Metals Company and the Illinois Institute of Technology Research Institute in Chicago, Illinois (IITRI). The mechanical properties of fiber metal that were measured in this program included strength and elongation in simple tension, Young's modulus, shear modulus, and torsional damping capacity.

The primary variables affecting properties are porosity and the alloy used in making the fiber metal. However, fiber diameter, fiber length, thermal history, and the orientation of the test specimen in the sheet can also have important effects upon the properties measured.

The properties of fiber metal can be understood if one carefully considers its composition. Fiber metal is a complex array of randomly oriented metal fibers. These are metallurgically bonded together at many points along the length of each fiber. Its composition is somewhat analogous to the structural steel network of a building that has load carrying members in three directions. In fiber metal, the load carrying members are curved rather than straight and are randomly oriented in three dimensional space. The first step in the manufacture of fiber metal is the preparation of uniform felts or mats of fibers. They are oriented more in the plane of the sheet than they are perpendicular to the sheet so that more strength will be provided in the sheet plane. However, there is sufficient vertical orientation and interlocking of fibers so that delamination will not occur in the finished fiber metal. Metallurgical bonds are provided at all of the fiber contact points by either diffusion bonding or brazing the felts in a protective atmosphere in a high temperature furnace. The fiber diameter and length of time at high temperature will determine the size of the diffusion bonds achieved in relation to the fiber sizes. The felts are compacted to their final thickness and porosity by either rolling or pressing. Several different combinations of compaction and bonding can be used to control the characteristics of the final product. Maximum strength and stiffness are obtained by providing as many metallurgical bonds as possible. This is done by bonding at the final density required in the fiber metal. Very weak, low modulus, highly damped fiber metal materials can be produced purposely by minimizing the size and number of metallurgical bonds.

Low density fiber metal structures are easily compressed. Most of the compressive deformation is permanent with little elastic recovery. With the normal metallurgical bonds present in fiber metal, there is little breakage of bonds when a sheet is compressed

in the direction perpendicular to the plane of the sheet. Instead, the primary mode of deformation during compression is a bending and yielding of individual fibers.

When a piece of fiber metal is considered as a material rather than a structure, some generalizations on its mechanical properties can be made in comparison to the solid alloy from which it is fabricated: it is weaker, less rigid, less ductile, more compressible, less uniform, and is a more highly damped material than the solid counterpart. It is also mechanically and structurally anisotropic, with more strength within the plane of the sheet than in the direction perpendicular to the sheet.

Experimental Apparatus and Procedure

Measurements were made on a number of fiber metal materials of Young's modulus, tensile strengths (ultimate and yield), elongation, shear modulus, and damping capacity. Rectangular bar specimens 10 in. (25. cm) long by 0.75 in. (1.9 cm) wide were used for all tests at thicknesses of 0.062 in. (0.157 cm) and 0.125 in. (0.318 cm). Young's modulus was calculated from data acquired by the visual observation of the deflection of both cantilever and simply supported beams, as known loads were applied. Tensile strengths and elongations were determined on a universal testing machine. Both shear modulus and damping capacity were calculated from data produced by allowing clamped, vertically suspended samples of fiber metal to oscillate under torsional loads over known amplitudes, with a rod of known moment of inertia firmly attached to its free end. A complete description of apparatus, procedures, and calculations is given in Appendix I.

Discussion of Results

Tensile stress strain behavior.- The results are summarized in Tables I-II and I-III. In all cases, as is described in Appendix I, the properties are calculated as if the fiber metal were a uniform, simple material rather than a complex assemblage of metal particles. Although this is not the most fundamental approach, it provides results that are the most useful in the conventional equations employed in stress analysis.

Inspection of the typical tensile stress-strain curves with and without periodic unloading shown in Figure I-1 provides some insight into the mechanical properties of fiber metal. Even at very low loads, the material starts to undergo permanent deformation so that upon release of the load, the sample retains a substantial fraction of the total strain at load. A prestrained sample, upon reloading, shows a true elastic behavior in which the strain is directly proportional to the applied stress.

This condition prevails until the sample is loaded to its previous level, where plastic deformation again begins. The elastic modulus increases with increasing levels of prestrain. The effect of prestrain on elastic modulus for the sample shown in Figure I-1 is shown in Figure I-2. Although fiber metal continuously yields with increasing load, it is desirable to know what loads can be applied that will not cause large permanent deformations of a material. For stainless steels and aluminum this has been typically (and arbitrarily) set at 0.2% offset, Reference 4. The yield strength of fiber metal is shown as a function of prestrain in Figure I-3. Just as the solid alloys harden with increasing strain past the yield points, this curve illustrates the strain hardening behavior of fiber metal. Strain hardening coefficients calculated for fiber metals are many times lower than those calculated for the corresponding solid metal.

Upon repetitive loading and unloading, with increasing levels of prestrain, the elastic hysteresis loops between the loading and unloading curves progressively broaden. In solid metals, this loop narrows with increasing strain levels. "The areas of these hysteresis loops, representing the energy dissipated per cycle, are of practical interest, as the amount of this energy determines the damping properties of the material," Reference 4. The areas of these loops also increase with decreasing apparent density of the fiber metal and are believed to be related to the average distance between interfiber bonds.

In a typical tensile stress-strain curve, the material appears to elongate uniformly out to the maximum or ultimate tensile strength. At this point, a visible flaw appears in the specimen and the sample continues to elongate in the area of the break as the load diminishes. Long fibers can be seen being pulled from the fiber metal in the zone of the break. The two broken pieces of the sample contain too many long fiber ends to permit piecing the sample together for measuring total elongation. Consequently, elongation is measured by cross-head movement and only includes the uniform elongation out to the ultimate tensile strength. The tensile break areas take on an appearance more typical of solid metals when the fiber metal is produced at higher densities and with shorter fibers. However, in no case do fiber metal samples have a "neck" in the break zone. The failures appear to be the combined results of shear failures at interfiber bonds and tensile failures of individual fibers. It is interesting to note that some "necking" of individual fibers in the break zone can be observed.

From the foregoing observations, it is believed that during the process of pulling a piece of fiber metal to failure, individual fibers will continuously reorient themselves so that they tend toward parallelism with the direction of load. Some interfiber bonds will break so that there is an increasing area of load-bearing fibers in tension with increasing levels of stress

and strain. The break will finally occur in that portion of the specimen which happens to have the smallest number of fibers per unit of volume. It seems clear that product uniformity is important in maximizing strength and ductility. Because product uniformity has an effect upon testing results, and because the chances for having a flaw in a sample increase with increasing sample length and cross sectional area, sample size probably can affect the results from mechanical properties testing.

Young's modulus.- Typical load deflection curves obtained from cantilever beam testing for Young's modulus are shown in Figure I-4. In all cases for the cantilever beam and the simply supported beam measurements, the deflection was linear with the applied load. The results from these tests are defined as "Method I results" in the discussion that follows. Young's modulus can be calculated from typical stress-strain curves from the multiple unloading technique (see Figure I-1) in two ways. Method II results are calculated from the slope of the stress-strain curve at the origin. This is similar to Method I but is less accurate because of the difficulty with obtaining an accurate slope at one point on a complex curve. Method III results are calculated by taking the slope of the straight line portion of the stress-strain curve after prestraining the material to 0.2% offset. A comparison of the results from the three methods is shown in the following table.

Fiber type	Apparent density, percent	Method of calculation					
		I		II		III	
		PSI X 10^6	MN/m^2 X 10^3	PSI X 10^6	MN/m^2 X 10^3	PSI X 10^6	MN/m^2 X 10^3
C18	25.8	0.36	2.48	0.40	2.76	0.54	3.72
C18	61.5	3.00	20.70	3.80	26.20	4.00	27.60
C38	25.4	0.19	1.31	0.18	1.24	0.19	1.31
C38	63.5	3.00	20.70	3.20	22.10	3.29	22.70

It is clear that Method I gives the most conservative results. In three of the four instances, Method I results were significantly lower than the other two, and in the fourth case, results from all three methods were virtually identical. The Method III results are consistently higher than the

other two because these modulus values were obtained on slightly prestrained samples. As pointed out previously, Figure I-2 shows the increase of Young's modulus with increasing levels of prestrain.

The correlations below are made with the use of the lower, more conservative, modulus data obtained with the beam deflection method. It should be noted that all of these correlations show the apparent modulus of the material in terms of percentage of the modulus of the solid counterpart. The physical meaning of this relative modulus is that this is the equivalent or effective cross sectional area that is actually carrying the load in the sample.

The Young's modulus data for C38 fiber metal are shown in Figure I-5 as a function of density.

First, Figure I-5 shows that the apparent Young's modulus increases exponentially with the apparent density of the fiber metal. Although the relationship is not quite a straight line on a logarithmic plot, the modulus increases approximately in proportion to the cubic power of apparent density.

The addition of screen to the surface of the fiber metal substantially increases the apparent Young's modulus. This is probably the result of two causes. The addition of screen provides a set of pre-aligned metal fibers which can immediately begin accepting a share of the load. The screen also increases the sectional moment of inertia by having the larger screen wire area at the sheet surface.

This stiffening effect of screen is even more noticeable in low density specimens or in the typical thin fiber metal sheets used for sound absorption applications because the screen represents a much larger percentage of the metal present. This can be seen in the photomicrograph of a cross section of product number FM128A in Figure I-6.

No effect was observed of sample thickness or sample orientation within a sheet on the apparent Young's modulus for unreinforced fiber metal. However, users of fiber metal have found some reduction in modulus and strength of thin screen reinforced materials by testing samples taken at a 45° orientation to the screen wires.

The Young's modulus data for the C18 fiber metal are shown in Figure I-7 in comparison with the curve for the C38 material. This curve reinforces the previous observation regarding sample orientation. It also shows a significant increase in Young's modulus with decreasing fiber diameter, particularly at the lower densities. The curves have been extrapolated to intersect the 100% density line at the Young's modulus of annealed Type 347SS.

The Young's modulus data for E58 aluminum fiber metal are shown in Figure I-8. Data are shown for both the as-received condition and for duplicate samples that have been heat treated at 750°F to anneal the alloy. The samples in the annealed condition appeared to have a slightly higher modulus. This is not understood since the modulus of solid aluminum alloys is essentially independent of the condition. Also, the modulus appears to increase linearly with apparent density rather than exponentially. It is important to note that these samples were metallurgically bonded only once at an apparent density of 25% with no subsequent bonding at the higher densities. Low modulus samples of stainless steel fiber metal have been produced at high apparent densities by omitting sintering after compacting. The many additional metallurgical bonds provided by rebonding at high densities help rigidify the fiber metal structure and provide more effective load carrying fibers. This lack of rebonding thus explains the anomalous results with increasing density.

Shear modulus.- The shear modulus results are presented in Figures I-9 through I-11. As with the Young's modulus results, these are shown as apparent values relative to the shear modulus of the solid metals. For comparison, the relative Young's modulus curves for unreinforced fiber metal are shown for each fiber type.

It is seen that apparent density is the major factor in influencing shear modulus. The shear modulus of stainless steel fiber metals increases exponentially with increasing apparent density.

In general, the values for relative shear modulus are essentially equal to the relative Young's modulus. This is not surprising since the same samples having the same real moment of inertia were used for measuring both moduli and because the moment of inertia has a similar role in determining both the flexural and torsional rigidities which were used to determine modulus.

There was no effect of sample thickness or sample orientation on shear modulus.

There was no effect of screen reinforcement on shear modulus. This is a surprising result and is not understood. The screen should increase the effective load bearing area and torsional rigidity of a sample, so that an observable effect of screen reinforcement was expected at low densities where the screen represents a significant portion of the total metal present.

Ultimate tensile and yield strengths.- The results showing the effect of apparent density on ultimate tensile strength of C38 fiber metal are shown in Figure I-12. The corresponding plot for yield strength is shown in Figure I-13. As with Young's modulus, ultimate tensile strength and yield strength increase exponentially with increasing apparent density. There is no significant effect

of sample thickness or sample orientation in a sheet. Screen reinforcement does have an effect at low apparent densities. It is important to note that the volume of screen present is included in the calculated apparent density of all materials discussed in this report. The ultimate tensile strengths of thin screen reinforced samples of C38 and C18 acoustical materials are plotted in Figure I-14, along with the average line for unreinforced C38 materials. This plot also demonstrates an increase in tensile strength with screen reinforcement of very thin samples. This point is illustrated further in Figure I-15 which shows the percent increase in strength for screen reinforcement of both C18 and C38 fiber as a function of the percent screen present in the material.

The ultimate tensile strengths and yield strengths for C18 fiber metal are plotted as a function of density in Figures I-16 and I-17 respectively. At high densities, the results with the finer C18 fibers [.002 in. (.005 cm) diameter] are equivalent to the C38 [.004 in. (0.010 cm) diameter] fibers. However, as observed with the modulus results, much higher yield and ultimate tensile strengths are achieved with the finer fibers at low densities. The most probable explanation for this is that low density fiber metal samples fail primarily at the bonds; the C18 fibers have (a) more mechanical interlocking of the fibers with twice the L/D ratio (b) more interfiber bonds per unit length of fiber and (c) a higher ratio of metallurgical bond area to fiber cross sectional area.

The yield strengths and ultimate tensile strengths for both conditions of E58 aluminum fiber metal are shown in Figures I-18 and I-19 respectively. The anticipated results were experienced: annealing of course reduces the strength of a hardened alloy. As with Young's modulus, the strength of the aluminum materials increased linearly with density rather than exponentially. This again was the result of a process employing only a single bonding between fibers at 25% density.

The smoothed curves of ultimate tensile strength of unreinforced fiber metals relative to the ultimate tensile strength of the solid metals are shown in Figure I-20 in comparison to the apparent Young's modulus and shear modulus curves. It is evident that the relative ultimate tensile strength curves are consistently higher than the relative modulus curves. When these relative values are interpreted as "effective load carrying areas," these results are reasonable. There is more reorientation of fibers and more load bearing area of fibers when a sample is fully strained at its ultimate strength than with the very low levels of strain used for measuring the moduli.

Elongation.- The observed elongations from the tensile specimens are shown in Figure I-21.

First, it seems clear that for unreinforced stainless steel fiber metal, elongation is near maximum at about 50 percent density, decreasing with both increasing and decreasing density from 50 percent. Screen reinforcement results in a substantial improvement in elongation, except at high density, where it could be expected to exert the least influence. Also as would be expected, screen reinforcement has a major influence on low density specimens. The effect of test direction with respect to rolling direction is negligible, and the effect of thickness is not clear from the available data.

Interpreting these results, it would seem that low density materials are unable to accept much strain before failure because they are primarily sinter-bond dependent for strength, and there are too few sinter bonds per fiber. Also, at high densities, fiber metal materials seem to behave like porous castings, which show poor ductility. Although the materials are fairly strong, there are large numbers of stress raisers (pores) within their structures which have largely lost their identification with their fibrous origins. Apparently at around 50 percent density, there are sufficient sinter bonds per fiber that the material's dependence on them for strength is minimized, yet at the same time the fibrous nature of the material is still influencing its behavior in a major way.

Further confirmation of the desirable influence of screen is shown in Figure I-22, which compares the results obtained above on 0.125 in. (0.318 cm) thick specimens with those obtained on specimens 0.020 to 0.040 in. (0.051-0.102 cm) thick. As expected, the thin materials generally show still greater elongation to failure.

Damping capacity.- It is obvious from the "dead" feel of fiber metal that it has high damping properties in comparison with solid metal. The torsional damping capacities obtained from oscillation data are shown in Figures I-23 through I-25. Low density samples with a minimum of interfiber bonding, in general, have the greatest damping capacity. However, the metallurgical properties of the individual fibers appear to have a major effect on damping capacity as evidenced by the extremes of damping capacity measured for the two conditions of the aluminum fiber metal, Figure I-25.

Figure I-23 shows small increases in damping capacity with the addition of screen reinforcement, with increased thickness, and when the sample was cut transversely to the rolling direction. However, Figure I-24 shows that there is no significant effect of sample orientation, with materials made from C18 fibers. No consistent effect of fiber diameter is apparent.

Conclusions

The following conclusions can be derived from the graphical interpretation of the data which resulted from the 52 samples employed in this study.

1. The ultimate tensile strength (UTS), yield strength (S), Young's modulus (E), and shear modulus (G) of fiber metal increase exponentially with apparent density when the material has been metallurgically bonded at or close to the final density of the fiber metal. Graphical correlations indicate that these values vary approximately with the cubic power of the apparent density.

2. These mechanical properties increase only linearly with apparent density when materials are produced by bonding at a single, low density followed by compaction only to the higher density.

3. There is no effect of sample orientation within a sheet of unreinforced fiber metal; it is isotropic in the plane of the sheet due to the random orientation of the fibers.

4. Screen reinforcement of fiber metal increases the strength and modulus in proportion to the percentage of screen in the material. As a result, the largest effect of screen reinforcement is observed in low density or thin materials.

5. Prestraining of fiber metal increases yield strength and elastic modulus by reorientation of the fibers in the direction of strain.

6. Sample thickness has no significant effect on the measured properties of fiber metal except damping capacity which decreases with decreasing thickness.

7. Torsional damping capacity is increased with decreasing apparent density and increased thickness and with the use of annealing and screen reinforcement.

8. Maximum ductility is achieved at apparent densities near 50 percent. At higher densities, reduced elongations are observed because fiber metal has smaller pores; it looks and behaves more like porous castings. At low densities, premature failure of interfiber bonds causes reduced elongations. Elongation is increased with screen reinforcement and with a higher fiber L/D ratio.

TABLE I-I

MECHANICAL PROPERTIES OF FIBER METAL

Alloy and fiber type	Specimen apparent density	Tensile testing: Yield strength, psi x 10^3	Yield strength, MN/m^2	Ultimate strength, psi x 10^3	Ultimate strength, MN/m^2	Elongation, percent	Young's modulus, psi x 10^6	Young's modulus, MN/m^2	Shear modulus, psi x 10^6	Shear modulus, MN/m^2	Damping capacity coeff
347 SS C18	11.4	0.38	2.62	1.07	7.37	5.1	0.16	1 120	0.03	210	0.295
	25.8	2.40	16.55	3.70	25.50	11.0	0.38	2 340	--	--	--
	47.2	2.88	19.85	9.65	66.50	12.5	2.07	14 250	0.64	4 410	0.485
	61.5	11.30	77.90	22.00	151.50	13.0	3.00	23 300	--	--	--
	79.4	18.20	125.50	36.50	251.50	5.4	10.50	72 500	3.97	27 350	0.275
347 SS C38	11.3	0.05	0.35	0.19	1.31	1.2	0.05	340	0.01	690	0.590
	25.4	0.78	5.38	0.83	5.72	--	0.19	1 310	--	--	--
	42.8	3.70	25.50	8.00	55.20	9.3	1.42	9 790	0.53	3 650	0.340
	63.5	10.70	73.70	17.50	120.50	9.0	3.00	22 650	--	--	--
	75.0	16.90	116.40	25.75	177.50	NIL	7.05	48 600	2.44	16 800	0.290
aluminum E58 as brazed	32.7	0.92	6.34	1.26	8.69	0.79	0.51	3 570	0.23	1 590	0.180
	51.3	1.73	11.92	2.45	16.90	0.14	0.85	5 860	0.42	2 890	0.220
	67.0	2.86	19.70	3.15	21.70	1.15	0.88	6 070	0.36	2 480	0.400
aluminum E58 annealed	32.2	0.61	4.21	0.86	5.92	1.46	0.64	4 410	0.19	1 310	0.820
	48.0	0.99	6.83	1.45	10.00	1.52	0.95	6 550	0.33	2 270	1.120
	71.5	0.93	6.41	1.98	13.65	3.00	1.25	8 620	0.31	2 140	1.330

TABLE I-II

EFFECT OF FABRICATION TECHNIQUES ON THE MECHANICAL PROPERTIES OF FIBER METAL

Fabrication technique investigated	Alloy and fiber type	Specimen apparent density	Tensile testing: Yield strength, psi x 10^3	Tensile testing: Yield strength, MN/m^2	Tensile testing: Ultimate strength, psi x 10^3	Tensile testing: Ultimate strength, MN/m^2	Tensile testing: Elongation, percent	Young's modulus, psi x 10^6	Young's modulus, MN/m^2	Shear modulus, psi x 10^6	Shear modulus, MN/m^2	Damping capacity coeff
Rolling direction (specimens transverse to rolling direction)	347 SS C18	45.4	4.27	29.40	8.85	61.00	8.30	2.40	16 550	0.86	5 930	0.38
		80.8	20.85	143.80	25.75	177.50	1.30	10.60	73 100	4.02	27 700	0.41
	347 SS C38	41.0	1.32	9.11	6.25	43.10	10.60	1.00	6 890	0.26	1 790	0.45
		77.9	17.70	121.90	25.35	174.80	6.45	7.80	53 700	2.67	18 400	0.33
Fiber metal thk (.062 in.(.159 cm) vs test .125 in.(.317 cm))	347 SS C38	25.0	0.99	6.82	1.17	8.07	1.00	0.36	2 480	0.06	410	0.43
		35.0	1.79	12.35	3.20	22.05	4.01	--	--	0.26	1 790	0.32
		77.8	16.95	116.80	22.52	155.20	3.75	8.60	59 300	3.29	22 650	0.21
Effect of screen reinforcement (18 mesh - .009 in. (.023 cm) wire)	347 SS C38	14.7	0.50	3.45	0.85	5.86	16.88	0.45	3 100	0.02	140	0.48
		47.1	4.40	30.35	10.15	70.10	13.30	2.60	17 930	0.58	3 990	0.39
		78.2	19.81	136.40	27.80	191.50	2.00	9.10	62 700	3.16	21 750	0.31

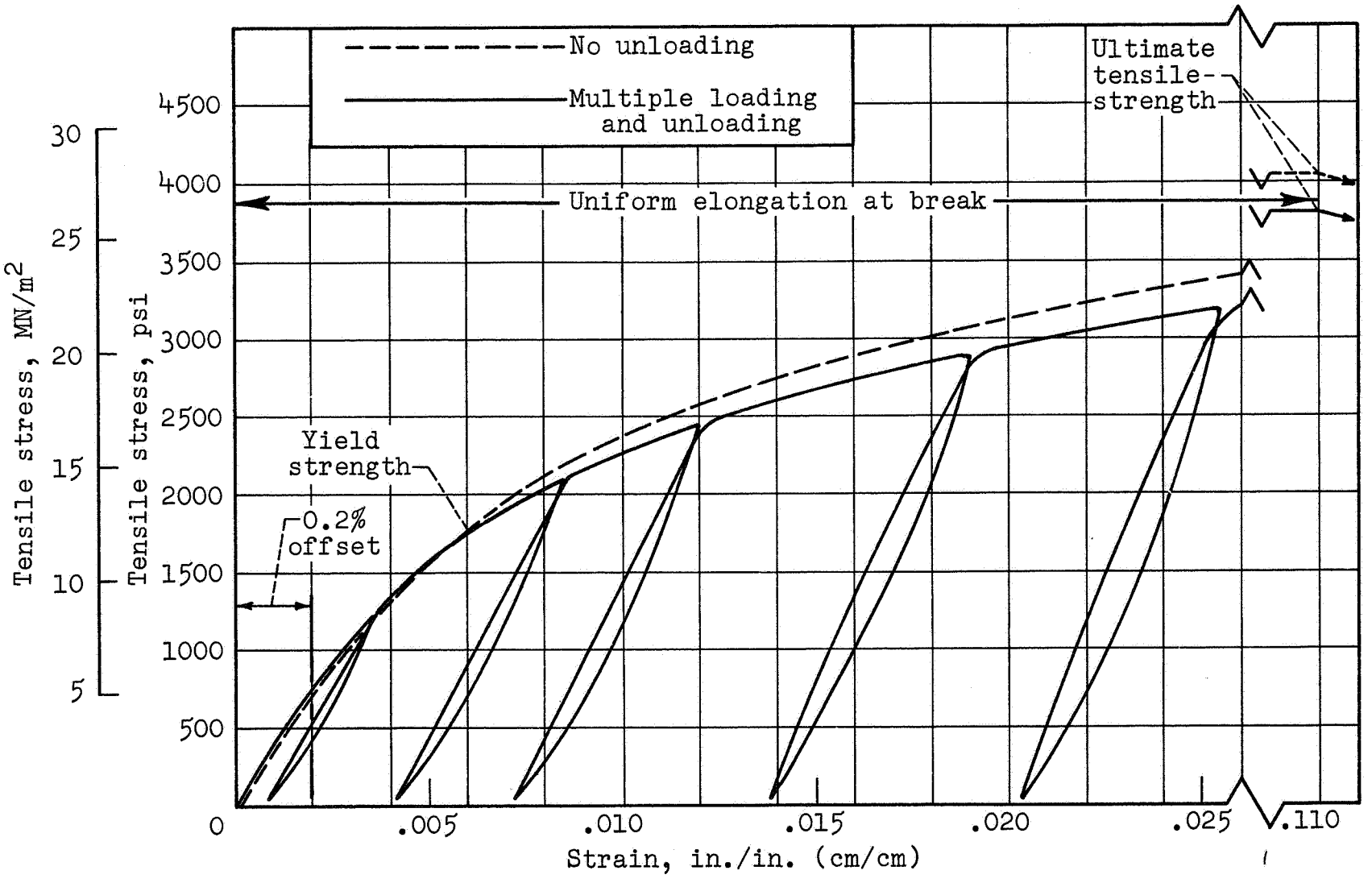

FIGURE I-1

TYPICAL STRESS - STRAIN PLOT FOR 347SS
FIBER METAL, 25.8 PERCENT DENSE C18 FIBER

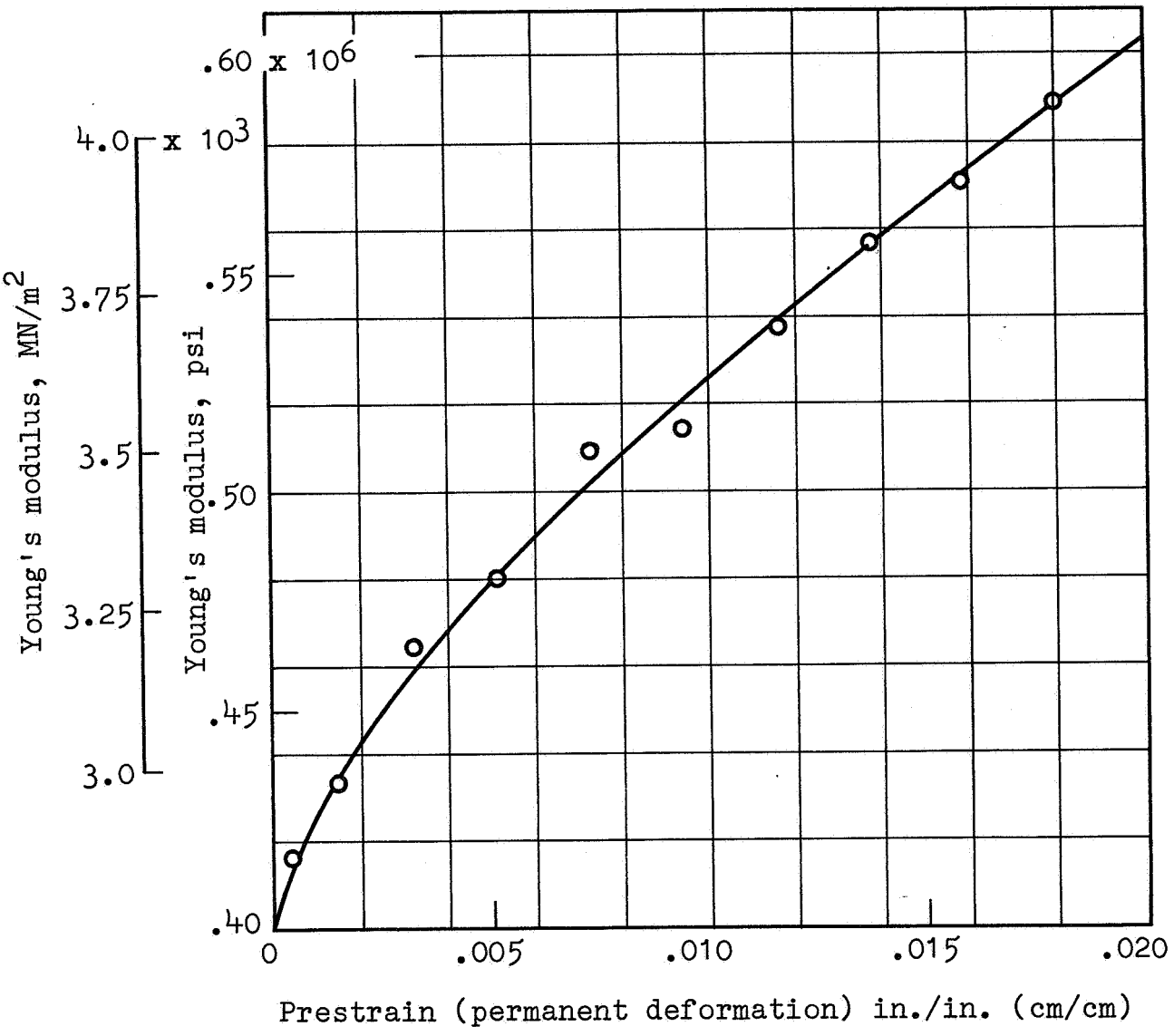

FIGURE I-2

EFFECT OF PRESTRAIN ON YOUNG'S MODULUS OF
347SS FIBER METAL, 25.8 PERCENT DENSE C18 FIBER

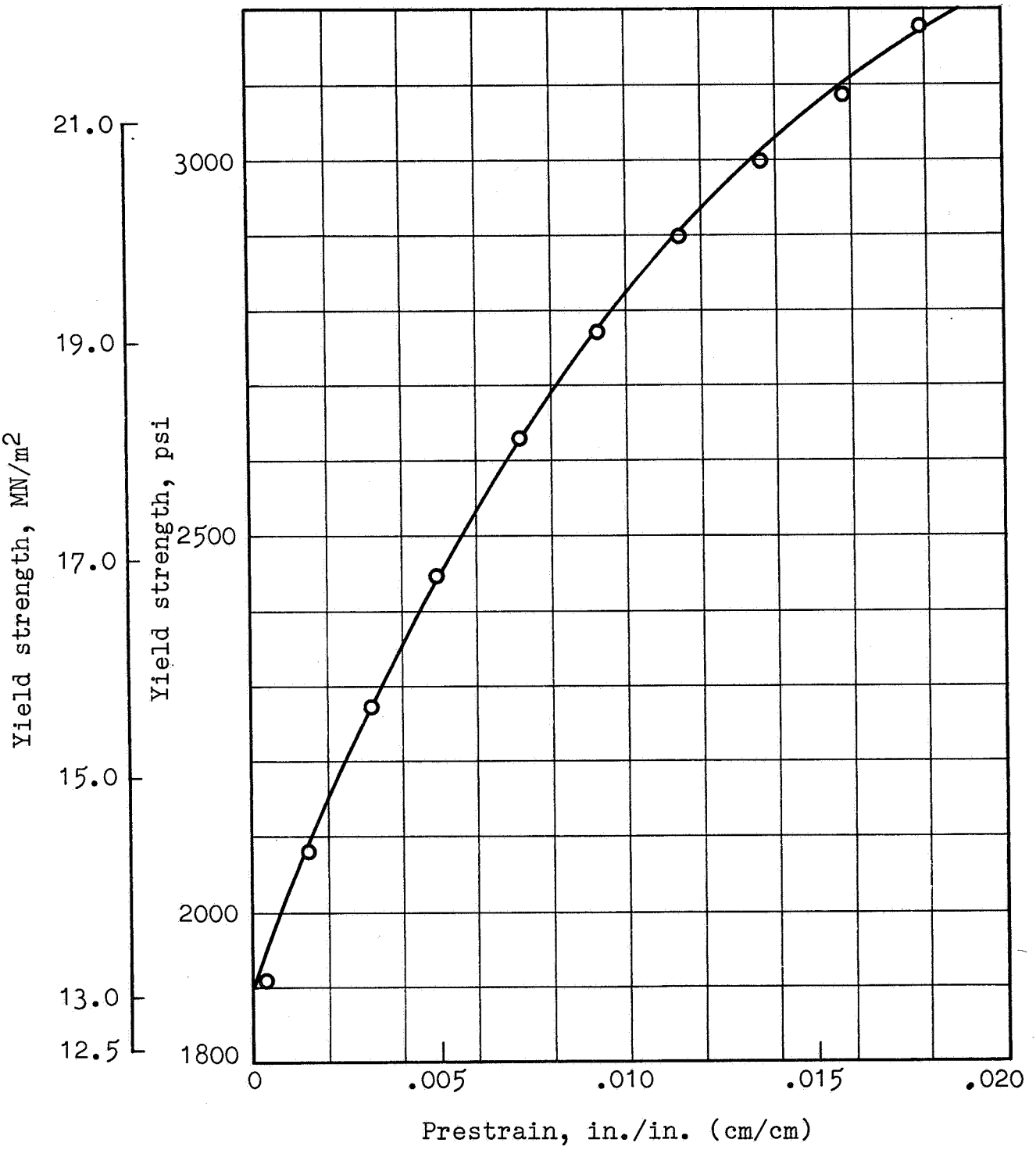

FIGURE I-3

EFFECT OF PRESTRAIN ON THE YIELD STRENGTH OF 347SS FIBER METAL, 25.8 PERCENT DENSE C18 FIBER

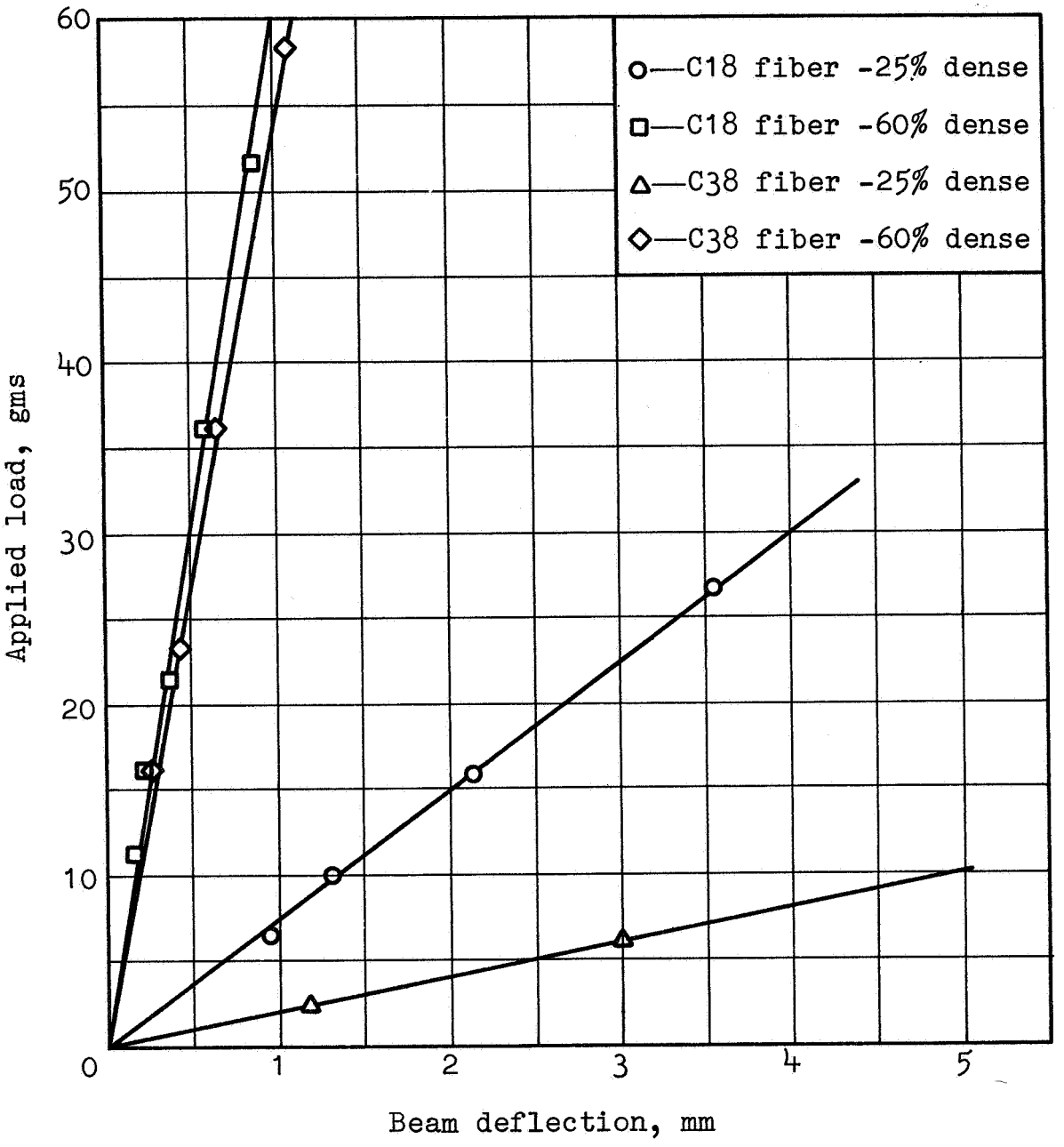

FIGURE I-4

CANTILEVER BEAM DEFLECTION TESTING FOR
YOUNG'S MODULUS DETERMINATION, 347SS FIBER METAL

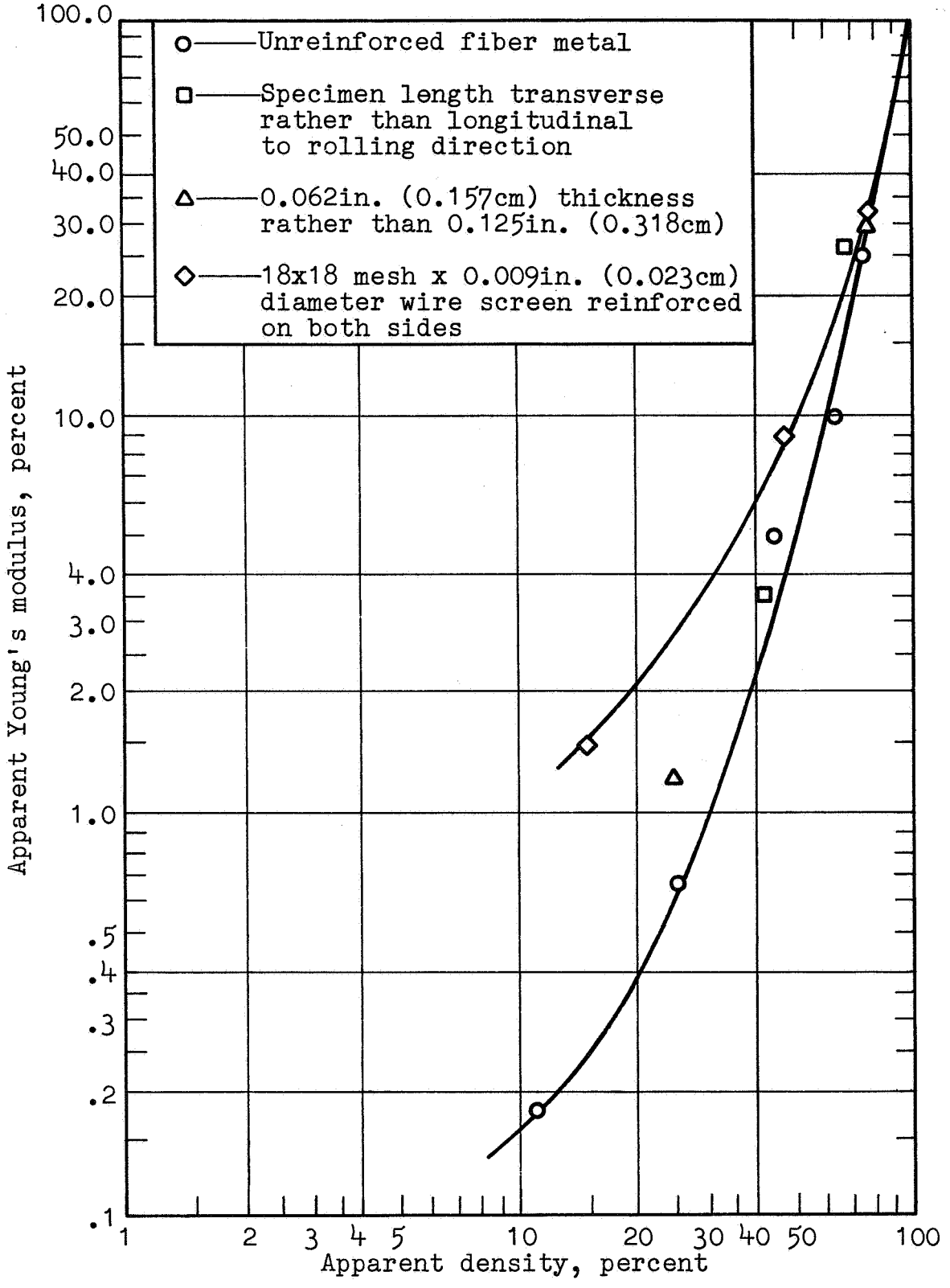

FIGURE I-5.- APPARENT YOUNG'S MODULUS VS APPARENT DENSITY, 347SS FIBER METAL TYPE C38 FIBER

FIGURE I-6

PHOTOMICROGRAPH OF FM128A FIBER METAL ACOUSTICAL MATERIAL, 347SS-TYPE C18 FIBER WITH 18 MESH x 0.009 in. (0.023cm) DIAMETER WIRE SCREEN REINFORCEMENT ON BOTH SIDES-x56

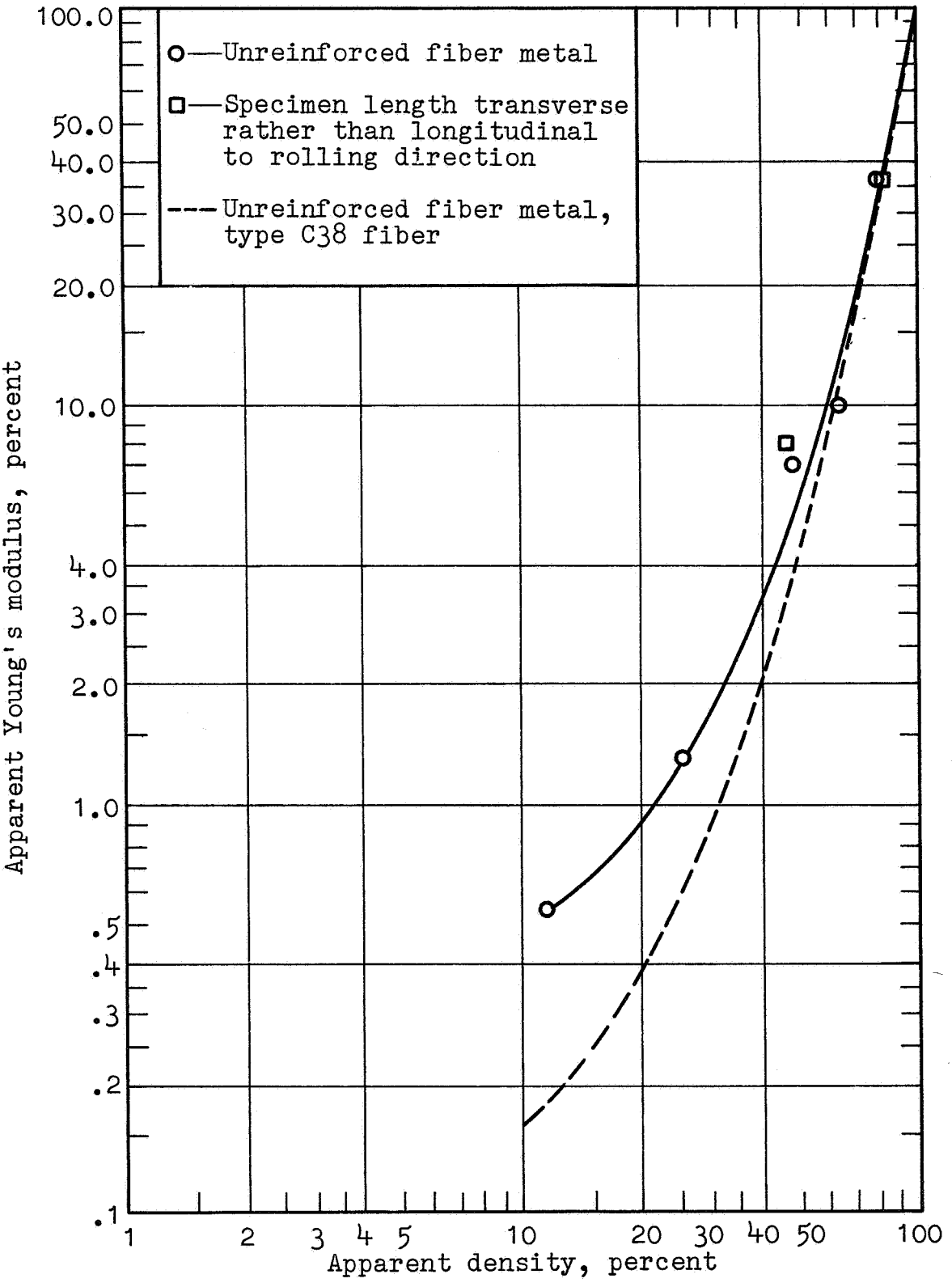

FIGURE I-7.- APPARENT YOUNG'S MODULUS VS APPARENT DENSITY, 347SS FIBER METAL TYPE C18 FIBER

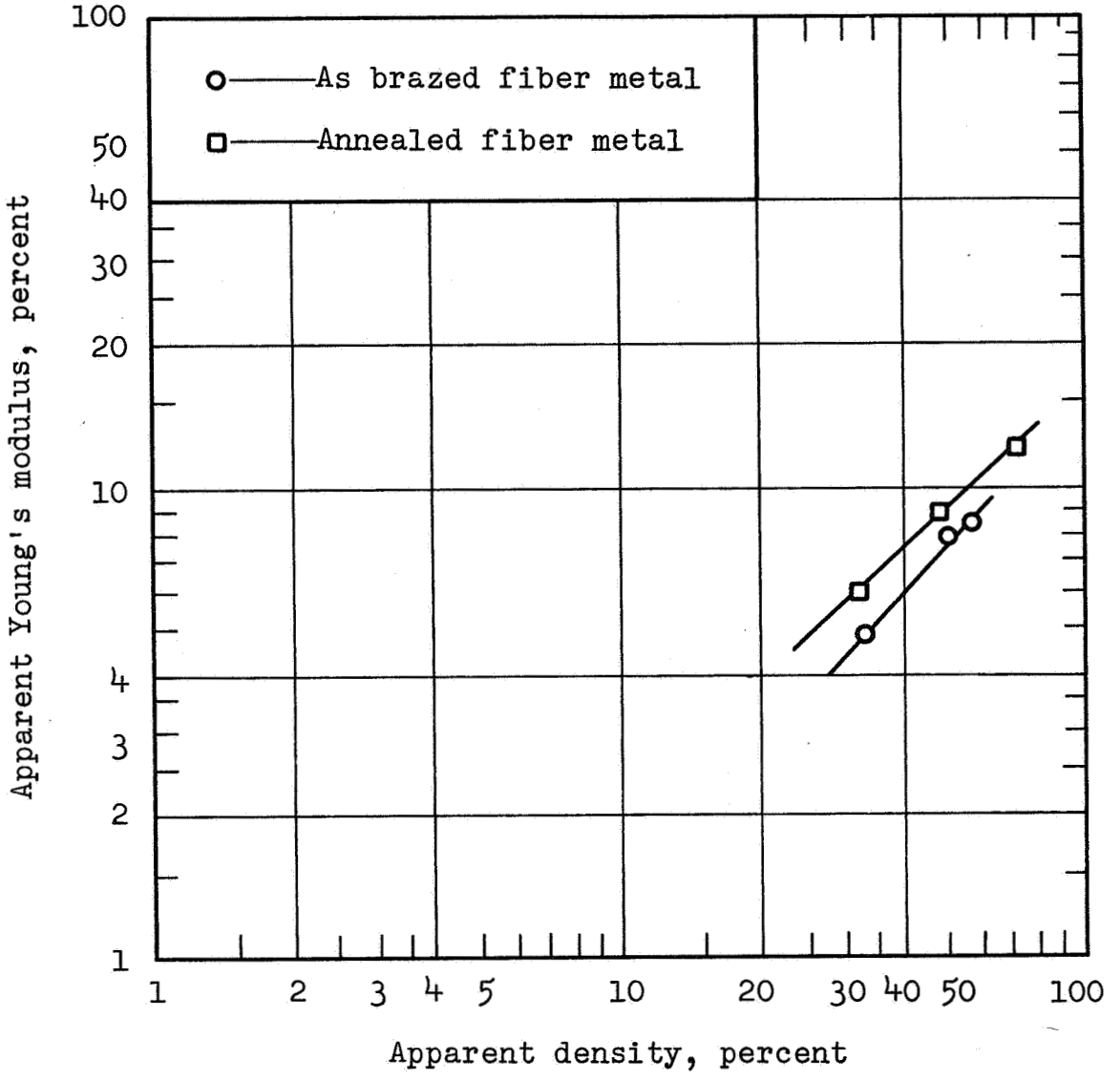

FIGURE I-8

APPARENT YOUNG'S MODULUS VS APPARENT DENSITY,
ALUMINUM FIBER METAL TYPE E58 FIBER

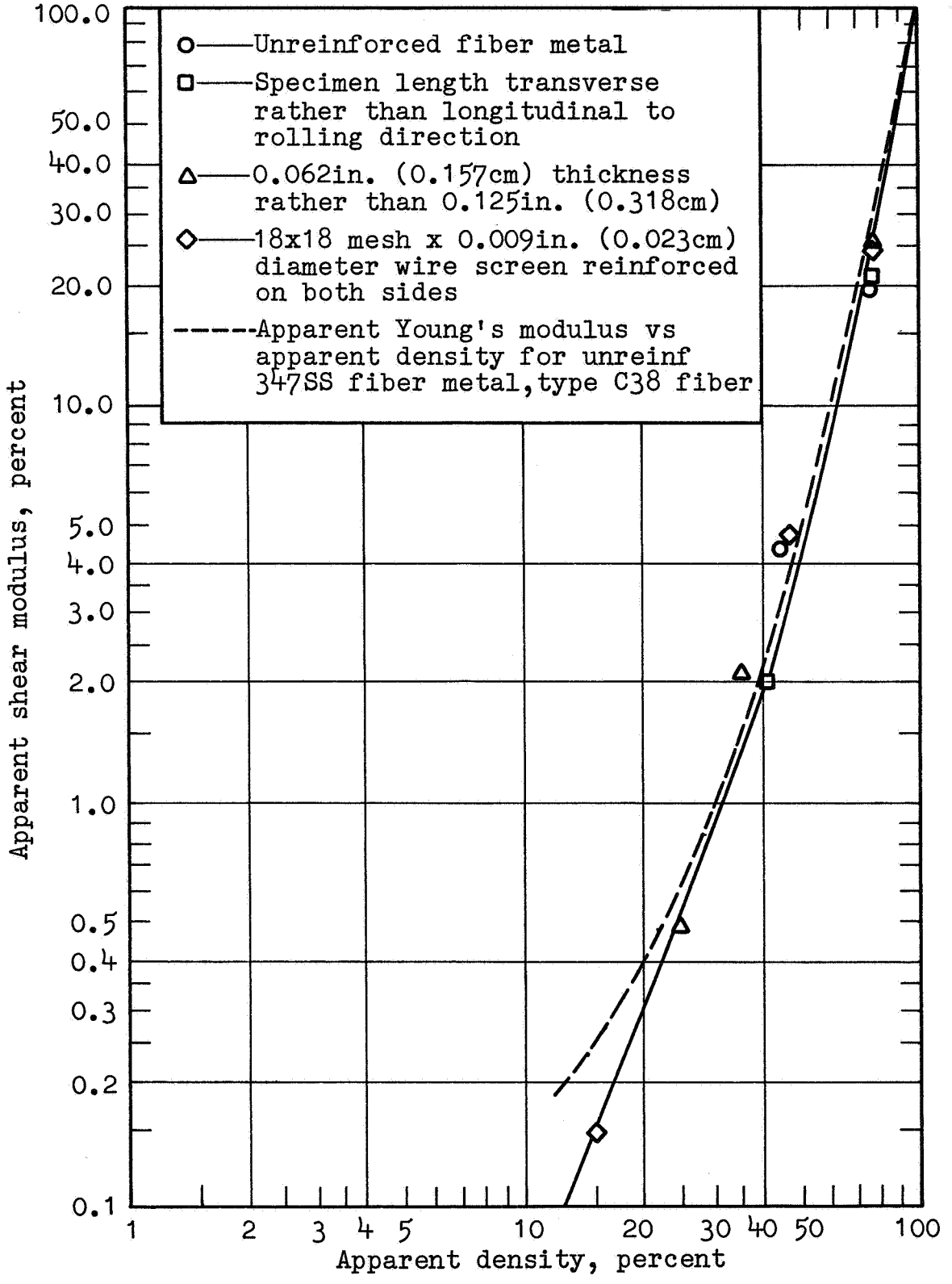

FIGURE I-9.- APPARENT SHEAR MODULUS VS APPARENT DENSITY, 347SS FIBER METAL TYPE C38 FIBER

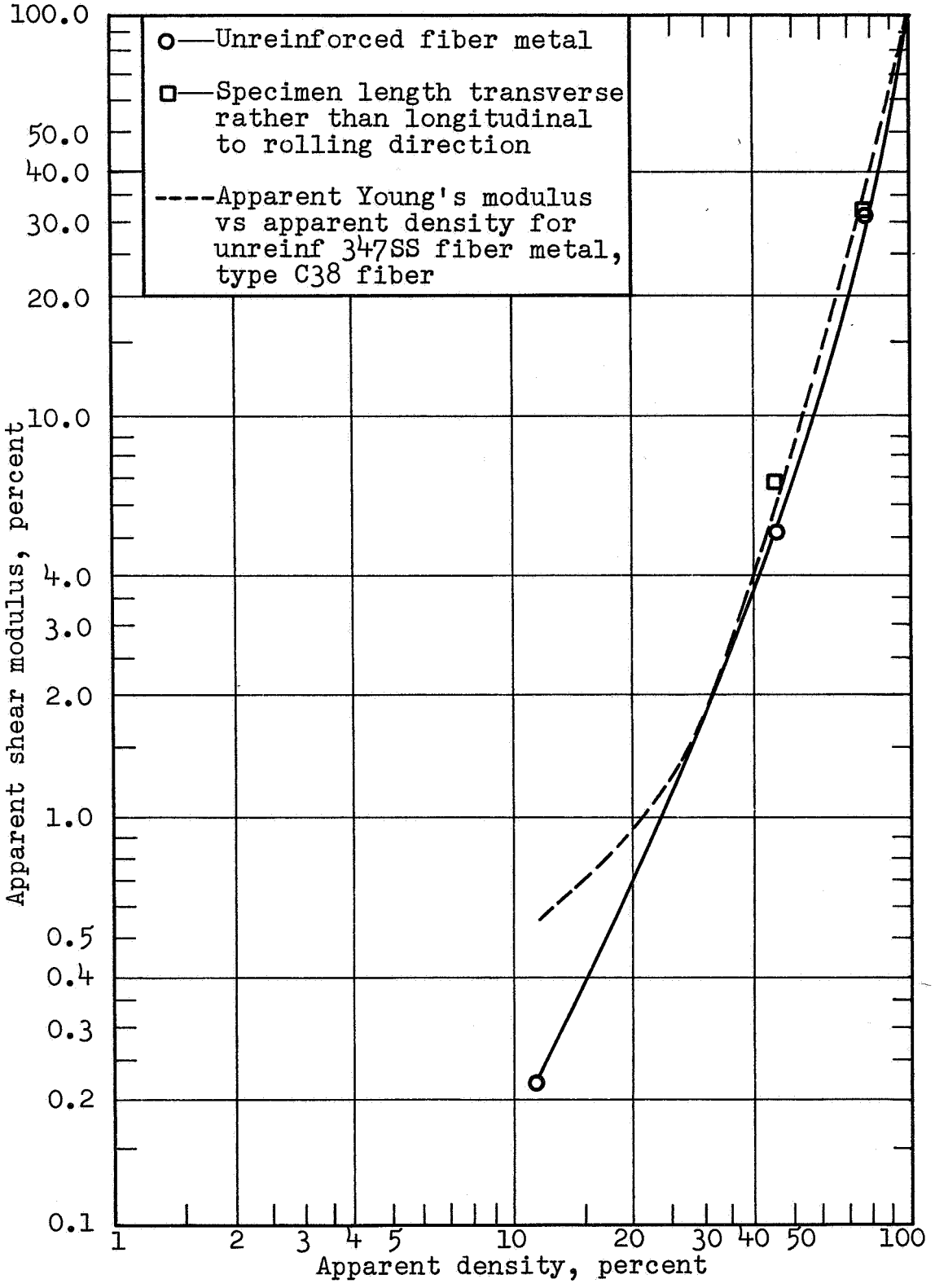

FIGURE I-10.- APPARENT SHEAR MODULUS VS APPARENT DENSITY, 347SS FIBER METAL TYPE C18 FIBER

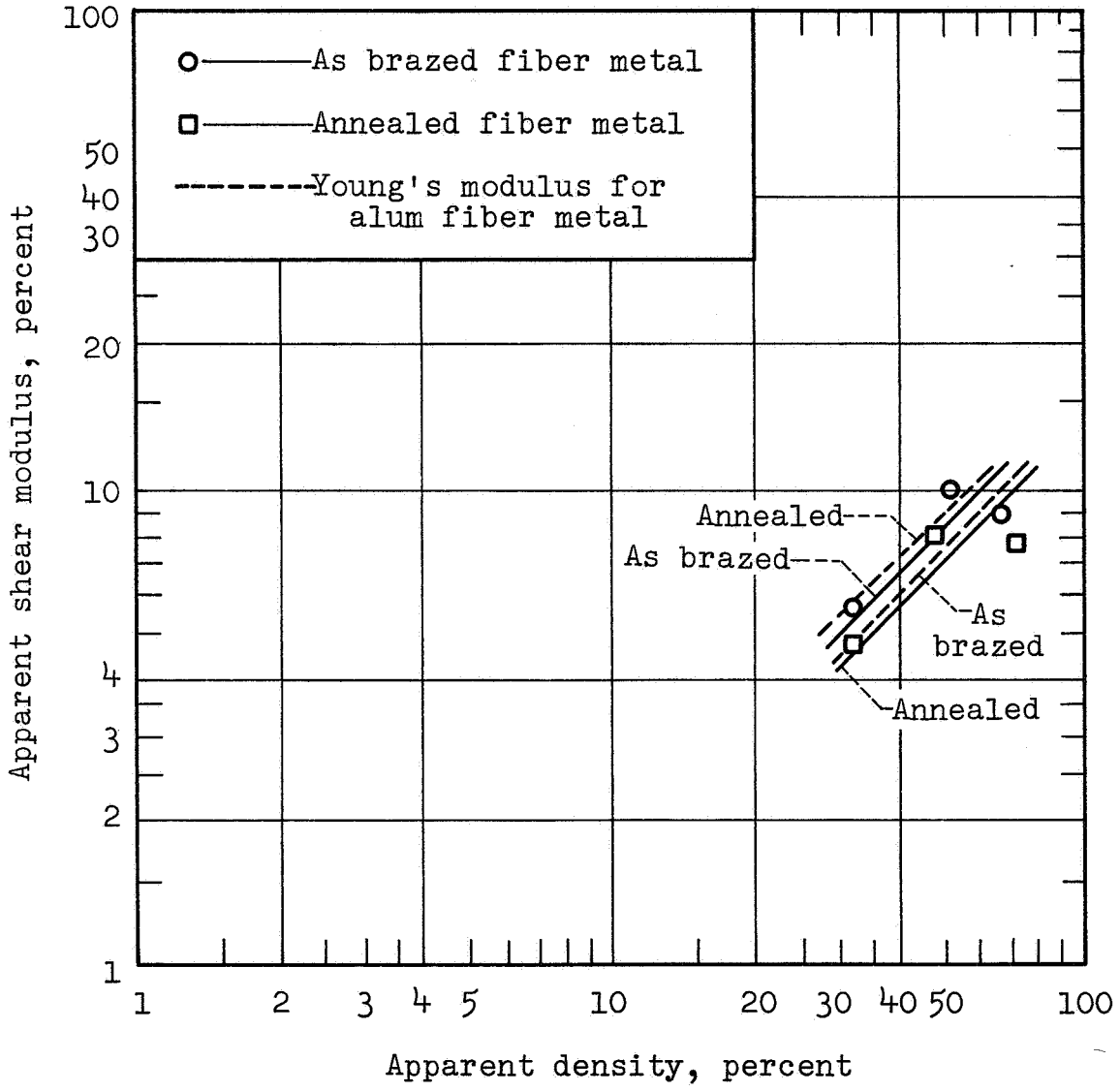

FIGURE I-11

APPARENT SHEAR MODULUS VS APPARENT DENSITY,
ALUMINUM FIBER METAL TYPE E58 FIBER

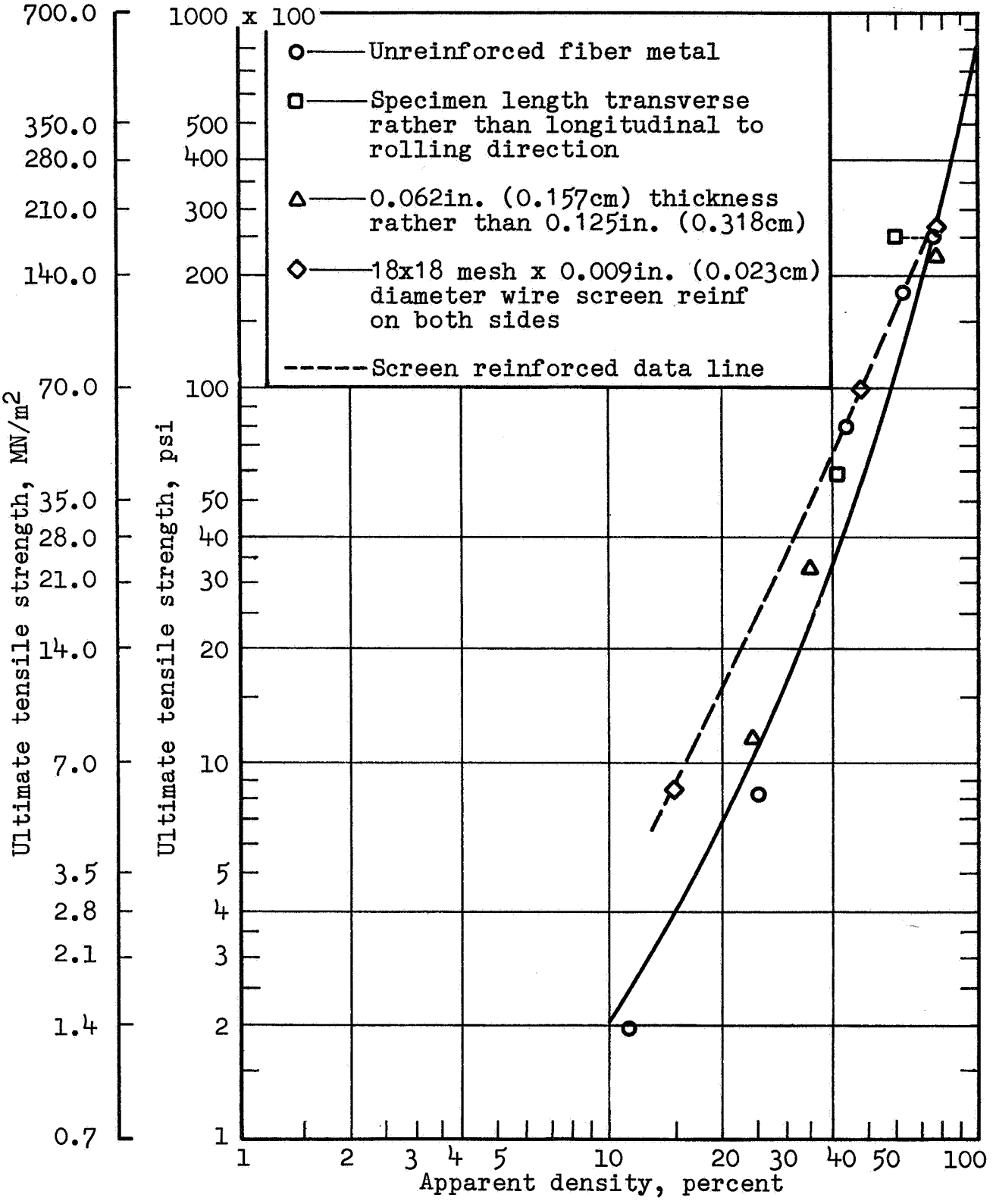

FIGURE I-12.- INFLUENCE OF APPARENT DENSITY ON ULTIMATE TENSILE STRENGTH, 347SS FIBER METAL - C38 FIBER

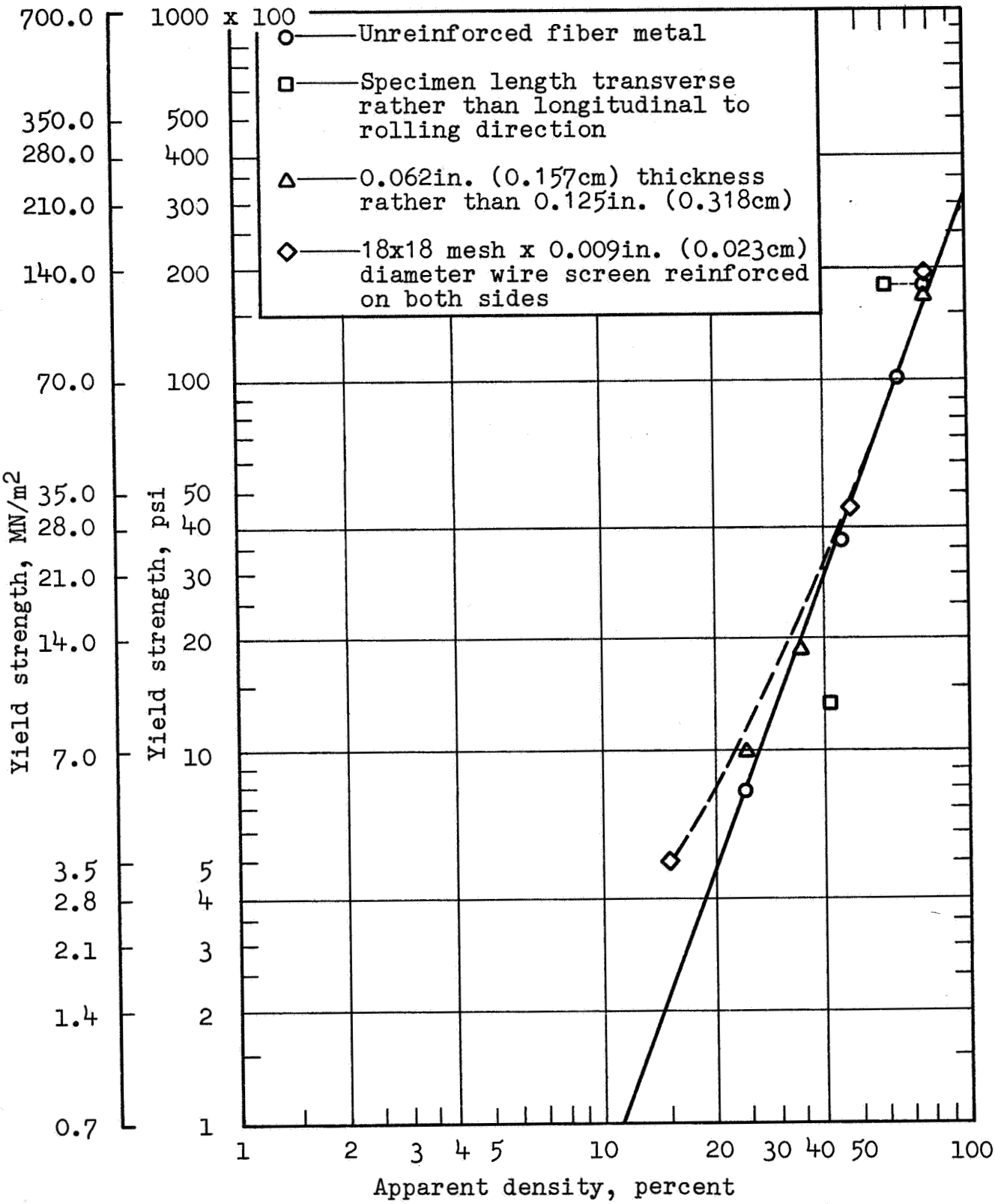

FIGURE I-13.- INFLUENCE OF APPARENT DENSITY ON YIELD STRENGTH, 347SS FIBER METAL - C38 FIBER

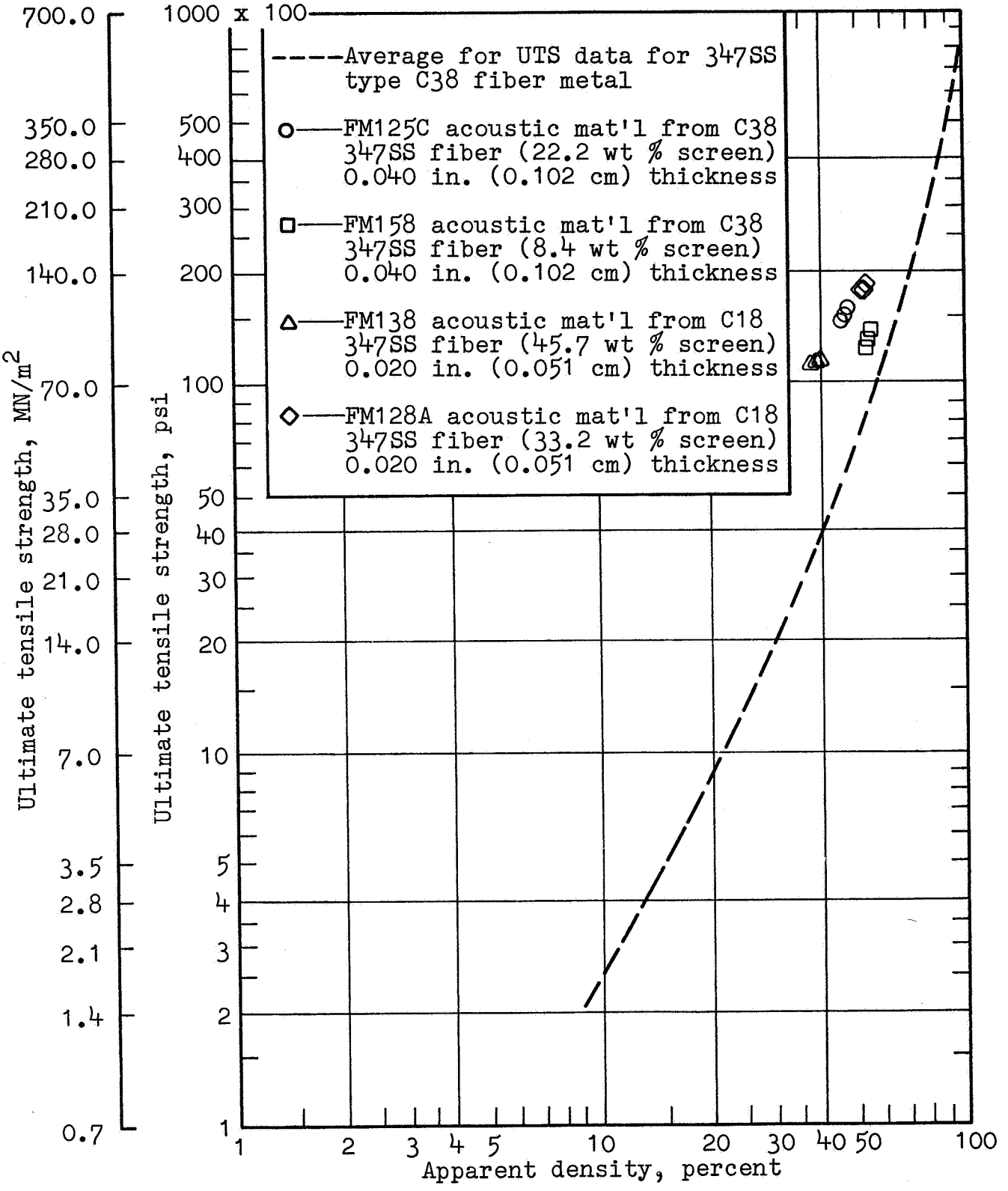

FIGURE I-14.- INCREASE IN ULTIMATE STRENGTH OF THIN 347SS FIBER METAL BY WIRE SCREEN REINFORCEMENT

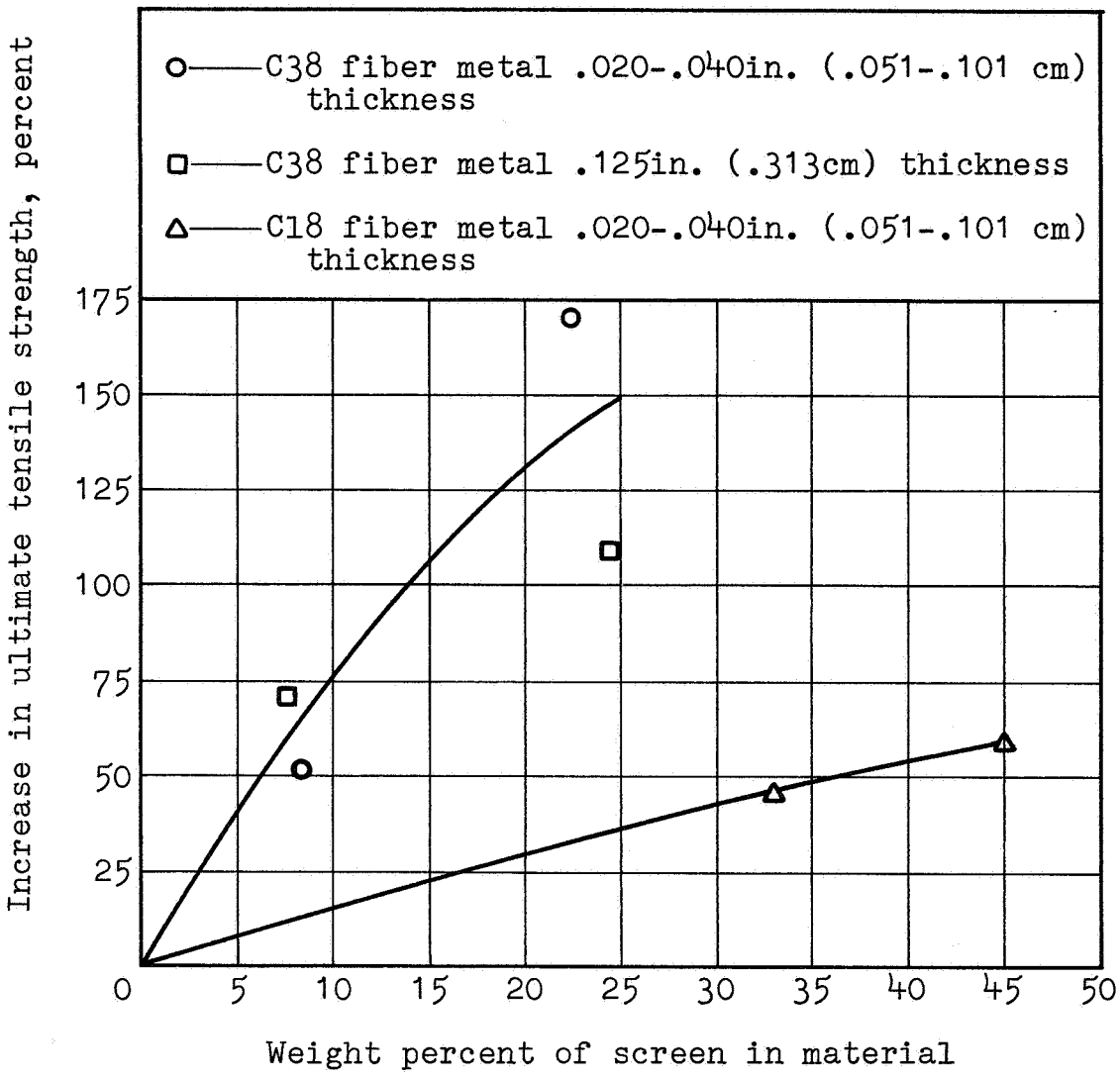

FIGURE I-15

INCREASE IN ULTIMATE TENSILE STRENGTH CAUSED BY 18x18 MESH x .009 in. (.023 cm) DIAM WIRE SCREEN REINFORCEMENT, TYPE 347SS FIBER METAL

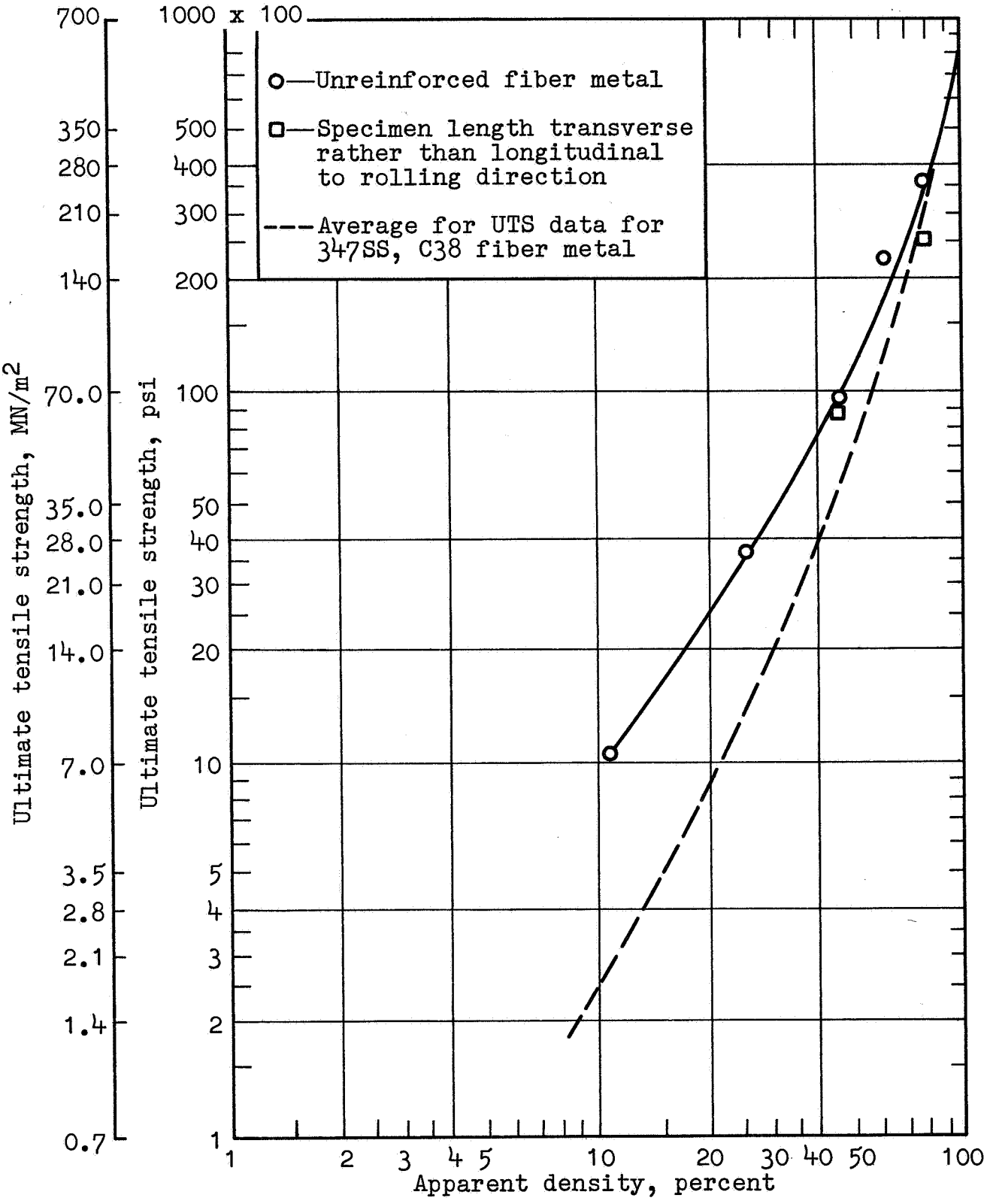

FIGURE I-16.- INFLUENCE OF APPARENT DENSITY ON ULTIMATE TENSILE STRENGTH, 347SS FIBER METAL - C18 FIBER

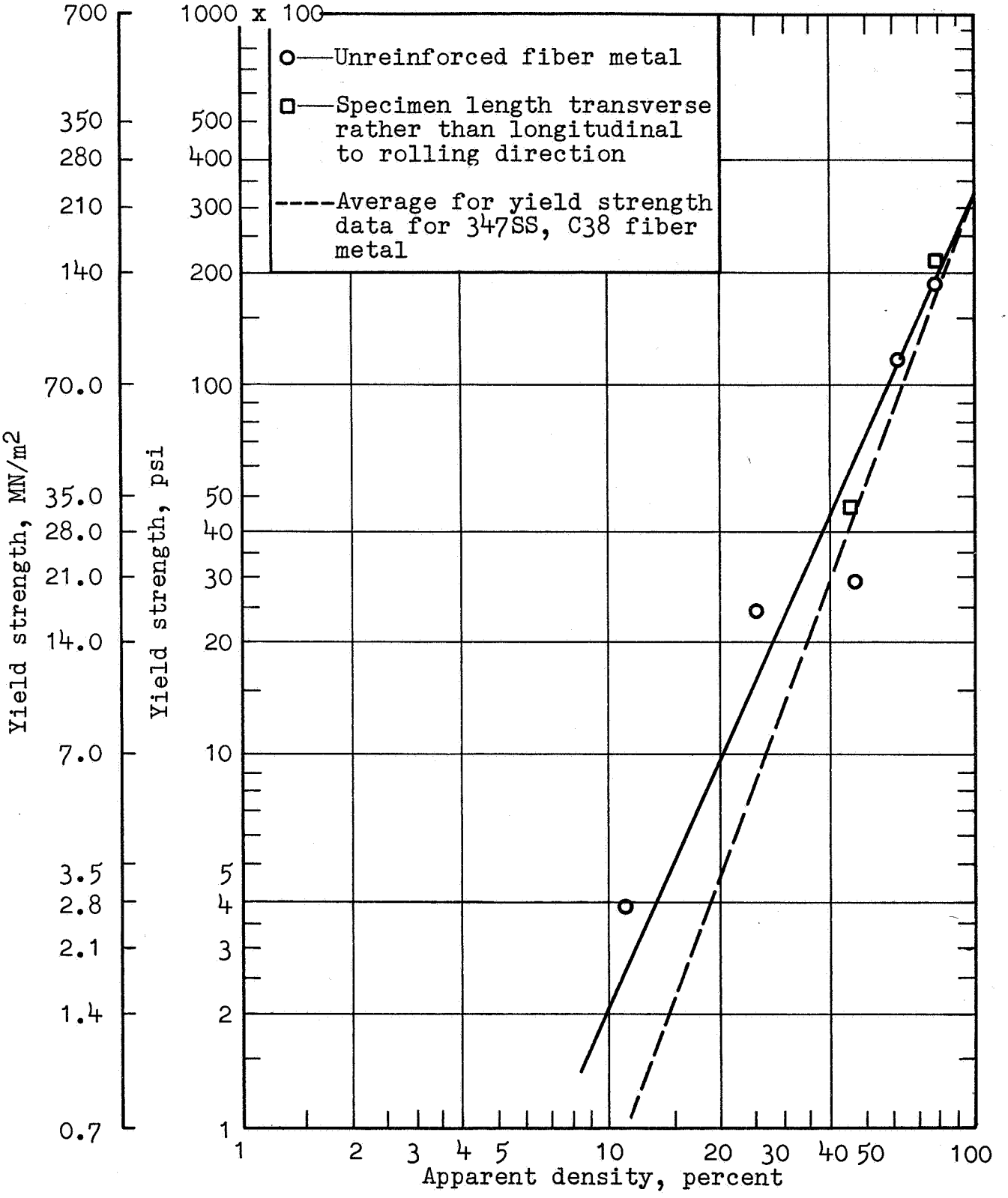

FIGURE I-17.- INFLUENCE OF APPARENT DENSITY ON YIELD STRENGTH, 347SS FIBER METAL - C18 FIBER

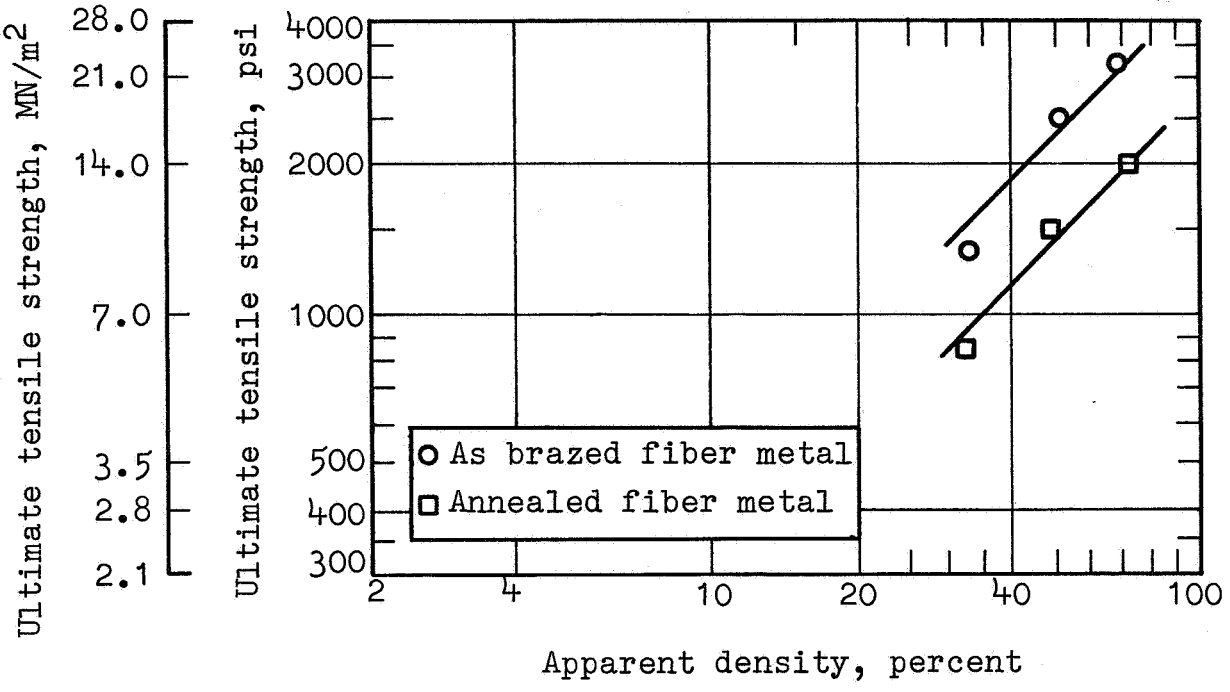

FIGURE I-18.- INFLUENCE OF APPARENT DENSITY ON UTS, ALUMINUM FIBER METAL - E58 FIBER

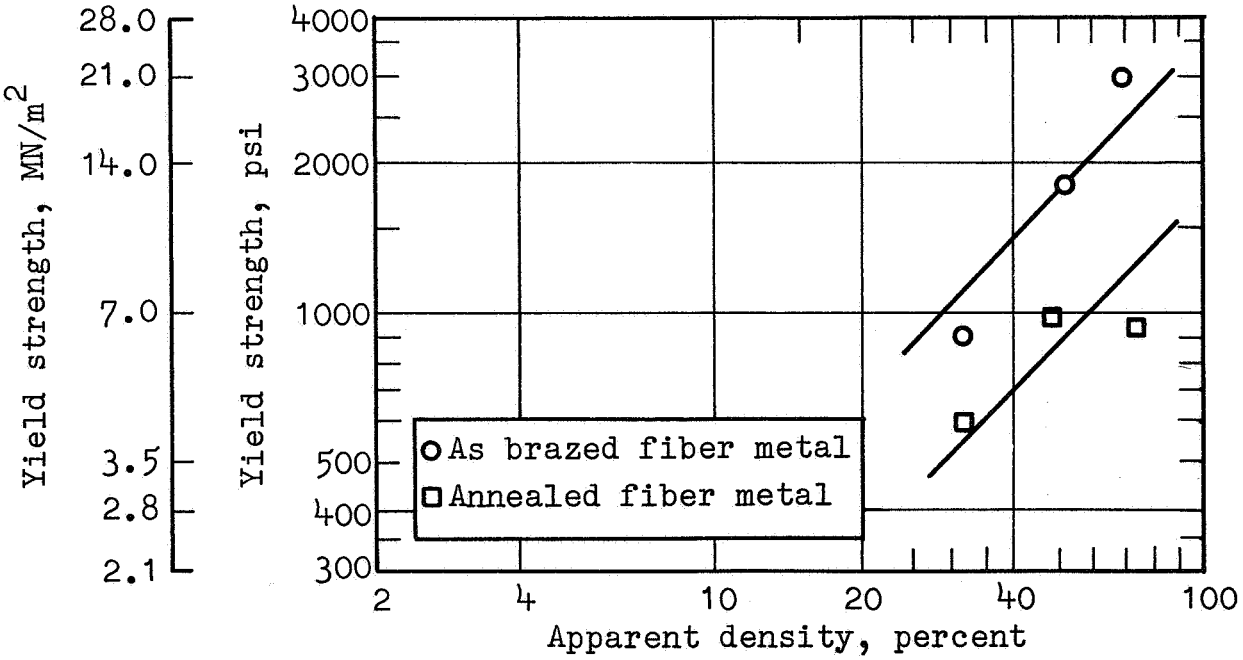

FIGURE I-19.- INFLUENCE OF APPARENT DENSITY ON YIELD STRENGTH, ALUMINUM FIBER METAL - E58 FIBER

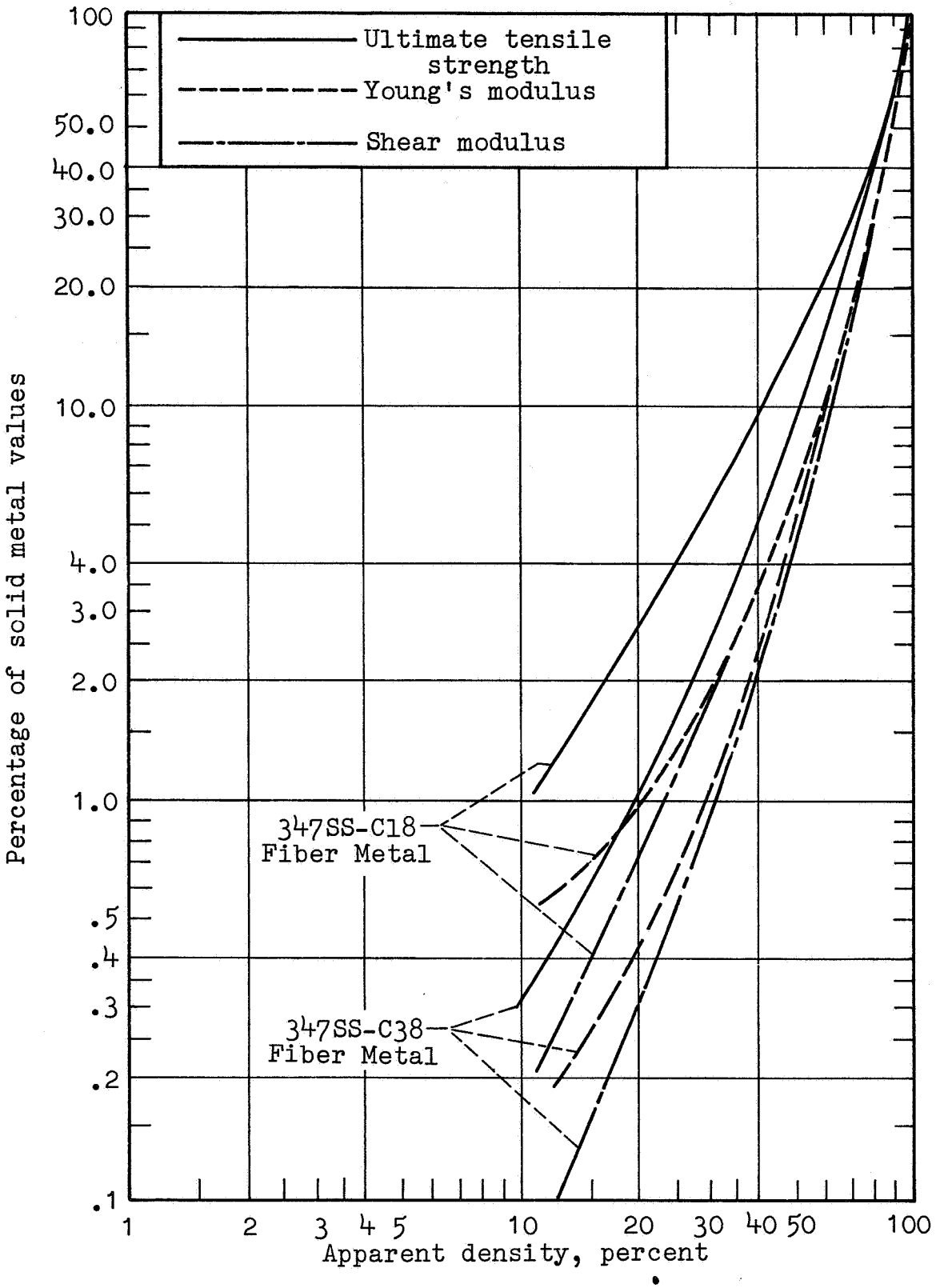

FIGURE I-20.- APPARENT VALUES OF ULTIMATE TENSILE STRENGTH, YOUNG'S, AND SHEAR MODULUS FOR FIBER METAL

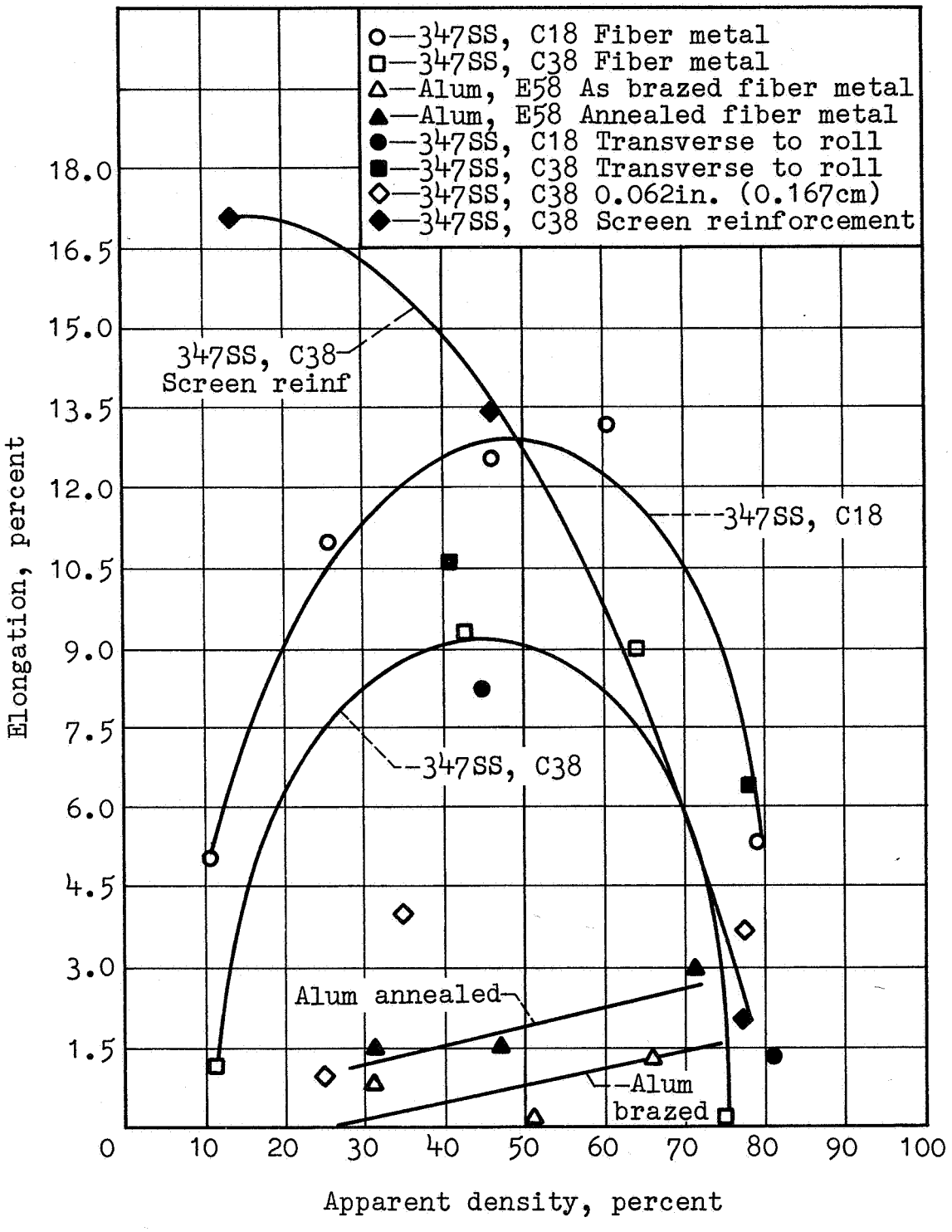

FIGURE I-21

INFLUENCE OF APPARENT DENSITY ON ELONGATION OF FIBER METAL, 7.0in. (17.8cm) TEST GAUGE LENGTH

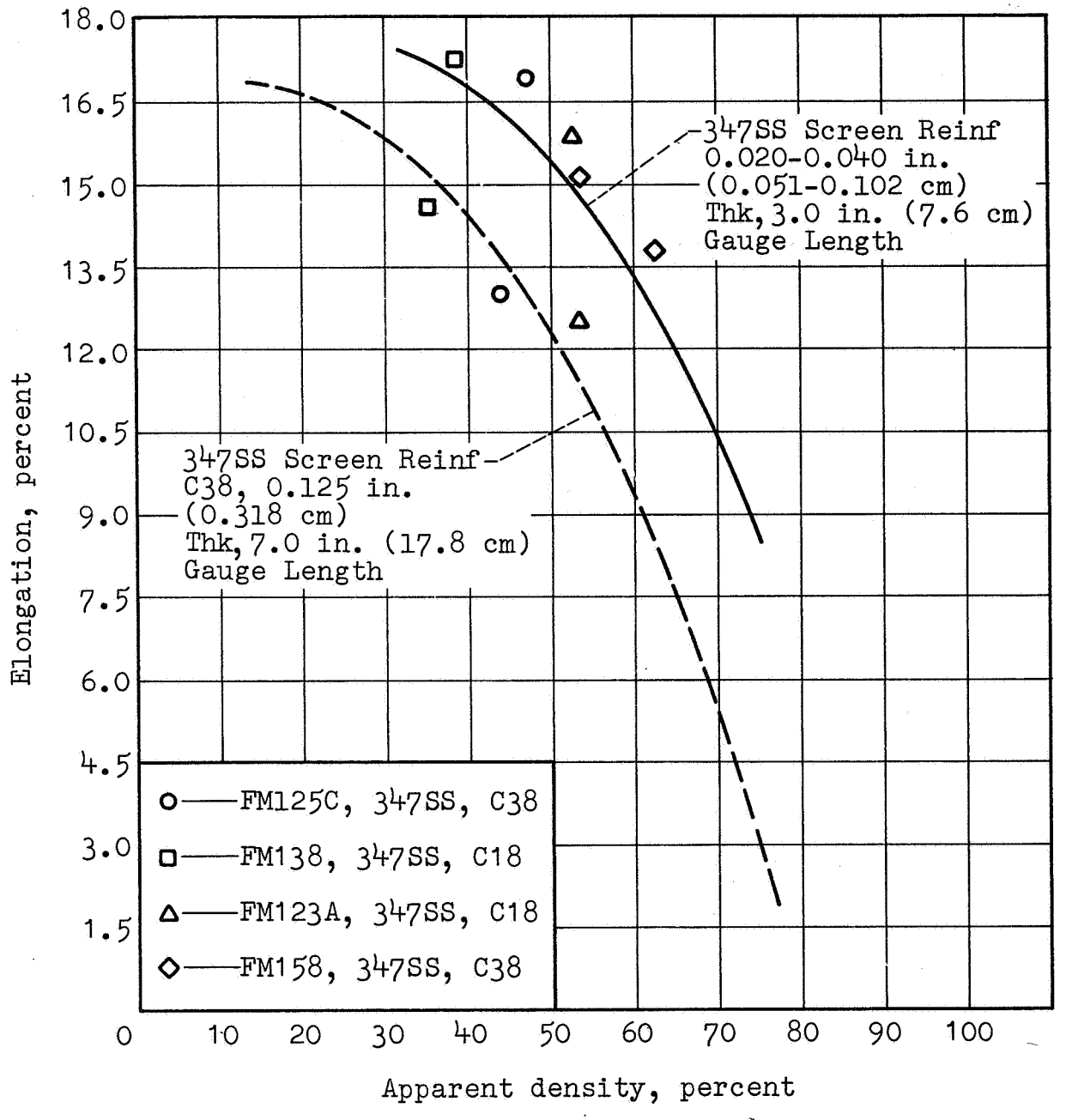

FIGURE I-22

EFFECT OF THICKNESS ON THE
DUCTILITY OF SCREEN REINFORCED
TYPE 347SS FIBER METAL MATERIALS

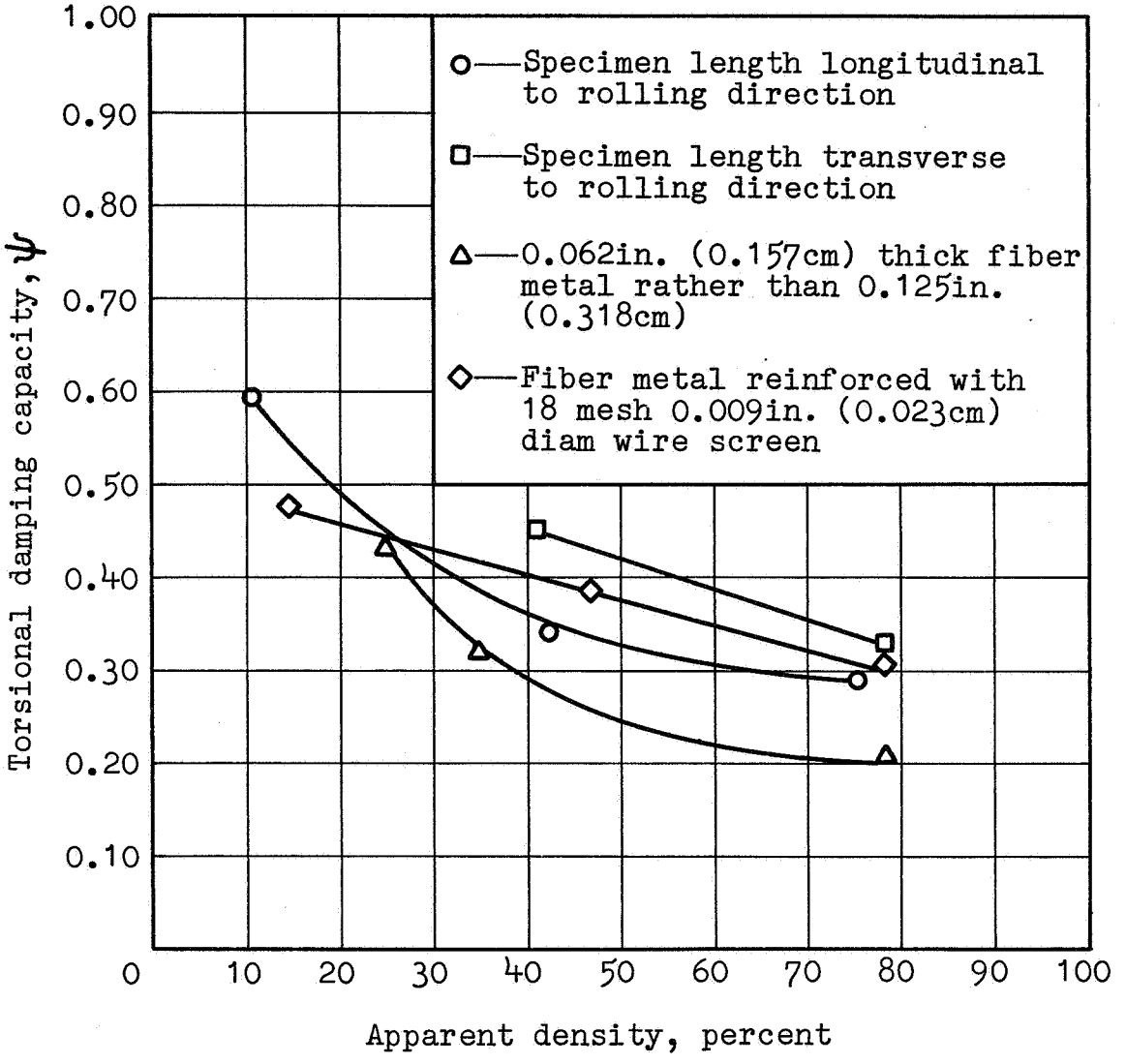

FIGURE I-23

TORSIONAL DAMPING CAPACITY
OF 347SS TYPE C38 FIBER METAL

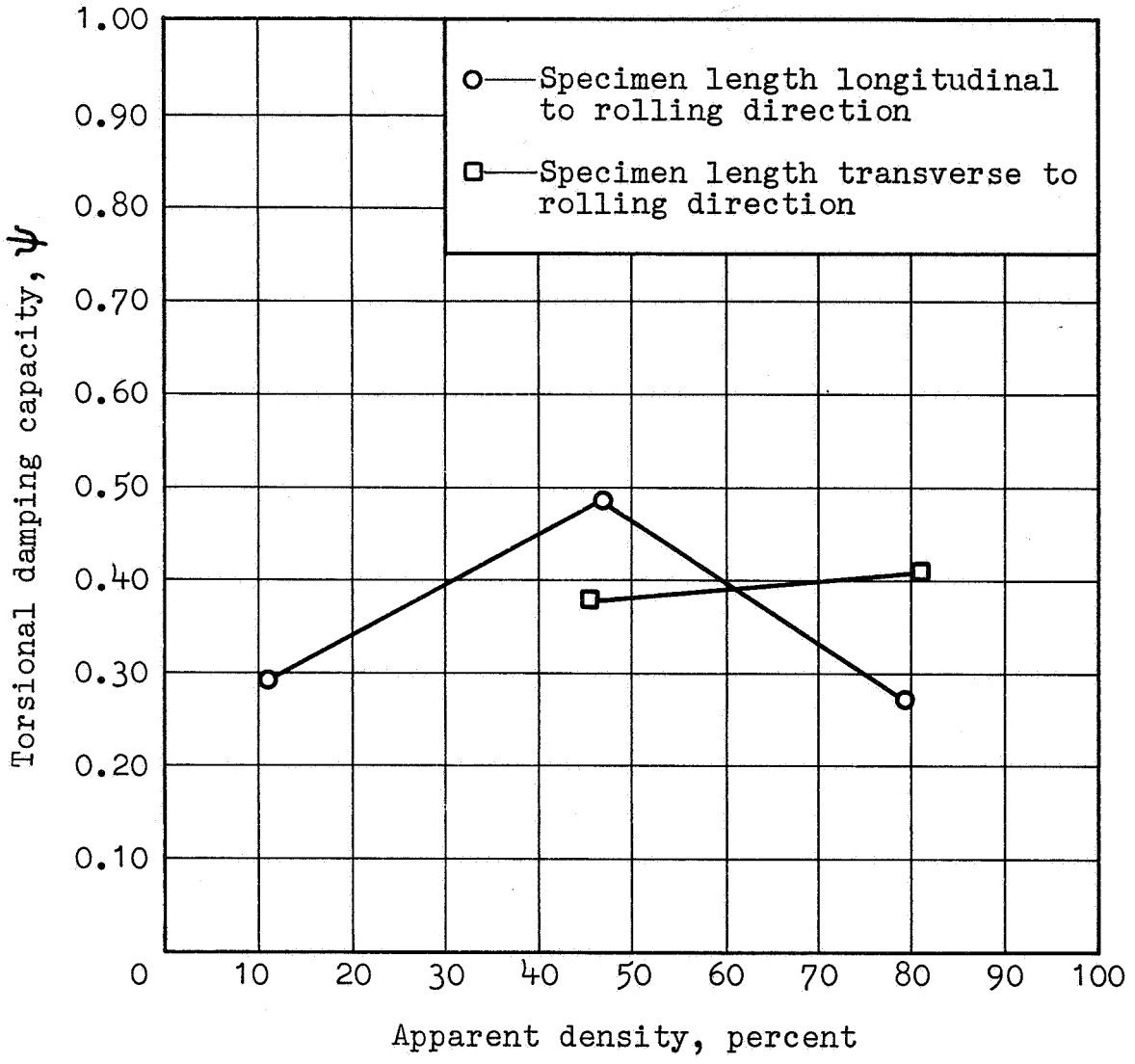

FIGURE I-24

TORSIONAL DAMPING CAPACITY
OF 347SS TYPE C18 FIBER METAL

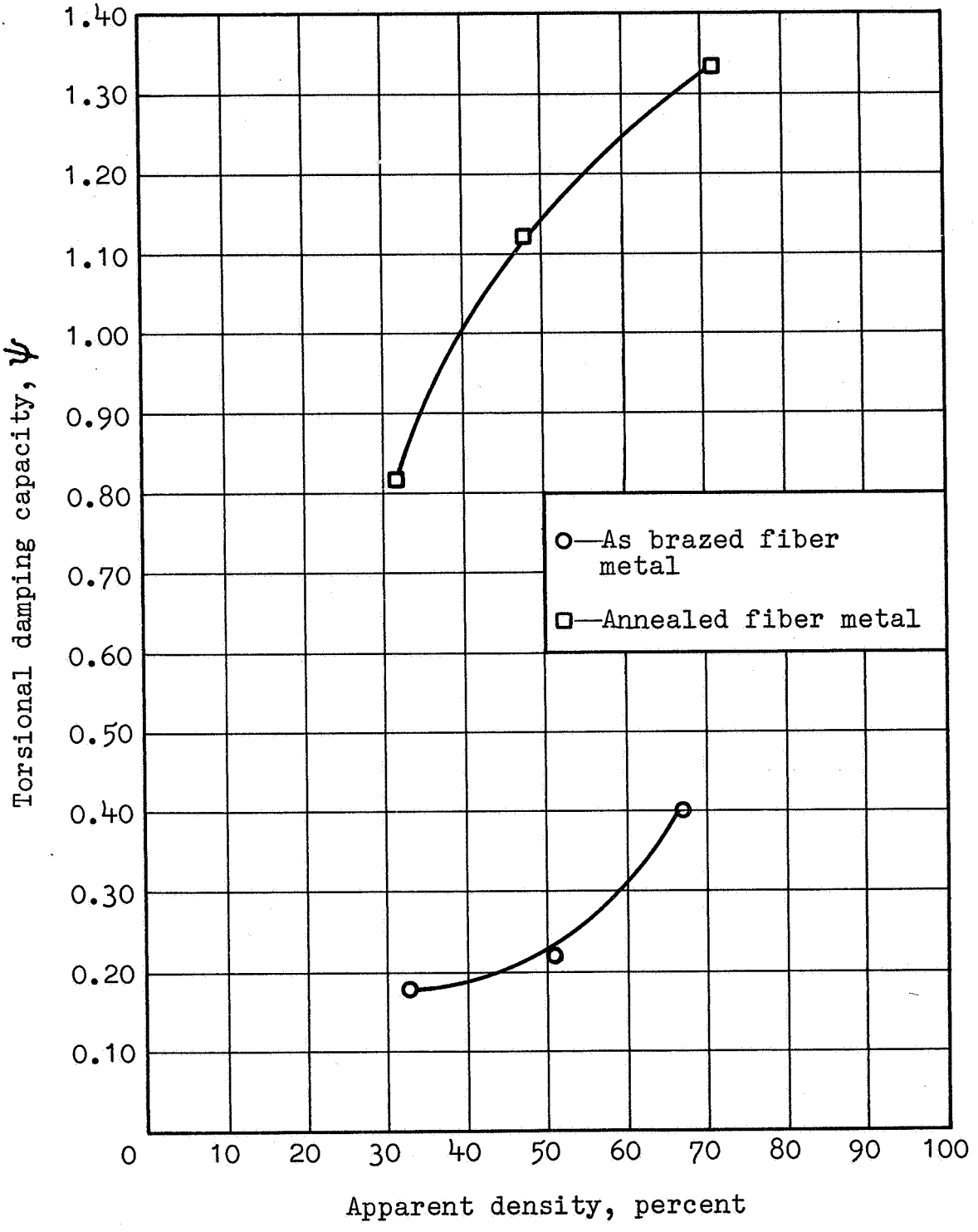

FIGURE I-25

TORSIONAL DAMPING CAPACITY OF
ALUMINUM TYPE E58 FIBER METAL

SUMMARY OF CONCLUSIONS

The principal conclusions of the program are summarized as follows:

TASK A - THERMAL EXPANSIVITY

1. Both aluminum and stainless steel fiber metal have thermal expansivities which are about 95 percent of the solid materials over the temperature range 70°F to 1000°F (21 to 538°C). In the temperature range of 70 to -275°F (-170°C) fiber metal expansion properties are equal to the solid metals.

2. Fiber metal materials are isotropic in thermal expansivity and this property is insensitive to variations in apparent density.

TASK B - AIR EROSION

The 45° impingement of a jet of air at sonic (nozzle) velocity for 100 hours on a variety of fiber metal materials had no measurable effect on them of any kind.

TASK C - FREEZE THAW CYCLING

Ten cycles of water saturation followed by freezing of the water had no measurable effect on any of several fiber metal materials tested.

TASK D - WATER SATURATION

The peak-to-peak pressures and air particle velocities associated with the high noise levels alone (e.g., 160 db) in fanjet engine inlets and fan exhaust ducts are more than sufficient to force water from and to rapidly dry any of the fiber metal materials tested in water retention capability. This should be true even with virtually zero air flow in the ducts.

TASK E - FUEL SATURATION AND COMBUSTION

Six cycles of saturating a series of fiber metal materials in JP4 jet fuel followed by combustion produced no detectable changes in any material properties.

TASK F - AIR OXIDATION

Fifty-hour stagnant air oxidation tests of both types of stainless steel and the aluminum alloy fiber metals showed:

1. Type 347 stainless steel fiber metal is oxidation resistant to 1000°F, (538°C) based on rate of weight gain consideration.

2. Type 17-4 PH precipitation hardening stainless steel lost strength due to overaging at temperatures above 900°F (482°C). Rate of weight gain for temperatures exceeding 900°F (482°C) also confirmed that 900°F (482°C) is the oxidation resistance limit for this alloy.

3. The aluminum alloy fiber metal was oxidation resistant at 700°F (372°C) from weight gain considerations. However, this temperature caused a loss of strength due to overaging, whereas 600°F (316°C) exposure produced no strength change.

4. Acoustical flow resistance of the tested materials is not affected significantly by the oxidation conditions employed.

TASK G - SALT CORROSION

Exposure of the two stainless steel and the aluminum alloy fiber metals to warm salt spray corrosion conditions (in accordance with F.T.M.S. No. 151A, Method 811.1 testing procedure) for up to 96 hours produced the following conclusions:

1. The 347 stainless steel materials underwent no significant property changes and are considered fully resistant to the test.

2. The 17-4 PH stainless steel materials showed some weight gain, loss in strength and increase in acoustical flow resistance, and are not considered to be resistant to the test.

3. The aluminum alloy materials increased in flow resistance and lost tensile ductility, but did not lose strength. These materials are also not considered to be resistant to the test.

TASK H - CLEANABILITY

1. For the contaminating test employed, in which silica sand, lampblack, and oil were caused to clog fiber metal specimens, it was determined that one or more simple cleaning procedures could fully restore all specimens to their original acoustical flow resistance.

2. The recommended procedure for cleaning fiber metal materials in place in engine ducts or inlets, is to spray with a solvent while simultaneously vacuum cleaning the material.

3. When fiber metal materials can be removed for cleaning, the recommended procedure is to immerse the materials in solvent and apply ultrasonic cleaning.

TASK I - MECHANICAL PROPERTIES

1. For a variety of stainless steel fiber metal materials, ultimate tensile strength, yield strength, Young's modulus, and shear modulus were found to increase exponentially with increasing apparent density. These properties increased approximately with the cubic power of apparent density.

2. If fiber metal materials are not resintered at the final density, the mechanical properties increased only linearly with the apparent density.

3. Screen reinforcement of fiber metal increases mechanical properties in proportion to the percentage of screen in the material.

4. Prestraining of fiber metal materials into their plastic deformation region increases both yield strength and elastic modulus. Typical results for a prestrain of 2 percent in a specimen of 26 percent density is that yield strength increased by 68 percent and Young's modulus by 50 percent.

5. Torsional damping capacity increases with decreasing apparent density, with increasing thickness, and with the application of screen reinforcement. The annealing of the aluminum materials resulted in a large increase in torsional damping.

6. Tensile ductility is maximum for fiber metal densities near 50 percent, with typical elongations for type 347 stainless steel ranging between 8 and 13 percent. Ductility falls to low values for both high- and low-density materials; 80 percent and 10 percent densities both showed typical elongations of about 1 to 5 percent.

7. Tensile ductility is increased by screen reinforcement and by decreasing fiber diameter.

8. For unreinforced fiber metal, sample orientation has no effect on mechanical properties, considering those properties in the plane of the sheet.

9. It is recommended that additional mechanical properties be measured under compressive loading. Also, additional information is needed on flexural damping properties, and a major body of information is required on fatique properties.

APPENDIX

APPENDIX A

Thermal Expansivity

Experimental apparatus.- The apparatus employed conformed to American Society for Testing and Materials method E 228-66 aT. It consisted essentially of a vitreous silica dilatometer, which encased the specimens and an extensometer (dial gage) for measuring length changes. An electric furnace was employed to achieve temperatures greater than ambient and a liquid nitrogen bath was used to create the sub-ambient temperatures. Calibrated iron-constantan thermocouples and a potentiometer were used to measure temperature. A laboratory oven was employed in the stress relief of the aluminum samples. An electrically heated laboratory tube furnace was used in the stress relief of the 347 SS samples. All weighings were conducted on an analytical balance.

Detailed experimental procedure.- The procedure followed ASTM method E 228-66 aT. It consisted of the following.

1. The test specimens were machined from larger blocks of fiber metal. They had a 0.312 in. (0.792 cm) square cross section and were approximately 2.0 in. (5.08 cm) in length.

2. The samples were stress relieved as follows:

   a. For aluminum fiber metal, the samples were heated to 650°F (343.3°C), held at temperature for 0.5 hours and retort cooled to room temperature at 200°F/hour (111.2°C/hr).

   b. For 347 SS fiber metal, the samples were slowly heated to 900°F (482.2°C), held for 0.5 hours at temperature and furnace cooled. An atmosphere of hydrogen was maintained at temperatures above 250°F (121°C).

3. The samples were dimensionally inspected, weighed to the nearest milligram and sent to York Research Corporation in Stamford, Connecticut for expansivity measurements.

4. The actual elongation testing consisted of the following:

   a. Each starting gauge length was precisely determined.

   b. The thermal elongation of the 347 SS samples was measured in 100°F (55.6°C) increments up to 1000°F (537.8°C) and then in 100°F (55.6°C) increments back down to room temperature. The thermal elongation of the aluminum samples was measured in 50°F (27.8°C) increments up to 400°F (204.4°C) and then again in 50°F (27.8°C) increments down to room temperature.

c. The gauge length of each sample was remeasured after the high temperature excursions.

d. Cooling curves were obtained for all samples by measuring the change in length, in 50°F (27.8°C) increments, below room temperature, down to -275°F (-170.6°C) and then in 50°F (27.8°C) increments up to room temperature.

e. The gauge length of each sample was rechecked, at room temperature, at the end of the cooling cycle.

APPENDIX B

Air Erosion

Experimental apparatus.- The air erosion test apparatus is shown in Figure AB-1. Plant compressed air was passed through a commercial oil trap and a 20 micron nominal porous metal filter. The air was supplied from a pressure regulator, through 0.5 in. (1.25 cm) and 0.25 in. (0.63 cm) copper tubing, to each of five 0.055 in. (0.140 cm) diameter solid stream flow nozzles which were constructed of type 303 stainless steel. Five specimens were tested simultaneously. Each specimen was sandwiched between 0.062 in. (0.157 cm) thick Neoprene rings with 3.4 in. (8.6 cm) outer and 1.4 in. (3.6 cm) inner diameters. Each sandwich was surmounted by an aluminum washer of the same dimensions as the Neoprene. Each specimen sandwich was securely fixed to the table portion of the apparatus with a welders clamp. This part of the apparatus was constructed of 0.5 in. (1.27 cm) diameter, holed, 304 SS, perforated, sheet, 0.062 in. (0.157 cm) thick. The discharge of each flow nozzle was located 0.010 in. (0.025 cm) above the test specimen and was directed to impinge air onto and through the fiber metal at an angle of 45 degrees.

The thickness of the target impingement area of each specimen was monitored by a micrometer that was fitted with 0.035 in. (0.089 cm) diameter flat tips.

Photographs at 21X magnification of the target impingement areas were taken on a metallographic microscope. An ultrasonic cleaner was employed in cleaning the test specimens and they were dried in an electric oven.

Experimental procedure.- The following procedure was employed in this test series:

1. A 2 in. (5.1 cm) square of each material was cut, weighed, and dimensionally inspected with the procedure described in Appendix L.

2. A 1.75 in. (4.45 cm) diameter disc was cut from each square using a hole saw. The edges were lightly sanded to remove burrs.

3. Each disc was ultrasonically cleaned in an alkaline cleaner, rinsed in deionized water, and dried to constant weight at 250°F (121°C). Weights were measured to the nearest 0.001 gm.

4. The 0.055 in. (0.140 cm) diameter target area of impingement was located by inking a 0.120 in. (0.305 cm) outer and 0.080 in. (0.203 cm) inner diameter circle in the center of each disc. To assist in the accurate relocation of this area, four, .020 in. (0.051 cm) diameter holes were lightly punched with a pin on the circumference of the circle.

5. Two thickness measurements of the target area were made and averaged. The thicknesses were estimated to the nearest 0.0001 in. (0.0002 cm).

6. The impingement area was photographed at 21X.

7. Flow resistance measurements were made at 0.556 ft per sec (16.5 cm per sec) flow velocity using the apparatus described in Appendix J. The 1 in. (2.54 cm) diameter test area was employed.

8. Each disc was subjected to the air blast, with a velocity of about 1130 ft per sec, (345 m/sec) for 100 hours. Each flow nozzle discharged to atmospheric pressure. The nozzles were operated as sonic orifices by maintaining the pressure drop across them at the critical ratio, which is 0.53 for air. Calculations indicated that the pressure drops in the system were negligible, so the air pressure in the manifold was maintained at 13-14 psig ($89.5 \times 10^3 - 96.5 \times 10^3$ N/m2). This air pressure was checked twice daily. Also, a bi-daily check to insure that the air blast was impinging on center was performed.

9. Following exposure, each disc was recleaned ultrasonically, to remove small amounts of oil that had penetrated the system. The discs were dried at 250°F (121°C) and reweighed to the nearest 0.001 gm.

10. The impingement area was relocated microscopically using the pin holes and re-inked.

11. The target area was rephotographed at 21X.

12. Each disc was rechecked for flow resistance.

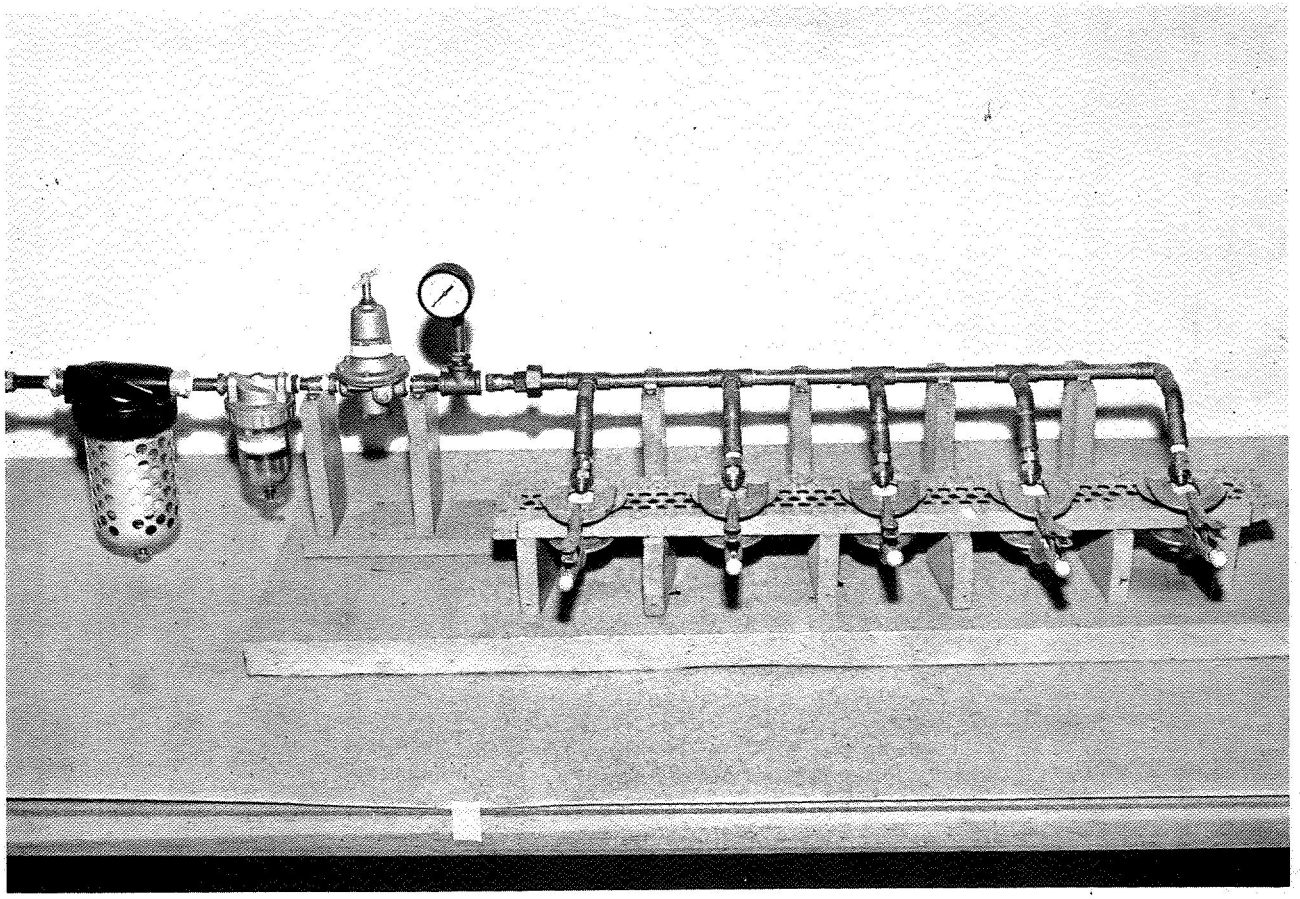

FIGURE AB-1

AIR EROSION TEST APPARATUS

APPENDIX C

Freeze-Thaw Cycling

Experimental apparatus.- The deionized water used in the saturation and freezing portion was produced by a laboratory deionizer and was prefiltered through a grade 7 laboratory filter paper.

Once saturated, the specimens were sealed in 1.7 in. (4.3 cm) x 8.0 in. (20.3 cm) polyethylene bags. The plastic clad specimens were frozen between 10.0 in. (25.4 cm) x 10.0 in. (25.4 cm) x 5.0 in. (12.7 cm) blocks of dry ice and this ice sandwich was placed within a polystyrene foam container which was located in a laboratory refrigerator. All specimens were thawed and dried in an electrically heated laboratory oven.

Experimental procedure.- The following procedure was employed in this test series:

1. Two 1.5 in. (3.8 cm) by 7.0 in. (17.8 cm) specimens of each material were cut. The dimensions and apparent densities of both were measured using the procedure described in Appendix L. One was designated a control specimen and set aside.

2. All specimens were flow resistance tested as described in Appendix J.

3. Each test specimen was saturated with deionized, filtered, water by immersing it horizontally into the water and moving it in a pumping motion up and down while immersed. The samples were check weighed to ensure that the available pore volumes were completely filled. The minimum filling that was observed was 95 percent. Care was taken at all times to maintain the samples in a horizontal attitude, in order to prevent drainage and ensure full volume filling of the pore network.

4. The specimens were quickly slid into the polyethylene bags and placed on the bottom layer of dry ice, which was already positioned in the insulated container. The top layer of dry ice was placed in position and the container was gently placed in a refrigerator.

5. The samples were allowed to freeze and cool to dry ice sublimation temperature (-109°F) (-78°C) overnight.

6. After 16 hours, the specimens were removed from the ice and placed in the drying oven. They were thawed and dried to constant weight at 220°F (104°C).

7. The specimens were dimensionally inspected and rechecked for flow resistance.

8. Steps 3 through 7 were repeated until a total of 10 freeze-thaw cycles had been completed.

9. Duplicate 0.6 in. (1.5 cm) by 6.0 in. (15.0 cm) tensile coupons were cut from each tested specimen and each control specimen.

10. Mechanical properties for all coupons were determined by the procedure described in Appendix K.

APPENDIX D

Water Saturation

Experimental apparatus.- The apparatus employed in this test series is shown schematically in Figure AD-1. It consisted of six calibrated flow orifices that delivered the desired quantities of air to the test fixture. The test fixture was made up of 1.75 in. (4.44 cm) diameter copper tubing, to which was attached tubing connections and a pipe union. The fiber metal test specimens were held in the pipe union which was machined with a recess to hold the fiber metal and gaskets. The specimens were gasketed with closed cell Neoprene to prevent leakage. Mercury and inclined water manometers were used to measure the differential pressures across the flow orifices and fiber metal specimens respectively. Valve A was left open until the desired flow velocities had been established. This prevented undesirable air flow through the wet fiber metal samples and premature, evaporative, dryout. The air flow discharged to atmospheric pressure. All weighings were conducted on an analytical balance. A laboratory ultrasonic unit and electric oven were employed in the ultrasonic cleaning and drying of the fiber metal samples.

Experimental procedure.- The following procedure was used in the execution of this test series.

1. A 1.75 in. (4.44 cm) diameter disc sample was cut for each fiber metal.

2. The discs were ultrasonically cleaned and dried at 250°F (121.1°C).

3. Each disc was weighed to the nearest milligram, dimensionally inspected, and their apparent densities calculated.

4. The edges of each disc were sealed with a thin layer of silicone rubber, in order to prevent edge flow.

5. Each disc was inserted in the test fixture and subjected to air flow velocities ranging from 0.008 to 11.1 ft per sec (0.244-338.5 cm per sec). A test area of 1.0 in. (2.54 cm) was exposed during testing. Differential pressures across the fiber metal were recorded at each flow velocity setting.

6. Each sample was saturated with filtered, deionized water without its being removed from the test fixture. The inlet tubing to the fixture was disconnected for this operation.

7. The break-through pressure was determined for each material by slowly increasing the air pressure on the upstream side of the sample until the first bubble appeared and broke free of

a .005-.010 in. (.013-.026 cm) thick water film on the top surface of the sample. Later, this water film was removed with a modified hypodermic syringe.

8. The profile of differential pressure-flow velocity was determined for the wet fiber metal. The same velocities as in step 5 were used. Premature evaporative dryout of the sample was eliminated by not allowing any air flow through the sample until the proper flow velocities had been established.

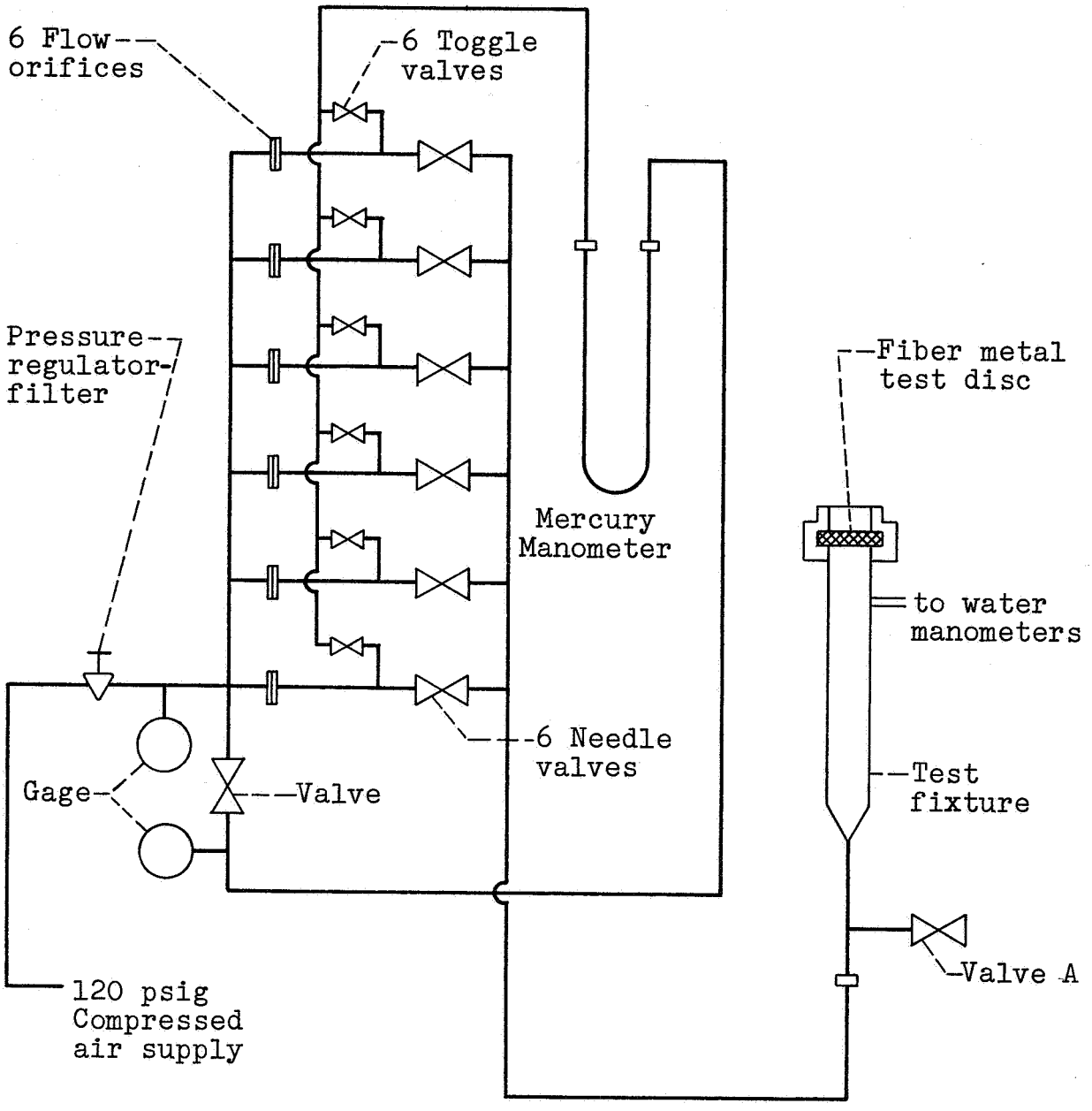

FIGURE AD-1

WATER SATURATION TEST APPARATUS

APPENDIX E

Fuel Saturation And Combustion

Experimental apparatus.- The specimens were saturated with JP-4 fuel from a 3000 ml glass beaker. Combustion of all specimens took place on a permeable grating located in a laboratory hood. A photograph of the grating with a specimen containing burning fuel is shown in Figure AE-1. The grating was made of 304 stainless steel, 10 mesh, screen, backed with 0.5 in. (1.27 cm) diam holed perforated stainless steel sheet, 0.062 in. (0.157 cm) thick. It was permeable so as to allow through-convection air currents and hence complete combustion.

Experimental procedure.- The following procedure was employed in this test series:

1. Two specimens of each material were cut; a 2.5 in. (6.4 cm) by 7.0 in. (17.8 cm) test specimen and a 1.5 in. (3.8 cm) by 7.0 in. (17.8 cm) control specimen.

2. Test specimens were tested for flow resistance by the procedure described in Appendix J.

3. The density and dimensions of all test specimens were determined with the procedure described in Appendix L.

4. Test specimens were allowed to wick JP-4 jet fuel completely into their pore network.

5. Test specimens were removed from the fuel, immediately oriented to the horizontal, to prevent drainage so as to insure full retention of the fuel in its pores, and placed on the combustion grating.

6. Test specimens were immediately ignited and allowed to burn to completion.

7. The test specimens were visually inspected, reweighed to the nearest milligram, and air permeability checked as in step 2.

8. Steps 4 through 7 were repeated until a total of six combustion cycles were completed.

9. Two tensile coupons were cut from each test specimen and a single coupon was cut from the control specimen. All coupons were tensile tested as described in Appendix K.

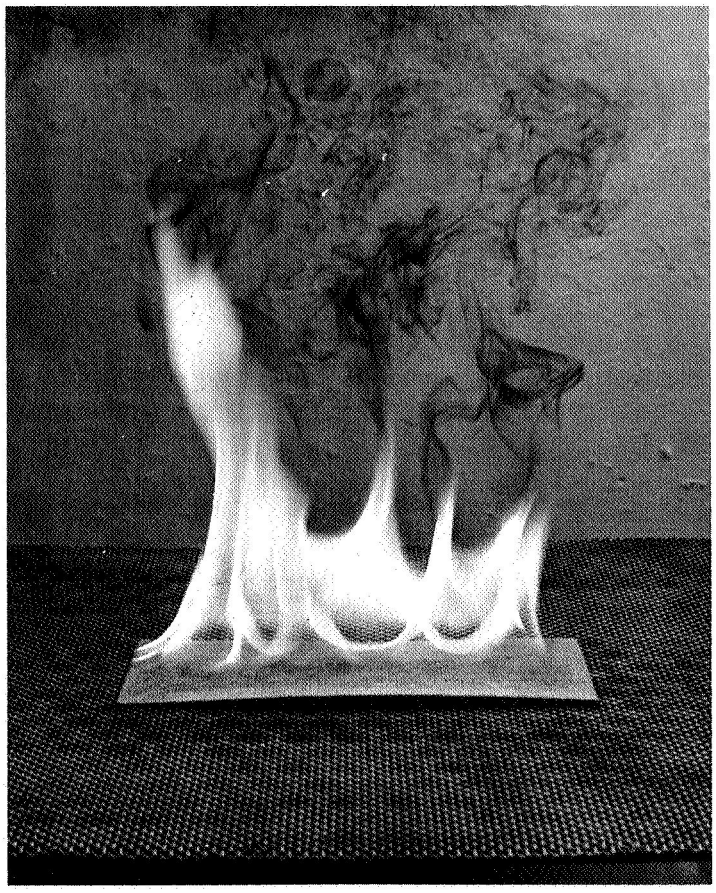

FIGURE AE-1

BURNING COMBUSTION SPECIMEN

APPENDIX F

Air Oxidation

Experimental apparatus.- The equipment in which the environmental exposures were conducted consisted of an electrically heated laboratory furnace, with inner dimensions of 4.5 in. (11.4 cm) x 4.5 in. (11.4 cm) x 14.0 in. (35.6 cm), a temperature indicator-controller, a potentiometer with a 4 position thermocouple switch, and a rack which contained the test samples. The rack held a total of 20 samples on 2 levels. Being only 6 in. (15.2 cm) in length, it minimized thermal gradients. It was constructed of perforated 347 stainless steel sheet. Four indicating thermocouples, located on diagonal corners, were present during each run. They indicated a deviation of not more than 3 percent from the nominal temperature set point.

Experimental procedure.- The following procedure was employed in this test series:

1. Sixteen test samples of aluminum fiber metal, and 21 samples each of 347 and 17-4 PH SS materials were cut. Each sample was 1.5 in. (3.8 cm) wide and 6.0 in. (15.2 cm) long. A similar sized reference control sample for each material was set aside for future use.

2. Each test sample was weighed and dimensionally inspected as described in Appendix L.

3. Each test sample was measured for flow resistance and a nominal rayl number was calculated. The procedure is described in Appendix J.

4. The samples were subjected to air oxidation for periods of 2, 4, 10, 20, and 50 hours.

The temperatures that were investigated were:

Aluminum	347 and 17-4 PH SS
500°F (260°C)	800°F (427°C)
600°F (316°C)	900°F (482°C)
700°F (372°C)	1000°F (538°C)
	1100°F (593°C)

5. After oxidation, each test sample was cooled, reweighed to the nearest milligram, rechecked dimensionally, and rechecked for flow resistance as in step 3.

6. Two tensile coupons were cut from each test sample, and a single coupon from the reference control.

All coupons were tested for mechanical properties as described in Appendix K.

APPENDIX F

Calculations.- The percentage weight gain data shown in Figures F-14 through F-18 were refined in the following manner:

1. It was assumed that the oxidation reaction rate was limited by the thickness of oxides formed on the fiber metal surface and therefore the reaction rate equation took the form.

$$(1) \quad \frac{dw}{dt} = \frac{K}{w^n}$$

Where

w is the cumulative weight gain of oxides per unit area of fiber surface, gm/cm^2

K the reaction rate constant

n the order of the reaction

$\frac{dw}{dt}$ the rate of weight gain of oxides per unit area per unit of time, $gm/cm^2/hr$

2. The basic data for each of the stainless steel alloys illustrated in Figures F-14 through F-18 were recalculated, expressing them in terms of w.

3. W was plotted as a function of time (t). On this basis, the data for all of the fiber diameters used fell on the same plot despite their different specific surface areas. This illustrated the fact that the weight increase is directly proportional to surface area. A smooth curve was drawn through the points on this plot.

4. The slope of the curve (dw/dt) was taken at several values of w and these values were then replotted on a log-log plot of dw/dt vs w. The slope of this plot, for each stainless steel alloy, appeared to be -2, indicating second order reactions.

5. The best straight lines at a slope of -2 were drawn through the data sets for each temperature level. The constants were calculated for each line (temperature) using the reaction rate equation in the form,

$$(2) \quad \frac{dw}{dt} = \frac{K}{w^2}$$

6. Using the relationship of Arrhenius which states that the logarithm of reaction rate constants vary inversely with the absolute temperature, T, a semi-log plot of K vs 1/T yielded the relationships shown in Figure F-19.

APPENDIX F

7. By integration of equation (2) the following equation is obtained which describes the weight gain of fiber metal resulting from air oxidation.

$$(3) \quad w^3 = 3Kt$$

By using equation (3), Figure F-19, and multiplying by the specific surface areas for the fiber metal materials, the smoothed curves were obtained which are shown in Figures F-20 and F-21. Experimental data points are also shown for comparison. In addition, some weight gains for extended times were calculated and these are shown in the text.

APPENDIX G

Salt Corrosion

Experimental apparatus.- The spray chamber used in Program A conformed to standards set forth in Federal Test Method Standard Number 151A, Method Number 811.1. Filtered, deionized, water was used to rinse the samples after testing and they were dried in an electrically heated laboratory oven. All specimens, both before and after testing, were stored in polyethylene bags.

Program B utilized the same equipment as in Program A, plus a laboratory dessicator.

Experimental procedures.- The following procedure was employed in the execution of this test series:

1. Four 3 in. (7.6 cm) by 6 in. (15.2 cm) specimens were cut from each material.

2. All surfaces were degreased with trichloroethane.

3. The dimensions and apparent density of each specimen was measured using the procedure described in Appendix L.

4. The flow resistance of each specimen was measured as described in Appendix J.

5. A color photograph was made of each material type.

6. Each sample was separately wrapped in polyethylene and sent to York Research Corporation for environmental exposures.

7. Three of the four specimens of each material were tested in Program A. This involved exposure to a fine mist of 5 percent sodium chloride solution at 95°F (35°C) for periods of 24, 48, and 96 hours. All testing was performed in accordance with Federal Test Method Standard Number 151A, Method Number 811.1.

8. The remaining specimen of each material was tested in Program B. This involved thoroughly spray wetting each sample weekly with a solution of synthetic sea water and allowing them to remain wetted in a closed laboratory dessicator at 75°F (23.9°C) for a period of 336 hours. All testing was conducted in a manner suggested by Mil-E-5009C, paragraph 4.3.9, Corrosion Susceptibility Test.

9. Following exposure, each sample from each program was rinsed with deionized water, dried at 250°F (121.1°C), individually repackaged in polyethylene, and returned to Huyck Metals Company for analysis.

10. Each sample was visually inspected, photographed in color and remeasured for length, width, thickness, and weight.

11. Each sample was remeasured for flow resistance as described in Appendix J.

12. Duplicate 0.6 in. (1.5 cm) by 6.0 in. (15.2 cm) tensile specimens were cut from each sample. They were tested for mechanical properties as described in Appendix K. Reference properties data were available from control specimens measured in Task F--Air Oxidation.

APPENDIX H

CLEANABILITY

Experimental Apparatus

Flow resistance test apparatus.- The apparatus employed in the low velocity (5-20 cm/sec) (0.16-0.65 ft/sec) flow resistance measurements is shown in Figure AH-1. A vacuum pump drew air from the room through a 10 cm (3.94 in.) diameter test area. The volume flow of air was determined by a rotameter type flow meter and the differential pressure across the fiber metal was measured by a water micromanometer. In order to prevent edge flow, the heavy weights shown, supplied sealing pressure to soft rubber gasketed flanges. The accuracy of the rotameter was about ± 2 percent and the micromanometer accurately indicated differential pressures as small as 0.001 in. (0.0025 cm) of water.

The high velocity (27-500 cm/sec) (0.89-16.4 ft/sec) flow resistance apparatus is shown in Figure AH-2. Plant compressed air was filtered of oil and water, passed through a gate valve and pressure regulator to control the flow rate, through a calibrated orifice meter to measure the flow rate, and then through the 10 cm (3.94 in.) diameter test area. Four orifice plates, with orifice diameters ranging from 0.25 to 1.25 in. (0.64-3.18 cm) were used to cover the range of air flow velocities. The pressure drop across the sample was measured by 40 in. (102 cm) long manometers. The accuracy of reading the meniscus of any of the mercury or water columns is estimated at ± 0.02 in. (± 0.05 cm).

The test samples were clamped between 0.5 in. (1.25 cm) wide soft rubber gasketed flanges at the end of a 60 in. (1.97 m) long straight section of pipe. This long section of pipe between the orifice meter and the test sample was used to smooth out the flow and produce air flow conditions into the test samples similar to those obtained with the low-flow apparatus.

Contamination test apparatus.- The samples were contaminated with the apparatus shown in Figure AH-3. The tests were conducted in a test cell in which a supply of dry compressed air was available and the flow rate of the air was monitored by a rotameter. The test specimens were clamped at the end of a vertical diffuser tube. The vertical orientation of the diffuser section, through which the contaminated air flowed, was chosen in order to contaminate the fiber metal specimens uniformly across their exposed surface. The contaminant was introduced into the diffuser by means of a plunger inside a special dispenser tube the end of

which was loaded with the contaminant. Details of the contamination test fixture are shown in Figure AH-4. The static pressure tap on the side of the diffuser tube was used with the differential pressure manometer to monitor the pressure drop across the specimen. Any contaminated air passing through the test specimen was exhausted directly into the room.

For the Part I tests with the fiber metal samples, the diameter of the opening at the end of the diffuser tube was six inches. For the Part II and Part III tests, a second diffuser tube, similar in appearance to the one shown in Figure AH-3, was fabricated with a 10 cm (3.94 in.) diameter end opening. The 10 cm (3.94 in.) diameter opening was required to fit into the flow-resistance apparatus.

For the Part II and Part III tests an aluminum ring, indicated in Figure AH-4, was used around the honeycomb bonded to the fiber metal sheets. The ring was an integral part of the sample holder at the end of the diffuser tube in that it formed a ledge on which to install the C clamps. The ring was also required in determining flow resistance in order to constrain the air flow to a 10 cm (3.94 in.) diameter test area when testing samples with honeycomb bonded to them. It was also needed in cleaning some of the bonded honeycomb samples where it was used to support an impervious backing plate, as shown in Figure AH-5.

Experimental Materials

Contaminant.- The contaminant consisted of 90 volume percent dust admixed with 10 volume percent lampblack. The dust was 140 mesh silica flour as defined by paragraphs 5.3.5 and 4.11.1 of Military Specification Mil-E-005272B (USAF). Its characteristics are shown below.

Distribution of sizes of particles

Quantity passing through mesh screen U.S. Standard Sieve Series, percent	Size of wire mesh screen, wires/inch
100	100
98 ± 2	140
90 ± 2	200
75 ± 2	325

Chemical analysis

Substance	Composition by weight, percent
SiO_2	97 to 99
Fe_2O_3	0 to 2
Al_2O_3	0 to 1
TiO_2	0 to 2
MgO	0 to 1
Ignition losses	0 to 2

APPENDIX H

The lampblack was a commercially available product with a 90 millimicron (3.5×10^{-5} in.) arithmetic mean particle diameter, 99.6 percent pure carbon, and 0.4 percent volatile material.

Turbine oil.- The turbine oil used in the contamination testing was a synthetic light lubricating oil with a viscosity of 27 centistokes (27×10^{-6} m^2/sec) at 100°F (37.8°C).

Solvent.- The solvent used in the cleaning evaluations was 1, 1, 1 trichlorethane.

Honeycomb support.- The honeycomb support used in Parts II and III of the program was made from fiberglass cloth impregnated with phenolic resin. The cell wall spacing on the honeycomb was a nominal 0.75 in. (1.91 cm) and its depth was 1.0 in. (2.54 cm) in Part II of the program and 0.5 in. (1.27 cm) in Part III of the program. A modified film epoxy adhesive was used to bond the layers of fiber metal to the honeycomb supports for both the Part II and Part III testing.

Additional materials.- Additional materials and equipment were employed in the various cleaning methods that were evaluated in this program. In the interest of clarity these items will be enumerated only in the specific discussions of these procedures.

Experimental Procedure

Part I testing.- Part I of the test program evaluated fiber metal without the honeycomb backing. It was conducted in the following manner:

1. Seven, 7 in. x 7 in. (17.8 cm x 17.8 cm) test specimens of each of the three material types were prepared.

2. Each specimen was flow resistance tested in an uncontaminated condition at air velocities of 5, 10, 16, 20, 27, 110, 250, and 500 cm per sec (0.16 to 16.4 ft/sec).

3. Each specimen was then contaminated in the following manner.

   a. The specimen was clamped at the end of the contamination test fixture as shown in Figure AH-3.

b. The air flow rate was adjusted until the pressure drop across the specimen became 6.9 in. (17.5 cm) of water. The air flow rate required to produce this pressure drop was noted.

c. The lampblack and silica-flour dust contaminant was introduced slowly and continuously into the diffuser section of the fixture and the air flow rate was decreased to maintain the pressure drop at 6.9 in. (17.5 cm) of water as the sample became contaminated and the flow resistance increased.

d. The addition of the dust contaminant was continued, maintaining a constant pressure drop, until the air flow rate dropped to approximately half the value at the start of the test. Contamination was terminated when this value of air flow was reached.

The contamination schedule for each material type is shown below.

Specimen No.	Contaminant
1	A
2	A
3	B
4	B
5	B
6	B
7	B

Contaminant A was the dry dust-lampblack mixture mentioned previously; contaminant B consisted of the same mixture but it was blown against specimens that had been prewetted in turbine oil. The wetting procedure consisted of immersing the specimen in the oil for a few seconds, removal, wiping with a cloth, and then allowing it to drain onto a piece of absorbent toweling. After draining until oil was no longer visible, excess oil was blown out of the specimen using a jet of high pressure air from a small nozzle directed onto the faces and edges of the sample.

4. Each specimen was then rechecked for flow resistance in the contaminated condition at air flow velocities of 10, 110, and 500 cm/sec (0.33, 3.6 and 16.4 ft/sec).

5. Each of the 7 specimens of each material type was then cleaned per the following schedule and by the following procedures.

APPENDIX H

Specimen No.	Method No.	Name	Description[a]
1	1	brush and vacuum clean	Brush the contaminated side of the fiber metal sheet with a wire brush. Keep brushing until no further improvement can be observed. Apply the nozzle of a vacuum cleaner to the contaminated surface and continue brushing and vacuum cleaning until no visible improvement can be detected.
2	2	scour with air jet	First, direct a jet of compressed air through the specimen from the uncontaminated side until contaminant removal appears to cease, and then repeat the procedure directing the air through from the reverse side.
3	3	wipe with solvent-soaked rag, and vacuum clean	Wipe the contaminated side of the fiber metal surface with a shop towel soaked in a solvent. After wiping away as much of the contaminant as possible, brush and vacuum clean, as in method 1, until no further improvement is visible.
4	4	dip, rinse, and soak in solvent, brush, and vacuum clean	Dip the specimen into a tank of solvent. Place the specimen in the solvent in a horizontal position, leaving it immersed for a few seconds. Upon removal let the solvent drain and evaporate, then brush and vacuum clean, as in method 1, until no further improvement is visible.

APPENDIX H

Specimen No.	Method No.	Name	Description[a]
5	5	dip, rinse, and soak in solvent, scour with air jet	Immerse the specimen in a tank of solvent as in method 4. Let the solvent drain and evaporate, then scour with a jet of compressed air as in method 2.
6	6	wipe with solvent-soaked rag, scour with air jet	Wipe with a solvent-saturated towel as in method 3. After removal of as much contaminant as possible, scour with a jet of compressed air as in method 2.
7	7	immerse in tank of solvent, expose to ultrasonic energy	Immerse the specimen in a solvent-filled tank on the bottom of which is attached an ultrasonic transducer. Place the specimen over the transducer for a short time and then invert the specimen and expose to ultrasonic energy for another short period.

[a]The wire brush used in cleaning methods 1, 3, and 4 was made from 1.0 in. long by 0.006 in. (2.54 x 0.015 cm) diameter brass bristles and had a cleaning surface area of 5.5 in.^{2} (35.4 cm^2). The vacuum cleaner was an industrial type fitted with a 1.5 in. (3.8 cm) diameter nozzle on the end of the hose. The vacuum-cleaner nozzle was always applied to just the side of the specimen that had been exposed to the contaminating air flow.

The air jet used in methods 2, 5 and 6 used compressed air, at a pressure of 80 lb/in.^{2} gage, (551 kN/M^2) passed through a 0.125 in. (0.318 cm) diameter nozzle. The angle of impingement of the air jet onto the surface was varied in order to blow out as much of the contaminant as possible.

The ultrasonic cleaning tank used for method number 7 was a commerical unit operated at a frequency of 22kHz. The electrical power input to the transducer was a nominal 200 watts. The transducer was located at the center of the bottom of the tank. The tank was 5.25 in. wide, 9.5 in. long, and 6 in. high

(13.3 x 24.1 x 15.2 cm) and had a capacity for about one gallon (0.0038 m3) of solvent. The height of the tank prevented complete immersion of the test specimens in the solvent and required that the contaminated specimens be inverted once in order to clean the total contaminated area. The distance between the transducer and the contaminated region of a test specimen varied from about 2 to about 4 inches (5-10 cm) because the contaminated specimens were placed in the tank at an angle in order to expose as much as possible of the surface area to the untrasonically agitated solvent.

6. The effectiveness of each cleaning method was observed by a recheck of the flow resistance of the cleaned specimens at air velocities of 10, 110 and 500 cm per sec (0.33, 3.6 and 16.4 ft/sec).

7. Steps 3 through 6 were repeated until all 7 test specimens of each material type had been subjected to a total of 3 contaminations and cleanings. The flow resistance results for the contaminated and cleaned specimens were averaged.

Part II testing.- Part II of the program tested FM171 epoxy bonded to honeycomb. Only the most effective cleaning methods from Part I were evaluated. This part of the program was conducted in basically the same manner as Part I and the contamination and cleaning schedule is shown below.

Specimen No.	Contaminant	Cleaning Method
1	A	2
2	B	4 - 4A
3	B	5 - 5A
4	B	7

Exceptions to Part I testing were as follows:

1. Cleaning method 4 was amended to 4A during the third cycle cleaning operation and an impervious 0.25 in. (0.635 cm) thick aluminum plate was clamped in place and a stream of solvent was poured directly onto the contaminated surface and into the honeycomb cells as shown in Figure AH-5. The vacuum-cleaner nozzle was applied to the surface concurrent with the application of the solvent. A slurry of dust particles, dissolved oil, and solvent was vacuum removed and this procedure was continued until no contaminant was visible and the surface appeared clean. The wire brush was not used during this operation.

2. Cleaning method 5 was amended to 5A during the third cycle cleaning operation and the aluminum backing plate was clamped into place. A stream of solvent was poured onto the contaminated surface as in method 4A. After pouring on solvent until the surface appeared clean, the specimen was turned over and the slurry of excess solvent, dissolved oil, and dust particles was poured out. The fiber metal surface was then scoured with the air jet until all traces of solvent appeared to have evaporated.

3. For the third cycle with cleaning method 7, the backing plate and fiber metal-honeycomb specimen was held together by hand and immersed into the solvent in the ultrasonic cleaning tank. The contaminated surface was placed toward the bottom of the tank and the specimen was rotated 180° to obtain complete exposure of the surface to the ultrasonic energy. After removal from the tank the solvent was allowed to drain and evaporate.

Part III testing.- Part III of the program tested FM125C and FM171, constructed into a two layer material. The fiber metals were epoxy bonded in alternating fiber metal-honeycomb-fiber metal-honeycomb layers. Four test specimens were constructed with the 10 rayl FM125C on the air flow side and a second set of four specimens with the 40 rayl FM171 on the air flow side. Since all of the cleaning methods evaluated in Part II were effective they were again evaluated in Part III. This part of the program was also conducted in basically the same manner as Part I and the contamination and cleaning schedule is shown below.

Specimen No.	Specimen Configuration	Contaminant	Cleaning Method
1	FM125C, FM171	A	2
2	FM125C, FM171	B	4 - 4A
3	FM125C, FM171	B	5 - 5A
4	FM125C, FM171	B	7
5	FM171, FM125C	A	2
6	FM171, FM125C	B	4 - 4A
7	FM171, FM125C	B	5 - 5A
8	FM171, FM125C	B	7

APPENDIX H

Exceptions to Part I testing were as follows:

1. Two contamination and cleaning cycles were conducted as opposed to three cycles in Part I.

2. Cleaning methods 4, 5, and 7 were amended as in Part II during the second and final cleaning cycle. The aluminum backing plate was again used.

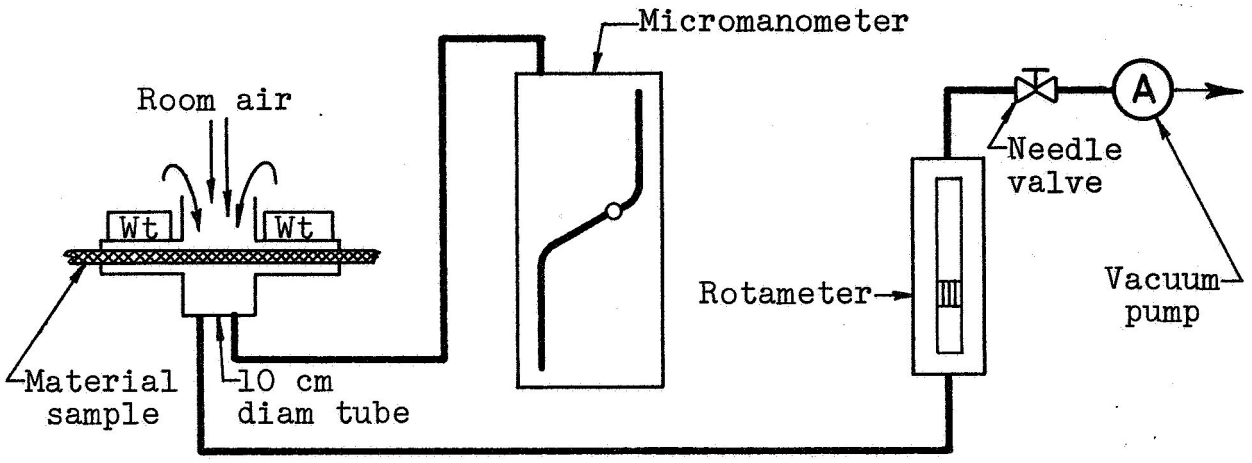

(a) Schematic

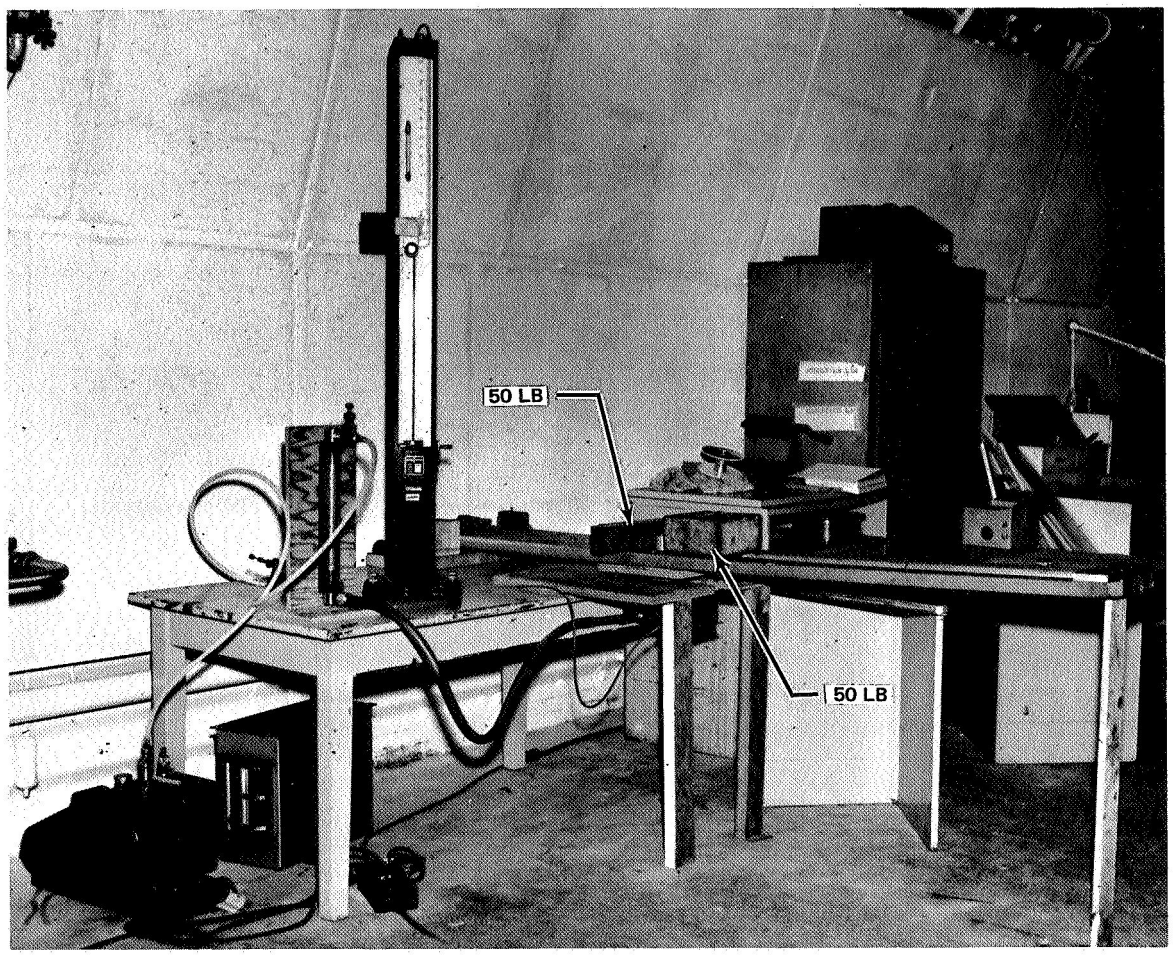

(b) Test setup

FIGURE AH-1.- LOW VELOCITY FLOW RESISTANCE APPARATUS - 5 TO 20 CM PER SEC (0.16-0.65 FT PER SEC)

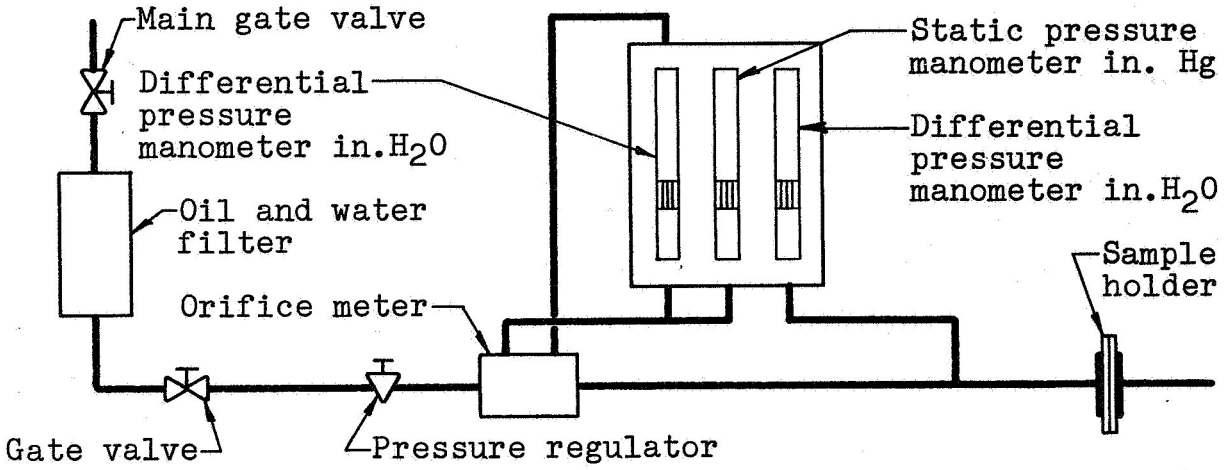

(a) Schematic

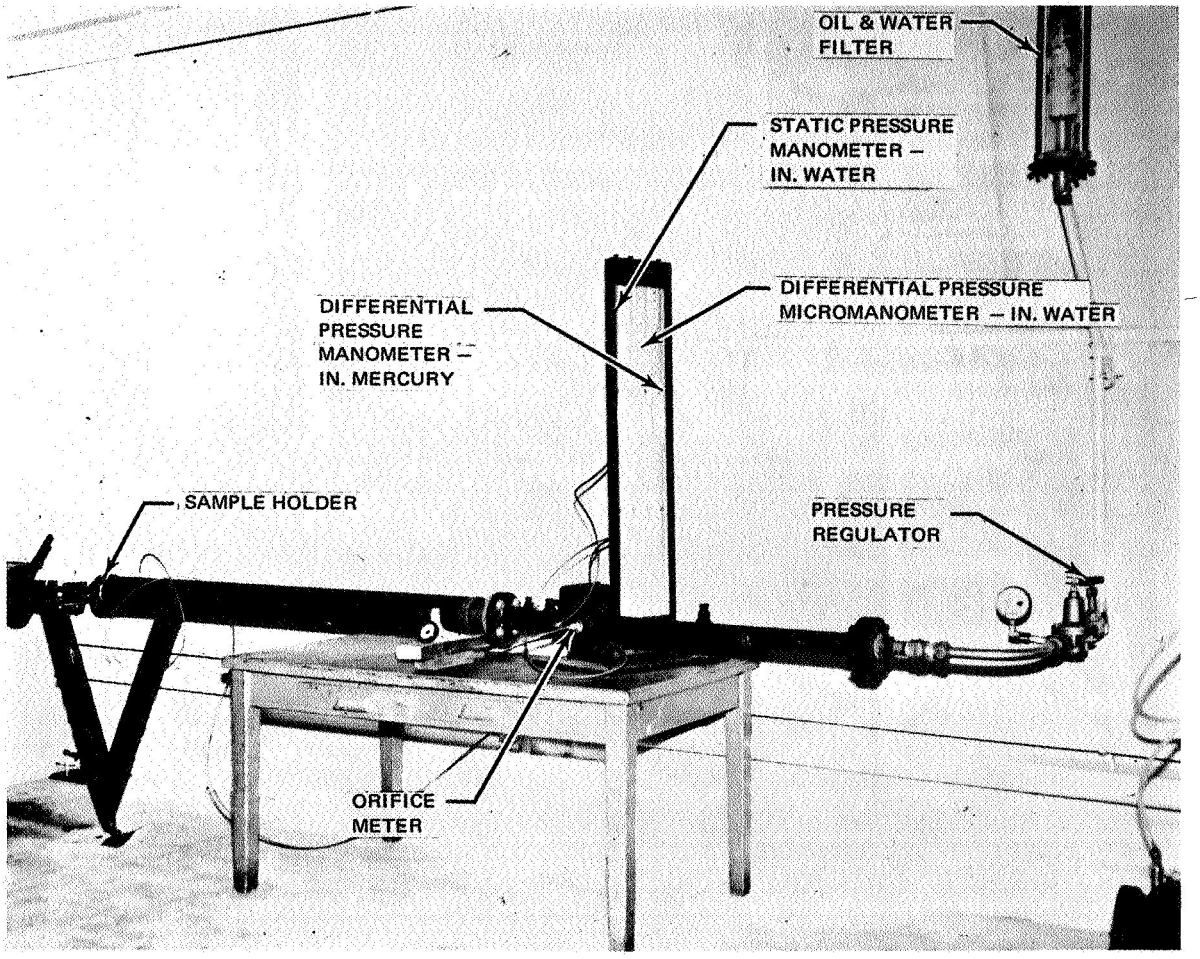

(b) Test setup

FIGURE AH-2.- HIGH VELOCITY FLOW RESISTANCE APPARATUS - 27 TO 500 CM PER SEC (0.89-16.4 FT PER SEC)

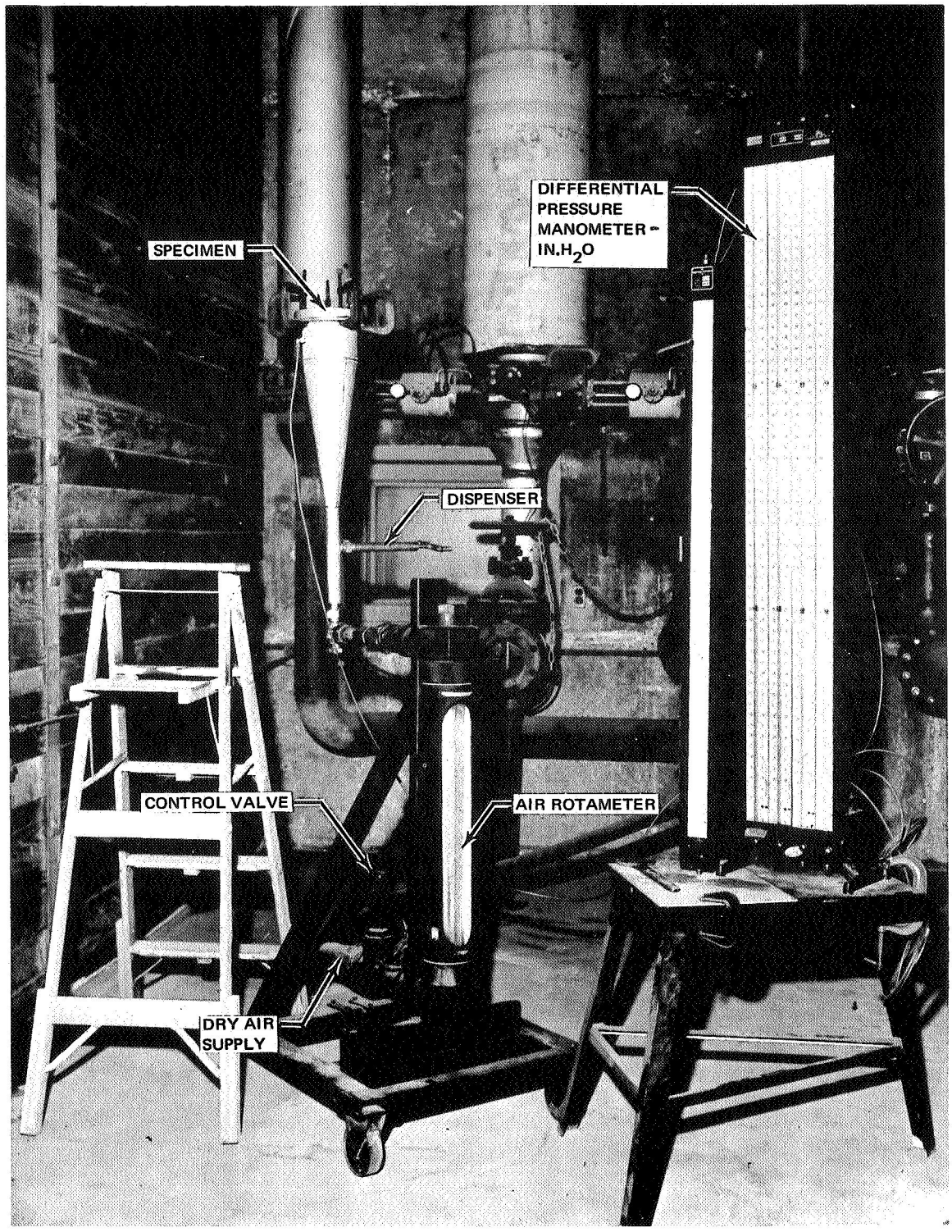

FIGURE AH-3

CONTAMINATION APPARATUS

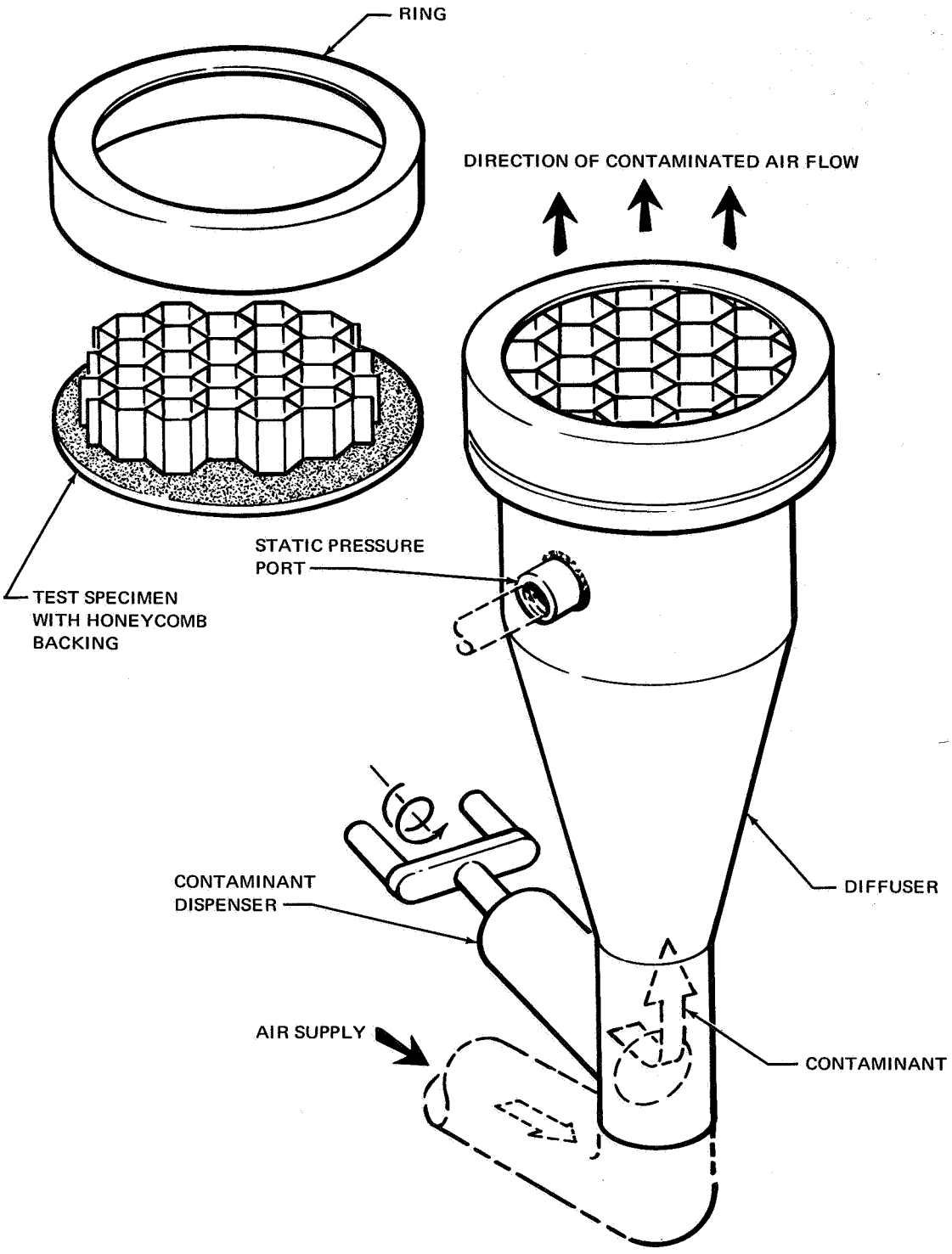

FIGURE AH-4

DETAIL OF CONTAMINATION TEST FIXTURE

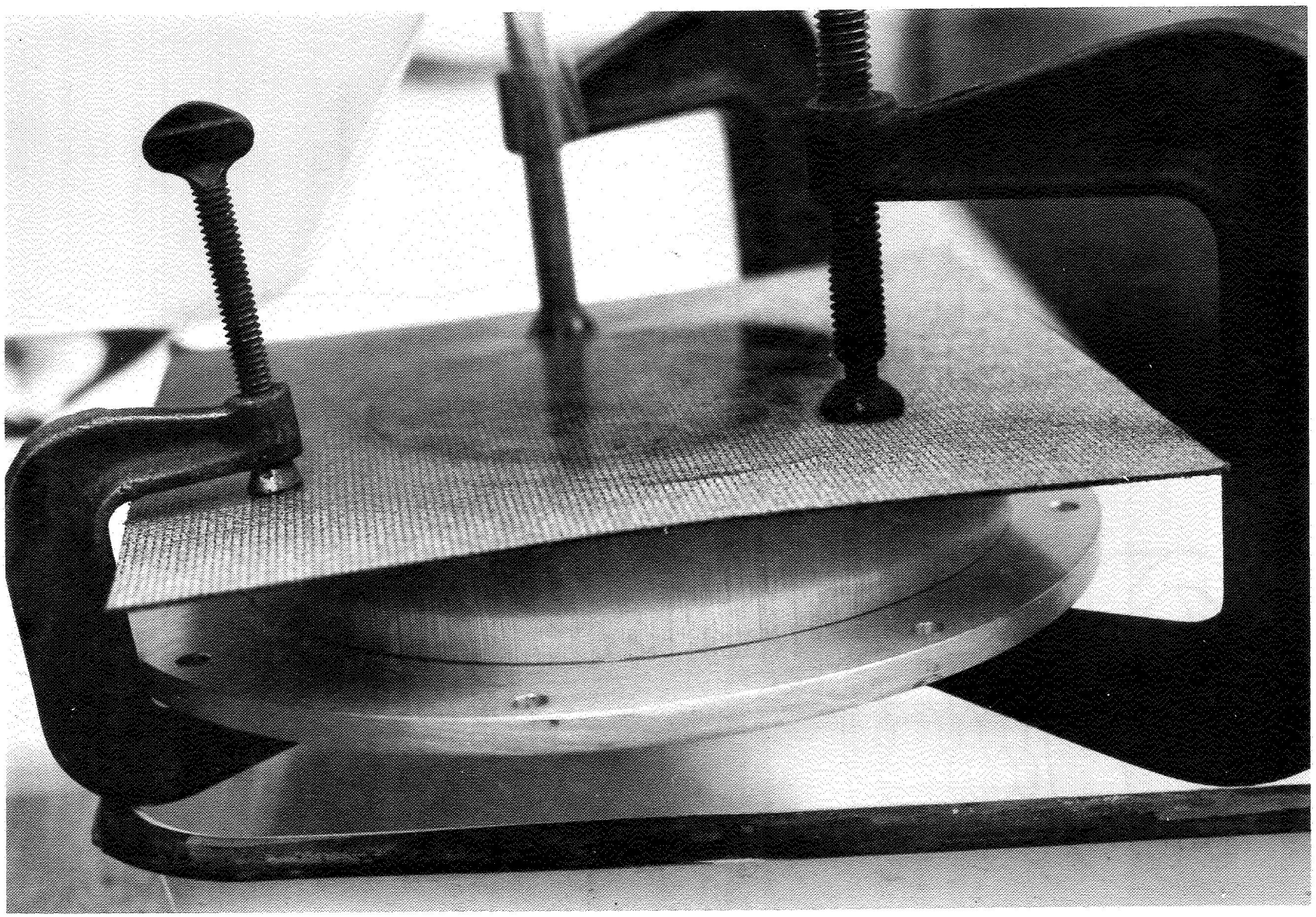

FIGURE AH-5

CLEANING METHOD 4A USED IN PART II AND III TESTING. IMPERVIOUS BACKING PLATE IN PLACE

APPENDIX I

MECHANICAL PROPERTIES

Experimental Apparatus

The apparatus for determining Young's modulus via the cantilever beam deflection technique is shown in Figure AI-1. Included in this equipment was a clamping device, a microscope for measuring beam deflection, a series of laboratory scale weights, and a light weight pan with attaching wire. Young's modulus was also determined, for very low apparent density test specimens, by a simply supported beam technique and this apparatus is shown in Figure AI-2. The microscope, scale weights, and pan previously mentioned were also included in this setup.

The tensile testing of the specimens was performed on a universal testing machine. This machine was fitted with both a strain gauge and an x-y plotter that made possible the measurement of the slope of the stress-strain curve, with repetitive loading and unloading of the test specimen.

The damping capacity and shear modulus of fiber metal was determined on the apparatus shown in Figure AI-3. Included in this apparatus were a specimen clamping device, an 8 ft (2.44 m), 1.89 lb (0.859 kg) aluminum rod, a light source, and a photo cell-recorder oscillation counter.

Experimental Procedures

Specimen description.- The specimen configuration employed in the testing is shown in Figure AI-4. As indicated, 0.062 in. (0.159 cm) thick specimens were used to determine the effect of thickness on mechanical properties. The specimens were normally cut from a sheet with their gauge lengths longitudinal to the rolling direction. However, some specimens were cut transverse to the rolling direction in order that the effect of rolling direction on mechanical properties might be determined. The apparent density of each test specimen was determined, prior to the adhesive bonding of the steel reinforcing tabs, by the procedure described in Appendix L.

Young's modulus.- Young's modulus testing (cantilever beam technique) was conducted in the following manner:

1. The specimen was clamped into position and the tared pan-wire assembly was hung immediately inboard of the adhesively bonded steel tab.

2. The deflection of the end of the specimen (beam) was measured with the microscope as the pan weight was progressively increased. Caution was exercised to end the testing before the applied load was sufficient to cause a permanent set to the specimen. Young's modulus testing (for the very low apparent density specimens) by the simply supported beam technique was conducted in a manner analogous to the cantilever beam testing. An unsupported span of 6.700 in. (17.018 cm) was used. Calculation of Young's modulus, by both techniques, is shown in a following section.

Tensile testing.- The destructive tensile and elongation testing were performed on the specimens that had been previously nondestructively tested for Young's modulus, shear modulus, and torsional damping capacity. The procedure that was employed was:

1. The specimen was placed in the universal testing machine and direct loaded in tension at a strain rate of 0.05 in./min (0.127 cm/min) until fracture. Some specimens were repetitively loaded and unloaded during a portion of the testing.

2. The elongation was determined by gaging the head travel distance and comparing this to the original gauge length.

Damping capacity and shear modulus.- The damping capacity and shear modulus of fiber metal were determined in the following manner. The technique is based on measuring the decay of torsional oscillations by the method used by Karplus et al, Reference 5.

1. The specimen was suspended vertically with one end being rigidly clamped.

2. An aluminum rod, approximately 8 ft (2.44 m) long and weighing 1.89 lb (0.859 kg), was attached at its center to the lower end of the specimen. This length of rod was selected so that a reasonably fast period of oscillation could be obtained.

3. The rod was displaced to a fixed stop at a predetermined chord distance from the light beam, thereby establishing a fixed initial amplitude of oscillation.

4. The rod was released and each time it swept past the light beam, focused on the photocell, the signal was recorded. The calculation of both damping capacity and shear modulus from these data is shown in a following section.

APPENDIX I

Calculation of Young's modulus.- Young's modulus by cantilever beam deflection was determined from the experimental data as follows:

$$(1) \quad d = \frac{PL^3}{3EI}$$

Where

d is the deflection, ft (m)

P is the applied load or force, lbs (N)

L is the length of the beam, ft (m)

E is Young's modulus, lb/ft^2 (N/m^2)

I is the moment of inertia, ft^4 (m^4)

For a cantilever beam,

$$(2) \quad I = \frac{Wt^3}{12}$$

Where

W is the width of the beam, ft (m)

t is the thickness of the beam, ft (m)

Combining equations (1) and (2),

$$(3) \quad E = \frac{4P}{Wd} \cdot \frac{(L)^3}{(t)^3}$$

Employing the same terms as above, Young's modulus can also be calculated from the simply supported beam deflection data as follows:

$\theta_1 = \theta_2$ = the slope at the free ends = $\frac{PL^2}{16EI}$

d = deflection at the center of the beam = $\frac{PL^3}{48EI}$

Then

$$(4) \quad E = \frac{P}{d} \cdot \frac{L^3}{48I}$$

$$(5) \quad I = \frac{Wt^3}{12} \text{ (for a simply supported beam)}$$

Combining equations (4) and (5),

$$(6) \quad E = \frac{1}{4} \cdot \frac{(P)}{(d)} \cdot \frac{1}{w} \cdot \frac{L^3}{t^3}$$

Calculation of damping capacity.- The damping capacity, ψ, of fiber metal was calculated from the torsional oscillation data as follows:

The initial amplitude of oscillation is taken as A_o. With a free decay of vibration, the amplitude of oscillation after n cycles, A_n, will be

$$A_n = A_o e^{-\alpha t}$$

Where

t is time

α is the attenuation coefficient

If $A_n/A_o = 1/e$, then $\alpha t = 1$ and $\log_e A_n/A_o = -1$. The damping capacity, ψ, and the log decrement, δ, are expressed by the equation.

$$\psi = 2\delta = \frac{2}{n} \log_e \frac{A_o}{A_n}$$

In order to simplify the calculation of ψ, the position of the stop (A_o) and the light beam (A_n) were adjusted so that $A_o/A_n = e$. Therefore, $\log_e (A_o/A_n) = 1$. Under these conditions, the expression for ψ reduces to, $\psi = 2/n$, where n is half the number of recorded photo cell signals. A_o was adjusted to insure that it was in the elastic range for the specimen.

The shear modulus, μ, of fiber metal was calculated from the torsional oscillation data as follows:

APPENDIX I

The torsion couple, Q, is related to the twist, ϕ, at the end of a strip of width, a, thickness, b, at a distance, c, from the clamp by the expression.

$$(1)\quad \frac{Q}{\phi} = \frac{\mu}{c}\, ab^3 \left[\frac{1}{3} - \frac{2b}{a}\left(\frac{2}{\pi}\right)^5 \cdot \sum_{m}^{\infty} \frac{1}{(2m+1)^5} \coth \frac{2b}{\pi a(2m+1)}\right] ,$$

$$(2)\approx \frac{\mu}{c}\, ab^3 \left(\frac{1}{3} - .21\frac{b}{a}\right) , \quad \text{(within 0.5\% for } b/a < 1/3).$$

For

If $b/a = 1/6$, then

$$(3)\quad Q/\phi = (\mu/c)\, ab^3\, (0.298).$$

The moment of inertia, I, of the long bar of mass, M, and length, L, that was clamped at its center to the lower end of the test specimens is:

$$(4)\quad I = \frac{ML^2}{12}$$

The frequency of oscillations, f, is given by the expression,

$$(5)\quad 2\pi f = \sqrt{(Q/\phi)\ 1/I}$$

Then

$$(6)\quad Q/\phi = 4\pi^2 f^2 I = \frac{\pi^2 ML^2}{3T^2} \quad \left(T = \frac{1}{f}\right)$$

Combining equations (3) and (6), and solving for the shear modulus, μ, yields,

$$(7)\quad \mu = \frac{\pi^2 ML^2}{3(0.298ab^3)} \cdot \frac{1}{T^2}$$

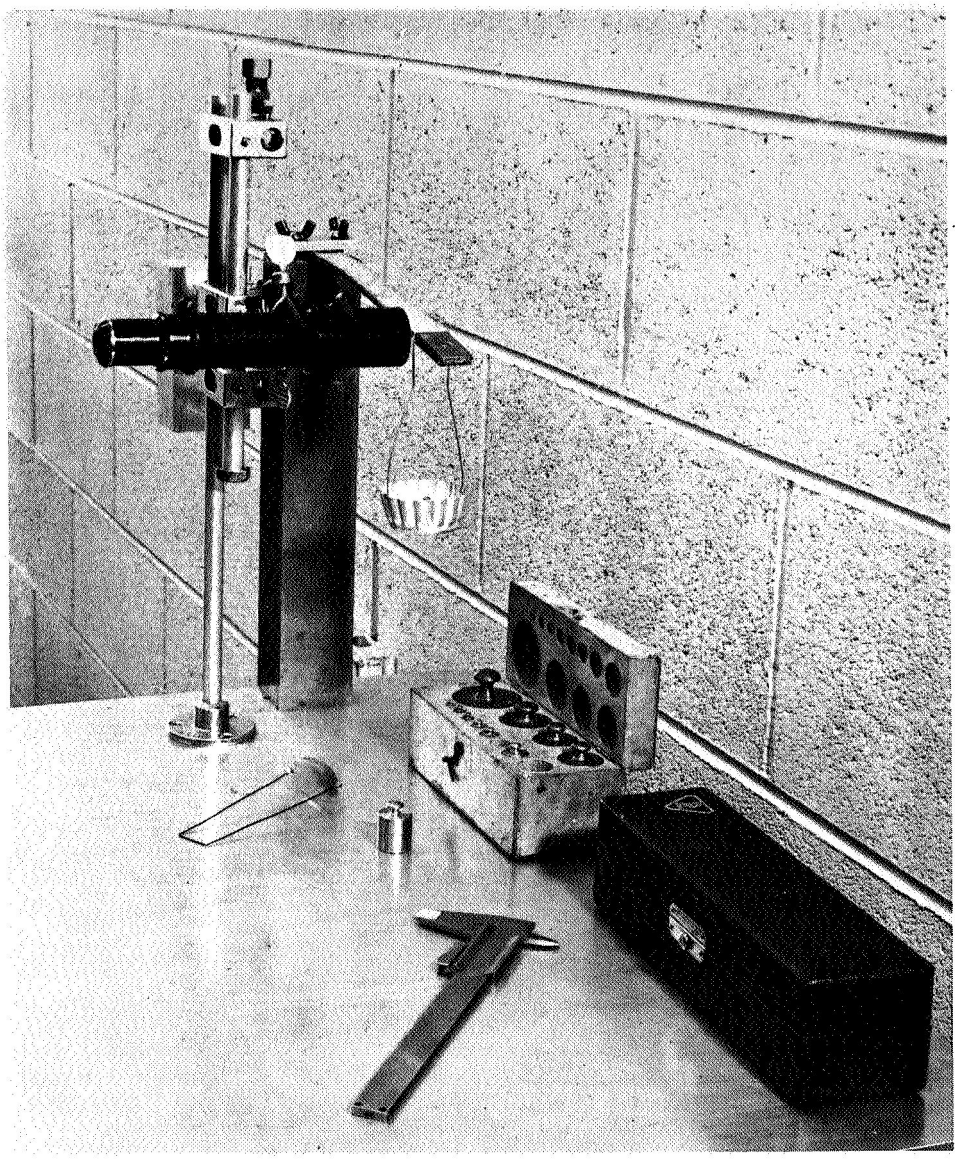

FIGURE AI-1

YOUNG'S MODULUS TEST APPARATUS CANTILEVER BEAM METHOD

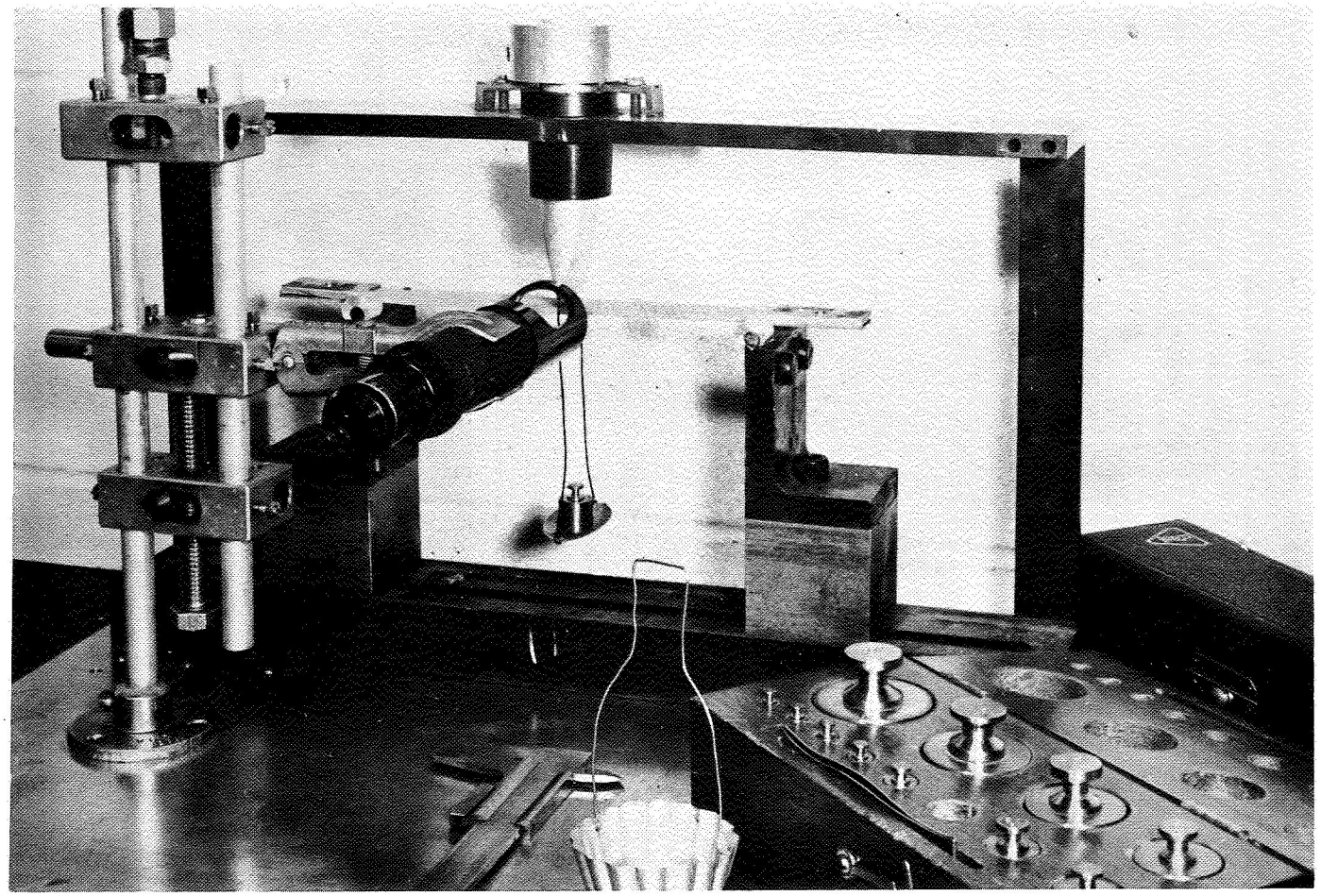

FIGURE AI-2

YOUNG'S MODULUS TEST APPARATUS SIMPLY SUPPORTED BEAM METHOD

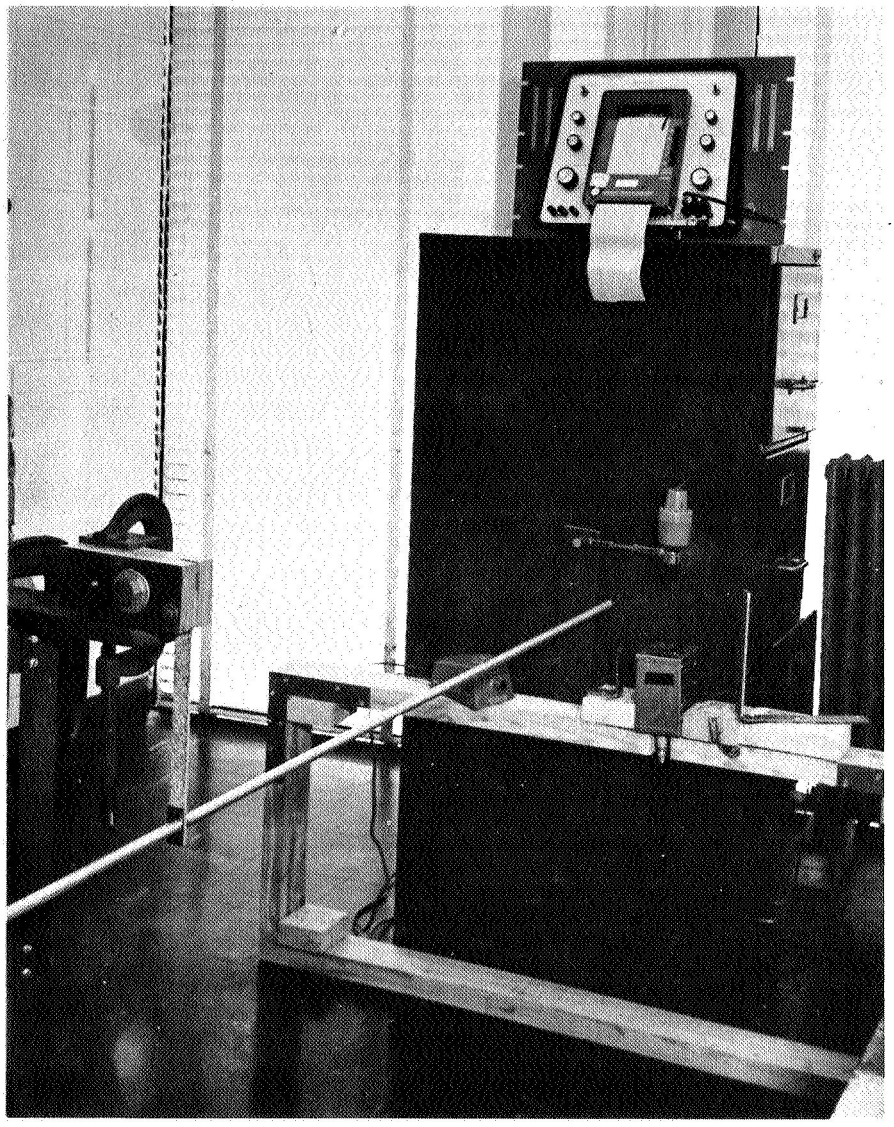

FIGURE AI-3

DAMPING CAPACITY AND SHEAR MODULUS TEST APPARATUS

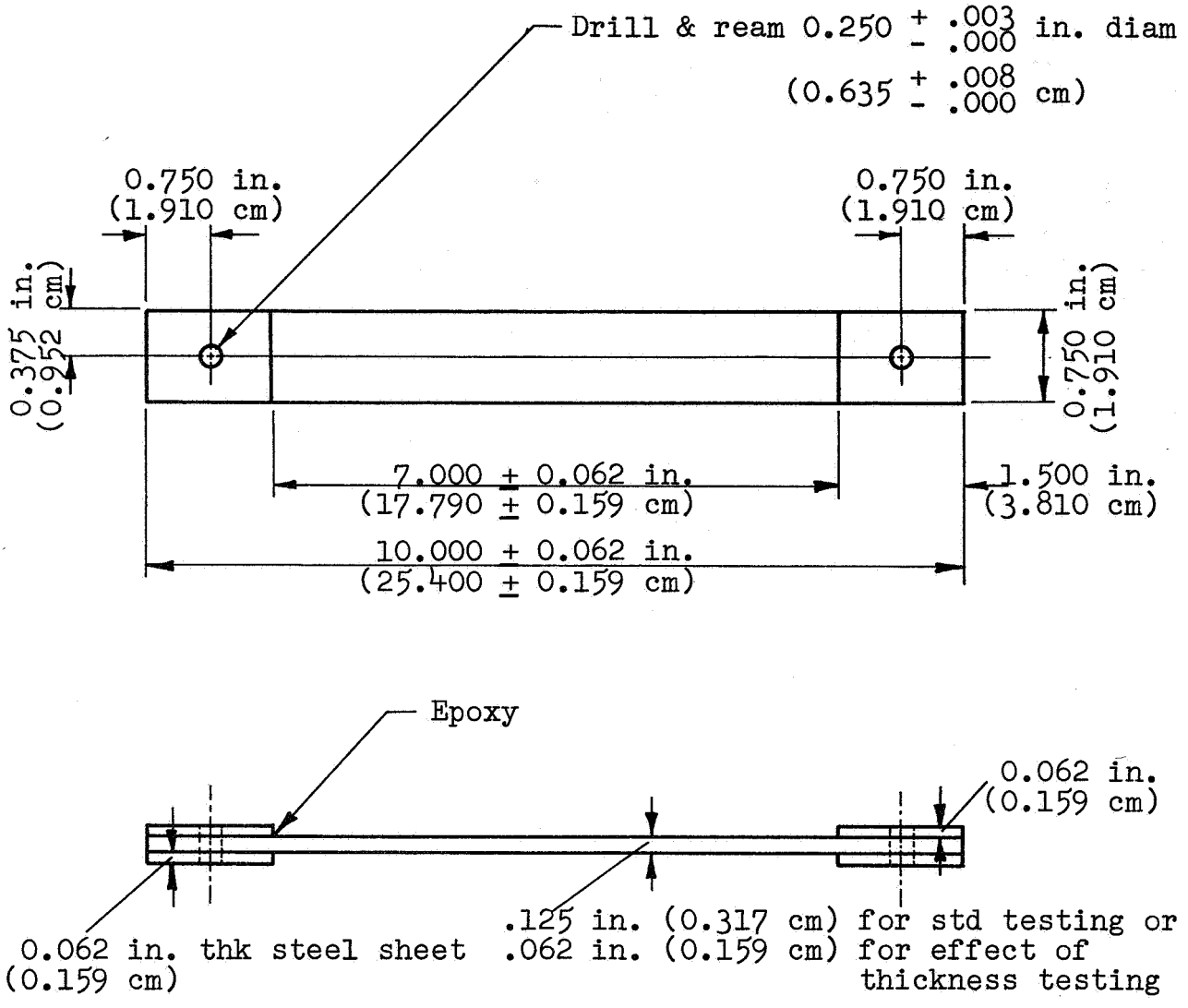

All tolerances ± 0.016 in. (0.040 cm)
except as noted

FIGURE AI-4

MECHANICAL PROPERTIES TEST SPECIMEN

APPENDIX J

Flow Resistance Testing--Tasks B Through G

Apparatus.- All flow resistance measurements performed in fulfilling NAS 1-6990 were conducted on the apparatus shown in Figure AJ-1. The apparatus consists of six calibrated flow orifices which can deliver precisely known volumes of air to gasketed test areas of 1 in. (2.54 cm) or 3.9 in. (10.0 cm) diameter. Mercury manometers are used to measure the differential pressures created by the air flow through the orifices and inclined water manometers are used to measure the differential pressures induced across the fiber metal materials being tested. This or similar apparatus is normally used in the proof testing of all fiber metal acoustical materials.

Procedure and calculations.- The flow resistance values in this report are normally expressed in the CGS unit of measurement, the rayl. One rayl is dimensionally equivalent to one dyne-sec/cm^3 (1 x 10^{-5} newton-sec/cm^3). The following procedure was employed in measuring flow resistance:

1. The test sample was placed on the 1 in. (2.54 cm) or 3.9 in (10.0 cm) diameter test area and subjected to an air flow velocity of 2000 cfh/ft^2 (equivalent to 0.556 ft/sec or 16.95 cm/sec). The differential pressure induced across the fiber metal was recorded. The test was repeated at a second location on the test specimen. Both test locations were marked, so that they could be accurately located for retest.

2. The differential pressures were averaged and a nominal rayl number calculated for the test specimen by the following equation:

$$R = \frac{\Delta P}{Va} \times C$$

where

R the air flow resistance, dyne-sec/cm^3

ΔP the average differential pressure, in. (cm) of H_2O

Va the air flow velocity at average pressure and temperature through the fiber metal, ft/sec (cm/sec)

C a constant; 81.7 if ΔP is measured in in. of H_2O and Va is in ft/sec; 979 if ΔP is measured in cm of water and Va is in cm/sec

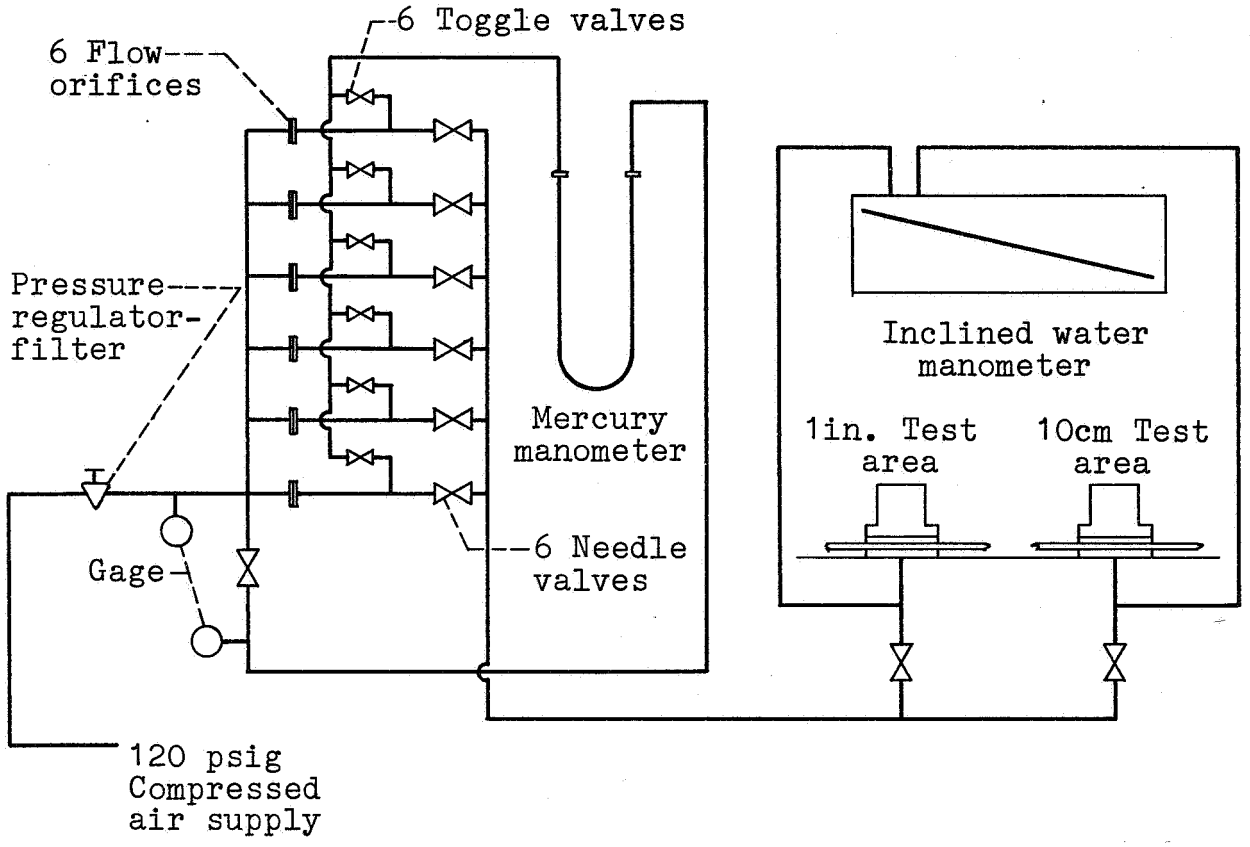

FIGURE AJ-I

FLOW RESISTANCE TEST APPARATUS

APPENDIX K

Mechanical Properties Testing--Tasks C, E, F and G

Apparatus.- All mechanical properties testing performed in fulfilling NAS 1-6990 were conducted on a testing machine capable of tensile, compression and bend testing. With modification, the machine is also capable of flexural, shear, hardness, notched bar and cupping testing. The machine is fitted with a recorder which has the displacement of the horizontal axis proportional to the elongation of the test piece. The machine was fitted with chucks of the standard quick-grip type.

Procedure and calculations.- Mechanical properties, as defined in this program, consisted of measuring the ultimate tensile strength (UTS) and the total percentage elongation of the test specimen at failure. Failure of the fiber metal was defined as the point at which a tear or crack developed. This was not always the point at which the test piece broke into two parts.

The following procedure was employed in testing both the reference control and environmental exposure test samples:

1. Rectangular test specimens were sheared from the parent sample. They measured, nominally, 0.6 in. (1.5 cm) wide and 6.0 in. (15.0 cm) long.

2. Dimensional and weight measurements were made and an apparent density and a cross sectional area was calculated for each specimen.

3. The ends of each specimen were reinforced on both sides with 0.6 in. (1.5 cm) wide and 1.5 in. (3.8 cm) long 24 gauge metal tabs. These tabs were epoxy bonded to the test specimen and are employed in all such fiber metal testing as a means of obtaining a gauge length. A nominal 3.0 in. (7.6 cm) gauge length remained and this was accurately determined for each specimen.

4. The specimen was then tensile tested, using the stress-strain recorder. A magnification factor of 16.0 was employed on the sample elongation-recording drum rotation.

5. The ultimate tensile strength was calculated by dividing the breaking force in lbs (N) by the cross sectional area in $in.^2$ (cm^2). It should be noted that this area is computed as if the specimen were solid.

6. The total percentage elongation was calculated as follows:

APPENDIX K

$$E = \frac{A - (B \times F)}{M \times G} \times 100$$

where

E sample elongation, percent

A total strain indicated on the recorder at failure, in. (cm)

B deflection characteristic of the beam employed in testing, in./lb force (cm/newton)

F breaking force, lbs (N)

G gauge length of the specimen, in. (cm)

M magnification factor for horizontal scale of recorder

APPENDIX L

Apparent Density And Dimensional Inspection

Apparatus.- The following apparatus was used in performing these tasks.

Weight determination	- Laboratory analytical balance
Length and width measurement	- A steel rule with subdivisions of 0.01 in. (0.025 cm)
Thickness measurement	- "Duckbill" type micrometer

Procedure and calculations.- The following procedure was followed:

1. The length, width and thickness of the specimen was determined. Lengths and widths were ordinarily measured to the nearest 0.01 in. (0.025 cm). Thicknesses were measured to the nearest 0.001 in. (0.0025 cm).

2. The weight of the specimen was determined to the nearest milligram.

3. The apparent density of the specimen was determined by the following formula:

$$D = \frac{A \times C}{L \times W \times T \times G}$$

where

D the apparent density of the specimen, percent

A the weight of the specimen, gms.

C a constant; 6.11 if L, W, and T are in in.; 100 if L, W, and T are in cm

L the length of the specimen, in. (cm)

W the width of the specimen, in. (cm)

T the thickness of the specimen, in. (cm)

G the specific gravity of the metal, gm/cc

REFERENCES

1. Rion, W.C. Jr.: Stainless Steel Information Manual for the Savannah River Plant Vol.1. Properties. Atomic Energy Commission report DP-860 (Vol.1), Engineering Department DuPont de Nemours (E.I.) & Co., Wilmington, Delaware, July, 1964.

2. Marsh, Alan H.: Study of Acoustical Treatments for Jet-Engine Nacelles. Douglas Paper 4146, Acoustical Society of America, Los Angeles, California, 2 November, 1966.

3. Hsu, J.S.: Fiber Metal Contamination and Cleaning Tests. Report No. DAC-66755 - Revision A, Douglas Aircraft Division, McDonnell Douglas Corporation, May 1968.

4. Timoshenko, S.; and MacCullough, Gleason H.: Elements of Strength of Materials. Third ed., D. Van Nostrand Co.Inc., 1949.

5. Karplus, H.B., Raelson, V.J., and Schwartzbart H.: Noise and Vibration Control with Fiber Metallurgy. Bulletin No. 35, Part 7, Illinois Institute of Technology Research Institute, April 1966.